*IN-15-CR*
*73941*
*p.214*
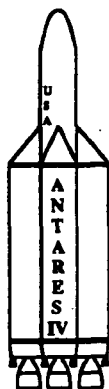
NASW-4435

# PROJECT ANTARES:

## A LOW COST MODULAR LAUNCH VEHICLE FOR THE FUTURE

## University of Washington

## Seattle, Washington

# PROJECT ANTARES:
## A LOW COST MODULAR LAUNCH VEHICLE FOR THE FUTURE

## FINAL REPORT

Space Systems Design, AA420/421
NASA/USRA Advanced Design Program

### Prepared By

| | | |
|---|---|---|
| Steve Aarnio | Bruce Detert | Sang Kim |
| Hobie Anderson | Miles Ervin | Steve Nicholls |
| El Mehdi Arzaz | Mike Filbin | Colin O'Connor |
| Michelle Bailey | Mark Foster | Steve Solomon |
| Jeff Beeghly | Kim Fricke | Matt Sullivan |
| Curt Cartwright | John Gailey | Jon Upham |
| William Chau | Howard Hu | Kurt Vold |
| Andrew Dawdy | Alvin Jackson | David Woodson |
| | Geneva Jacobson | |

### Instructor

Prof. Adam P. Bruckner

### Teaching Assistant

David Carlile

Department of Aeronautics and Astronautics
University of Washington
Seattle, Washington 98195

June 14, 1991

# ABSTRACT

The single stage to orbit launch vehicle Antares is based upon the revolutionary concept of modularity, enabling the Antares to efficiently launch communications satellites, as well as heavy payloads, into Earth's orbit and beyond. The basic unit of the modular system, a single Antares vehicle, is aimed at launching approximately 10,000 kg (22,000 lbs) into low Earth orbit (LEO). When coupled with a Centaur upper stage it is capable of placing 3,500 kg (7,700 lbs) into geostationary orbit. The Antares incorporates a reusable engine, the Dual Mixture Ratio Engine (DMRE), as its propulsive device. This enables Antares to compete and excel in the satellite launch market by dramatically reducing launch costs. Antares' projected launch costs are $610 per pound ($1,340 per kg) to LEO which offers a tremendous savings over launch vehicles available today.

Inherent in the design is the capability to attach several of these vehicles together to provide heavy lift capability. Any number of these vehicles, up to seven, can be attached depending on the payload and mission requirements. With a seven vehicle configuration Antares' modular concept provides a heavy lift capability of approximately 70,000 kg (154,000 lbs) to LEO. This expandability allows for a wider range of payload options such as large Earth satellites, Space Station Freedom support, and interplanetary spacecraft, and also offers a significant cost savings over a mixed fleet based on different launch vehicles.

# PREFACE

This report is the seventh in a series that began in 1985, when the University of Washington was invited by NASA to participate in what would become the highly successful NASA/USRA Advanced Design Program. Under this program our students have examined various innovative design problems relating to the critical needs of space prime power, propulsion, and transportation, such as solar and nuclear power systems, ram accelerator mass launchers, and solar propulsion systems, all based on ongoing research at the University.

This year our design project delved into the topic of space transportation, in the form of Antares, a new class of low-cost, modular, single-stage-to-orbit (SSTO) launch vehicle. The concept grew out of the ideas and suggestions of several individuals. When we began the course in the Winter Quarter it was my intention that the class investigate the various SSTO proposals that had surfaced during the past three decades, and proceed to design a flyback SSTO vehicle which would represent the "last word" on the concept. Following presentations to the class early in the term by Dana Andrews, Eric Wetzel, and John Jordan on Boeing's SSTO, Personnel Launch System (PLS), and Advanced Launch System (ALS) concepts, our thinking began to shift. Teaching Assistant David Carlile suggested we design a two or three unit modular booster, smaller than the ALS, which would serve not only to deliver the PLS to orbit but also to carry a variety of moderate to heavy payloads, depending on the number of units attached together. At a departmental seminar the following day, Dale Myers, former Deputy Administrator of NASA, spoke about the lack of an effective, low-cost launch capability in the U.S. and the success of Arianespace, the European launch consortium, in capturing more than half the commercial satellite market. He went on to suggest that some form of small, two or three unit, modular launch vehicle was needed to make the U.S. competitive again in the commercial launch market. Discussions with other visitors, such as

former U.S. astronaut George "Pinky" Nelson and Yuri Stekolchikov of the Lavochkin Association in the U.S.S.R., added to our growing fund of ideas.

Finally, drawing from these various ideas and incorporating suggestions from our students, David Carlile and I came up with the basic concept of our project: a partially reusable, SSTO modular launch vehicle, which would be capable of placing payloads ranging from ~10,000 to ~70,000 kg (22,000 to 154,000 lb) into low Earth orbit and, when coupled with an upper stage such as the Centaur, delivering up to ~4000 kg (8800 lb) to geosynchronous orbit. The prime considerations were to be simplicity and low cost. The students enthusiastically accepted this challenge and proceeded to skilfully develop the vehicle design presented in this report: the Antares. Their work has been creative and of high quality, and has met all our original objectives. Although much work remains to be done, it is our belief that the Antares is an innovative and straightforward approach to the problem of lowering the cost of space missions and returning the U.S. to a preeminent position in commercial space. We look forward to the day when Antares will become a reality.

Adam P. Bruckner
Research Professor
June 14, 1991

# ACKNOWLEDGEMENTS

Furthermore, we would like to extend our gratitude and apologies to anyone who was inadvertently not acknowledged above. Due to the length and scope of this project, some individuals who helped us may have been omitted by accident.

Finally, thanks goes to NASA/USRA and Frank Swalley, our center mentor, for sponsoring this program and giving us the chance to develop this project. Thanks also goes to the Department of Aeronautics and Astronautics here at the University of Washington for additional funding and other help.

# TABLE OF CONTENTS

# 1.0 INTRODUCTION
(Howard C. Hu)

The expanding applications of communications and military satellites over the last decade have increased the demand for reliable, low cost launch vehicles. Recent projections made by the Office of Commercial Space Transportation (OCST) indicate that the average number of payloads launched per year will continue to increase [1]. This OCST study, covering the period between 1993 and 2005, predicts that the number of communications satellites launched into low Earth orbit (LEO) will increase from 10 to 17 per year. However, the number of communications satellites placed into geosynchronous equatorial orbit (GEO) are expected to remain fairly constant. The study also indicated that there will be a modest increase in the number of remote sensing satellite launches, from 4 to 6 per year. Deliveries of other payloads into orbit, such as orbital microgravity experiments, are projected to increase from 7 to 10 per year during 1993 to 2005. The National Aeronautics and Space Administration (NASA) has estimated that 11-14 flights per year are needed to construct and supply the proposed Space Station *Freedom* [2]. Other analyses done by NASA, the Air Force's Space Systems Division, and the NASP program reveal that a vehicle able to lift 9000 kg (20,000 lbs) into LEO could carry 80% of NASA's civil payloads, 60% of the Defense Department's payloads, and most of the commercial payloads [3]. With a backlog of payloads waiting to be launched and a projected increase in the number of launches needed in the future, the current U.S. launch fleet, comprised of reusable Space Shuttle Orbiters and expendable launch vehicles (ELV's), will not be able to adequately meet these demands.

The Space Shuttle, initially hailed as America's dependable, low-cost, all-purpose launch vehicle, has encountered numerous technical problems, causing delays to scheduled launches. Originally, in the early 1970s, NASA projected that a reusable Shuttle would deliver payloads to orbit for one-tenth the cost of any expendable launch vehicle available at that time [4]. However, in order to achieve these cost savings, the Shuttle had to be flown frequently, allowing the operations costs to be spread out over the many missions. As late as 1981,

NASA's Office of Space Transportation Systems Operations was predicting that the Shuttle could achieve a flight rate of 40 missions per year [4], but unexpected delays to scheduled launches have severely reduced this number, thus resulting in the current high cost of launching payloads on the Orbiters. The Shuttle, being a man-rated vehicle, requires multiple redundant systems in order to ensure the safe launch and return of the crew. This in turn has caused NASA to create a "standing army" of technicians and engineers to keep the Space Shuttle Orbiters in operation and on schedule. The man hours involved significantly increase the Shuttle's launch costs, making it less attractive to potential launch customers. The reduction in the number of launches per year caused by the delays, and the increased cost to consistently maintain the Space Shuttle reduces its effectiveness as a reliable vehicle for launching satellites and space probes.

With the delays of the Shuttle reducing the number of launches available, satellite launch customers have had to rely on expendable launch vehicles, such as the Atlas, Delta, and Titan [4]. However, the ELV's, originally developed in the 1960s as intermediate range ballistic missiles (IRBM's), and intercontinental ballistic missiles (ICBM's), impose mass and size restrictions that limit their payload capacities. These restrictions have created a gap in the payload range to GEO between 1,500 kg (3,300 lbs) and 4,000 kg (8,800 lbs) as shown in Table 1.1. Arianespace, a consortium of European aerospace companies and banks, predicts that satellites heavier than 1,200 kg, particularly in the 2,000 to 3000 kg range, will dominate the future [5]. Without an American expendable launch vehicle that is able to compete in the 1,500 kg to 4000 kg payload range, and with the uncertainty of the Space Shuttle launches, U.S. companies have turned to Arianespace for their launch needs [2]. To date, Arianespace has effectively captured a 50% share of the satellite launch market [5].

The high cost of launching a satellite on the shuttle or an ELV places another constraint on satellite manufacturers. It currently costs from $50,000 to $120,000 per kilogram ($22,700 to $54,500 per pound) to launch a payloads into GEO [6]. To reach LEO, the cost range is from $6,600 to $26,450 per kilogram ($3,000 to $12,000 per pound) [7].

The mass and size restrictions and high launch costs of the current mixed fleet of Space Shuttle Orbiters and ELV's have severely hindered America's ability to compete in the satellite launch market. It is apparent that a new flexible and cost-effective launch vehicle must be developed to ensure America's continued presence as a leader in the commercial launch market. Current vehicles under consideration, such as the Advanced Launch Development Program (ALDP), formerly the Advanced Launch System (ALS) [8], and the fly back single-stage-to-orbit (SSTO) manned vehicle [9], do not meet the above mentioned criteria. The ALDP is designed as a heavy lift launch vehicle, thus limiting its effectiveness for launching payloads into orbit to a small percentage of the market. The totally reusable manned SSTO requires many additional systems that not only increase the overall cost of the vehicle, but makes it more complex. As evident from the problems experienced by the Shuttle, very complex vehicles tend to encounter more technical problems, which in turn increases the launch costs.

Antares, the new launch vehicle proposed in this report, is the flexible and cost-effective launch system that will be able to meet the nation's growing launch needs both in the near and long term. Antares is a single-stage-to-low Earth orbit launch vehicle that can deliver a wide range of payloads into orbit. The basic Antares vehicle for LEO and GEO missions utilizes an advanced reusable liquid hydrogen and liquid oxygen engine, the Dual Mixture Ratio Engine (DMRE), as its main engine [10]. The DMRE is retrieved for reuse in future missions via the Engine Return Unit (ERU), resulting in a substantial reduction of the launch costs. For LEO missions, the Antares vehicle has the capability to be clustered together to provide heavy lift. The LEO mission vehicles (see Fig. 1.1), which are identical modular units, can be combined to form various modular configurations, from a two booster configuration (Antares II), up to a seven booster configuration (Antares VII), as illustrated in Fig.1.2a and 1.2b. This modular concept reduces cost on the basis that a large, heavy lift vehicle is a cluster of simple, generic boosters, thus, giving Antares an unprecedented advantage over any other existing or proposed launch vehicle. The Antares vehicle used for GEO missions, which is basically the same vehicle as the LEO mission vehicle (see Fig. 1.3), launches payloads into a

suborbital trajectory, and then utilizes a Centaur upper stage to deliver the payloads the rest of the way to GEO. By utilizing reusable engines and the concept of modularity, Antares provides a low-cost, reliable alternative to the existing fleet of launch vehicles.

For Antares to be successful, it needs to recapture a large portion of the U.S. satellite market that has been lost to Arianespace. One Antares vehicle can place a payload of 4,000 kg (8,800 lbs) into GEO, thus allowing it to effectively compete against Arianespace for launch customers. Antares' modular capability provides another distinct advantage over other launch vehicles and is instrumental in making the Antares a potentially dominant player in the commercial launch market. The ability to attach several vehicles together provides launch customers with a wide range of payloads to LEO, from 10,000 kg (22,000 lbs) with Antares I to 70,000 kg (154,000 lbs) with Antares VII. The low launch costs of the Antares vehicle, $1,340 per kg ($610 per lb) to LEO and $16,200 per kg ($7,350 per lb) to GEO, cannot be matched by any existing launch vehicles. Antares' unique ability to deliver a variety of payloads into LEO and GEO and its low launch costs, allows it to effectively compete not only against Arianespace, but other foreign competitors such as the Chinese and the Japanese. The concept of modularity and the cost savings attributed to reusable engines makes Antares a reliable, inexpensive, and flexible launch vehicle of the future.

This report provides a detailed analysis of the systems that make up the Antares vehicle. A complete mission profile is given along with discussions of the vehicle's systems which include the ERU, propellant tanks, structural connecters, and fairings. These sections are followed by an analysis of ground operations scenarios and a thorough discussion of the modular configurations. An evaluation of the cost per unit mass to launch payloads into orbit concludes the report. The scope of this report is to convey the main concepts developed for the Antares vehicle. The ideas elaborated in the following sections will act as a precursor for further research into developing Antares as America's reliable launch vehicle for the 21st century.

4

Table 1.1: Payload Capacities of Various Launch Vehicles.

| VEHICLE | LEO | | GEO | |
|---------|-----|-----|-----|-----|
| | (kg) | (lbs) | (kg) | (lbs) |
| DELTA | 3,500 | 7,800 | 700 | 1,500 |
| DELTA II | | | | |
| 6920/6925 | 3,900 | 8,600 | 600 | 1,300 |
| 7920/7925 | 5,000 | 11,000 | 800 | 1,750 |
| ATLAS I | 5,900 | 13,000 | 1,000 | 2,200 |
| ATLAS II | | | | |
| II | 6,700 | 14,700 | 1,150 | 2,500 |
| IIA | 7,000 | 15,400 | 1,250 | 2,750 |
| IIAS | 8,600 | 18,900 | 1,500 | 3,300 |
| TITAN III | 14,700 | 32,300 | 4,150 | 9,100 |
| TITAN IV | 17,700 | 39,000 | 4,500 | 9,900 |
| SPACE SHUTTLE | 23,000 | 50,500 | 2,300 | 5,000 |
| ARIANE IV | | | | |
| 40 | 4,800 | 10,500 | 1,150 | 2,500 |
| 42P | 6,000 | 13,000 | 1,600 | 3,500 |
| 42L | 6,800 | 14,900 | 1,850 | 4,050 |
| 44P | 7,300 | 16,000 | 1,900 | 4,150 |
| 44LP | 8,200 | 18,000 | 2,200 | 4,850 |
| 44L | 9,600 | 21,100 | 2,500 | 5,500 |

Key: LEO = Low Earth Orbit
     GEO = Geosynchronous Equatorial Orbit

SOURCE: References 5,6,7,11,and 12

5

## 1.1 NOMENCLATURE

| | |
|---|---|
| ALDP | Advanced Launch Development Program |
| ALS | Advanced Launch System |
| Antares I | Single Antares vehicle |
| Antares II | Two vehicle configuration |
| Antares III | Three vehicle configuration |
| Antares IV | Four vehicle configuration |
| Antares V | Five vehicle configuration |
| Antares VI | Six vehicle configuration |
| Antares VII | Seven vehicle configuration |
| DMRE | Dual Mixture Ratio Engine |
| ELV | Expendable Launch Vehicles |
| ERU | Engine Return Unit |
| GEO | Geosynchronous Equatorial Orbit |
| ICBM | Intercontinental Ballistic Missile |
| IRBM | Intermediate Range Ballistic Missile |
| LEO | Low Earth Orbit |
| NASA | National Aeronautics and Space Administration |
| OCST | Office of Commercial Space Transportation |
| SSTO | Single-Stage-to-Orbit |

## 1.2 REFERENCES

1. U.S. Department of Transportation, Office of Commercial Space Transportation, The Future of the Commercial Space Launch Market: 1993-2005, Decision Science Consortium, Inc. and Berner, Lanphier, and Associates, Inc., May 1991, pp. 8-30.

2. Frazer, L., "Lead, Follow or Get out of the Way," Space World, May 1988, pp. 12-15.

3. Payton, G. and Sponable, J.M., "Single Stage to Orbit: Counting Down," Aerospace America, April 1991, pp. 36-39.

4. Simon, M.C. and Hora, R.P., "Return of the ELV's," Space World, January 1988, pp. 15-19.

5. Jaeger, R.W. and Claudon, J., "Ariane - The First Commercial Space Transportation System," The Fifteenth International Symposium on Space Technology and Science, Volume II, Tokyo 1986, pp. 1431-1438.

6. Wertz, J.R. and Larson W.J., Editors, Space Mission Analysis and Design, Kluwer Academic Publishers, Dordrecht, The Netherlands, 1991, p. 671.

7. U.S. Congress, Office of Technology Assessment, Access to Space: The Future of U.S. Space Transportation Systems, OTA-ISC-415, U.S. Government Printing Office,Washington, DC, April 1990, p. 59.

8. DeMeis, R., "New Life for Heavy Lift," Aerospace America, March 1991, pp. 32-35.

9. Payton, G. and Sponable, J.M., "Designing the SSTO Rocket," Aerospace America, April 1991, pp. 40-45.

10. Limerick, C.D., "Dual Mixture Ratio $H_2/O_2$ Engine for Single Stage to Orbit Application," Journal of Propulsion, Vol. 7, No. 1, January - February 1991, pp. 31-36.

11. Wilson, A., ed., Interavia: Space Directory, Jane's Information Group, Coulsdon, Surrey, United Kingdom, 1990, pp.256-290.

12. Reichert, R.G., "Space Launcher Upper Stages-Design for Mission Versatility and/or Orbital Operations," The Fifteenth International Symposium on Space Technology and Science, Volume II, Tokyo 1986, pp. 1463-1474.
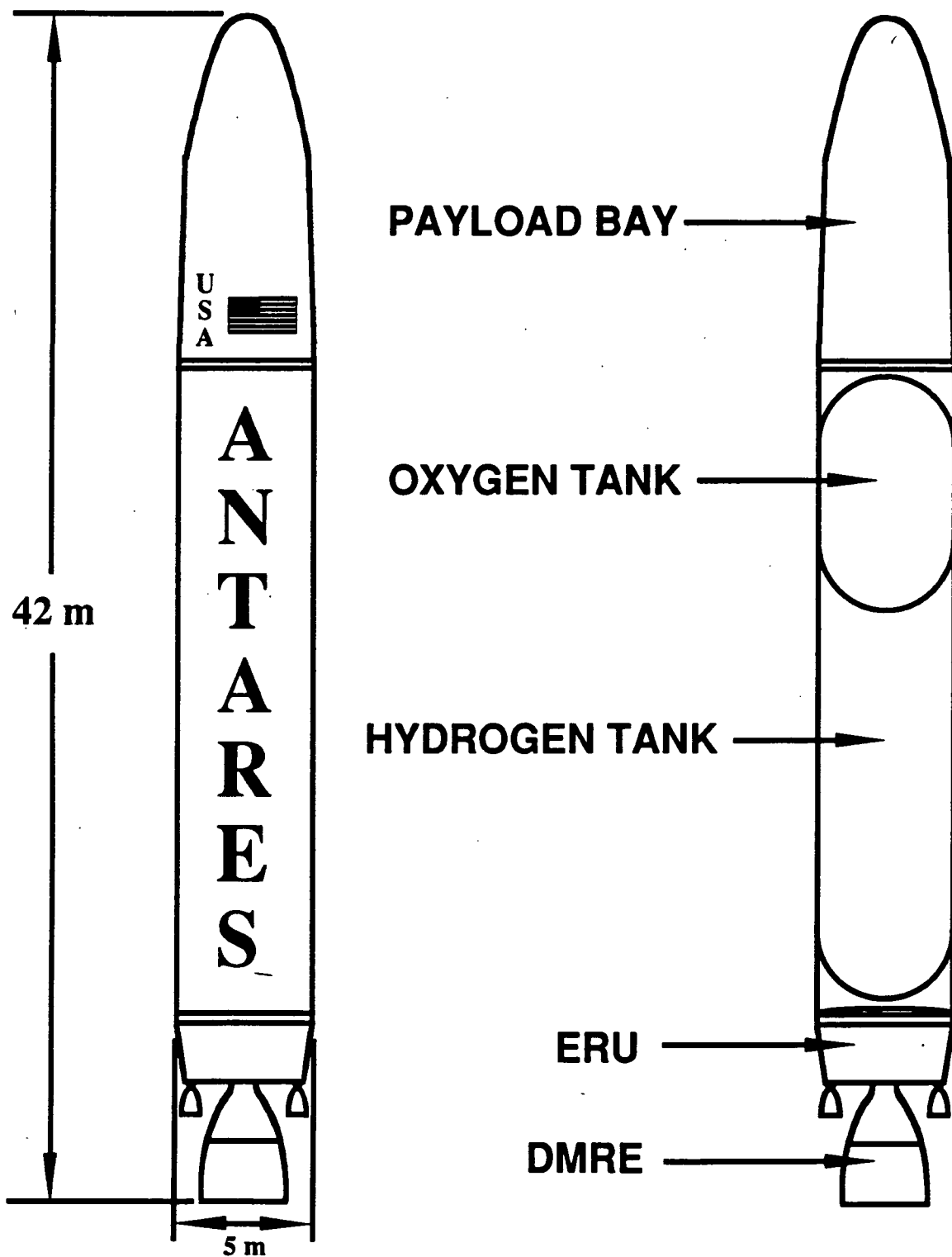
Fig. 1.1. Antares I - configured for LEO missions.

# PLAN VIEW
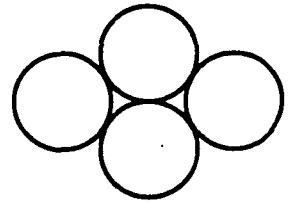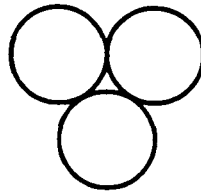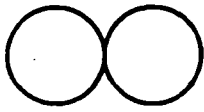
# SIDE VIEW
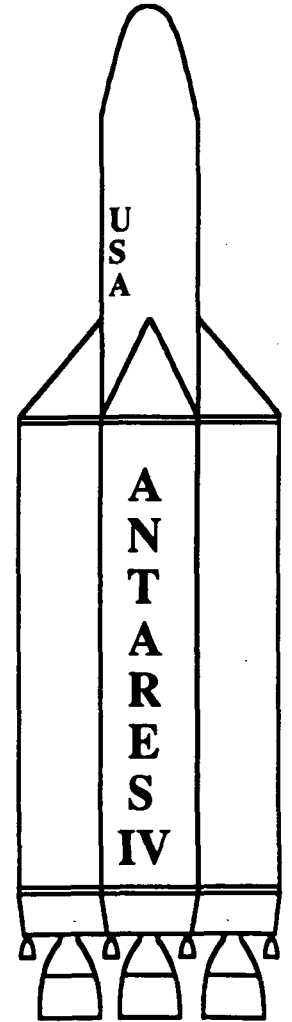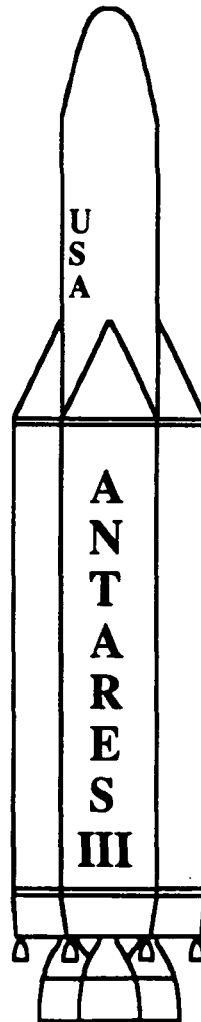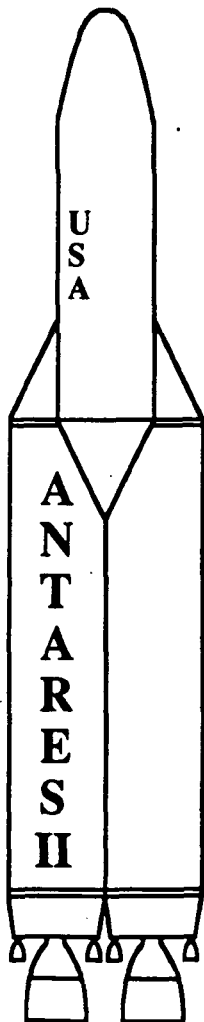


Fig. 1.2a. Antares modular configurations.

# PLAN VIEW
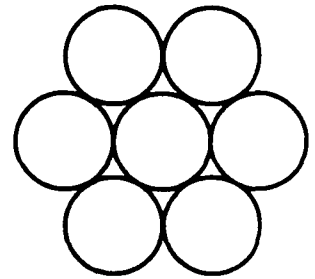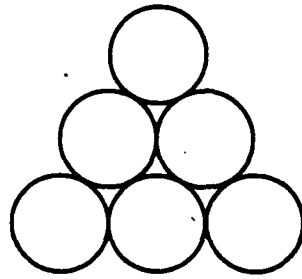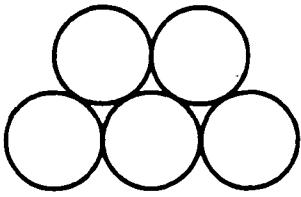
# SIDE VIEW
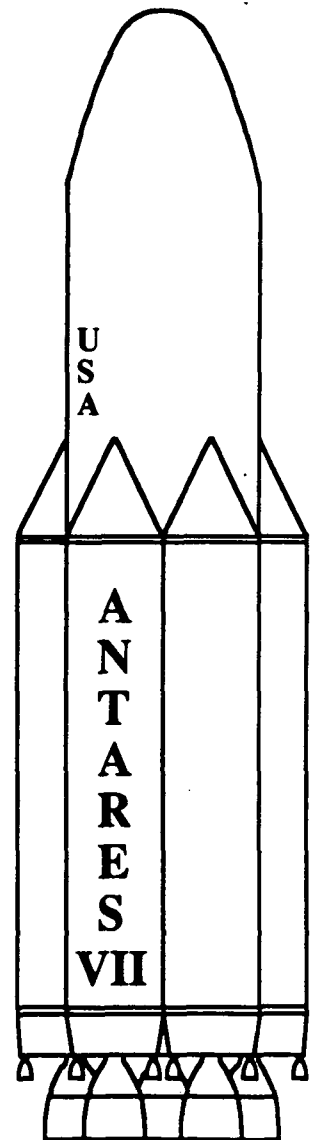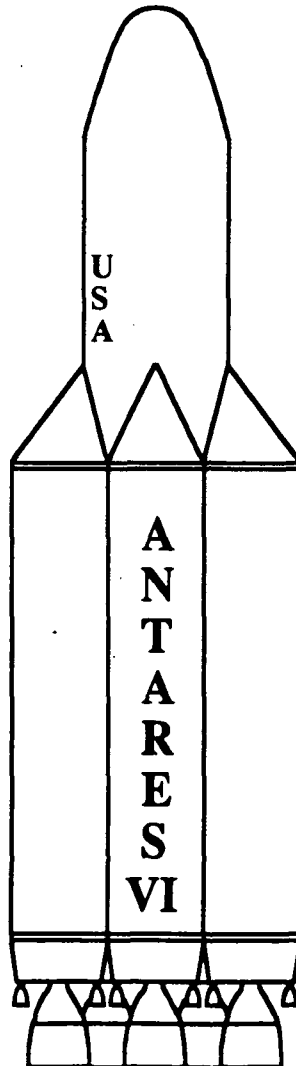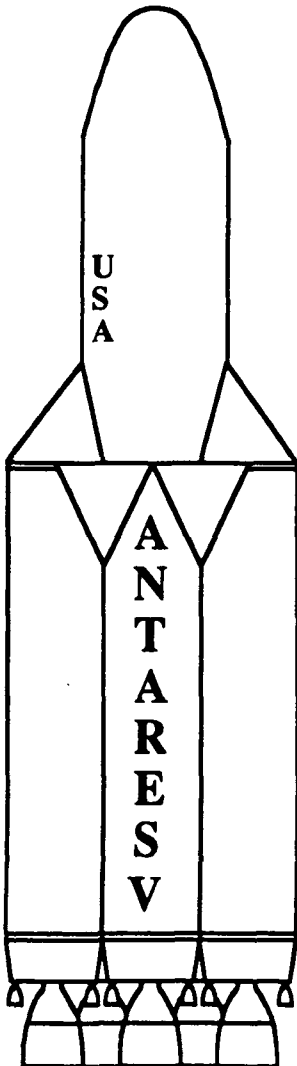


Fig. 1.2b. Antares modular configurations.

**53 m**

**5 m**

**PAYLOAD BAY**

**CENTAUR UPPER STAGE**

**OXYGEN TANK**

**HYDROGEN TANK**

**ERU**

**DMRE**
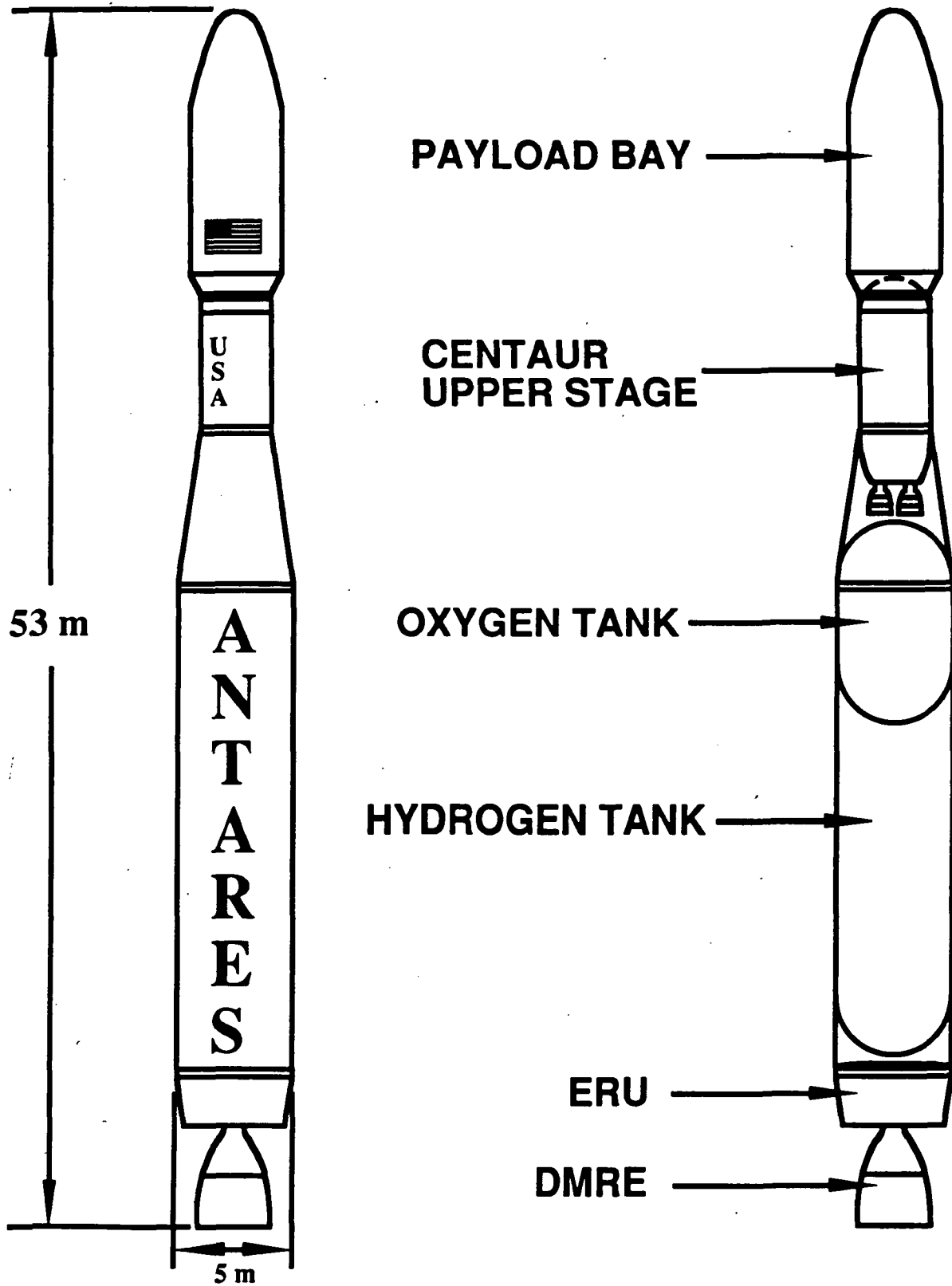
Fig. 1.3. Antares I - configured for GEO missions.

11

# 2.0  MISSION ANALYSIS

The Antares is designed to launch payloads into low Earth orbit and geostationary orbit. Both of these missions require an optimized launch trajectory, which is highly dependent on atmospheric influences during the initial launch phase. OPGUID, a launch analysis routine obtained from NASA Marshall Space Flight Center [1], was employed in order to optimize the Antares' launch trajectory for both low Earth orbit and geostationary missions (see Appendix A.1). Included in the OPGUID program are atmospheric profiles that provide a model of the variations with increasing altitude of typical atmospheric characteristics, such as density and pressure. This allows OPGUID to accurately analyze the forces that act on the vehicle during its atmospheric ascent. The results from OPGUID were checked by an in-house trajectory optimization routine. The routine involves numerically integrating the equations of motion that apply to the vehicle during ascent (see Appendix A.2). In addition, a launch stability analysis was also done to assure that the Antares would be able to react to wind gusts during launch. Deorbit is also included in the flight trajectory analysis, in which the deorbit trajectory is analyzed from the equations of motion for a body re-entering the Earth's atmosphere.

## 2.1  MISSION SCENARIOS
(Michael Filbin)

A primary mission for the Antares is launching payloads into low Earth orbit. The vehicle reaches LEO in a single stage. At take-off, the payload is surrounded by a fairing that absorbs the dynamic pressure loads that result from high velocity atmospheric flight (see Fig. 2.1). The fairing is jettisoned at an appropriate altitude, where the dynamic pressure has fallen to a sufficiently low value. At main engine cut-off, when the vehicle has reached orbital altitude and velocity, the payload is deployed from the Antares vehicle. Each payload is required to carry its own kick booster if it needs to attain a specific altitude and inclination. For example, to circularize the payload into a 300 km circular orbit, the kick booster would perform

**PRECEDING PAGE BLANK NOT FILMED**

a burn at the apogee of the low Earth parking orbit (see Fig. 2.2). The Antares' orbital maneuvering system is also capable of placing the entire vehicle, including the payload, into a circular orbit up to 300 km. This provides flexibility to payloads that may need to be launched into specific orbits.

After the payload has been delivered to low Earth orbit, the Antares orbits the Earth until the first available deorbit opportunity. Orbital maneuvering engines, located in the Engine Return Unit (ERU), are used to deorbit the vehicle. Following the deorbit burn, the ERU separates from the tank, and the two components enter the Earth's atmosphere separately. The tanks burn up during re-entry and are not retrieved, whereas the ERU survives re-entry. After the ERU has been decelerated through the atmosphere, a parafoil system deploys from hatches located on the ERU to further slow the vehicle before it splashes down on the ocean.

Increased payload capacities to low Earth orbit are achieved with the modular configurations of Antares. For these configurations, Antares II through Antares VII vehicles, the mission profile is identical to that of the Antares I configuration to low Earth orbit. During the launch phase, the boosters in the modular cluster burn in parallel until the main engines simultaneously cut-off. At this time, the payload is deployed from the multiple Antares configuration. For the deorbit of the modular vehicle, each ERU separates individually from the Antares tanks. The tanks remain attached to each other as they re-enter the atmosphere, whereas the ERU's re-enter separately. Each ERU is equipped with a parafoil system that deploys prior to splashdown.

Another primary mission of the Antares is the launch of communications satellites into geostationary orbit. This is accomplished in the Antares I configuration, where the vehicle is equipped with a Centaur upper stage. Although the Antares is a single-stage to orbit vehicle, the GEO mission requires the booster to launch into a ballistic trajectory, because the Centaur is capable of completing the launch insertion into low Earth orbit, in addition to transferring the payload into a geostationary orbit.

During the launch phase of the geostationary mission, the Centaur and payload are surrounded by a fairing that is jettisoned at an appropriate altitude (see Fig. 2.3). The Centaur separates from the booster as the main engine cuts off, and continues its flight into geostationary orbit. Following the upper stage separation, the Antares falls back toward the Earth. The ERU jettisons from the main tank assembly and deorbits into the Atlantic Ocean as previously described. The expendable tank burns up during re-entry.

The Centaur upper stage, following its separation from the tank, continues upward until it attains an intermediate low Earth parking orbit. While in this orbit, the Centaur waits for the appropriate time, corresponding to the satellite's desired location in GEO, to initiate its burn to a geosynchronous transfer orbit (GTO) (See Fig. 2.4). The Centaur initiates the GTO burn at the perigee of the parking orbit, which minimizes propellant usage. When the Centaur reaches the apogee of the GTO it again fires its engines to circularize the satellite in GEO. Due to the $28.5°$ inclination of the Kennedy Space Center launch site, the Centaur must also perform an out-of-plane burn to rotate the orbital plane and place the satellite directly above the Earth's equator. This plane change is accomplished with out-of-plane burns at both the perigee and apogee of the geostationary transfer orbit. Thus, GEO payloads do not require a kick booster, because the Centaur performs all the necessary orbital maneuvers to attain GEO.

## 2.2   PERFORMANCE ANALYSIS
(Andrew Dawdy)

The performance analysis provides data on the Antares capabilities and limitations. Data for this analysis are generated by solving the general equations of motion with numerical integration techniques. By establishing mission criteria, the data can be used to evaluate different engine configurations for overall suitability. Prediction of optimum payload masses helps to establish propellant tank volumes, and ascent parameters provide data for the stability analysis.

## 2.2.1 LEO PERFORMANCE OPTIMIZATION

The goal of the LEO performance optimization is to generate data for the design of the baseline Antares vehicle. Marshal Space Flight Center's OPGUID trajectory optimization program (see Appendix A) is used to calculate the optimum payload mass using different engines and varying amounts of propellant in the vehicle's tanks. For simplicity, the structural mass (12,700 kg) and diameter (5.0 m) are assumed to be the same in each of the configurations examined. The basis for these initial approximations will be discussed in subsequent sections. All preliminary analysis is performed with an east launch from the Kennedy Space Center into a 150x300 km elliptical orbit of 28.5° inclination.

Three different engines were examined for use on this vehicle: the Space Shuttle Main Engine (SSME), the Space Transportation Main Engine (STME), and a staged combustion, dual mixture ratio engine (DMRE) under study at Pratt & Whitney Co.[3]. The SSME, and the STME were both found to be less than ideal, as they cannot be throttled sufficiently to limit burnout acceleration to 4 G's or less. In addition, the STME's specific impulse (427 sec in vacuum) was found to be insufficient for the missions considered. The DMRE satisfies the requirements of a Single-Stage-To-Orbit (SSTO) vehicle as it produces high thrust at takeoff, high specific impulse at altitude, and is deeply throttleable. The engine is able to operate at oxidizer to fuel ratios (O:F) of 12:1 and 6:1 and is equipped with a nozzle extension capable of deployment at altitude. Parameters relevant to the mission analysis are listed in Table 2.1. A more detailed presentation of the DMRE is given in Section 3.1 and a detailed comparison of the engines considered is presented in Appendix B.

Performance of the engine is primarily dependant on the altitude at which it operates. At low altitudes atmospheric pressure is greater than the static pressure of the exhaust. This results in a normal shock within the nozzle. As the exhaust passes through the normal shock

Table 2.1: DMRE Parameters.

| | Area Ratio 40:1 | Area Ratio 150:1 |
|---|---|---|
| Exit Area | 2.06 m$^2$ | 7.73 m$^2$ |
| Vacuum Thrust<br>O:F=12:1<br>O:F=6:1 | 2670 kN (600,000 lbs) | 2790 kN (628,000 lbs)<br>1850 kN (417,000 lbs) |
| Sea Level Thrust<br>O:F=12:1 | 2460 kN (553,000 lbs) | |
| Vacuum Isp<br>O:F=12:1<br>O:F=6:1 | 362 sec | 379 sec<br>467 sec |
| Sea Level Isp<br>O:F=12:1 | 333 sec | |

the static pressure is increased to atmospheric levels, this reduces the velocity of the exhaust and hence the thrust. As the rocket gains altitude, and the atmospheric pressure drops, the shock losses decrease and the engine produces more thrust. When the static pressure at the exit plane of the nozzle is equal to the atmospheric pressure, the engine is said to have reached its design altitude. At the design altitude the nozzle is said to be ideally expanded; prior to this the nozzle is over-expanded. As the rocket attains even higher altitudes the nozzle becomes under-expanded. The thrust generated by both over- and under-expanded nozzles increases throughout the flight of the rocket, but it is never as great as the thrust generated by an ideally expanded nozzle at the same altitude. Nozzles with smaller area ratios have lower design altitudes. For this reason it is often desirable to have an extendable nozzle. This improves the

efficiency at both low and high altitude by having two different design altitudes, so that the engine is able to operate closer to the design conditions for longer periods in the flight.

The thrust of an engine is dependent on three factors: combustion chamber pressure, exit to throat area ratio and atmospheric pressure. The DMRE has been designed to vary both its chamber pressure and exit area. The thrust of an engine can be determined analytically, based on these factors. For optimum performance the extendable nozzle should lowered when the thrust produced in either position is equal. The DMRE produces identical thrust levels with both nozzles at between 9 and 12 km (30,000-40,000 ft), at the high chamber pressure corresponding to an O:F of 12:1.

At takeoff and during the early phases of the ascent, gravity and drag resist the force of the engine. During this phase of the mission it is important that the vehicle generate as much thrust as possible. When the flight path angle of the vehicle relative to the local horizontal becomes small, and the vehicle approaches orbital velocities, the effects of gravity are diminished. This usually occurs in the later phases of the flight, as the rocket reaches the outer reaches of the atmosphere. Under these flight conditions it is more important for the engine to make efficient use of the propellent that it carries. Specific impulse ($I_{sp}$) is frequently used to measure how efficient a rocket uses its propellant. $I_{sp}$ is defined as the thrust divided by the weight flow rate. The DMRE is capable of reducing its O:F from 12:1 to 6:1. This reduces the weight flow rate of the engine and increases the $I_{sp}$. Analytical modeling of the Antares vehicle shows that the O:F should be changed at an altitude of between 25 and 30 km (80,000-100,000 ft).

Once the propulsive characteristics are established it is possible to optimize the structural sizes and payload masses for the mission. The initial thrust to weight ratio (T/W) of the vehicle is an important consideration in sizing the propellant tanks. If the T/W is decreased, through the addition of payload or propellant, there is a corresponding decrease in the vehicle's acceleration during the early portion of the ascent. The net result is that the vehicle is retarded by the earth's gravity longer and it therefore requires more energy to complete its mission. If

18

the propellant mass is increased further, a point is reached beyond which it requires more energy to fly the added propellant than this propellant contains. This trend can be seen in Fig. 2.5 where LEO payload mass is plotted vs. propellant mass. This curve's maximum provides the design criterion for the tank sizes (see Section 4.1).

Once the dynamic and propulsive characteristics of the vehicle are known, a sample mission profile can be constructed. With the help of the OPGUID program it is possible to optimize this sample trajectory and generate data necessary for the structural and stability analyses. The results of the sample trajectory become the baseline performance for the Antares system, as all other missions will be performed with one or more vehicles of the same design. Statistics concerning the operation of the Antares are presented in Table 2.2. The following is a sample mission that was created using the OPGUID software..

T-0:00 (min:sec)

> An Antares vehicle fueled for takeoff has a gross liftoff mass of 197,600 kg (435,500 lbs). This is composed of 12,700 kg (28,000 lbs) of structural mass, 174,900 kg (383,300 lbs) of liquid oxygen and hydrogen, and a payload of 10,000 kg (22,000 lbs). At take-off the DMRE operates at an O:F ratio of 12:1 and an area ratio of 40:1. With its high mass flow rate and small area ratio it produces 2460 kN (553,000 lbs) of thrust at sea level. The $I_{sp}$ at this time is 333 sec. (If the DMRE were operating in vacuum in this same configuration it would produce 2670 kN (600,000 lbs) of thrust at an $I_{sp}$ of 362 sec). The thrust to weight ratio (T/W) at take-off is 1.27.

T+0:76

> As Antares reaches an altitude of 12 km (40,000 ft) the engine produces 2630 kN (592,000 lbs) of thrust and the $I_{sp}$ is 357 sec. At this point the nozzle extension is lowered and the thrust continues to increase, but at a higher rate.

19

**T+1:50**

When the Antares reaches an altitude of 27 km (88,000 ft) it is traveling at a velocity of 1,100 m/s (3,500 ft/s) at an angle of 32° above the local horizontal. Here, the O:F ratio changes to 6:1 and the thrust is reduced from 2780 kN (625,000 lbs) to 1840 kN (414,000 lbs). The efficiency of the engine becomes a bigger concern than the thrust generated. This is achieved through the increased $I_{sp}$, which changes from 377 sec to 463 sec. The reduced thrust generates an acceleration of 1.5 G's at this altitude, and is sufficient to carry the vehicle out of the gravity well.

**T+3:45**

At an altitude of 97 km (317,000 ft) atmospheric heating effects become minor and the payload fairing is jettisoned. The jettisoning of the payload fairing is delayed until the heat transfer due to friction is less than that produced by solar radiation. The velocity at this point in the flight is 3,000 m/s (9,840 ft/s). The drop mass of the payload fairing is 1,400 kg (3,100 lbs).

**T+4:33**

As the total mass of the Antares decreases, the acceleration experienced by the vehicle increases proportionally. A design criterion of 4.0 G's maximum acceleration was chosen and as such, the vehicle must begin to throttle back at this point. A continuous throttling of the engine will occur from this time until burnout when the thrust will reach 47% of its maximum value.

**T+6:00**

Burnout is achieved six minutes after lift off with the completion of orbital insertion into a 150 x 300 km elliptical orbit of 28.5° inclination. This orbit was chosen for the sample profile analysis as it provides a wide range of final orbital altitudes for the payload. The burnout mass of the Antares vehicle consists of 11,300 kg (24,900 lbs) of structure and 10,000 kg (22,000 lbs) payload. The total Δv required for this mission profile is 9.29 km/s.

Table 2.2: Optimized Baseline Performance.

| | |
|---|---|
| Liftoff Mass | 197,600 kg (435,500 lb) |
| Propellant Mass | 174,900 kg (383,300 lb) |
| Initial Thrust to Weight Ratio (T/W) | 1.27 : 1 |
| Time to Burnout | 361 sec |
| Payload mass to LEO | 10,000 kg (22,000 lb) |
| Burnout Acceleration | 4.0 G's |
| Total $\Delta v$ | 9.29 km/s |

## 2.2.2 GEO PERFORMANCE OPTIMIZATION

Many launch vehicles are of the staged variety. They are optimized utilizing stages of varying thrust and burn time. The jettisoning of stages eliminates the need for carrying the mass of empty propellant tanks to orbit. The Antares system is a single-stage-to-orbit design based on the belief that the efficiency lost by taking the entire structure to orbit will be more than compensated by the simplicity of design and operation. When designing a mission profile for the GEO mission, a transfer vehicle is required to carry the payload from LEO to GEO. As the mass of this transfer vehicle plus that of a marketable payload exceed the payload mass that the Antares I can place in LEO, the Antares must adapt to become a staged vehicle. This is accomplished by using Antares as the first stage of a two stage vehicle. The transfer vehicle will serve a dual mission as both a second stage and a LEO-GEO transfer vehicle. The Antares will not be placed into LEO in this mission scenario but will perform a suborbital flight that will cause it to fall into the ocean for recovery.

21

The mission to GEO presents a more difficult optimization problem, as the vehicle is now composed of two stages. If the mission is seen to be composed of two vehicles, one, the Antares, powered by a DMRE and a second, the Centaur, powered by two RL10-4A engines, a maximum mass taken to LEO can be found. When optimizing a staged rocket it is important to drop the mass of the propellant tanks as soon as the propellant is consumed. The most physically efficient rocket possible would consist of infinite stages that would be jettisoned as soon as the fuel was consumed. Constraining the problem to that of a two stage vehicle, it is desirable to jettison the mass of the Antares tanks as quickly as possible. This reduces the weight of the vehicle and allows the lighter Centaur to lift the payload. This suggests that the Antares should have a relatively short burn time.

There are two physical constraints that limit the payload mass to GEO. The first is the initial thrust to weight ratio, and its effect on payloads delivered to LEO, as discussed in Section 2.2.1. The second is that as the burn time of the second stage increases, the amount of propellant left to perform the LEO-GEO transfer is decreased. In designing our GEO mission profile to suit an available second stage / transfer vehicle, the Centaur, the volume of available propellant is predefined. Thus, for an optimum mission profile using these two vehicles, the Antares must have a fairly long burn time compared to an optimally designed staged vehicle using the same engine characteristics. This is done to utilize the large propellant tanks of the Antares and to conserve fuel in the Centaur.

In analyzing the GEO mission with the Centaur upper stage it is assumed to be equipped with two RL10-4A engines which are currently being developed by Pratt & Whitney, and insulation sufficient to prevent fuel evaporation during the Geosynchronous Transfer Orbit (GTO) coast. Table 2.3 presents the specifications of the Centaur that were used in the GEO mission analysis.

Table 2.3: Centaur Vehicle Specifications.

| Structural Mass | 1404 kg (3100 lbs) |
|---|---|
| Fuel Capacity | 17,000 kg (37,500 lbs) |
| Vacuum Thrust | 180.2 kN (40,500 lb) |
| Vacuum Isp | 449 sec |

Optimization of the GEO mission involves balancing the Antares propellant mass and the Centaur stage burn time. The initial T/W of the vehicle must be considered, along with the propellant available for the GEO transfer. Examination of the curves in Fig. 2.6 shows how the trade between these two consideration affects the GEO payload mass. It can be seen that as the second stage burn time is increased, the payload mass becomes limited by the amount of propellant remaining in the Centaur's tanks.

The mission profile driven by these considerations is very similar to the LEO mission during the first portion of the flight. The characteristics of the DMRE do not change and hence the nozzle area and mixture ratio changes occur at the same altitudes as they do in the LEO mission. A sample mission profile is presented here that details those points that differ from the LEO mission. Table 2.4 follows the mission profile and lists specific information obtained from the sample mission optimization.

T+4:21

The Antares and Centaur reach an altitude of 97 km (317,000 ft) and the payload fairing is jettisoned. Since the GEO payload is smaller than a LEO mission payload the fairing has a reduced size. This results in a drop mass of 1,200 kg (2,600 lbs).

T+4:30

Acceleration of the vehicle has reached the 4 G limit and the DMRE begins to throttle back. The DMRE will throttle back continuously to 73% of maximum before burnout.

23

**T+5:06**

At an altitude of 115 km (380,000 ft) the Antares booster achieves burnout. A $\Delta v$ of 7.25 km/s has been given to the Centaur and the payload. At this point the Centaur's engines ignite, producing 180 kN (40,500 lbs) at an $I_{sp}$ of 449 sec. The Antares performs a suborbital trajectory that will end in the Atlantic Ocean 2,060 km (1,250 mi) off the coast of Florida. The ERU separates from the tanks and splashes down to be recovered by ship for reuse. The tanks break up on re-entry and are discarded.

**T+8:21**

The Centaur inserts itself and the 4000 kg (8,800 lb) payload into a parking orbit that is 150 x 300 km at 28.5° inclination. The specifics of the Centaur's transfer maneuvers will be covered in the following section.

Table 2.4: Optimized GEO Mission Performance

| | |
|---|---|
| Booster Propellant Mass | 162,100 kg  (357,500 lb) |
| Booster Burn Time | 306 sec |
| Second Stage Burn Time | 195 sec |
| Propellant for GTO and GEO insertion | 9000 kg  (19,800 lb) |
| Antares $\Delta v$ | 7.25 km/s |
| Centaur $\Delta v$ | 1.92 km/s |
| Total $\Delta v$ | 9.17 km/s |
| GEO Payload Mass | 4000 kg  (8800 lbs) |

To maintain an optimum thrust to weight ratio at take-off, the Antares propellant tanks are only partially full. As the mass of the Centaur and a 4,000 kg payload are greater than the LEO payload, this is done to reduce the take-off mass to achieve a T/W of 1.27. The reduced propellant in the Antares reduces the first stage $\Delta v$ generated, but this is not critical as it does not reach orbit. The Centaur's propellent provides the remaining $\Delta v$ needed to place the payload and itself into the LEO parking orbit prior to the transfer to GEO.

## 2.3    GEO MISSION ANALYSIS
(John Gailey)

GEO missions are completed in two stages. The first stage consists of a single Antares vehicle that lifts the second stage Centaur and its payload part-way to a 150/300 km parking orbit. After the vehicle separates, the Centaur continues its insertion into the parking orbit, acting as a second stage. From LEO, it can then initiate the transfer to the higher GEO orbit. The following orbital analysis encompasses this upper stage transfer from LEO to GEO.

### 2.3.1   UPPER STAGE ORBIT OPTIMIZATION

Acting as a second stage, the Centaur separates from the Antares during the launch phase and inserts itself and the payload into a 150/300 km elliptical orbit, as noted earlier. The Centaur then waits for the optimal insertion time and proceeds to change orbits, starting from the perigee at 150 km. The geosynchronous transfer orbit (GTO) is a combined plane change and Hohmann transfer maneuver. The GTO efficiently transfers the payload from the original orbit with an inclination of 28.5° to an equatorial geosynchronous orbit at 35,786 km. A diagram of the mission profile is shown in Fig. 2.7.

Using the equation for the velocity of an object in an elliptical orbit [3],

$$v = \sqrt{2\mu\left[\frac{1}{a_1} - \frac{1}{(a_1 + a_2)}\right]}$$  (2.1)

$a_1$ = perigee radius
$a_2$ = apogee radius
$v$ = velocity
$\mu$ = gravitational parameter of Earth = 398,601 km$^3$/s$^2$

the following velocities are calculated, with $a_1 = a_2$ for the GEO orbit:

$v_G$ = Velocity at GEO = 3.075 km/s

$v_{Ta}$ = Velocity at apogee of transfer orbit (GTO) = 1.59 km/s

$v_{Tp}$ = Velocity at perigee of transfer orbit (GTO) = 10.28 km/s

$v_{Lp}$ = Velocity at perigee of LEO orbit = 7.86 km/s

Figure 2.8 is a vector diagram of the original orbital velocity vector, $\vec{v}_1$, and the final velocity, $\vec{v}_2$. As seen in Fig. 2.8, the shortest vector and therefore most efficient method of changing planes and orbit is a combined maneuver, shown as $\Delta \vec{v}$. This is more efficient than $\Delta v_1$, which represents an increase in velocity from $\vec{v}_1$ to $\vec{v}_2$ first, and then the plane change, and $\Delta v_2$, which represents a plane change first, and then the increase in velocity to $v_2$.

The $\Delta v$ for the combined plane and velocity change is obtained from the law of cosines. Thus, the transfer to GTO burn ($\Delta v_{GTO}$) is:

$$\Delta v_{GTO} = \sqrt{v_{Lp}^2 + v_{Tp}^2 - 2v_{Lp}v_{Tp}\cos(\Delta\theta)}$$  (2.2)

where $\Delta\theta$ is the amount of plane change performed at perigee.
The second, GEO circularization burn ($\Delta v_{GEO}$) is:

$$\Delta v_{GEO} = \sqrt{v_G^2 + v_{Ta}^2 - 2v_G v_{Ta}\cos(28.5^\circ - \Delta\theta)}$$  (2.3)

The most efficient plane change is that composed of a small plane change at LEO and the rest of the plane change at GEO. Figure 2.9 shows the total LEO to GEO transfer $\Delta v$'s for

different incremental plane changes at LEO. The plane change in LEO for the lowest $\Delta v$ shown on the graph is $\Delta\theta = 2.11°$.

Therefore:

$\Delta v$ from LEO to GTO is $\Delta v_{GTO} = 2.447$ km/s

$\Delta v$ from GTO to GEO is $\Delta v_{GEO} = 1.794$ km/s

This yields the best total LEO to GEO **$\Delta v = 4.241$ km/s.**

To illustrate that this result is the most efficient the following two alternatives were studied:

i) Optimal transfer starting from the 300 km position: $\Delta v = 4.275$ km/s

ii) Transfer without a LEO plane change at 150 km: $\Delta v = 4.265$ km/s

The chosen $\Delta v$ of 4.241 km/s is therefore a saving of 34 m/s and 24 m/s, respectively, over these alternate transfers.


## 2.3.2 SEPARATION OF SATELLITE FROM CENTAUR

Once the satellite is in GEO, it must be able to freely rotate or execute whatever maneuvers its mission requires. Therefore, the Centaur upper stage must be separated and moved some distance away to prevent it from interfering with the satellite's operation and to prevent any possibility of collision over time. With the amount of fuel remaining, the Centaur has the option of either increasing or decreasing altitude to another orbit. An altitude change of 1,000 km to another circular orbit is initially specified for a safe separation distance. Using a Hohmann transfer orbit, this maneuver requires a total $\Delta v = 37.1$ m/s for the lower orbit, and a total $\Delta v = 35.8$ m/s for the higher orbit. Although a higher orbit results in a slightly lower $\Delta v$, the difference is small and a lower orbit might be more attractive if the means are developed in the future to retrieve the Centaur upper stage and reuse it.

## 2.4 STABILITY AND CONTROL
(John Gailey)

The stability of the Antares is dependent upon the forces acting on the rocket, the center of pressure, the center of mass, and the amount the rocket nozzle is gimbaled. There are three forces acting on the vehicle. The thrust acts on the base, gravity acts on the center of mass, and aerodynamic lift acts on the center of pressure. These forces are illustrated in Fig. 2.10.

The center of pressure (c.p.) is the point along the length of the vehicle where the moments created by the aerodynamic forces above that point and the moments below that point are equal. Therefore all of the lift generated can be simplified for moment calculations by applying it at that point. Likewise, the center of mass (c.m.) is the point at which the moments caused by the weight of the vehicle above and below the c.m. are equal. For calculational purposes, all of the weight of the vehicle can be considered to be applied at the c.m..

The Antares vehicle is subjected to aerodynamic and gravity forces over much of its trajectory, but for the purposes of stability and control, it is sufficient to examine the worst case scenario. This occurs during the LEO mission at what is called the maximum dynamic pressure, or max. Q, the point along the flight trajectory at which aerodynamic forces are at a maximum due to a combination of density and velocity. The LEO configuration is used as the worst case as the payload mass above the tanks is less than the Centaur and payload in the GEO mission. This means that the c.m. on the LEO mission is farther below the c.p. than on the GEO mission and, therefore, the LEO configuration is more aerodynamically unstable. As a further complication, a 54 m/s (120 mph) wind gust is assumed. If the control system can keep the Antares stable at max. Q with a wind gust of this velocity, then it is capable of handling the rest of the flight as well.

### 2.4.1 AERODYNAMIC FORCES

The LEO Antares vehicle is 5 m in diameter, has a parabolic nose cone roughly 6 m in length, and is 40 m long, including the nose. During supersonic flight, an essentially constant

28

normal force coefficient ($C_N$) of 0.0559 per degree is encountered [4,5]. The center of pressure is one-half the body diameter below the joint between the nose and the body, i.e. the distance from the nose tip to the center of pressure, $X_{cp}$, is 8.5 m (see Fig. 2.10) [4].

From OPGUID, the conditions at max. Q are:

$\rho$ = atmospheric density = 0.434 kg/m$^3$

v = Antares booster velocity = 330 m/s

$v_g$ = wind gust velocity = 54 m/s.

Therefore the apparent angle of attack is

$$\alpha = \tan^{-1}\left(\frac{v_g}{v}\right) = 9.25° \tag{2.4}$$

and the total velocity is

$$v_{total} = \sqrt{v^2 + v_g^2} = 334 \ m/s \tag{2.5}$$

The actual normal force on the vehicle is then calculated from:

$$F_N = \left(\frac{1}{2}\rho v_{total}^2\right)\left(\frac{\pi}{4}d^2\right)C_N\alpha \tag{2.6}$$

where d = 5 m. Therefore the maximum normal force on the vehicle is $F_N$ = 245,000 N.

## 2.4.2 CENTER OF MASS

The center of mass of the Antares at max Q is found by first calculating the c.m. of the tank, given the tank's components and the amount of liquid hydrogen and oxygen remaining at max. Q, and then calculating the overall c.m. using the masses and centers of mass from the other components of Antares.

The tank components with the center of mass distances relative to the top of the tank are shown in Table 2.5:

Table 2.5: Tank Components and Centers of Mass

| Tank component | Mass | Center of Mass Relative to Top of Tank |
|---|---|---|
| LH$_2$ cylinder wall | 1900 kg | 13.76 m |
| LO$_2$ cylinder wall | 440 kg | 4.41 m |
| Top hemisphere | 220 kg | 1.56 m |
| Bottom hemisphere | 440 kg | 22.14 m |
| Common wall | 550 kg | 7.25 m |
| Insulation | 100 kg | 11.85 m |
| Propellant lines | 200 kg | 16.26 m |
| Remaining LH$_2$ | 15,330 kg | 17.09 m |
| Remaining LO$_2$ | 105,890 kg | 5.65 m |
| Whole tank | 125,070 kg | 7.25 m |

From this information and a fairing and payload connector length above the tank of 12 m, the center of mass of the tank is located 19.25 m from the nose cone tip of the Antares vehicle.

To find the overall center of mass based on the individual components of Antares, the masses and center of mass distances relative to the tip of the nose cone are shown in Table 2.6: The result, is a center of mass for the entire LEO Antares located at $X_{cm}$ = 19.13 m from the tip of the nose cone (see Fig. 2.10).

## 2.4.3 ENGINE GIMBALING

To stabilize the booster, the method Antares uses is the moment created by gimbaling the engine. Therefore, it is important to know that the amount the engine will be required to gimbal in a worst case scenario is less than the maximum designed engine gimbal angle of

Table 2.6: Antares Components and Centers of Mass

| Component | Mass | C.M. |
|---|---|---|
| ERU | 5800 kg | 38.2 m |
| ERU/Tank connector | 950 kg | 35.4 m |
| Tank (at Max Q) | 125,070 kg | 19.25 m |
| Payload | 10,000 kg | 7.40 m |
| Fairing | 1400 kg | 5.50 m |
| Payload connector | 700 kg | 11.5 m |
| Antares | 143,920 kg | 19.13 m |

$\phi = 10^{\circ}$ from the centerline. There are actually two cases where an engine would have to be gimbaled to maintain stability: a side gust as explained above, and an engine out situation in a multiple unit modular configuration (Antares II-VII).

For the side gust problem, the moment about the c.m. created by gimbaling the engine must equal the moment about the c.m. created by the aerodynamic side force $F_N$. The moment created by the wind gust is:

$$M = F_N \left( X_{cp} - X_{cm} \right) = 2,600,000 \ \text{N} \cdot \text{m} \tag{2.7}$$

To counter this moment with a total thrust of 2,611,000 N (value at max. Q point) will require:

$$\phi = \sin^{-1} \left( \frac{M}{T \cdot X_{cm}} \right) = 2.74^{\circ} \tag{2.8}$$

This is well within the allowable limit of 10°.

For the engine out case in the multiple unit modular configurations, the remaining engines must be gimbaled to make up for the unequal distribution of thrust. The remaining

engines have to be angled such that the resulting thrust vector is redirected through the center of mass.

Among the possible multiple unit modular configurations, the worst case occurs when an engine goes out in the Antares II, which consists of two modules. This is due to the fact that in the 3 to 7 modular configurations, more engines and thus more thrust is available to correct for the lost thrust from the one engine. Therefore, in the worst case scenario, a gimbal angle of $\phi = 7.46°$ is required to redirect the thrust of the remaining engine through the center of mass. This angle will decrease once the vehicle has had time to drop the malfunctioning ERU, as the c.m. will then move closer to the centerline of the module which has the working engine.

### 2.4.4 THRUST VECTOR CONTROL

In most large rockets without wings or fins, the center of pressure is above the center of mass, making the booster aerodynamically unstable [6]. This means that without proper control from the engine, the rocket will start to tumble as soon as it deviates from the flight path. Therefore, a control loop such as the one shown in Fig. 2.11 must be used to gimbal the rocket engine and right the vehicle.

The control loop will use the inertial navigation system gyros to provide feedback to the computer, which will enter the rocket angle required by the mission into the control system, shown by $\alpha_{COM}$. This angle is compared with the true angle, $\alpha$, shown by the gyros and an error is calculated, $\alpha_{ERR}$. The amplifier then takes this error and sends a command to the engine actuators to gimbal the engine a certain amount, $\phi_{COM}$. This vectoring of the thrust moves the rocket to a new angle, which is noted by the gyros and put back into the control system as feedback.

## 2.5  DEORBIT
(Kim Fricke)

After the Antares performs its launch portion of the mission, it is necessary to return the vehicle. For GEO launches, the vehicle follows a suborbital trajectory and will automatically splashdown in the Atlantic Ocean, 2,060 km (1,250 mi) downrange of the Kennedy Space Center launch site. This point is near 60° west longitude. For LEO missions, however, the Antares vehicle itself enters a parking orbit and must be given a short impulse to deorbit. This section of the report gives the details of the reentry trajectory and splashdown area.

### 2.5.1  BURN POINT DETERMINATION

The 150/300 km parking orbit achieved by the Antares vehicle during LEO missions has an orbital velocity of 7,726 m/s at perigee and 7,682 m/s at apogee. The eccentricity of this orbit is about 0.0113. In other words, the orbit can be closely approximated as circular. The orbital velocity variation between apogee and perigee is only 44 m/s.

The burn point for re-entry was determined using the FORTRAN program described in Appendix A.3. A 50 m/s deorbit burn results in a re-entry trajectory that carries the Engine Return Unit (ERU) for approximately 13,000 km (8,080 mi) before splashdown. Therefore, by firing the deorbit engines that distance uprange from the splashdown area, the Antares will drop down into the Atlantic at the desired location for recovery and reuse.

### 2.5.2  SPLASHDOWN AREA

The target zone is the Atlantic Ocean east of Florida and as close the the United States as possible, to try and reduce recovery and transportation costs. With the planned deorbit impulse of 50 m/s, the deorbit burn would have to occur 13,000 km (8,080 mi) uprange of the desired target. The most efficient point for the deorbit burn is at the apogee of the parking orbit. However, this creates the problem of splashing the ERU down at too low a latitude. The Kennedy Space Center launch site is at 28.5° north latitude. If the deorbit burn is done at

apogee, splashdown occurs at an undesirable location somewhere just above the equator. Therefore, it is necessary to do the burn when the ERU is somewhere between apogee and perigee, such that the re-entry trajectory drops it near 28.5° north latitude.

The ground track of the 28.5° inclined orbit shows that the point at which the ERU crosses the equator drifts 22.7° westward every orbit. This means that the optimum time for the re-entry burn is during the fifteenth or sixteenth orbits, which occur at 22.5 hours and 24 hours into the mission. These orbits are the first re-entry opportunities for the Antares vehicle.

## 2.6 CONCLUSIONS
(Michael Filbin / Andrew Dawdy)

Optimization of the launch and orbital flight characteristics is an important aspect in the design of the Antares to minimize the energy required to accomplish the mission. Energy savings translates directly into a savings of propellant and an increased payload lift capability. A parking orbit of 150/300 km was chosen, as the apogee is high enough to provide a wide range of final orbits for a LEO payload, and the perigee is beyond the significant drag effects of the earth's atmosphere, allowing sufficient time on-orbit for the ERU to be brought back accurately. This orbit also works well for GEO missions, because the Centaur can reach its destination without excessive propellant consumption.

Selection of the Antares main engine and sizing of the vehicle's propellant tanks were based on the analysis of the OPGUID program. The optimized launch characteristics and vehicle masses include $\Delta v_{launch}$=9.29 km/s, and initial propellant and Gross Lift Off Masses of 173,900 kg and 197,600 kg, respectively. This results in a payload capability to LEO of 10,000 kg.

Equatorial GEO missions have been planned by optimizing the orbital trajectory for the Centaur upper stage burn from LEO to GEO. This requires, in addition to a Hohmann transfer, a plane change of $\Delta\theta$=2.11° at the perigee of GTO and a 26.4° plane change at the

apogee. This results in an optimal $\Delta v = 4.241$ km/s for the LEO to GEO transfer, and a payload capability of 4,000 kg to GEO.

## 2.7 NOMENCLATURE

| | |
|---|---|
| ERU | Engine return unit |
| LEO | Low earth orbit |
| GEO | Geosynchronous earth orbit |
| GTO | Geosynchronous transfer orbit |
| $\mu$ | Gravitational parameter of earth |
| $a_1$ | Perigee of elliptical orbit |
| $a_2$ | Apogee of elliptical orbit |
| $v$ | Velocity |
| $v_G$ | Circular velocity at GEO |
| $v_{Lp}$ | Velocity at perigee of LEO orbit |
| $v_{Ta}$ | Velocity at apogee of transfer orbit (GTO) |
| $v_{Tp}$ | Velocity at perigee of transfer orbit (GTO) |
| $\Delta v_{GTO}$ | Velocity increment from LEO to GTO |
| $\Delta v_{GEO}$ | Velocity increment for GEO circularization |
| $I_{sp}$ | Specific impulse |
| $m$ | Vehicle mass |
| $T$ | Thrust |
| $C_D$ | Coefficient of drag |
| $A$ | Frontal area |
| $\rho$ | Atmospheric density |
| $R$ | Radius of the Earth |
| O:F | Oxidizer to Fuel ratio |
| T/W | Thrust to Weight ratio |
| c.p. | Center of pressure |
| c.m. | Center of mass |

| | |
|---|---|
| $X_{cm}$ | Position of center of mass relative to nose tip |
| $X_{cp}$ | Position of center of pressure relative to nose tip |
| $F_N$ | Normal force on booster |
| $W$ | Weight of booster |
| $\alpha$ | Vehicle angle of attack |
| $\alpha_{COM}$ | Vehicle angle of attack commanded by the flight computer |
| $\alpha_{ERR}$ | Error between the commanded and actual vehicle angles of attack |
| $\phi$ | Actual gimbaled engine angle |
| $\phi_{COM}$ | Gimbaled engine angle commanded by the flight computer |

## 2.8  REFERENCES

1.  OPGUID Program, NASA-Marshall Space Flight Center, courtesy of D. Mercier, August 1989.

2.  Limerick, C. D., "Dual Mixture Ratio H2/O2 Engine for Single Stage to Orbit Application," AIAA Journal of Propulsion and Power, Vol. 7, No. 1, pp. 65-67, 1991.

3.  Bate R., Mueller D., and White J., Fundamentals of Astrodynamics, Dover Publications Inc., New York, 1971, p.164.

4.  Ferguson S., Boeing Defense and Space Group, Seattle WA, private communication, May, 1991.

5.  Brebner G., "General Missile Aerodynamics," Missile Aerodynamics, Brebner B., Richards B., and Stahl W., Technical Editing and Reproduction Ltd., London, 1979, pp. 2-12.

6.  Koelle H., ed., Handbook of Astronautical Engineering, McGraw-Hill Book Company, Inc., New York, 1961, p.114.

Payload separates at
main engine cut-off
150 km
T + 6:00 min

Deorbit maneuver

Fairing jettisons
96 km
T + 3:45 min

ERU separates

Tank breaks up
during re-entry

ERU re-enters

Parafoil deploys

Flotation devices deploy

Fig. 2.1. LEO mission profile.

39

300 km Circular Orbit

Parking Orbit
150 - 300 km

Apogee burn
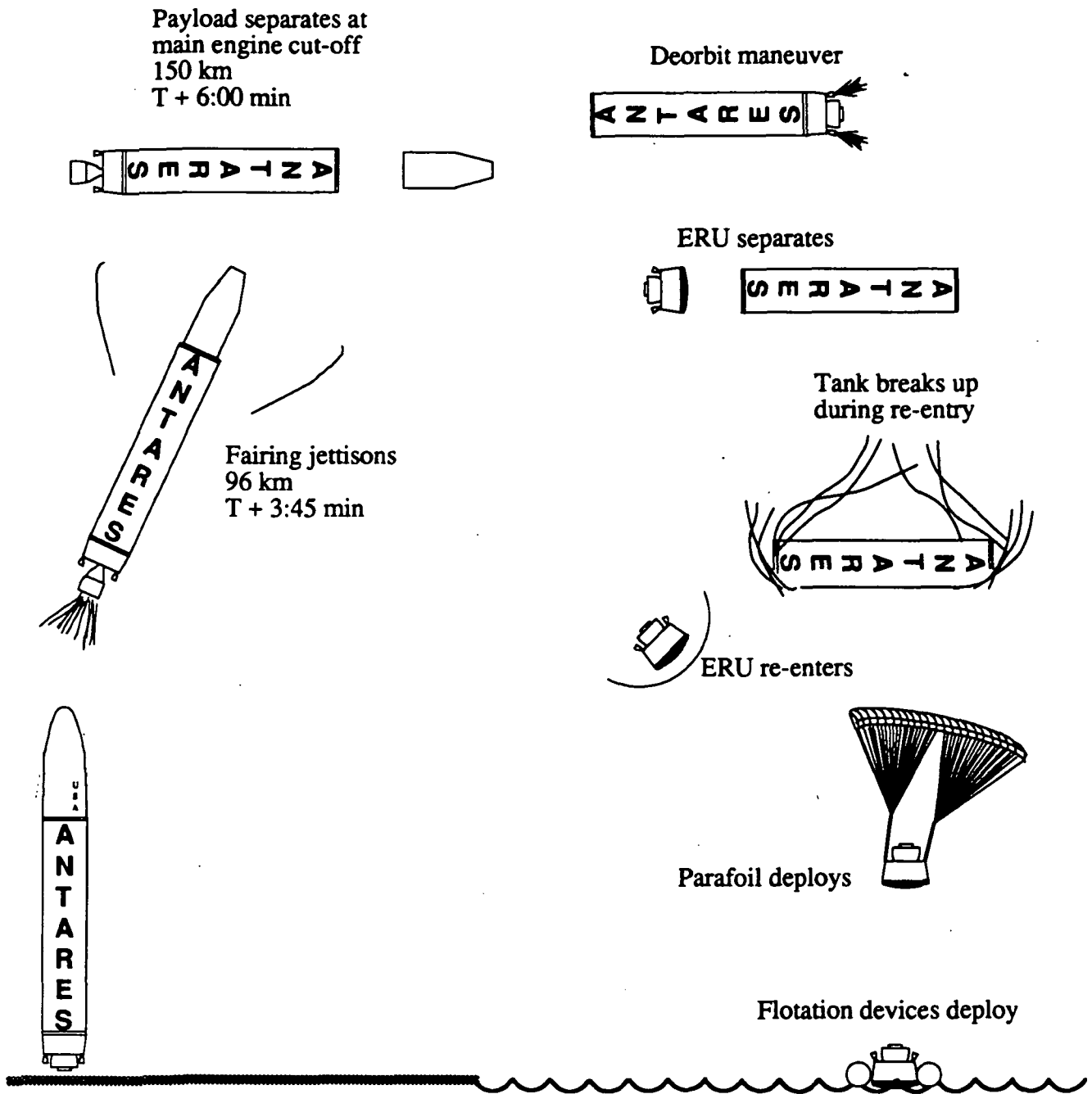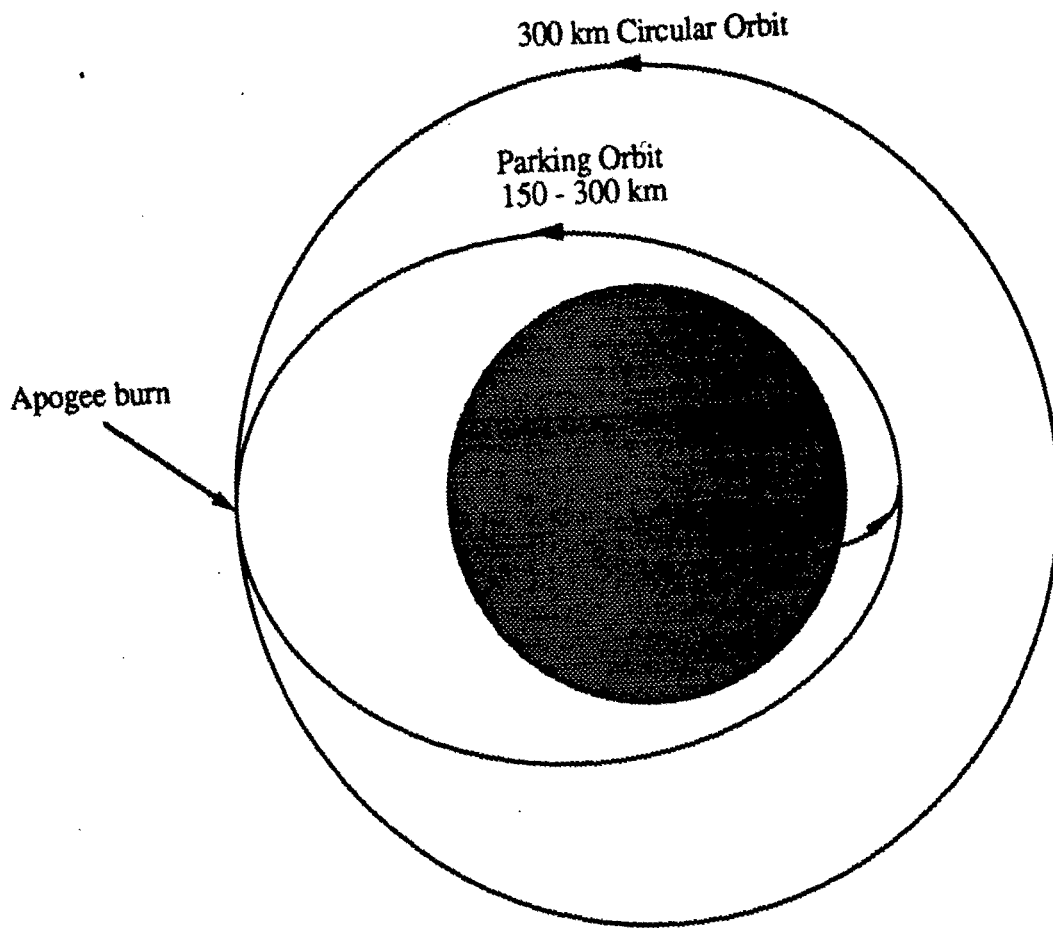
Fig 2.2. Orbital diagram for LEO orbit insertion.

Centaur separates at
main engine cut-off
115 km
T + 5:06 min

ERU separates

Tank breaks up
during re-entry

Fairing jettisons
100 km
T + 4:21 min

ERU re-enters

Parafoil deploys

Flotation devices deploy

ANTARES

ANTARES

Fig. 2.3. GEO mission profile.

Geo Transfer
Orbit

Parking Orbit
150 - 300 km

Geostationary Orbit at
35,786 km
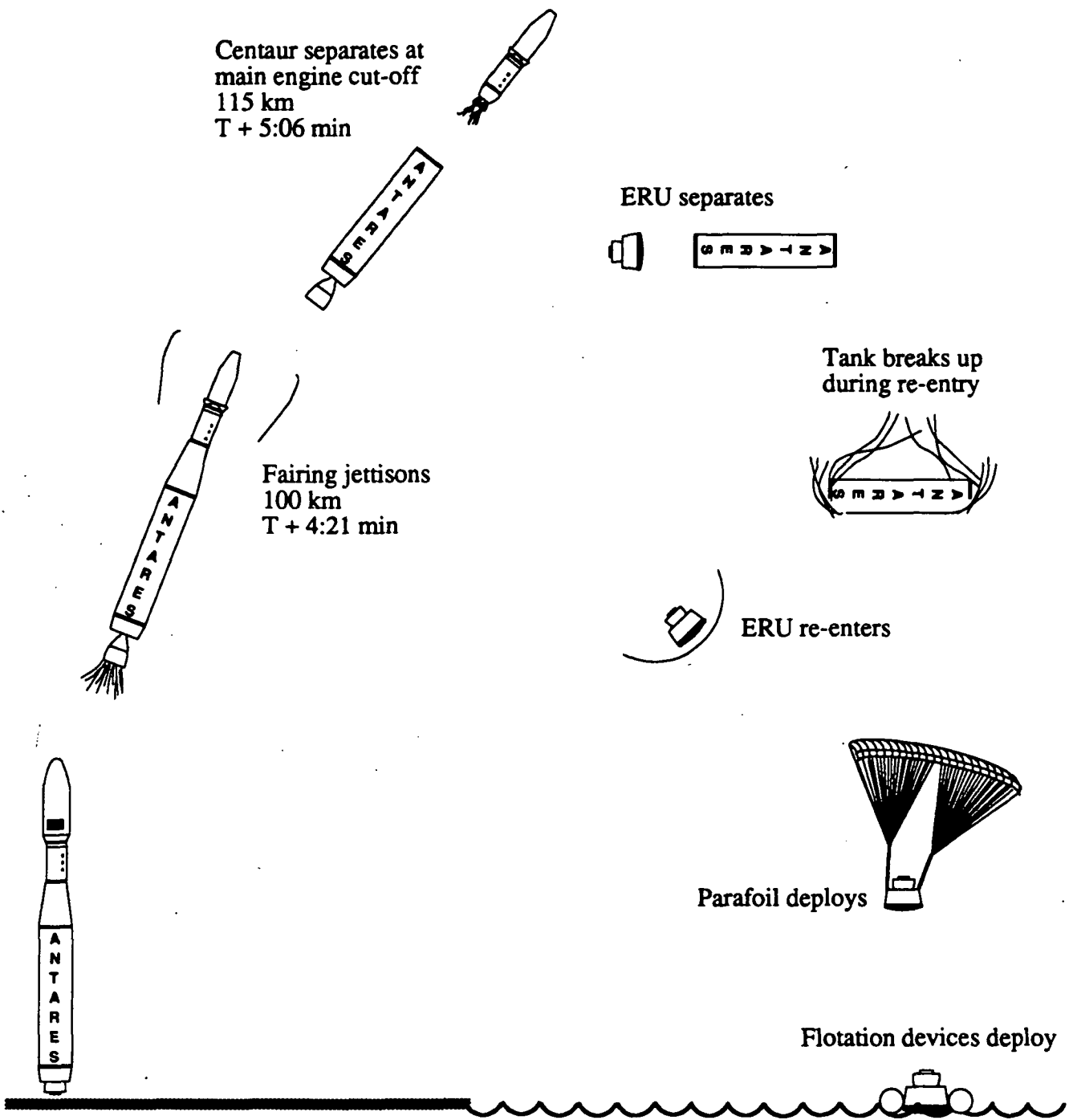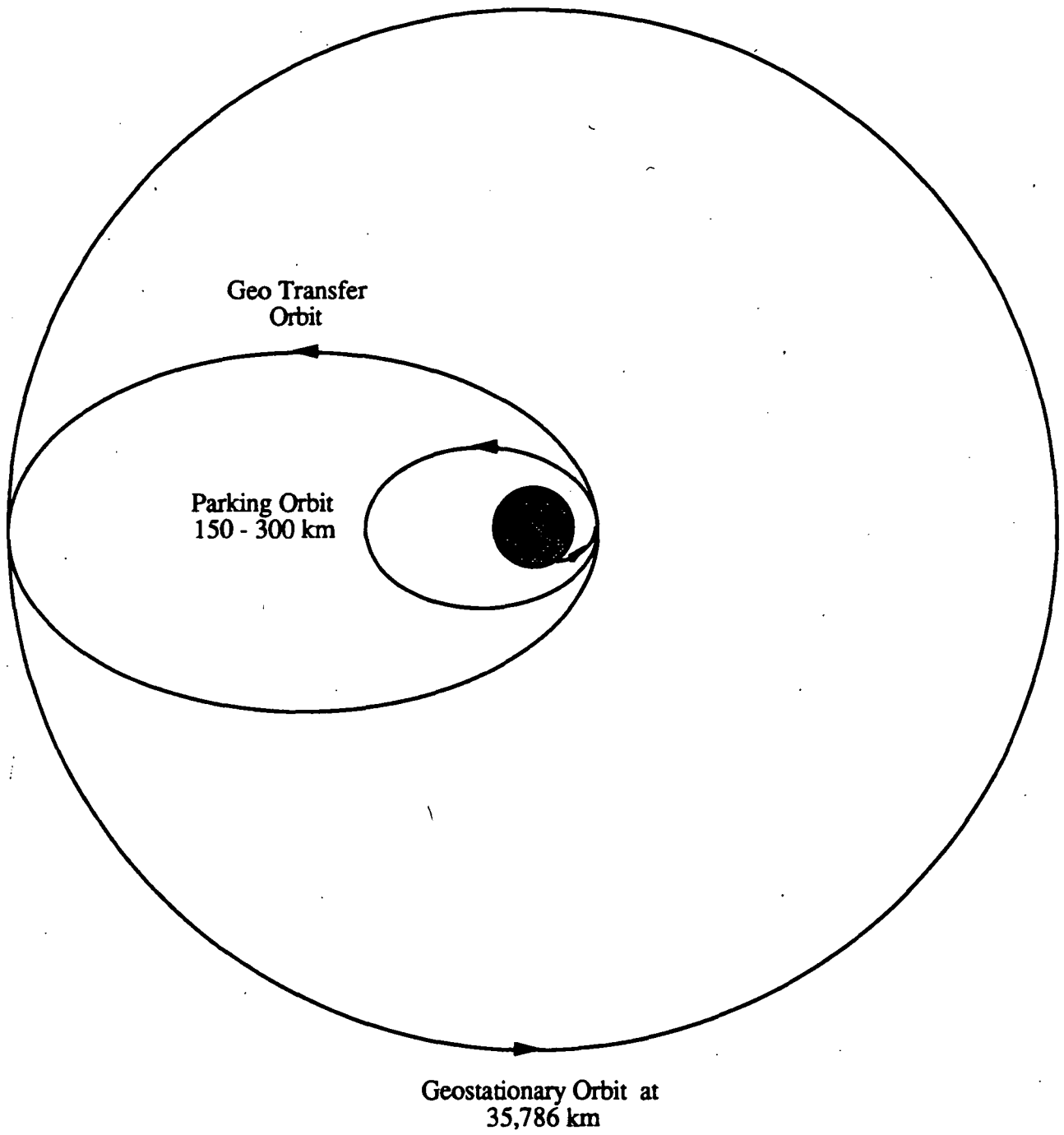
Fig. 2.4. Orbital diagram for LEO to GEO transfer (not to scale).
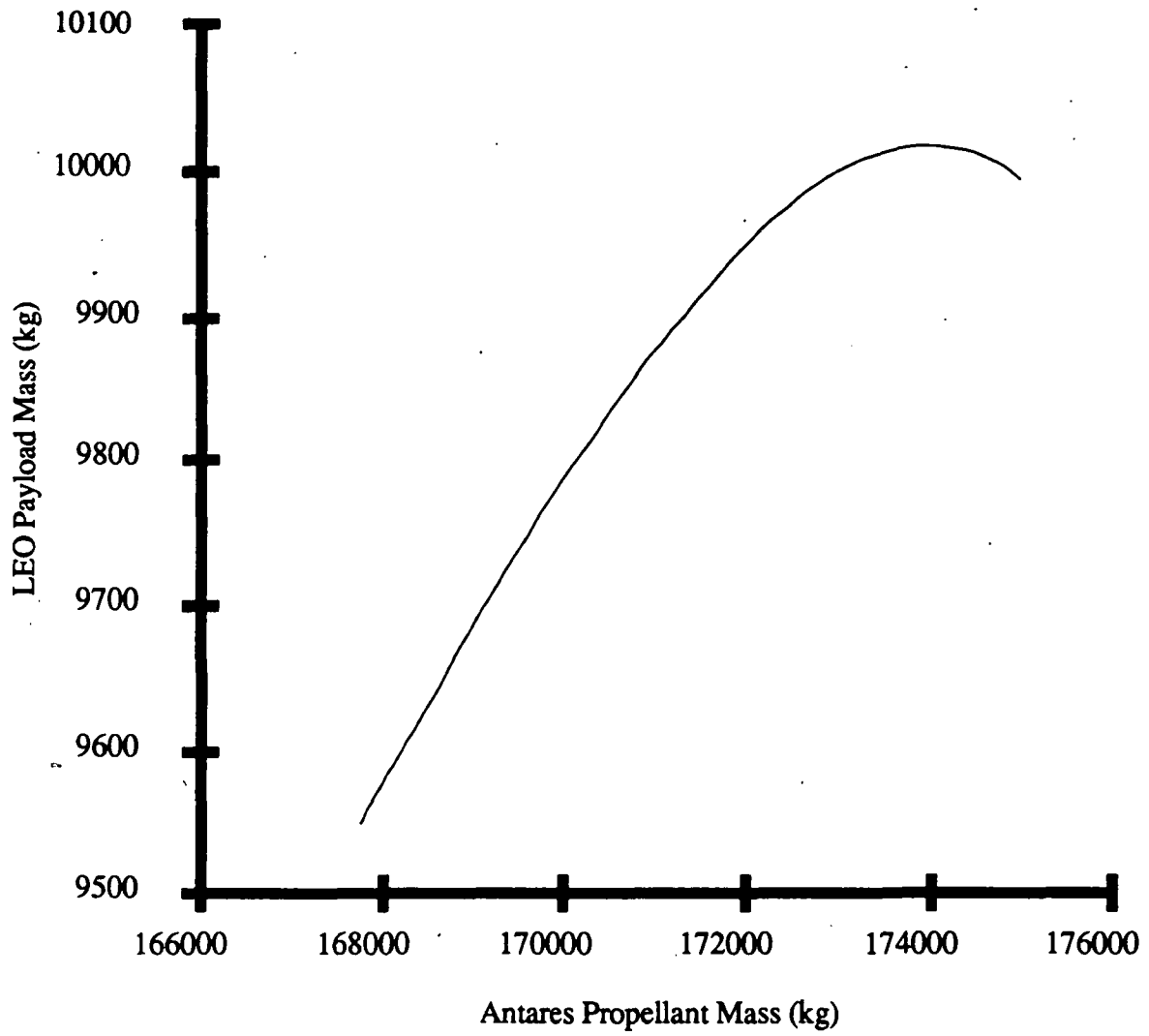
Fig. 2.5. Effect of propellant mass on LEO payload mass.
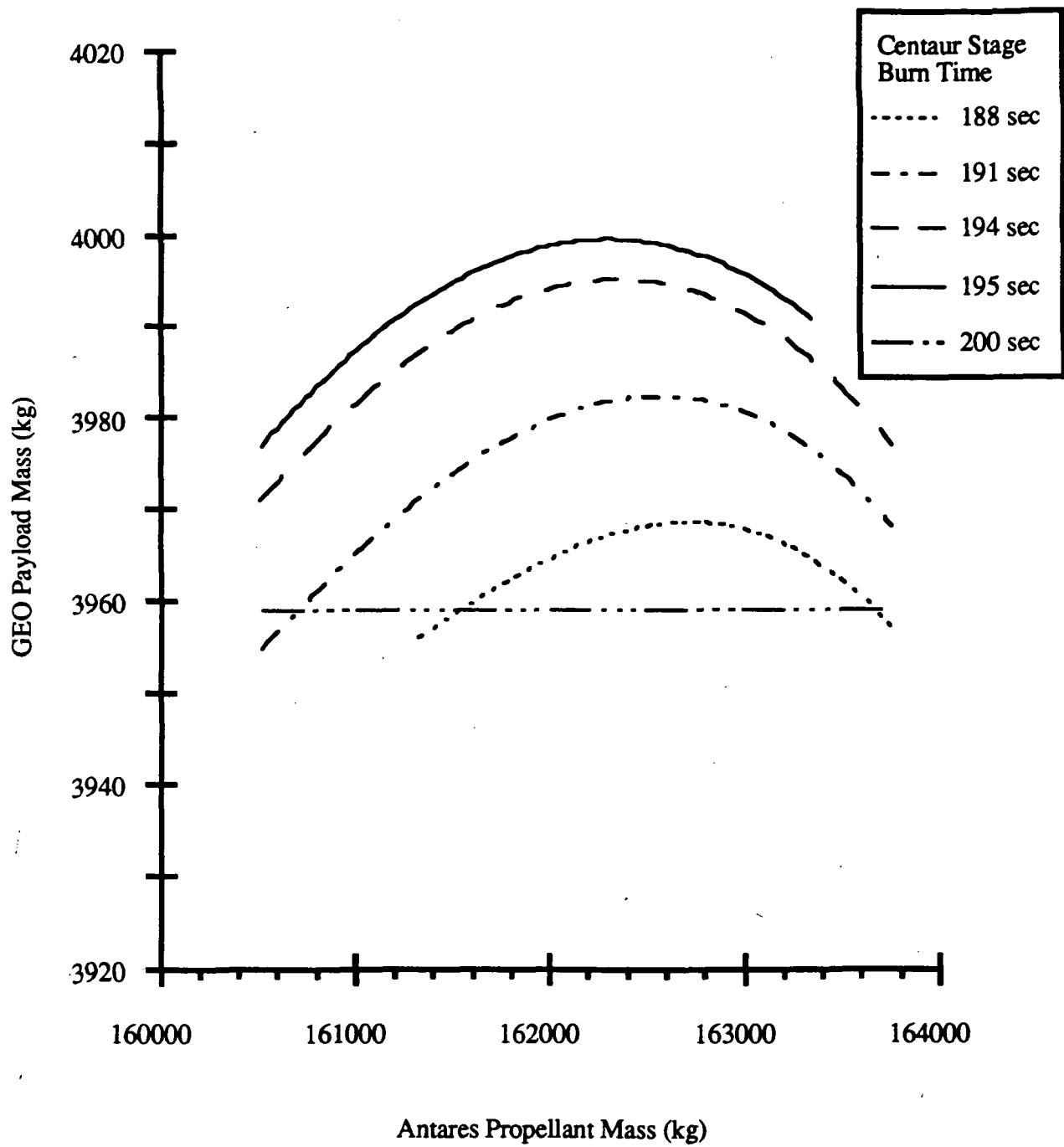
Fig. 2.6. Effect of Antares propellant mass and
Centaur burn time on GEO payload mass.
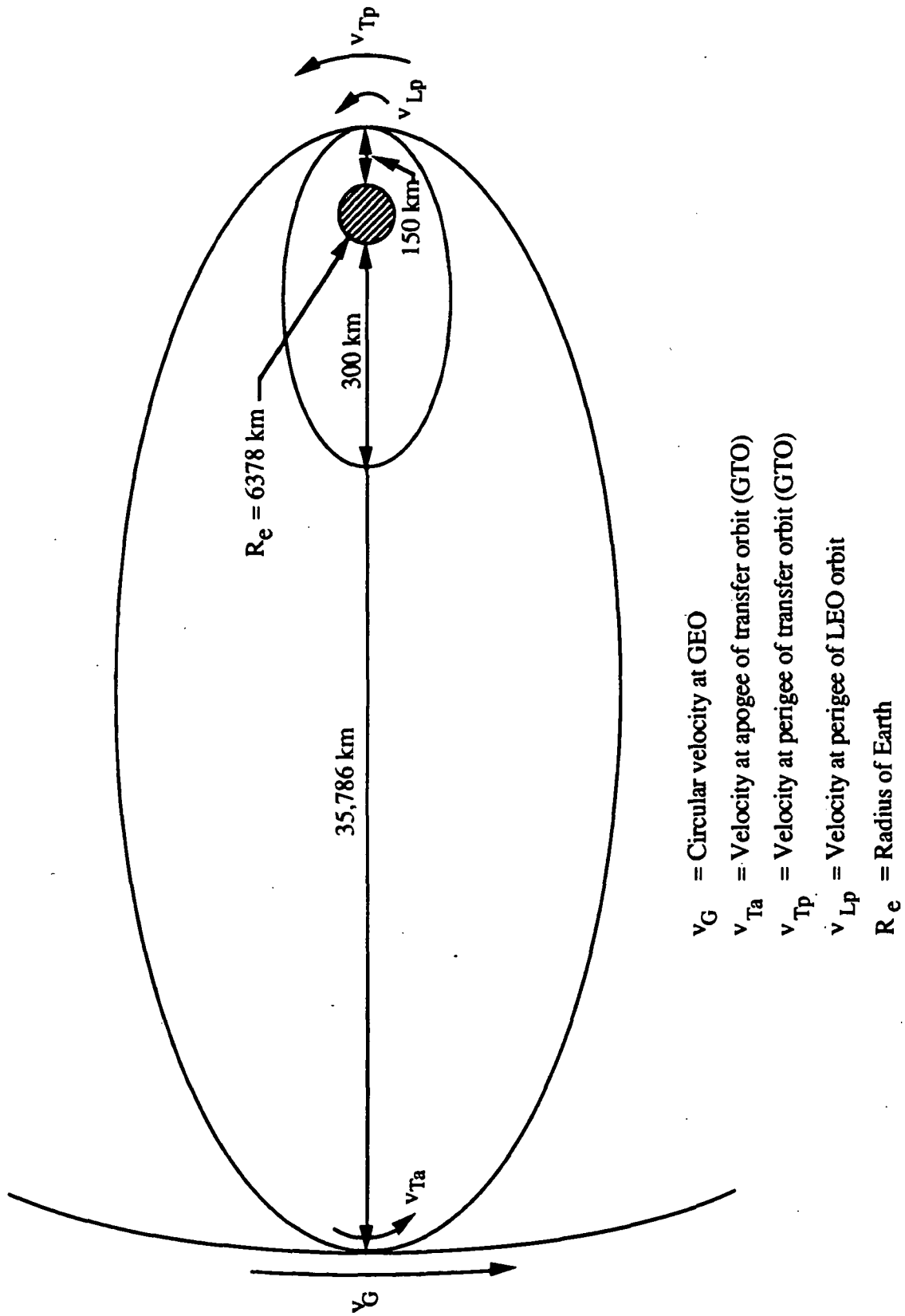
Fig. 2.7.  Mission profile diagram  (not to scale).

$v_G$   = Circular velocity at GEO

$v_{Ta}$  = Velocity at apogee of transfer orbit (GTO)

$v_{Tp}$  = Velocity at perigee of transfer orbit (GTO)

$v_{Lp}$  = Velocity at perigee of LEO orbit

$R_e$   = Radius of Earth

35,786 km

300 km

150 km

$R_e$ = 6378 km

$v_{Tp}$

$v_{Lp}$

$v_{Ta}$

$v_G$

45
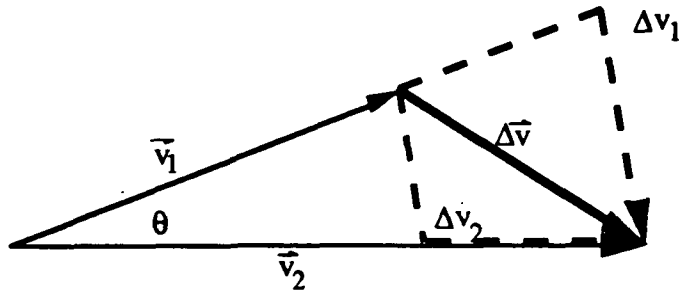
$\vec{v}_1$ = Initial velocity vector
$\vec{v}_2$ = Final velocity vector
$\theta$ = Plane change
$\Delta v_1$ = Increase in velocity followed by plane change
$\Delta v_2$ = Plane change followed by increase in velocity
$\Delta \vec{v}$ = Combined plane and velocity change

Fig. 2.8. Velocity diagram for velocity and plane change.
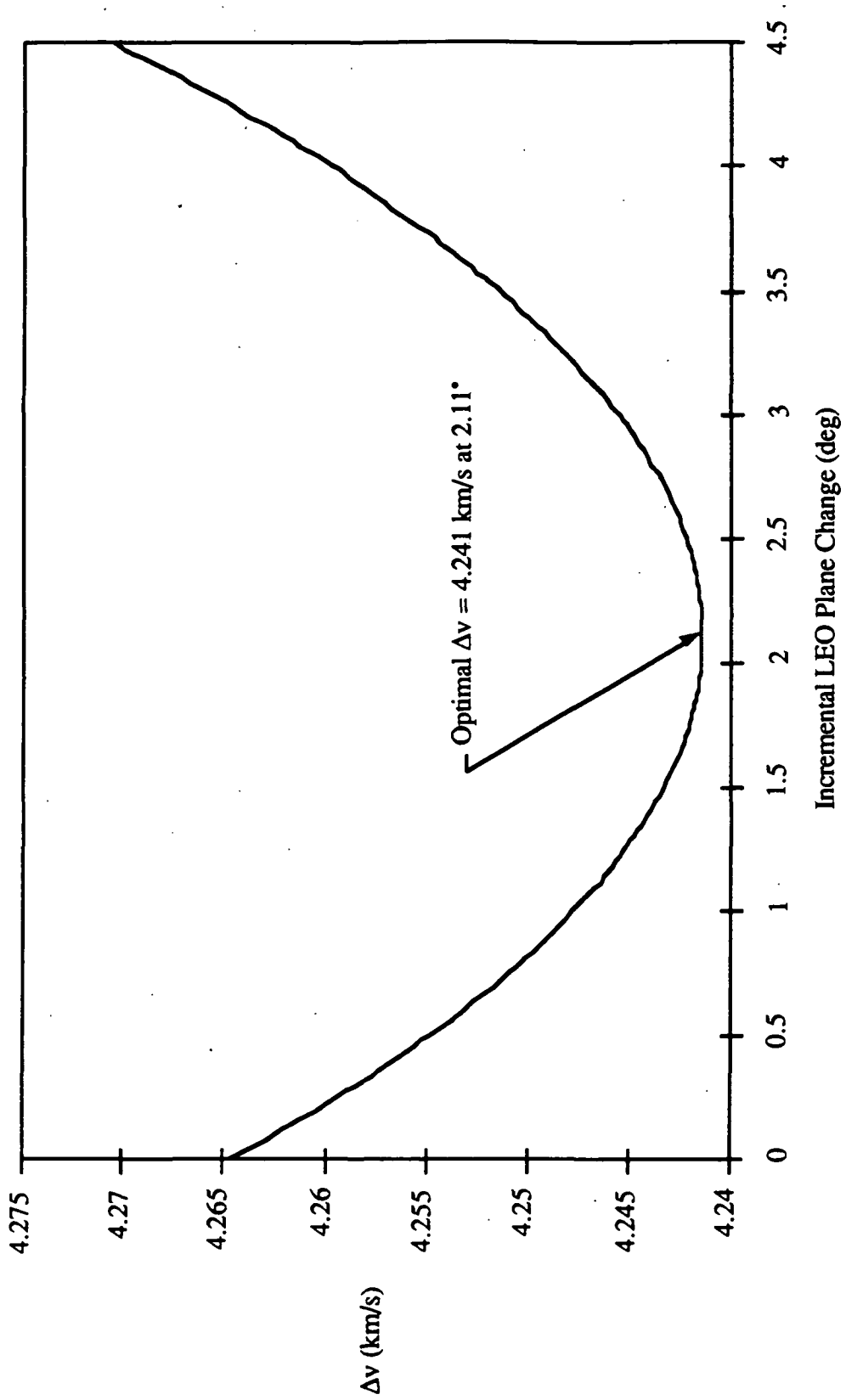
Fig. 2.9. Δv optimization using an incremental LEO plane change.

Direction of travel

CENTER LINE

α

REFERENCE
LINE

$X_{cp}$

$F_N$

$X_{cm}$

W

T

φ
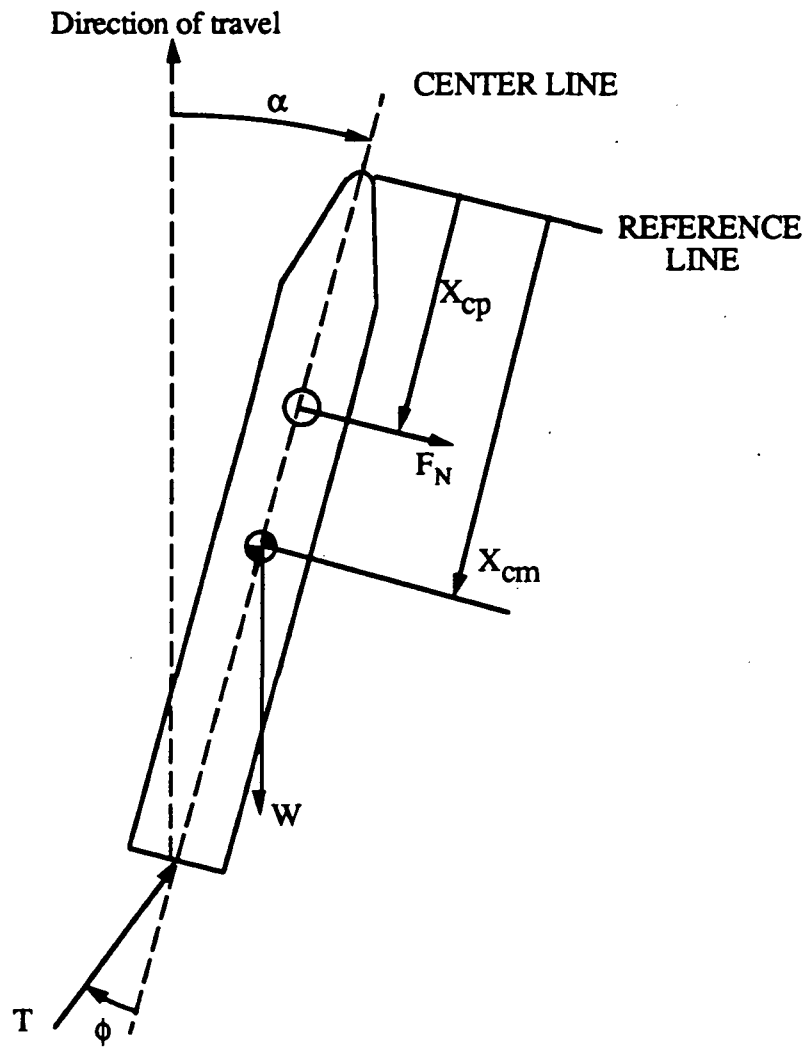
$F_N$ = Normal force
$X_{cp}$ = Distance of center of pressure from nose tip
W = Weight
$X_{cm}$= Distance of center of mass from nose tip
T = Thrust

Fig. 2.10. Forces acting on the vehicle.

48
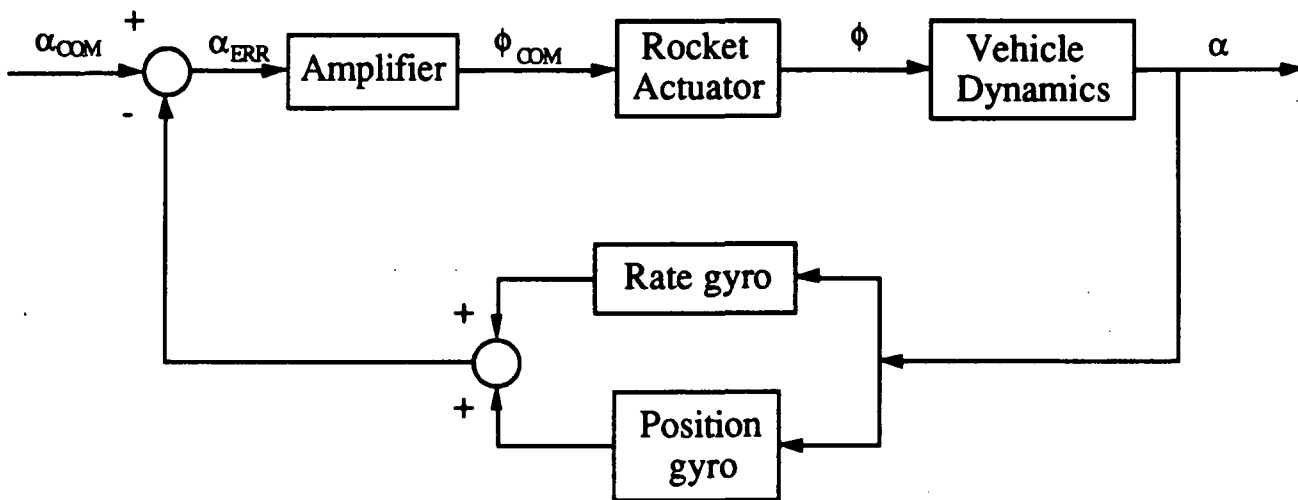
$\alpha$ = vehicle angle of attack with respect to vertical
$\alpha_{COM}$ = vehicle angle of attack commanded by the flight computer
$\alpha_{ERR}$ = error between the commanded and actual vehicle angles of attack
$\phi$ = actual gimbled engine angle
$\phi_{COM}$ = gimbled engine angle commanded by the flight computer

Fig. 2.11. Control system loop.

# 3.0 PROPULSION SYSTEM AND ENGINE RETURN UNIT

In the design of any space launch vehicle, a few of the many components tend to account for the majority of the cost of the system. Traditionally, the propulsion system and the avionics are the most significant financial investments in development and operation of unmanned launch vehicles. It was a primary focus of the Antares research and design team to address the high cost of placing payloads in orbit. The capability of reusing these costly components was found to be the best practical solution to decreasing the cost of launching payloads into orbit.

The Engine Return Unit (ERU) is the key element in the reusability aspect of the Antares launch vehicle. It houses the most expensive components of the vehicle, such as the Dual Mixture Ratio Main Engine (DMRE), secondary propulsion, and avionics. These components travel within the ERU back through the atmosphere, so that they may be reused on subsequent missions.

Figures 3.1a and 3.1b show cutaway views of the ERU in low earth orbit (LEO) and geosynchronous earth orbit (GEO) configurations, respectively. Top and bottom views of the ERU are displayed in Figs. 3.2 and 3.3, respectively. The ERU's diameter tapers from 5 m where it joins the body of the Antares to 4.5 m at its rear surface.

The ERU is designed with consideration of all phases of its mission: launch, orbital flight, re-entry, and landing. Of all of these phases, the launch phase imposes the greatest loading on the ERU. During this phase of the mission, the ERU must withstand the stress due to the DMRE's thrust. A thrust frame within the ERU must distribute the thrust vector from the engine to the outer perimeter, where the load is transmitted to the propellant tanks above.

For the re-entry phase, the ERU must have the appropriate thermal protection to withstand the extreme heating due to high velocity travel through the atmosphere. The forward surface, which encounters the most severe heating, is protected by a heat shield. The other

**PRECEDING PAGE BLANK NOT FILMED**

exposed surfaces are protected by a high temperature alloy thermal casing. Aerodynamic stability is another important consideration in the design of the ERU. The center of mass must be far enough forward for the body to be dynamically stable so that the ERU's heat shield will remain facing forward during re-entry.

Another critical phase of the ERU's mission occurs during landing. Initial impact with the water will cause landing loads on the order of 1,400 kPa (~ 200 p.s.i.) on parts of the unit. After the ERU has landed, it must be stable enough to withstand ocean waves without overturning.

## 3.1 DUAL MIXTURE RATIO ENGINE
(Geneva Jacobson)

The Antares is powered into orbit by the Dual Mixture Ratio Engine (DMRE), proposed and studied by Pratt and Whitney Inc. [1]. The engine uses liquid hydrogen and oxygen as propellants and is configured to meet the Single-Stage-to-Orbit (SSTO) vehicle propulsion requirements of high thrust to weight, high specific impulse ($I_{sp}$), deep throttling, and reusability. The engine can operate at oxidizer to fuel (O/F) ratios of 12:1 and 6:1 and has an extendable nozzle skirt that allows area ratios of 40:1 and 150:1.

During low altitude operation, the thrust is needed to overcome the gravitational and aerodynamic drag losses. Therefore, at takeoff, a high thrust is needed, and to achieve this the DMRE operates with a fuel mixture ratio of 12:1 and a nozzle area ratio of 40:1. At the higher mixture ratio, the mass flow rate is higher and with the lower nozzle area ratio, the exit pressure is higher (more closely matches atmospheric pressure). At high altitude, where the flight path angle is small, the gravitational and drag losses are minimal and $I_{sp}$ is the driving factor because a high thrust is no longer needed to overcome gravitational and drag losses. At 12,000 m the extendable nozzle skirt lowers to increase the area ratio to 150:1 [1]. Increasing the nozzle area ratio makes the engine more efficient for flight at higher altitudes because nozzle exit pressure can be more closely matched to the low ambient pressure. At 27,000 m the

mixture ratio is reduced to 6:1. This reduces the thrust because the mass flow is decreased, however, the $I_{sp}$ is increased because the molecular weight of the exhaust is reduced. The engine operates with a chamber pressure of 27.6 MPa and 18.6 MPa at the two different mixture ratios, respectively. Table 3.1 lists the overall characteristics of the DMRE, and table 3.2 compares the engine characteristics at the two mixture ratios.

Table 3.1: Overall Characteristics of Dual Mixture Ratio Engine [1].

| Cycle | Staged |
|---|---|
| Thrust to Weight Ratio | 109.5:1 (O/F=12, sea level) |
| Dry Mass | 2,272 kg (5050 lbs) |
| Throttling Ability | 10-100% |
| Projected Mission Life | ~100 missions |

Table 3.2: Engine Characteristics at 12:1 and 6:1 O:F Ratio [1].

| O/F / Area Ratio | 12:1 / 40:1 | 6:1 /150:1 |
|---|---|---|
| Specific Impulse (sea level) | 334 sec | N/A |
| Specific Impulse (vacuum) | 362 sec | 467 sec |
| Thrust (sea level) | 2,460 kN (552,000 lbs) | N/A |
| Thrust (vacuum) | 2,670 kN (600,000 lbs) | 1,850 kN (417,000 lbs) |
| Chamber Pressure | 27.6 MPa | 18.6 MPa |

## 3.2 PROPULSIVE ORBIT / DEORBIT SYSTEM
(Miles Ervin and Mike Filbin)

The Propulsive Orbit/Deorbit System (PODS), which provides the Antares with orbital maneuvering and deorbiting capability for LEO missions, is an independent propulsion system integrated into the structure of the Engine Return Unit (ERU). The PODS becomes active

after the payload has been deployed, maintaining the vehicle's attitude while it coasts in the parking orbit. Normally, the PODS carries enough propellant to deorbit the ERU and main tank from the 150-300 km parking orbit. As an added option, the PODS can carry enough propellant to raise the Antares and its payload into a 300 km circular orbit, and deorbit the rest of the vehicle from this altitude.

## 3.2.1 PODS ENGINES

The Rocketdyne XLR-132 engine has been selected for providing the $\Delta v$ for deorbiting the Antares and performing any needed orbital maneuvers. The XLR-132 uses monomethyl hydrazine (MMH) as fuel and nitrogen tetroxide ($N_2O_4$) as oxidizer. The engine is pump-fed and produces 16.68 kN of thrust. In the Antares I configuration, two XLR-132 engines are mounted on opposite sides of the ERU (see Fig. 3.1a). In addition to providing symmetrical thrust through the ERU's center of mass, the use of two engines allows for engine-out capability. The XLR-132 engines are configured in each ERU similarly for modular Antares configurations (see Figs. 3.4a, 3.4b, and 3.4c). The ERU's are oriented in the multiple configuration so that the engines are positioned symmetrically around the vehicle's center of mass. Table 3.3 lists the characteristics of the XLR-132 engines.

Marquardt R-1E thrusters, which are currently used in the Space Shuttle's reaction control system (RCS), have been selected to provide reaction control for the Antares. Like the XLR-132, the R-1E's use MMH and $N_2O_4$ as propellants. Each thruster produces 110 N of thrust, which makes it possible to point the Antares in any desired direction. These thrusters are pre-mounted in removable thruster racks that contain four Marquardt RCS thrusters each. The thruster racks are mounted on the bottom end of the ERU to enable easy access to PODS/ERU components, as well as flexibility in outfitting the Antares for multiple-booster missions. In the Antares I configuration, two thruster racks are mounted on the ERU, as shown in Fig. 3.3. This results in two thrusters directed outward in each of the coordinate directions perpendicular to the primary axis of the Antares, giving the vehicle the ability to pitch, roll, and

spin. In the multiple Antares configurations, one thruster rack is mounted in each ERU on the periphery of the vehicle (refer to Figs. 3.4a, 3.4b, and 3.4c). Since the vehicle is more massive, thruster racks used in modular configurations are equipped with eight thrusters. Table 3.3 lists the characteristics of the Marquardt R-1E thrusters.

Table 3.3: Rocketdyne XLR-132 and Marquardt R-1E Engine Specifications.

| ENGINE | Thrust (N) | $I_{sp}$ (sec) | mass (kg) | length (cm) | Expansion ratio |
|--------|-----------|----------------|-----------|-------------|-----------------|
| XLR-132 | 16,680 | 340 | 54.0 | 120.0 | 400:1 |
| R-1E | 110 | 280 | 3.7 | 27.9 | 100:1 |

## 3.2.2 PODS TANKS

The XLR-132 engine and the R-1E thrusters use common propellant tanks since they both burn MMH and $N_2O_4$ propellants. The propellants are pressure fed to the engine manifolds using a helium pressurization system. The tanks are equipped with rubber bladders, which allow the helium to exert pressure on the propellants and prevents the propellant from floating in the tank while in a zero-g environment. All of the tanks, including the helium pressurization tank, are spherical and manufactured from 7075-T6 aluminum.

A single, high pressure helium tank provides pressurant for the two propellant tanks (see Fig 3.5). The helium separates into two paths that lead to the MMH and $N_2O_2$ tanks. Helium isolation valves are located along each path and are switched to the "open" position when the engines are ready to fire. A pressure regulator is used to adjust the helium pressure to the required manifold inlet pressure of the engines. An isolation valve is located at the inlet of the oxidizer tank to prevent oxidizer vapors from backflowing through the check valve and reacting with fuel vapors. Overboard vents are also located on the XLR-132 propellant leg to prevent tank overpressurization.

The tank sizes were determined from the Δv requirements of the mission. The Δv provided by the two XLR-132 maneuvering engines is 150 m/s, up to 100 m/s of Δv for deorbit and 50 m/s of Δv for orbital maneuvering. From the rocket equation, it was determined that 330 kg is required to deorbit the Antares. The predicted propellant usage for the vehicle's attitude control in orbit is approximately 1 kg/hr per Antares booster, which is based on usage rates of similar size vehicles. The maximum hold in a parking orbit is approximately 15 revolutions, or 23 hours, based on the available time window for deorbit. This results in 23 kg of RCS propellant used for RCS operations. An additional 27 kg is required for attitude maintenance during orbital maneuvers, and spin control. Therefore, 50 kg of propellant is required for the R-1E thrusters. This results in a total of 400 kg of propellant needed for both the OMS and RCS engines, including an extra 20 kg of reserve propellant. The tanks are sized to accommodate an extra 280 kg of propellant that is used if the payload needs to be circularized to a 300 km orbit. Therefore, using the 1.8:1 mixture ratio for both the XLR-132 and Marquardt thrusters, it was determined that the inside diameter of both tanks must be 83 cm. Finally, to provide a constant manifold inlet pressure of 1.24 MPa (180 psia) to the propellant tanks, 2.0 kg (4.4 lbs) of helium is required. This corresponds to a 45.0 cm inside diameter for the helium tank, assuming a temperature of 300 K and a pressure of 20.7 MPa (3000 psia). Table 3.4 contains the specifications of the PODS tanks.

Table 3.4: PODS Tank Specifications.

| TANK | Diameter (cm) | Thickness (mm) | Empty mass (kg) | Full * mass (kg) | Pressure (MPa) |
|------|---------------|----------------|-----------------|------------------|----------------|
| MMH | 83.0 | 2.0 | 12.0 | 148 | 1.24 |
| $N_2O_4$ | 83.0 | 2.0 | 12.0 | 256 | 1.24 |
| Helium | 45.0 | 6.0 | 11.0 | 13.0 | 20.70 |

* Not including propellant to circularize payload to 300 km orbit.

In order to prevent the propellants from freezing while the Antares is in orbit, the tanks and propellant lines are equipped with area and line heaters. These heaters are powered from the principal battery power supply contained in the ERU. Additional insulation is also required for the tanks and propellant lines. The total mass of the PODS is 600 kg.

### 3.2.3 PODS OPERATIONS

The PODS becomes active following main engine cut-off. The RCS thrusters are used in orbit to maintain the vehicle's attitude. Prior to the deorbit maneuver, the RCS thrusters orient the Antares so that the XLR-132 engines are pointing in the direction of flight (see Fig. 3.6). At the appropriate time, these engines fire to decelerate the vehicle, providing the necessary $\Delta v$ to place the Antares into its deorbit trajectory.

When the XLR-132 engines have completed their deorbit burn, the RCS thrusters rotate the Antares 180°, orienting the tank forward of the ERU relative to the vehicle's flight path. The main tank assembly then separates from the ERU, sending the tank structure ahead of the ERU in the deorbit path. Once the separation between the ERU and tank is approximately 100 m, two small solid rocket motors mounted in the tank structure are fired. These solid rockets provide an additional 45 m/s of $\Delta v$ in the direction of flight, deorbiting the empty tank downrange of the intended ERU deorbit site. This maneuver is necessary in order to avoid tank debris damage to the ERU, which might occur if the two components deorbited in the same area.

Two STAR 13B solid rocket motors, manufactured by Morton Thiokol, are mounted in the aft bulkhead of the tank assembly (see Fig. 3.7). The STAR 13B produces a thrust of 7.0 kN, with a specific impulse of 286 seconds. These solid rocket motors are oriented at a 15° angle with respect to the tank's primary axis, in order to spin the tank, as well as providing it with forward thrust. The angular momentum resulting from spinning the tank structure keeps the tank oriented in the direction of flight while the solid rocket motors are

burning. The ERU simply remains in its original deorbit trajectory, re-entering the Earth's atmosphere.

In modular Antares configurations, the PODS on each ERU work together to maintain attitude control and to deorbit the vehicle. The operation of the combined system is coordinated through one set of avionics, which is located in one of the ERU's. The engines are configured on each multiple vehicle ERU the same as on the Antares I ERU (see Figs. 3.4a-3.4c), with the exception that the solid rocket motors are repositioned in the multiple tank structure (see Fig. 3.8). The deorbit maneuver for the multiple Antares configuration is identical to that of the Antares I mission. Following the deorbit burn, and 180° rotation maneuver, the ERU's separate from the tanks sequentially (see Fig. 3.9). The last ERU to separate makes final attitude corrections to assure that the tank assembly is oriented correctly for the separation maneuver. As the final ERU separates, it initiates the burn sequence for the solid rocket motors that are mounted on the tank assembly. The solid rocket motors fire shortly after ERU separation to spin up the tanks and send them downrange of the ERU deorbit trajectory. The multiple tanks remain attached to each other throughout their re-entry trajectory.

After the ERU's separate they are controlled autonomously through avionics and RCS thrusters located in each ERU. The RCS thrusters maintain the ERU's attitude to prevent the module from tumbling as it enters the atmosphere. The controllability of each ERU is also important in order to minimize the landing site dispersion, and make the recovery process as efficient as possible.

## 3.3 AVIONICS
(Michelle Bailey)

The avionics housed in the Engine Return Unit are controlled by a distributed command and data handling system (C&DH). This system is responsible for Antares subsystems, such as the guidance-navigation and control system and the communications system. The C&DH

system distributes electric power to all of the vehicle's equipment, and it consists of a central data processing unit, an on-board computer, and many remote sensors located on the vehicle. The central processing unit receives ground-based information and distributes it to either the remote units or the on-board computer. The computer is used to sequence operations such as propulsion firing and the powering down of vehicle components, for example the Dual Mixture Ratio Engine (DMRE). The remote units process and execute commands received from the computer. All information from the payload and the vehicle is routed through the central processing unit before it returns to Earth. The total mass of the C&DH system is 20 kg [2].

The guidance, navigation, and control system (GN&C) consists of an inertial navigation system (INS) and two horizon sensors. The INS is a complex system of accelerometers and gyros for attitude and position control, and the horizon sensors provide updated information to the INS. This GN&C system is ideal for the Antares vehicle as it allows precise positioning for re-entry, is lightweight (25 kg), and is very reliable [2].

The communications subsystem uses a transponder which is compatible with the Space-Ground Link System (SGLS) on the S-band. This is necessary because the Antares does not fly any long-term missions, and compatibility with the SGLS allows commands from the ground to reach the vehicle in a minimum time after launch. Some of the communication system's duties include transmission of signals to Earth, responding to autonomous commands, execution of mission commands, and system status reports to the C&DH system. The mass of the communications system is 40 kg [2].

The avionics themselves will use approximately 100 watts of power for both LEO and GEO missions. The entire power supply for the vehicle, however, varies greatly depending on the mission [3]. For LEO missions the booster may be orbiting the Earth for a matter of days, so in addition to a primary battery the booster will employ Nickel-Cadmium (NiCd) secondary batteries for energy storage. This is because primary batteries are not rechargeable, and therefore as a sole power source they are too massive for long term flights (days or weeks). Secondary batteries can be recharged (cyclically), and even though NiCd batteries are

associated with a limited amount of energy discharge,the LEO mission is not long enough to manifest a degrading effect on the mission because of this. For the GEO missions all of the booster's electric power will be supplied by a silver zinc primary battery since the mission duration is very short. Work is in progress for determining battery mass; at this point an estimate of 400 kg is used [4].

## 3.4  ERU STRUCTURE
(Steve Aarnio)

The ERU structure is divided into four separate units; the main thrust frame, the internal frame, the thermal casing, and the outer heat shield. Each of these is a separate entity, and they are all interconnected. The thermal casing is connected around the outside and over a portion of the bottom of the internal frame. The internal frame is, in turn, connected to the main thrust frame via titanium struts, and the heat shield is bolted to the titanium struts from the top. The function of each component is different from that of the others, and therefore, each structure has a different construction. The main thrust frame is responsible for transferring the thrust from the DMRE and the PODS engines directly to the main tanks and withstanding the re-entry and splashdown loads on the DMRE, the PODS engines, and the heat shield. The internal frame is designed to withstand only the re-entry and splashdown loads on the thermal casing. The heat shield and thermal casing are non-load bearing structures designed to protect the interior of the ERU from the extreme temperatures of re-entry.

### 3.4.1  THRUST FRAME
(Matt Sullivan)

The thrust frame for the ERU must withstand the loads placed upon it by the DMRE. In the maximum thrust condition the ERU experiences a force of 2,670 kN. The thrust frame consists of a four-member tensile square as the upper unit, which connects to four compressively loaded struts that connect directly to the gimballing joint of the DMRE (see Fig. 3.10). The struts that make up the tensile square encounter a tension of 944 kN each,

while the four other struts are under compression loads of 1,493 kN each. The struts are all constructed from Titanium Ti-5Al-2.5 Sn (MIL-T-9047) because of its high strength to weight ratio [5].

To compute the diameters of the compressive struts, analysis was done considering Euler's critical buckling load.

$$P_{CR} = \pi^2\left(\frac{EI}{L^2}\right) \tag{3.1}$$

$P_{CR}$ is the load at which Euler column buckling occurs for a strut with a cross-sectional moment of inertia I, a length L, and a Young's modulus E. The inner diameter for the compression struts is 8.0 cm while the outer diameter is 12.6 cm. The upper tensile struts were evaluated for the yield stress point, $\sigma_{yd}$, for titanium of

$$\sigma_{yd} = \frac{F}{\pi\left[\left(\frac{d_o}{2}\right)^2 - \left(\frac{d_i}{2}\right)^2\right]} = 7.58 \times 10^8 \text{ N}/\text{m}^2 \tag{3.2}$$

where $d_i$ and $d_o$ are the inner and outer diameters, respectively. For the tensile struts, the inner diameter is 10.0 cm while outer diameter is 11.1 cm. These struts were designed as tubing to increase their stiffness.

A factor of safety of 1.5 was employed throughout the thrust frame design process. The lengths of the struts are determined by the geometry of the ERU, and are 2.82 m and 2.23 m for the tensile struts and the compression struts, respectively. The masses of the struts are 74.2 kg for each of the compression struts, and 23.7 kg for each of the tensile struts, giving the entire thrust frame a total mass of 391 kg.

### 3.4.2 PODS THRUST FRAME
(Steve Aarnio)

The PODS thrust frame, illustrated in Fig. 3.11, is connected directly to the corners of the DMRE thrust frame. The three frame members are made of titanium for ease of connection to the titanium of the DMRE thrust frame. The main vertical member is a round tube with an

outside diameter of 5 cm and an inside diameter of 4 cm. These dimensions give the vertical member enough buckling strength to support the entire 16 KN of thrust from each PODS engine. The two diagonal supports are also round tubes. The outside diameter of the diagonals is 2.5 cm and the inside diameter is 2.25 cm; these dimensions give the diagonals enough strength to support the thrust of the PODS engines at full gimbal. The mass of one PODS thrust frame is about 12 kg, for a total mass of 25 kg for the two frames.

### 3.4.3 ERU INTERNAL FRAMING
(Steve Aarnio)

The ERU internal structure must be able to support the external thermal casing of the ERU during the initial launch acceleration, the aerodynamic forces during re-entry, the impact of the ERU on the water at splashdown, and the buoyant forces which act on the casing after splashdown. The ERU internal structure is a cylindrical conic frame made from DuPont Kevlar 49 composite, and is shown in Fig. 3.12. In this configuration, the upper support ring is 1 cm thick with an outside diameter of 4.90 m, to allow for the thickness of the heat shielding, and have an inside diameter of 4.85 m. The lower outer support ring has an outside diameter of 4.00 m and an inside diameter of 3.95 m. The lower inner support ring has an outside diameter of 2.05 m and an inside diameter of 2 m. All cross members are round tubes with an outside diameter of 2.5 cm and an inside diameter of 2.25 cm. With a mass of approximately 100 kg, this construction allows the structure to remain extremely light and strong.

The very large temperature changes which the structure encounters require the use of a thermally stable material, and the precise placement of the outer heat shield requires a thermally rigid structure as well. Kevlar is a good choice for both of these requirements. It has a very small thermal expansion coefficient ($-2 \times 10^{-6}$ /$^\circ$K), shows no sign of structural degradation within the temperature range from 77$^\circ$K to 523$^\circ$K, and little weakening at temperatures above this when exposed for durations of less than eight hours [6]. This slight degradation of properties is not a problem for the ERU structure, as the ERU spends very little time above

these temperatures, and even with this deterioration the Kevlar remains stronger than other materials [6].

The negative value of the thermal expansion coefficient means the structure will actually shrink as the temperature increases. This is not a desirable feature because the thermal casing is a thin sheet of ductile material, and is subject to plate buckling under the compressive forces of the shrinking ERU structure. However, because the expansion coefficient is so small, the effect of shrinkage is negligible over the size of the structure. During launch the temperature inside the ERU drops well below atmospheric conditions because of the liquid hydrogen and liquid oxygen lines running to the engine, and at a temperature of 77°K the ERU internal structure lengthens approximately 1.1 mm and the outside diameter increases by about 2 mm During re-entry the temperature inside the ERU is expected to be very high due to atmospheric friction, and at a temperature of 523°K the internal structure shortens approximately 1.4 mm and the outside diameter decreases by about 2.5 mm.

### 3.4.4  THERMAL CASING
(Steve Nicholls)

The ERU thermal casing consists of the cylindrical shell aft of the heat shield and the rear bulkhead. It is supported by the internal frame, as shown in Fig 3.13, and protects the internal components. Although most of the heating during re-entry occurs at the heat shield, the thermal casing must also withstand moderate thermal loads. The thermal casing is 1 mm thick and made of Inconel 718 alloy. This material combines very high strength with low thermal expansion and relatively low thermal conductivity. The mass of the thermal casing is 180 kg.

## 3.5  RE-ENTRY AND RECOVERY
(Kurt Vold)

After payload deployment in LEO, the PODS in the ERU deorbits the propellant tank and ERU. For GEO missions, the PODS is not needed. The separation system decouples the

tank from the ERU and the tank is sent into the atmosphere to burn up. The ERU returns through the atmosphere with the aid of a heat shield, and when the vehicle has slowed sufficiently, a parafoil is deployed which brings the ERU safely down for landing in water or on land.

### 3.5.1 SEPARATION SYSTEM
(Kurt Vold)

The ERU is designed to decouple from the propellant tank through the use of the separation system (see Fig. 3.14) and Section 5.0. The ERU is connected to the propellant tank by four explosive bolts (see Figs 3.1 and 3.2). These bolts have springs compressed around them that will push the ERU and propellant tank apart after the bolts have broken. Section 5.1.2 shows details of the bolts and how they are connected to the tank structure. The bolts run through attachment blocks, shown in Fig. 3.15a, at the corners of the thrust frame. The attachment blocks provide a path for the force from the trust frame to the explosive bolts while providing access to the underside of the bolt from outside the ERU. They are made of Ti16 A1-4 V titanium to withstand the high thermal and mechanical loads which they encounter. The attachment blocks are connected to access channels, shown in Fig. 3.15b, to provide a passageway to the attachment blocks to the outside of the ERU. This passageway is used during mating of the ERU and tank for tightening the explosive bolt and connecting it to the detonation system. The channels are made from Ti16 A1-4 V titanium because they are also subject to high thermal loads during re-entry. Replaceable bolt sleeves, shown in Fig. 3.15c, mount on top of the access channels to help in the mating process by providing male-female type connections between the tank and ERU. The sleeves, which are made from light gauge aluminum and carbon-carbon composite material, burn away during re-entry and are replaced upon refurbishment of the ERU. This arrangement is watertight for ocean landing. Seawater can fill the separation system components but goes no farther since there is no direct pathway between the inside of the components and the rest of the ERU. This feature minimizes mass because no doors are needed to shut and seal-off the ERU, and no back-up

system is necessary. A complete diagram of how these parts interconnect is given in Fig. 3.14, and a list of the components is given in Table 3.5.

Table 3.5: Separation System Components.

| Part | Number | Dimensions | Material | Mass |
|------|--------|-----------|----------|------|
| Attachment Blocks | 4 | l = 0.20 m<br>w = 0.20 m<br>h = 0.20 m<br>t = 2.0 cm | Titanium Ti16 Al-4 V | 18.8 kg |
| Access ports | 4 | l = 0.5 m<br>w = 0.20 m<br>h = 0.20 m<br>t = 2.0 cm | Titanium Ti16 Al-4 V | 9.4 kg |
| Replaceable Bolt Sleeve | 4 | h = 2.5 cm<br>d = 0.20 m | Aluminum, Carbon-Carbon Composite. | 2.0 kg |
|  |  |  | Total | 121 kg |

## 3.5.2 PROPELLANT DOORS
(Kurt Vold)

The hydrogen and oxygen lines decouple and slip apart at the propellant access door through the use of slip joint connectors and cryogenic o-rings. A spring retracts the flexible propellant lines into the housing and the propellant access door closes via a solenoid and spring, sealing off the ERU (see Fig. 3.16). The entire unit is contained in the propellant access housing. This housing provides the system back-up by sealing-off the propellant access door from the rest of the ERU. In the event of propellant access door failure, water could get into the propellant access housing and propellant lines, but would not enter the ERU.

A time line of events for the separation procedure is as follows: during mating of the ERU and the propellant tank, the springs are compressed and the explosive bolts tightened and connected into the detonation system. The propellant lines are then connected through the propellant line access door. At the proper time in the re-entry phase of the mission, the bolts explode, the propellant lines separate and are retracted into the ERU, the propellant access door closes, and the ERU detaches from the propellant tank. Expanding springs push the ERU and propellant tank safely apart.

### 3.5.3 HEAT SHIELD
(Kurt Vold)

Two methods of atmospheric re-entry exist. First is the slender body ballistic re-entry where the vehicle pierces through the atmosphere, losing little of its kinetic energy. Second is blunt body re-entry where nearly all the initial kinetic energy is dissipated to the atmosphere and the vehicle in the form of heat. The choice of which method to employ is a function of the overall mission. Given the requirement that the ERU is to be returned intact, i.e. the final velocity is effectively zero, a blunt body configuration is the obvious choice for the design of the heat shield. This configuration is shown in Fig. 3 17.

The total heat load, Q, on the re-entry vehicle is [7]:

$$Q = \frac{1}{2}\left[\frac{C_f' \cdot S}{C_d \cdot A}\right] \cdot \frac{1}{2}m\left(v_e^2 - v_0^2\right) \tag{3.3}$$

where

$C_f'$ = Effective average coefficient of friction    m = Total mass

$C_d$ = Coefficient of drag    $v_e$ = Initial re-entry velocity

S = Wetted surface area of the ERU    $v_0$ = Final velocity

A = Frontal area of the heat shield.

For blunt bodies, the fraction, $\eta$, of the total dissipated kinetic energy absorbed by the vehicle in the form of heat is [7]:

$$h = \frac{1}{2}\left[\frac{C_f' \cdot S}{C_d \cdot A}\right] \tag{3.4}$$

Minimizing the ratio within the brackets of Eq. 3.4 causes more energy to be transferred to the atmosphere and less to the vehicle. The heat shield of the ERU is designed to meet this criterion by using a flat top with curved edges (see Fig. 3.17). For this configuration, the frontal area is 19.6 $m^2$ and the surface area of the vehicle, not including the bottom, is 65 $m^2$

The heat shield is comprised of two separate layers, the top layer being an ablator and the bottom a metal base plate. The ablator's function is to absorb enough heat during re-entry to vaporize and be carried away in the boundary layer. An ablator will allow more payload to be returned for the same mass of heat shield than a non ablating shield [8]. Also, the interaction between the vaporized ablator material and the boundary layer lowers the coefficient of friction, thus lowering the heat transfer to the vehicle even more [8].

Ideally, all of the ablator material should vaporize during the re-entry phase. The mass of the ablator is determined from [8]:

$$\frac{m_f}{m_i} = e^{-\frac{C_H \cdot S \cdot V_e^2}{4 \cdot C_d \cdot A \cdot \xi_v}} \tag{3.5}$$

and $\qquad\qquad m_a = m_i - m_f \tag{3.6}$

where

$m_a$ = Ablator mass $\qquad\qquad\qquad\qquad$ $C_H$ = Stanton number = $C_f'$ /2

$m_i$ = Initial mass upon re-entry                                   $\xi_v$ = Heat of vaporization (J/kg)

$m_f$ = Final mass of vehicle at touchdown.

The heat of vaporization should be as high as possible so that the most heat is absorbed with the least mass. The ablator material selected is carbon-carbon composite which has a $\xi_v$ of $2.2 \times 10^7$ J/kg and a density, $\rho$, of 1500 kg/m$^3$ [9]. From Eq. 3.4 and a factor of safety of 1.5, the total mass of ablator material needed is 350 kg. A large safety factor is used to minimize the possibility of holes burning completely through the shield in the presence of nonuniform ablation.

The ablator is applied on top of the metal base plate to a depth of 3.0 cm with slightly more near the edges, as shown on Fig. 3.17. Upon refurbishment of the ERU, a new shield can be reapplied on top of the metal base using standard composite material construction techniques.

The metal base plate is made from 3 mm thick Ti16 Al-4 V titanium and supported from underneath by the thrust frame and by additional titanium cross-bracing anchored to the thrust frame so it will be able to withstand the max Q loads of re-entry and splashdown impact. Titanium has a large heat capacity and melting temperature so structural integrity is assured during the maximum heat load point in the flight. The mass of the titanium base plate and its cross bracing is 330 kg. As discussed in Section 3.4.4, the sides of the ERU are composed of Inconel and are angled inward, as shown in Fig.3.1.

## 3.5.4 RECOVERY
(Steve Nicholls)

In order to be a reusable system, the ERU must not only survive re-entry, but also must be slowed sufficiently to withstand impact with the Earth's surface. Two often proposed methods for deceleration through the atmosphere are: 1) propulsive retrorockets and 2) high drag and high lift devices such as wings and parachutes. Retrorockets require a large amount of propellant to operate, which in turn causes a large weight penalty. Rigid aerodynamic

surfaces (wings) are heavy and complicated. Parachutes, the usual medium for vehicle return, have very limited control characteristics. Advances in parafoil technology provide a high lift, low weight solution to vehicle recovery [10]. Parafoils provide the high drag characteristics of parachutes with the lift and control characteristics of hang gliders.

The reliable control characteristics of the parafoil allow for very accurate landings. With careful deorbit procedures, the ballistic ERU will be able to impact a cleared landing site, possibly as small as 1 to 2 km in diameter. Computer generated simulations are producing control algorithms for similar vehicles, carefully considering all variables of re-entry, including changing wind conditions. These studies show that the ERU landing site can be estimated to within 213 m with a 95% certainty [11].

The high degree of landing accuracy of the parafoil system will make recovery of the ERU simple and relatively inexpensive. During the GEO mission, in which the Antares booster does not reach orbit, splashdown of the ERU will be approximately 2,060 km downrange of the Kennedy Space Center. A recovery vessel will be waiting at the landing site. This will greatly decrease the ERU's exposure time to the corrosive salt water of the Atlantic Ocean. During the LEO mission, the entire Antares will achieve orbit. Following deorbit, the ERU could possibly land on the ground, a circular grass-covered site 1 to 2 km in diameter. The vehicle will have two landing opportunities per day to return to the Kennedy Space Center, where it can be refurbished and reused with little transportation cost. Initially, a sea landing will still be preferable. Perhaps, as the operations mature, ground landings can be attempted.

Figure 3.18 shows the ERU descent sequence. After separation from the tankage, the ballistic ERU attains a terminal velocity of approximately 325 m/s (Mach 1.2) at an altitude of 30,000 m [12], at which point a 16 m diameter drogue parachute is deployed. This chute stabilizes the vehicle and slows it to a terminal velocity of 49 m/s. When the ERU reaches an altitude of approximately 5000 m, the drogue chute is shed in favor of the main parafoil. Initially, only about 70% of the total possible wing area is used. This high wing loading configuration decelerates the system to a horizontal velocity of 25 m/s and a vertical velocity of

11 m/s. At such a high vertical velocity, the vehicle penetrates high winds quickly, reducing landing inaccuracy. At an altitude of around 1000 m, the entire parafoil wing area of 490 m² is deployed. This slows the vehicle to a vertical velocity of 5.2 m/s. At 30 m, just before touch down, a flare maneuver is performed by rapid trailing edge retraction. This reduces the vertical velocity at landing to 3.8 m/s. The horizontal velocity at impact is 14.3 m/s. Air bags are deployed to absorb landing impact. Flotation collar air bags are also deployed in a water landing scenario.

The complete parafoil system has a mass of 680 kg and is capable of delivering a vehicle weighing 7,400 kg, more than enough for the 5,800 kg ERU. The system is fully redundant i.e. an entire backup system ensures the safety of the ERU. The entire package is contained in a volume of approximately 0.85 m³. Table 3.6 lists the components of the parafoil system.

Table 3.6: Parafoil Components.

| ITEM | MASS (kg) | COMMENTS |
|------|-----------|----------|
| Drogue chutes | 132 | Terminal velocity=49m/sec, 16m diameter, mortar deployed |
| Backup drogue chute | 132 | Fully redundant system |
| Main parafoil | 150 | Full open vertical velocity = 3.8 m/sec, wing area = 490 m² |
| Backup parafoil | 150 | Fully redundant system |
| Parachute controls | 23 | For high glide control lines |
| Backup controls | 23 | Fully redundant system |
| Parachute support/installation | 70 | |
| TOTAL | 680 | |

## 3.6 SUMMARY
### (Matt Sullivan)

The high cost of the propulsion and avionics of expendable launch vehicles is always a problem. For the Antares launch vehicle, the ERU is the solution to this problem. The most expensive components return to the earth inside the ERU, so that they may be reused on subsequent missions.

The ERU design is consistent with the commitment to modularity in the design of the Antares. A listing of the individual component masses for each ERU is shown in Table 3.7. The total mass of the ERU configured for LEO missions is 5,800 kg. ERU's which perform missions to GEO will not need the secondary propulsion system for deorbit purposes but will retain the reaction control system. Otherwise, the components within each ERU are identical in design and manufacture.

The design of the ERU requires that the it remain oriented with the heat shield forward during re-entry. Because aerodynamic stability during re-entry is an important consideration in the ERU design, an aerodynamic analysis needs to be performed. This study is on-going and will be reported at a later date.

Table 3.7: ERU Component Masses.

| Item | Mass |
| --- | --- |
| Thrust Frames | 415 kg |
| Internal Frame | 100 kg |
| PODS | 600 kg |
| DMRE and Piping | 2,270 kg |
| Avionics | 85 kg |
| Thermal Casing and Fasteners | 200 kg |
| Heat Shield | 350 kg |
| Heat Shield Base Plate and Framing | 330 kg |
| Parafoil | 680 kg |
| Separation System | 120 kg |
| Batteries | 400 kg |
| Miscellaneous Hardware | 250 kg |
| Total ERU Mass | 5,800 kg |

## 3.7 NOMENCLATURE

| | |
|---|---|
| $P_{cr}$ | Critical Euler buckling load |
| $E$ | Young's modulus |
| $I$ | Sectional moment of inertia |
| $L$ | Length of structural member |
| $d_o$ | Outer diameter |
| $d_i$ | Inner diameter |
| $Q$ | Total re-entry heat load |
| $C_f'$ | Effective average coefficient of friction |
| $C_d$ | Coefficient of drag |
| $S$ | Wetted surface area of the ERU |
| $A$ | Frontal area of the heat shield |
| $m$ | Total mass |
| $v_e$ | Initial re-entry velocity |
| $v_0$ | Final velocity |
| $m_a$ | Ablator mass |
| $m_i$ | Initial mass upon re-entry |
| $m_f$ | Final mass of vehicle at touchdown |
| $C_H$ | Stanton number |
| $\sigma_{yd}$ | Yield stress |
| $\rho$ | Density |
| $\eta$ | Energy fraction |
| $\xi_v$ | Heat of vaporization |

## 3.8 REFERENCES

1. Limerick, C.D., "Dual Mixture Ratio $H_2/O_2$ Engine for Single Stage to Orbit Application," Journal of Propulsion and Power, Vol. 7, No.1, 1991, pp 23-24.

2. Wertz, J. R. and Larson, W. J., (ed.), Space Mission Analysis and Design, Kluwer Academic Publishers, 1991, pp 301-370.

3. Steadman, J. K., "$H_2$-$O_2$ Fuel Cells," United Technologies/NASA Report, June, 1981.

4. "Electrochemical Cell Technology for Orbital Energy Storage," NASA/General Electric Report, June, 1981.

5. "Metallic Materials and Elements for Flight Vehicle Structures," Military Standardization Handbook, MIL-HDBK-5C, Sept. 15, 1976.

6. E.I. DuPont DeNemours and Co., "Characteristics and uses of Kevlar 49 Aramid High Modulus Organic Fiber," DuPont Technical Information, Wilmington, DE, September 1981, pp. 4-5.

7. Allen, H. J., and Eggers, A. J., "The Study of the Motion and Aerodynamic Heating of Missiles Entering the Earth's Atmosphere at High Supersonic Speeds," NACA TN 4047, Ames Aeronautical Laboratory, Moffett Field, CA., October 1957.

8. Allen, H. J., "The Aerodynamic Heating of Atmosphere Entry Vehicles a Review," Fundamental Phenomena in Hypersonic Flow, J. Gordon Hall, Ed., Cornell University Press, 1966, pp. 5-29.

9. Tauber, M.E. "Atmospheric Entry into Jupiter," Advisory Group For Aeronautical Research and Development, North Atlantic Treaty Organization, The MacMillan Company, New York, 1964.

10. Wailes, B., Pioneer Aerospace Corporation, Florida, personal communication, April, 1991.

11. Wetzel, E., Boeing Defense and Space Group, Seattle, WA, personal communication, March, 1991.

12. Johnson, G. W., "Advanced Recovery Systems," Research and Technology 1990: Annual Report of Marshall Space Flight Center, NASA TM-103510, 1990, pp. 2-4.

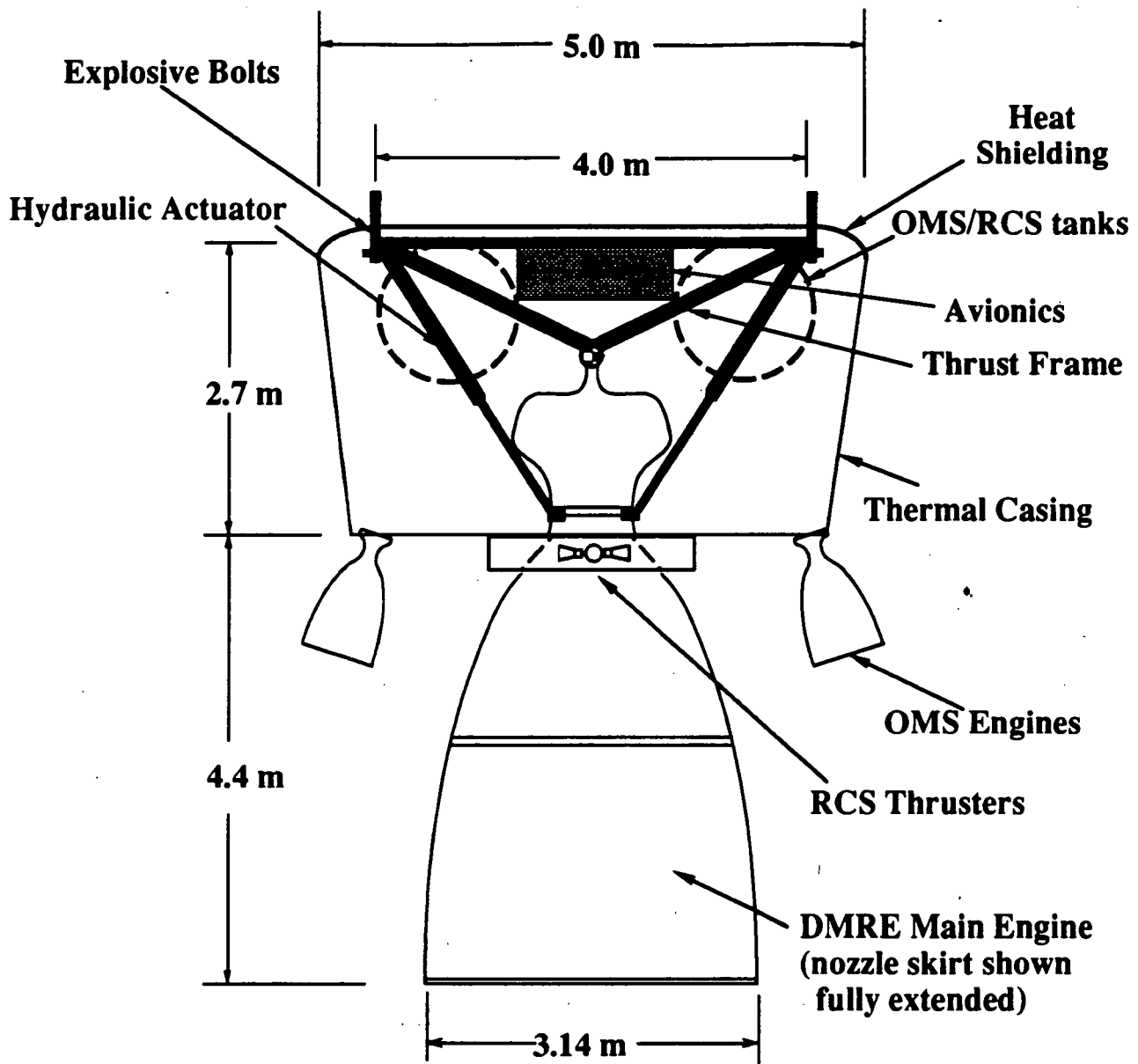Fig. 3.1a. Schematic cutaway view of Engine Return Unit (ERU): LEO configuration.
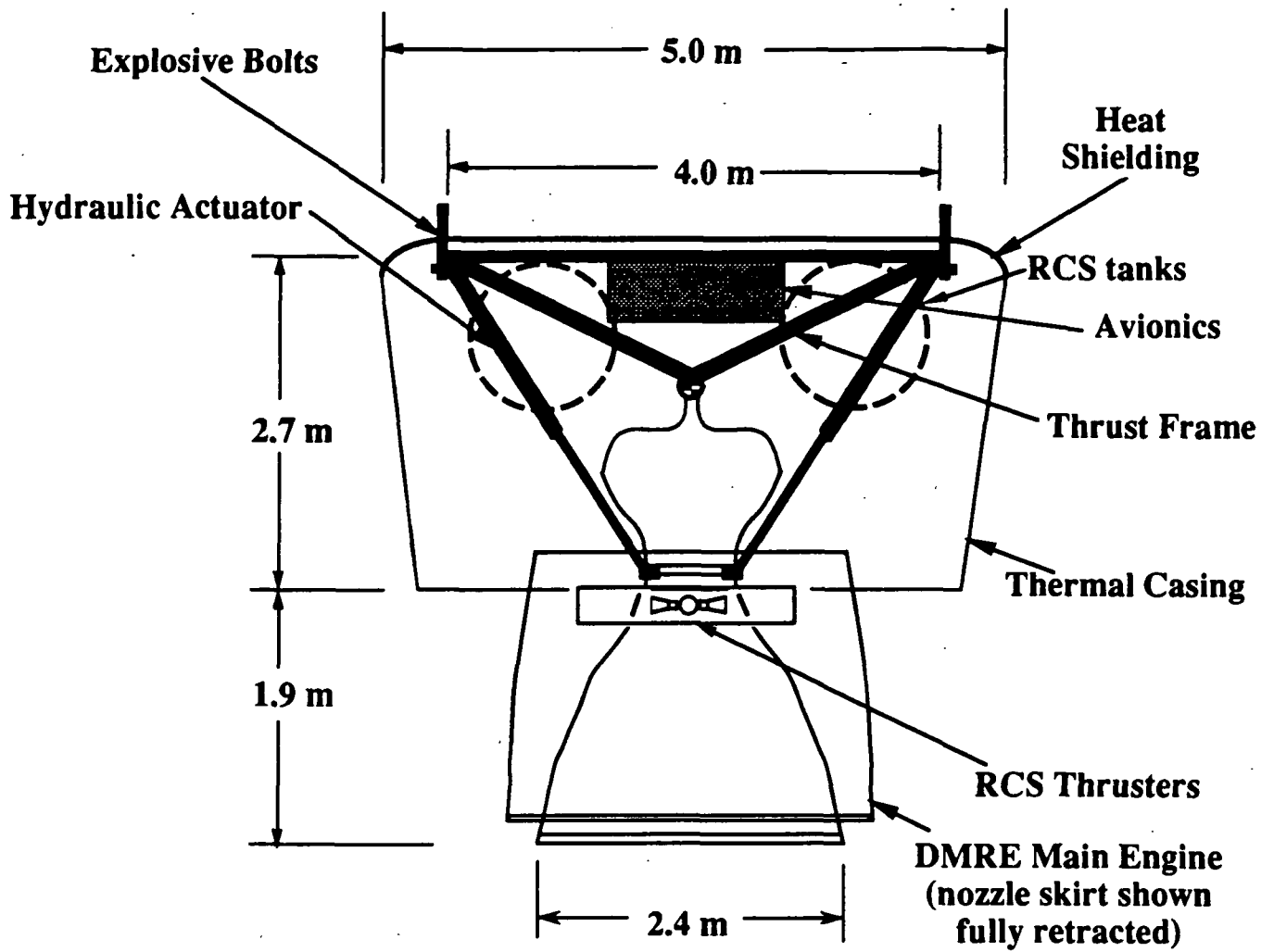
Fig. 3.1b. Schematic cutaway view of Engine Return Unit (ERU) : GEO configuration.

Fig. 3.2. ERU top view.

Main Engine
Nozzle

Recovery
System
Hatch

OMS
Engines

4.5 m

.3 m

RCS Thruster Racks

Fig. 3.3. ERU bottom view.

XLR-132 engines

RCS thruster racks

DMRE engines

Parafoil hatches
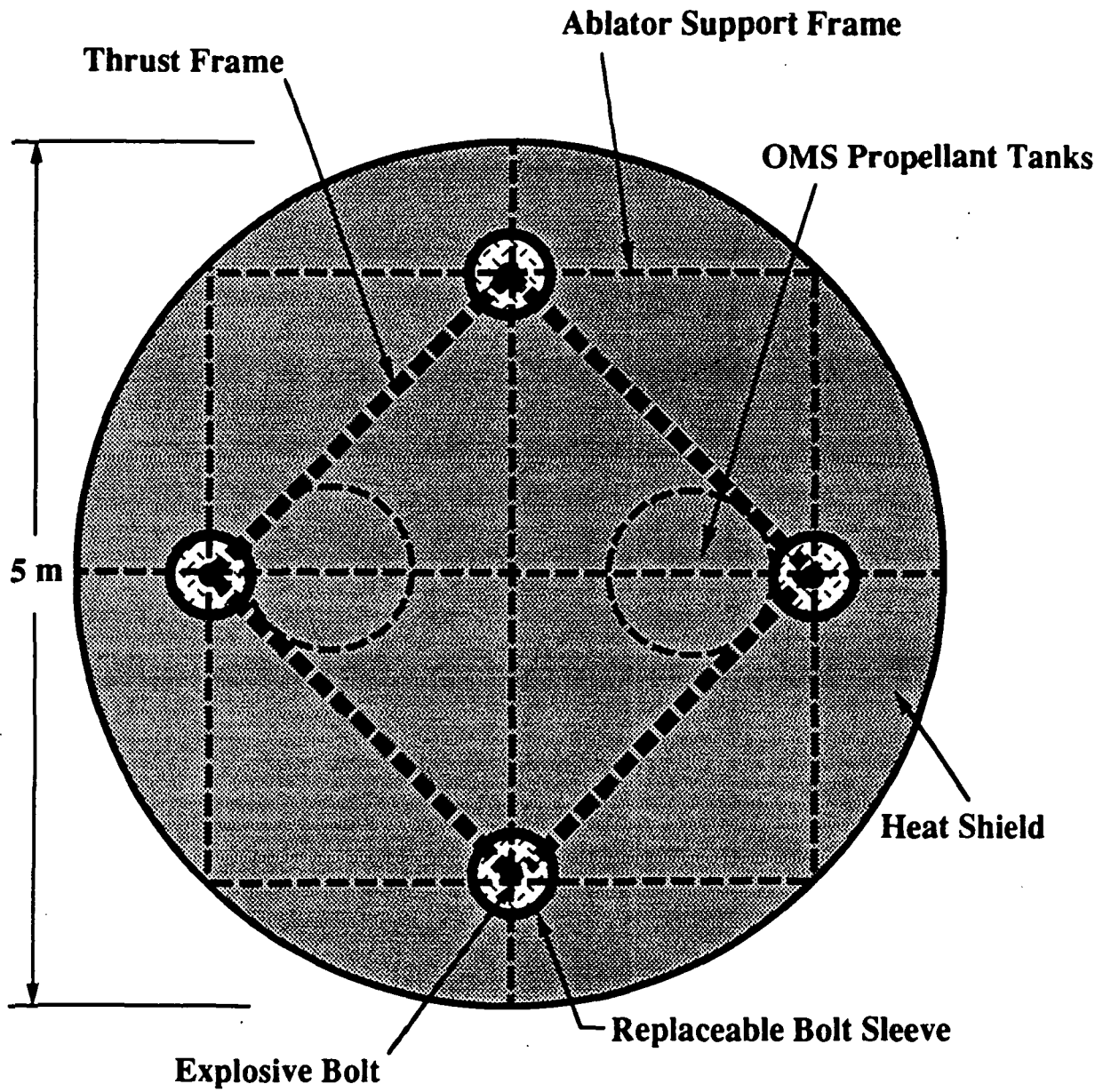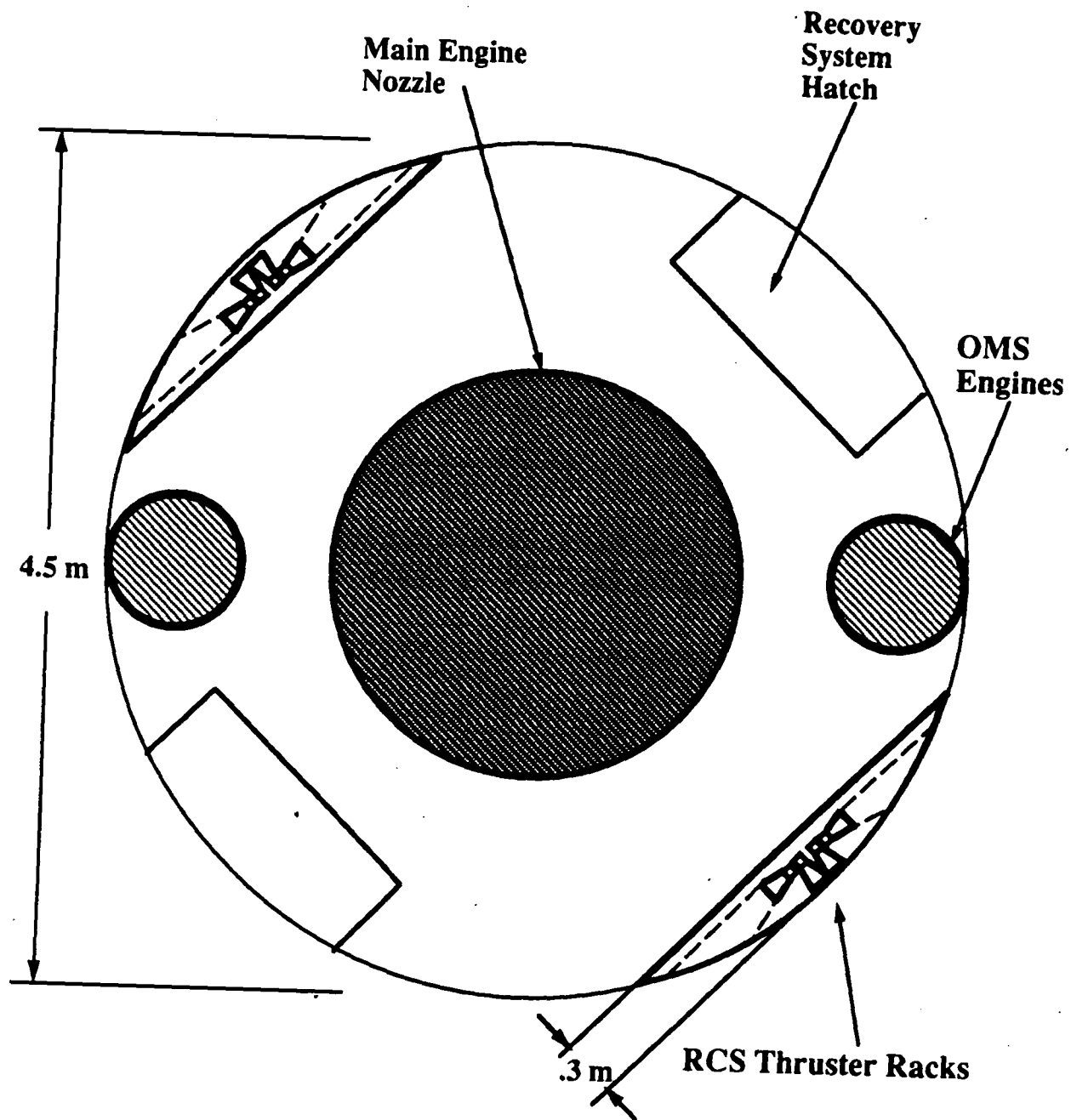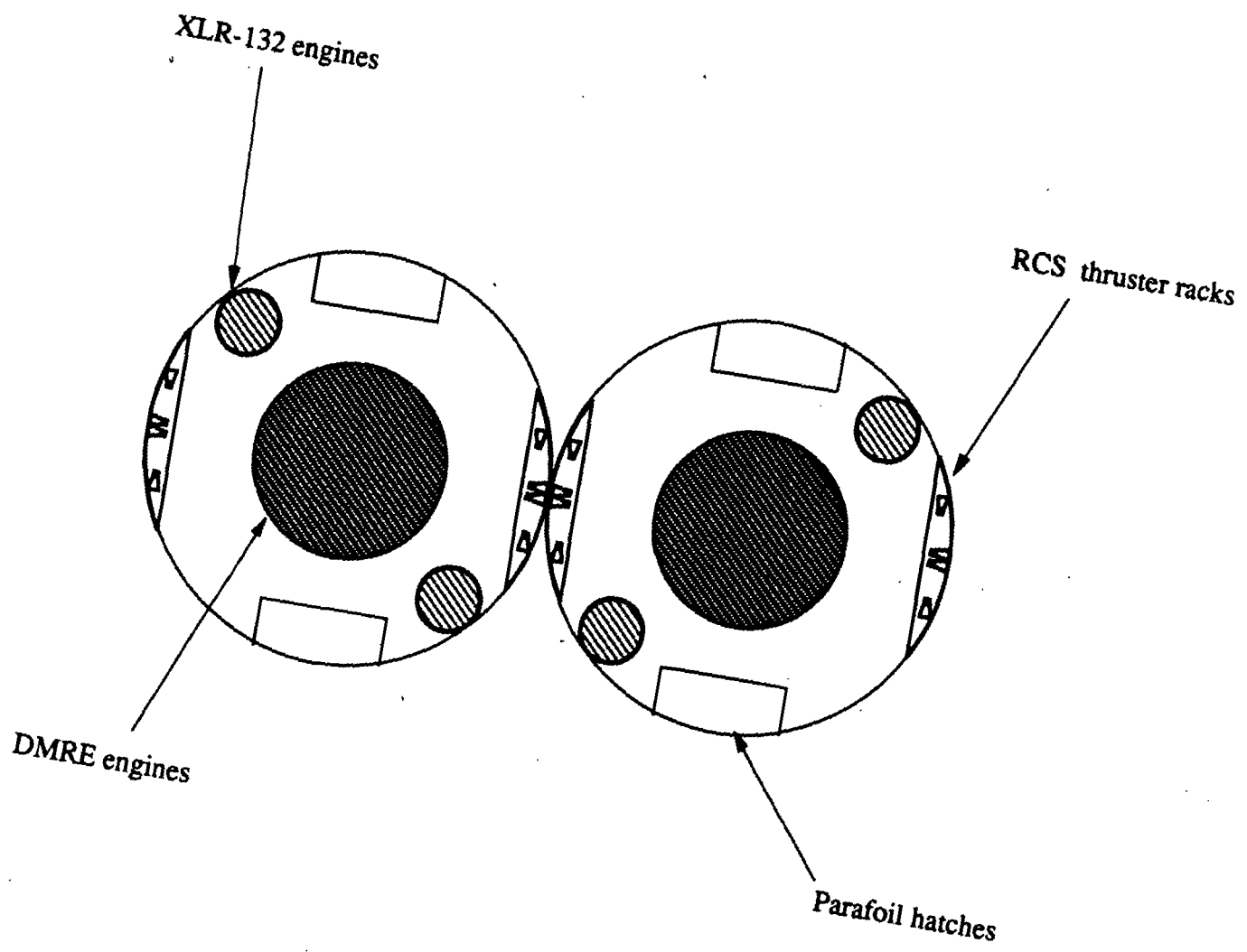
Fig. 3.4a. Antares II propulsion system configuration.

XLR-132 engines

RCS thruster racks

DMRE engines

Parafoil hatches
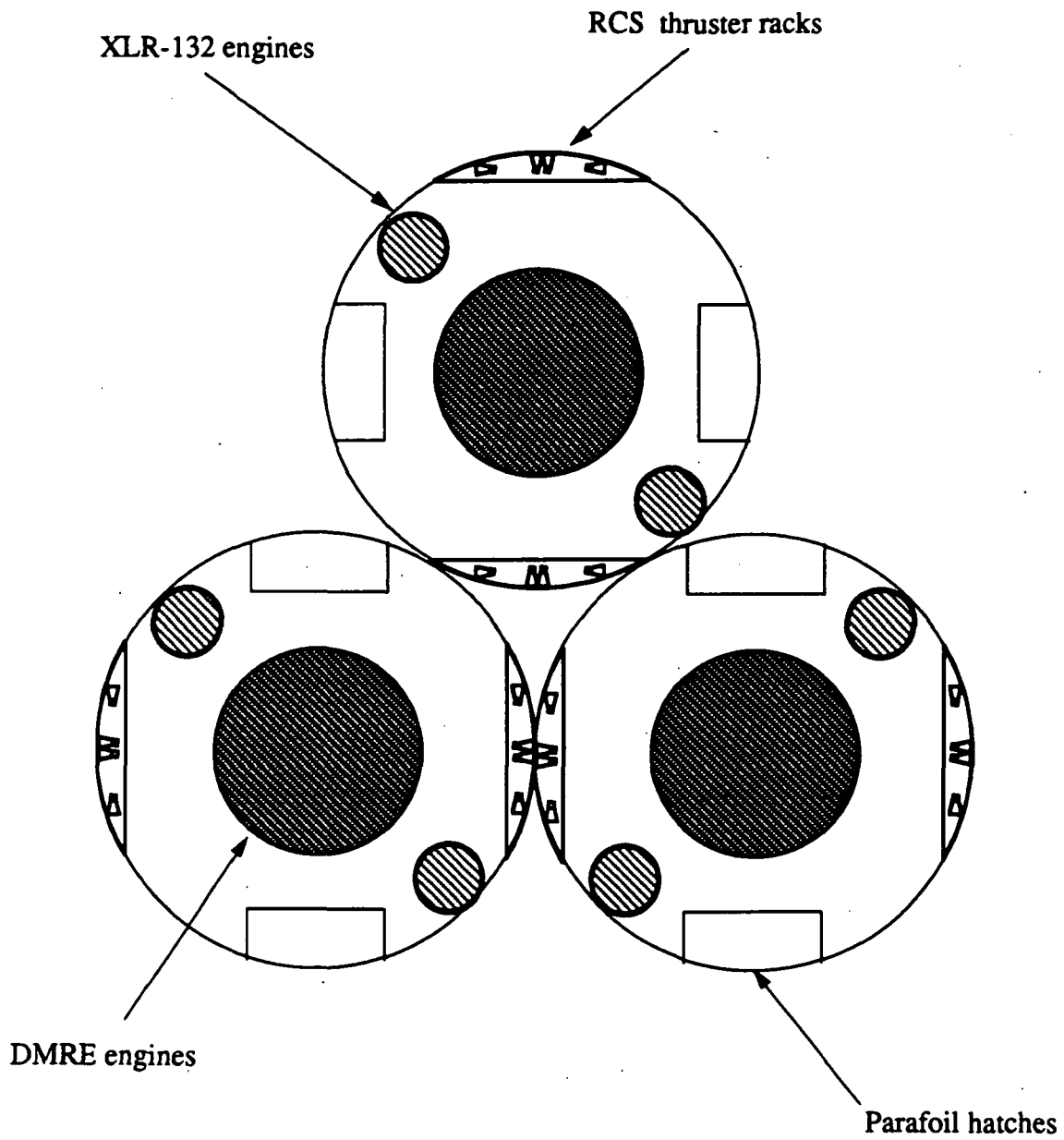
Fig. 3.4b. Antares III propulsion system configuration.

RCS thruster racks

XLR-132 engines

DMRE engines

Parafoil hatches
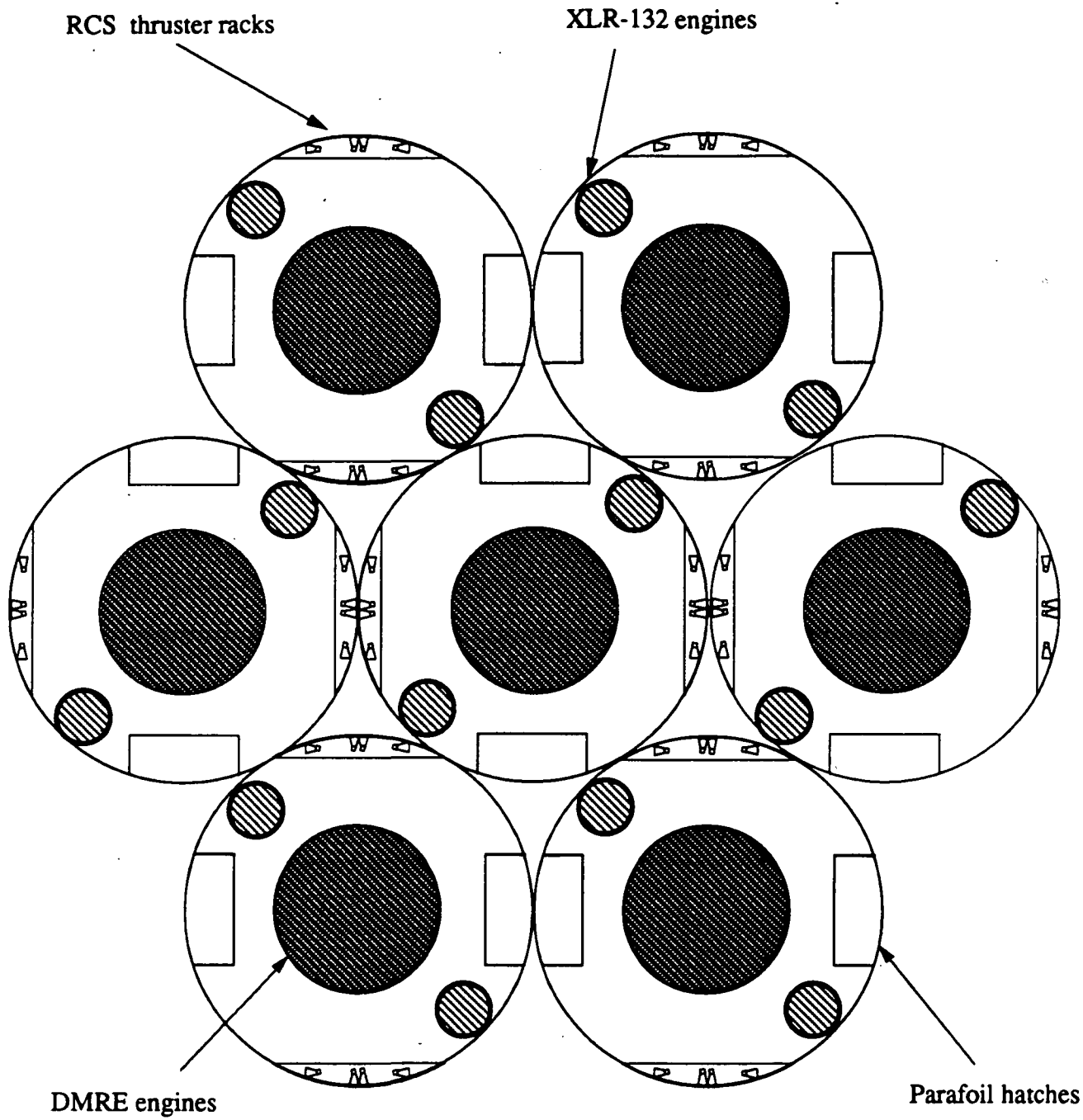
Fig. 3.4c. Antares VII propulsion system configuration.
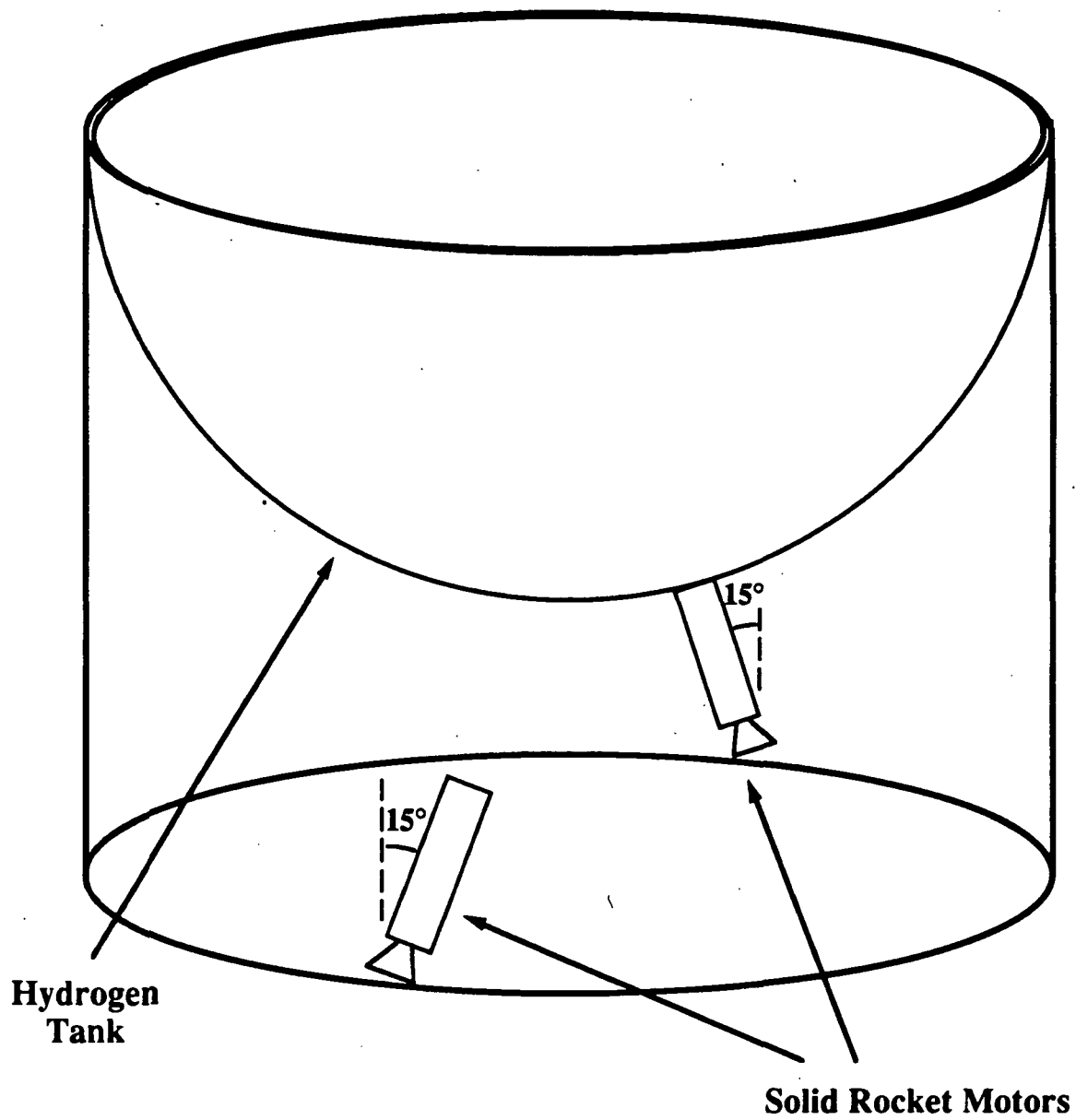
Fig. 3.7. Mounting of solid rocket motors in tank structure.
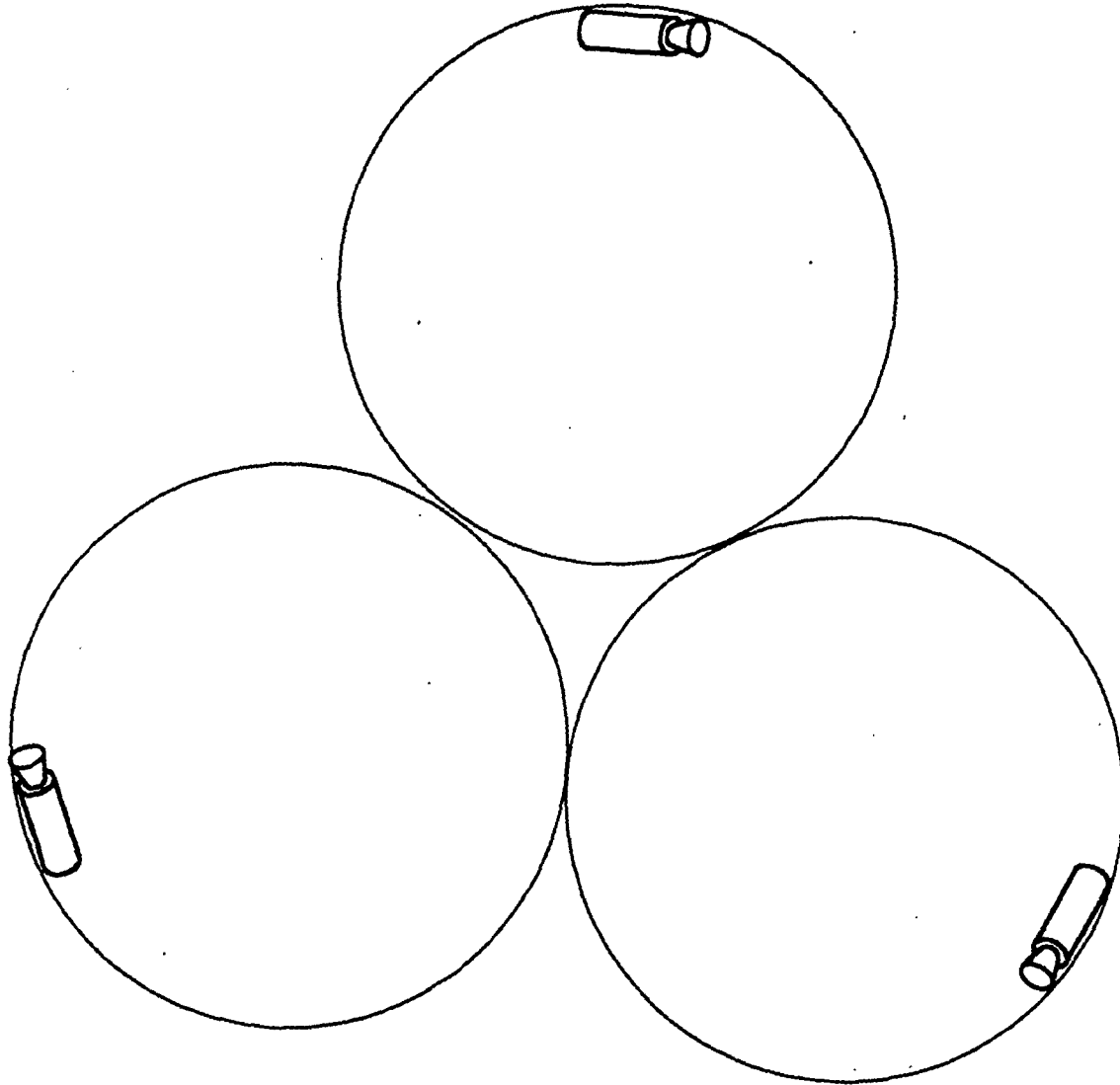
Fig. 3.8. Antares III solid rocket motor configuration.
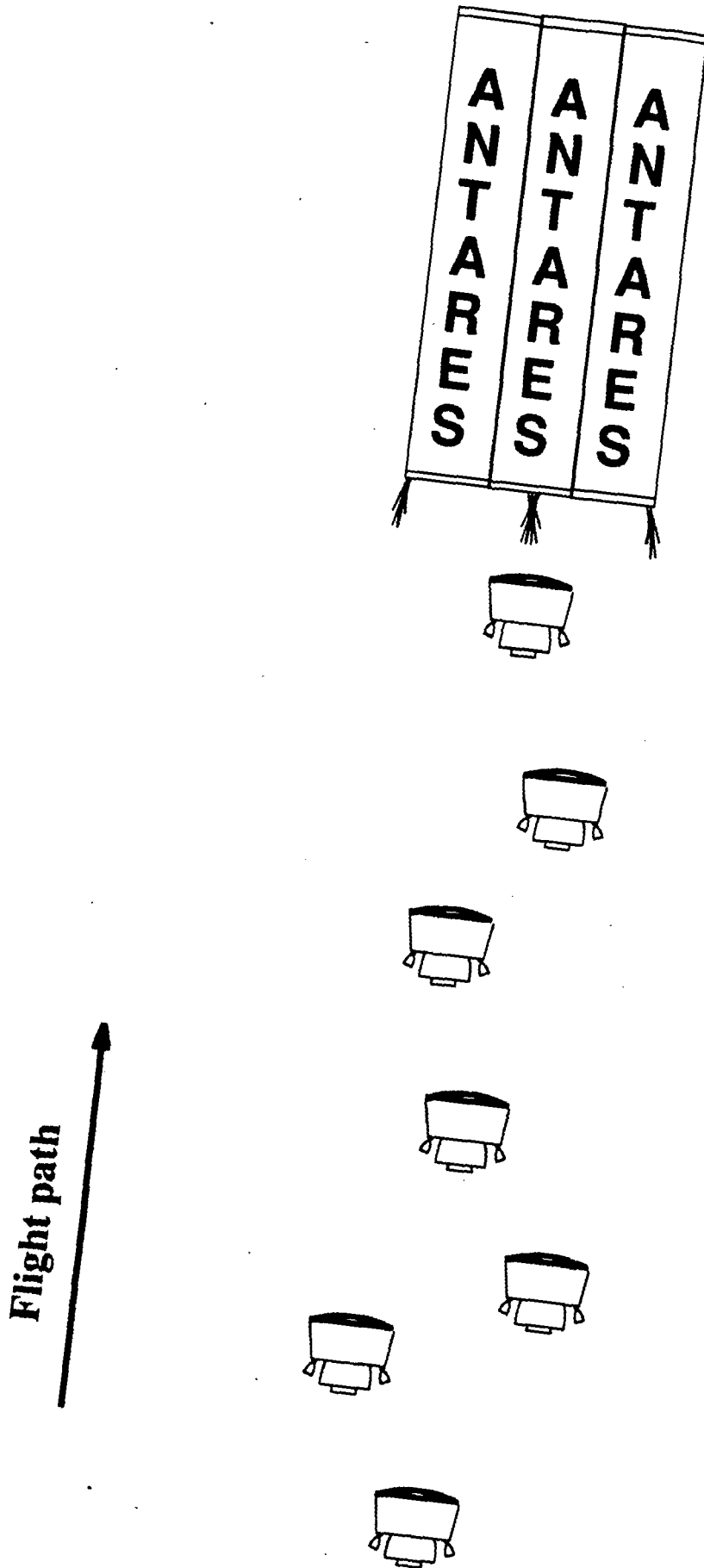
Fig. 3.9. Sequential ERU separation in Antares VII mission.

Flight path

**UPPER TENSILE STRUTS**

- Titanium tubing
- Inner diameter = 10.0 cm
- Outer diameter = 11.1 cm
- Length = 2.82 m

**LOWER COMPRESSIVE STRUTS**

- Titanium tubing
- Inner diameter = 6.0 cm
- Outer diameter = 12.6 cm
- Length = 2.23 m

- Total thrust frame mass = 391 kg.

Gimbal
Attach
Point

2.82 m

2.23 m
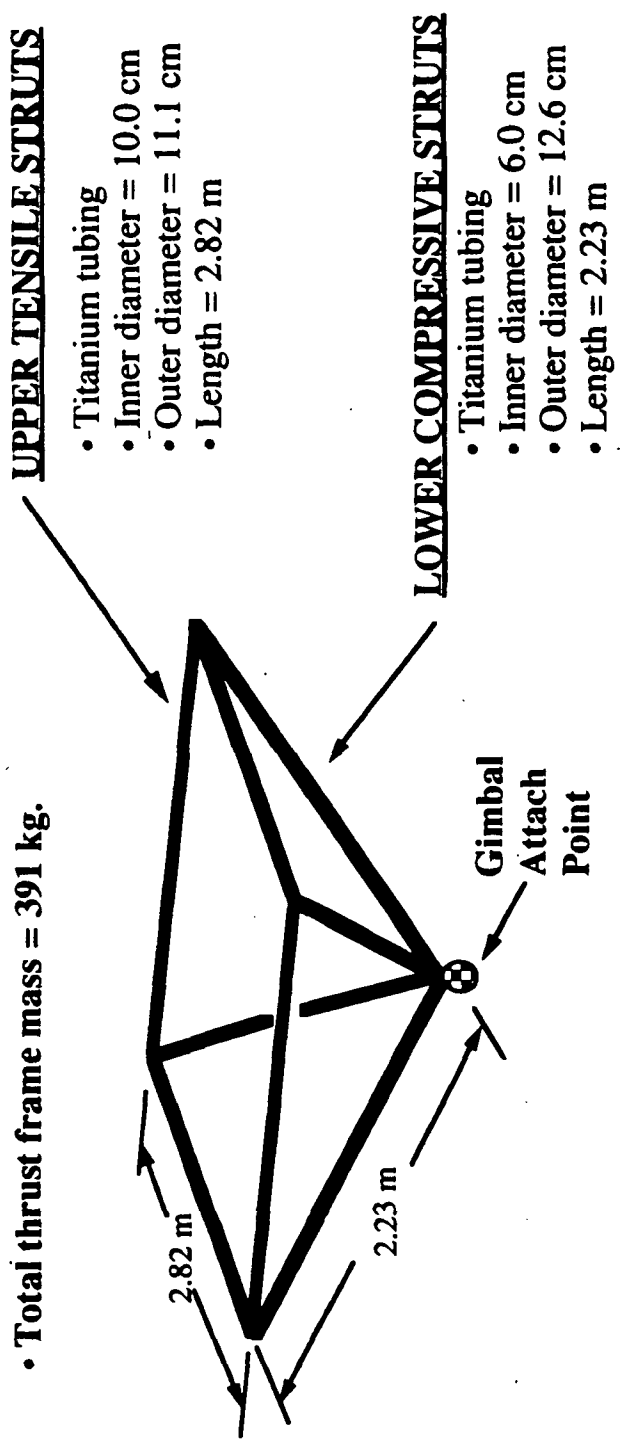
Fig. 3.10. Main thrust frame.

**Main Thrust Frame**
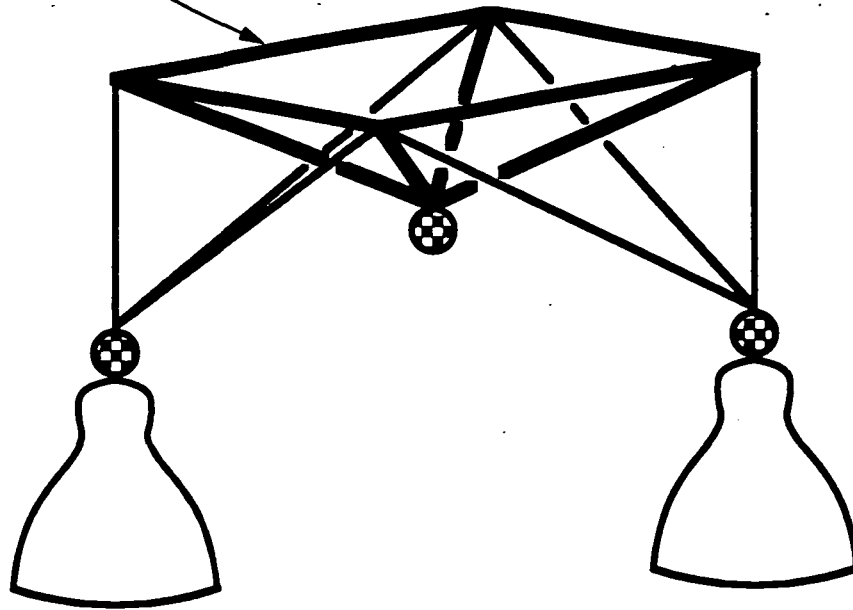
PODS thrust frame connected to DMRE thrust frame

4 m

2.7 m

4.826 m
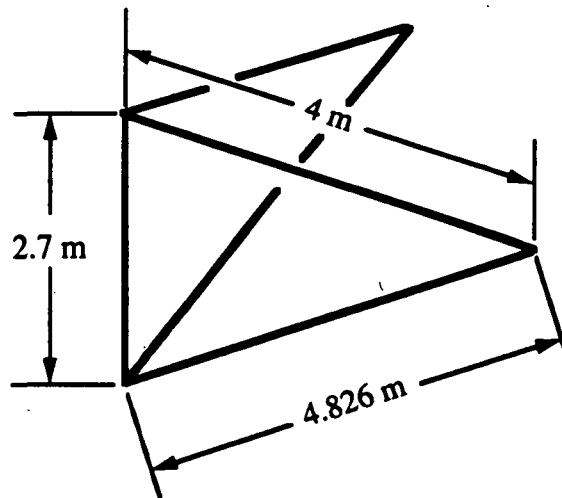
PODS thrust frame dimensions

Fig. 3.11. PODS thrust frame.
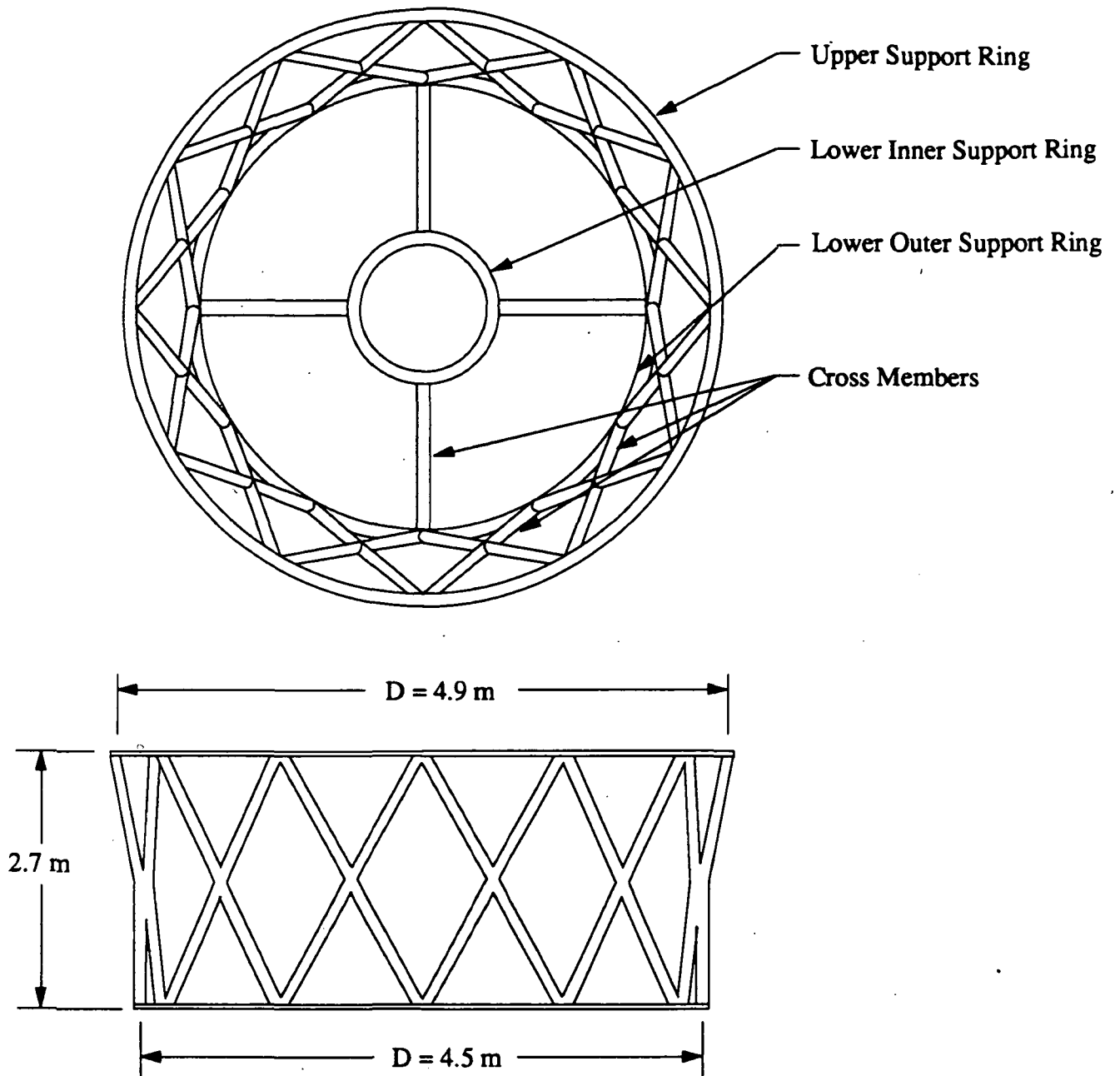
Fig. 3.12. Schematic of Engine Return Unit (ERU) internal framing.

ERU STRUCTURE
MEMBER

RIVET

FASTENER
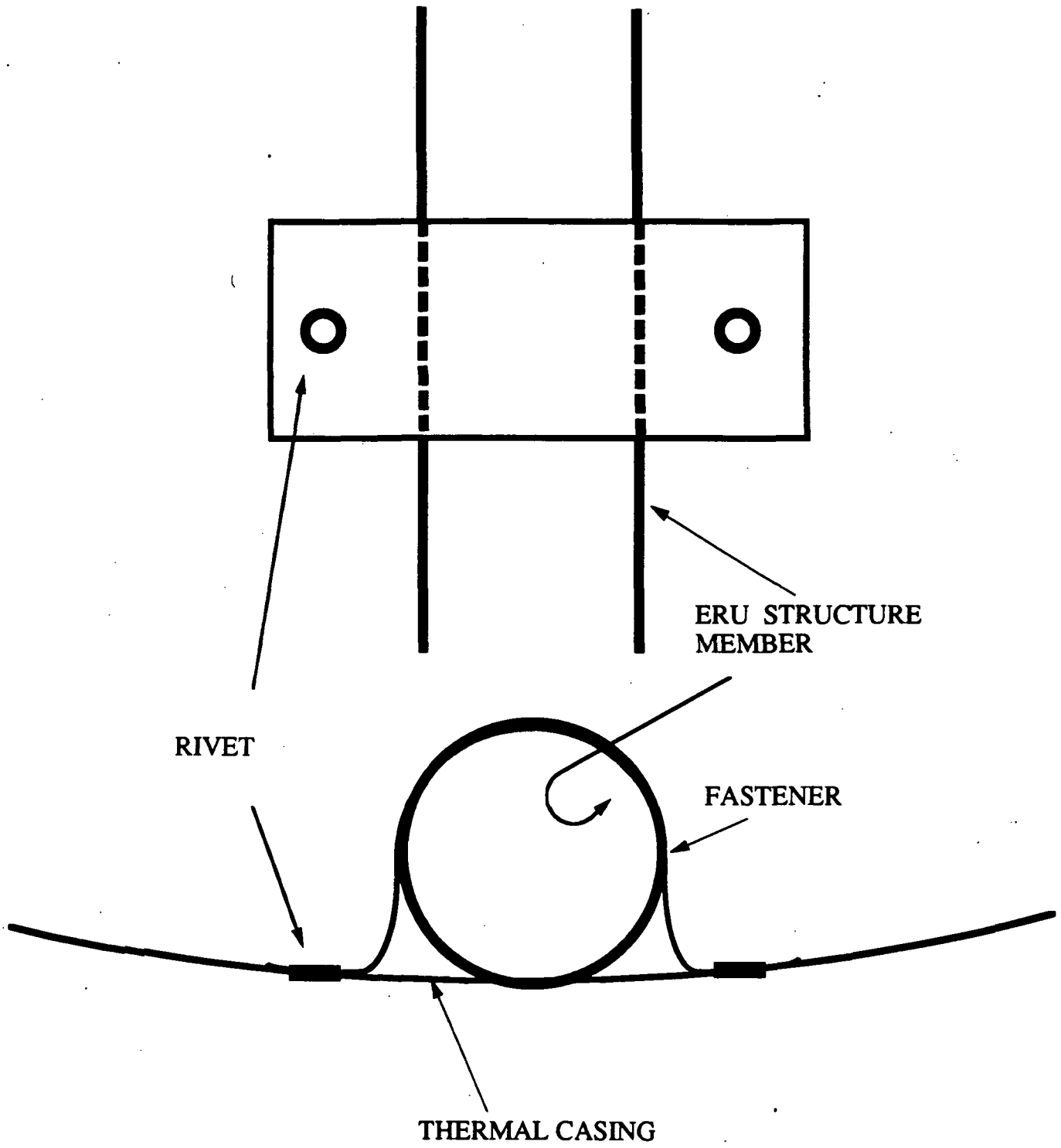
THERMAL CASING

Fig. 3.13. Thermal casing support.

90

C-2

Explosive Bolt

Carbon-Carbon
Ablator

Replaceable Bolt Sleeve

Titanium
Substraite

Thrust Frame

Attachment
Block

Access Hatch

Detonation
system
plug in

Access
Channel
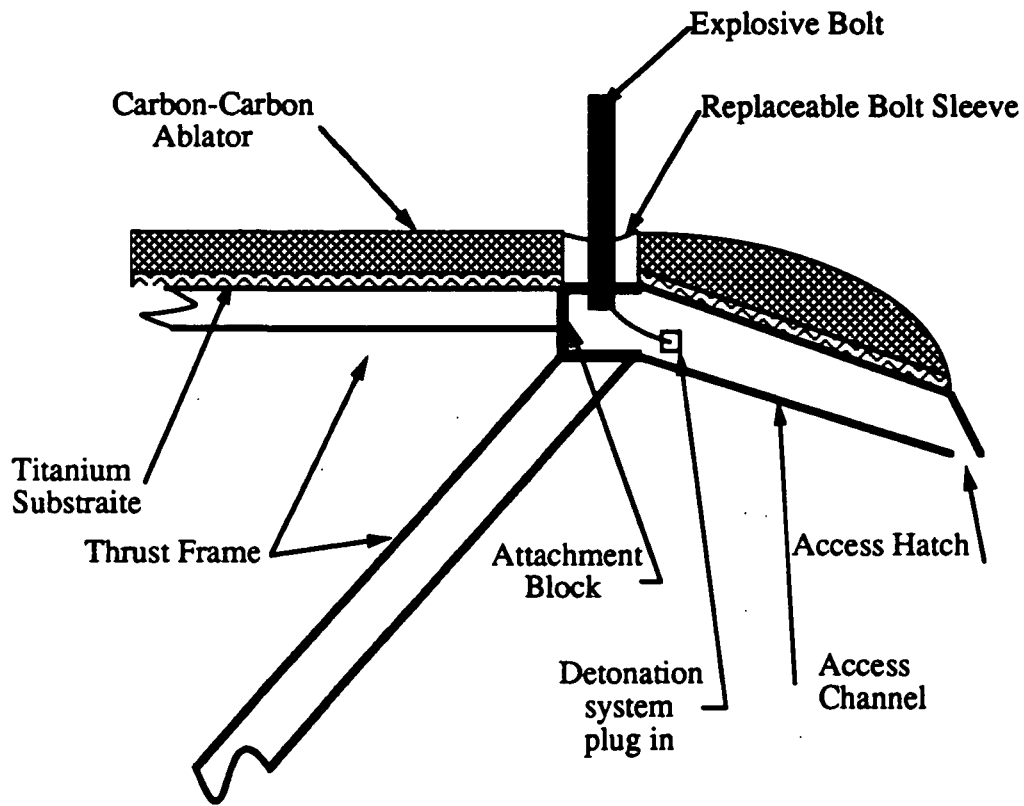
Not to scale to show component layout more clearly.

Fig. 3.14. Separation system side view.

5.0 cm

0.2 m

0.2 m

2.0 cm

0.2 m

Material:
Titanium

a) Attachment block.

0.2 m

0.2 m

0.5 m

Material:
Titanium

5 mm

b) Access channel.

Bolt Hole

Carbon-Carbon
Ablator

3.0 cm

Aluminum
Casing

0.2 m

c) Replaceable bolt sleeve.

Fig. 3.15. Separation system components.

92

Thrust Frame
(end view)

ERU Side

Propellant
Line
Coupling

Release Solenoid

Door

Door
Tracks

Break
Plane

Spring

Door
Lock

Flexible
Propellant
Line

Spring

Propellant Access Housing
(Aluminum)
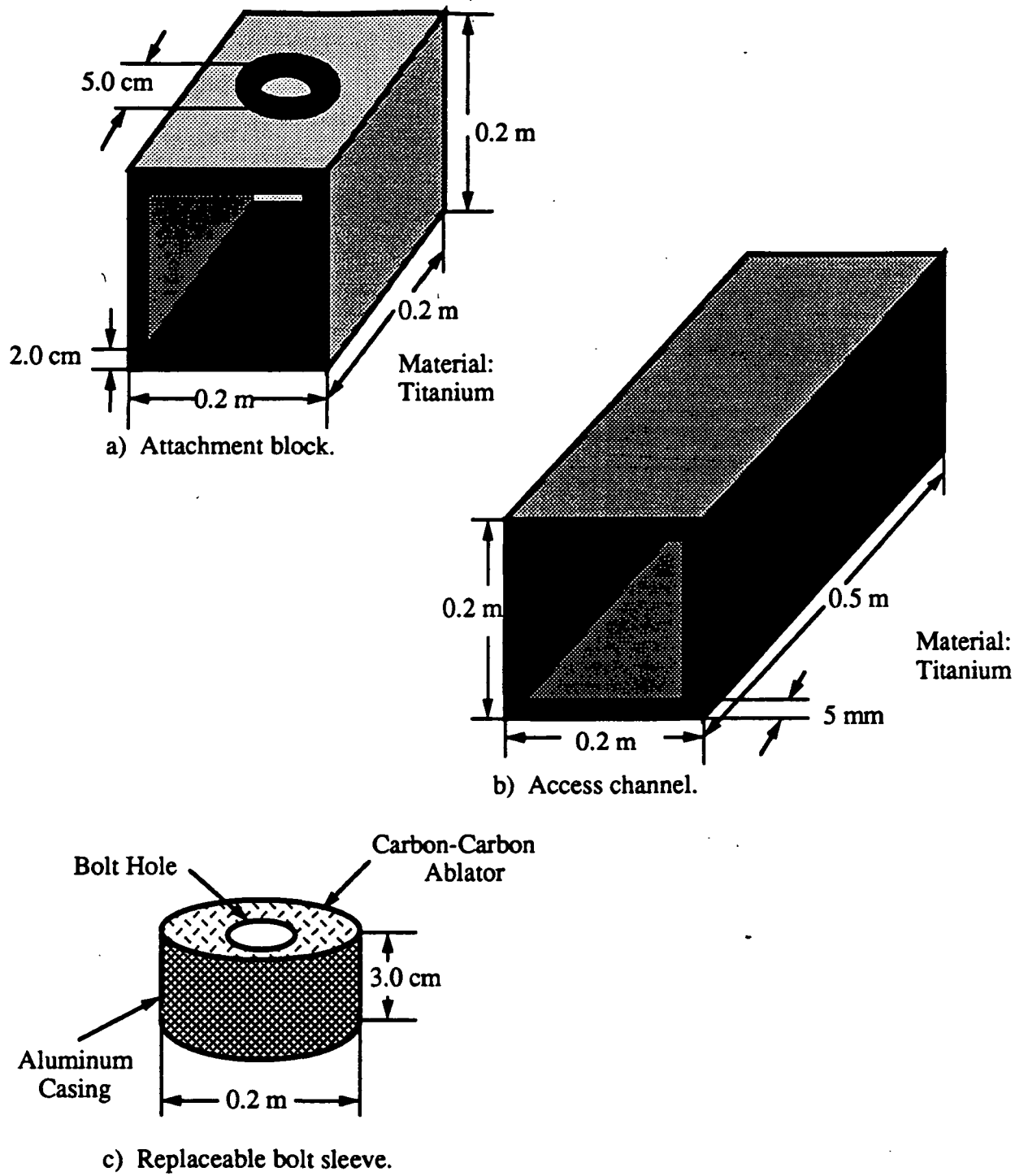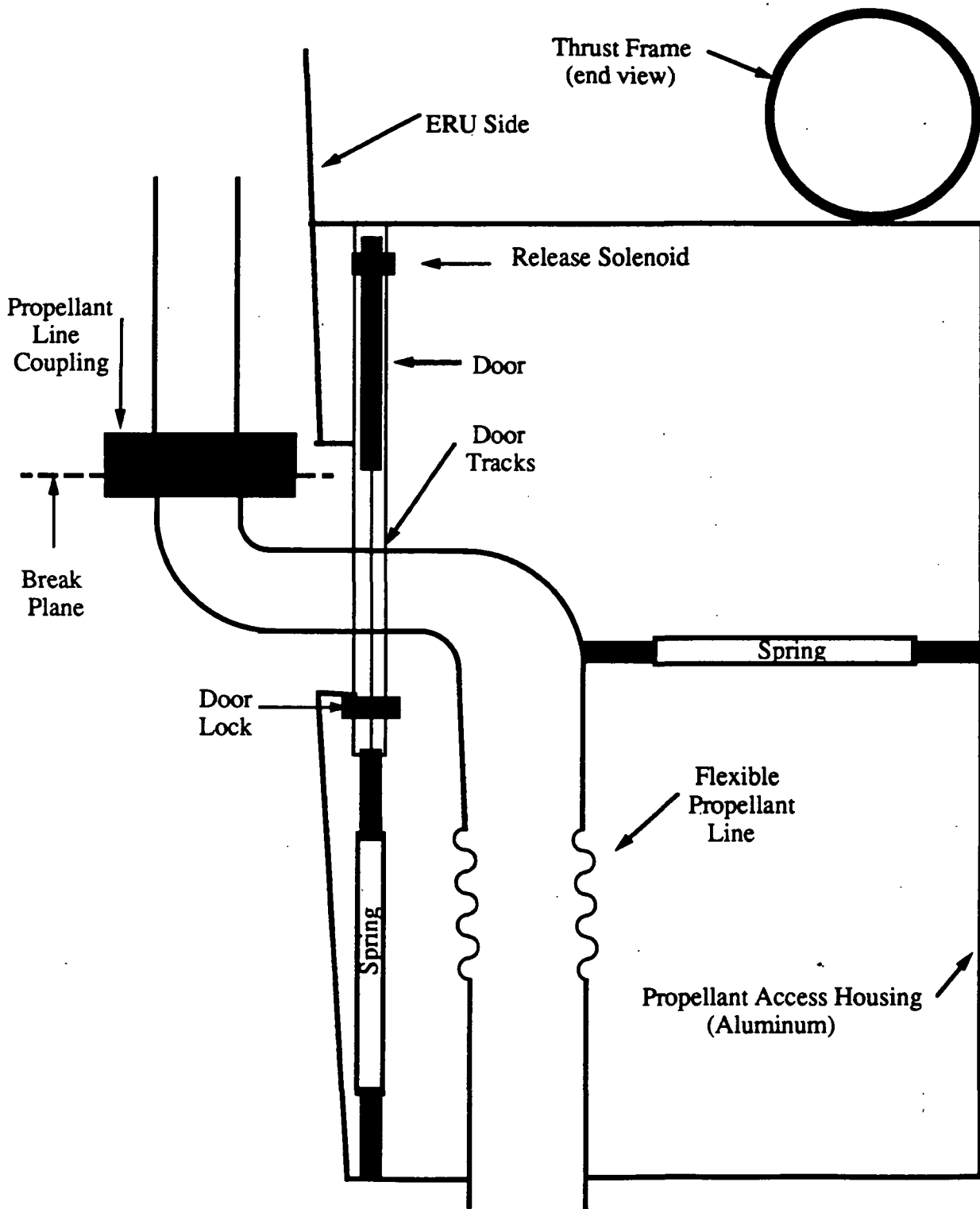
Fig. 3.16. Propellant inlet compartment.
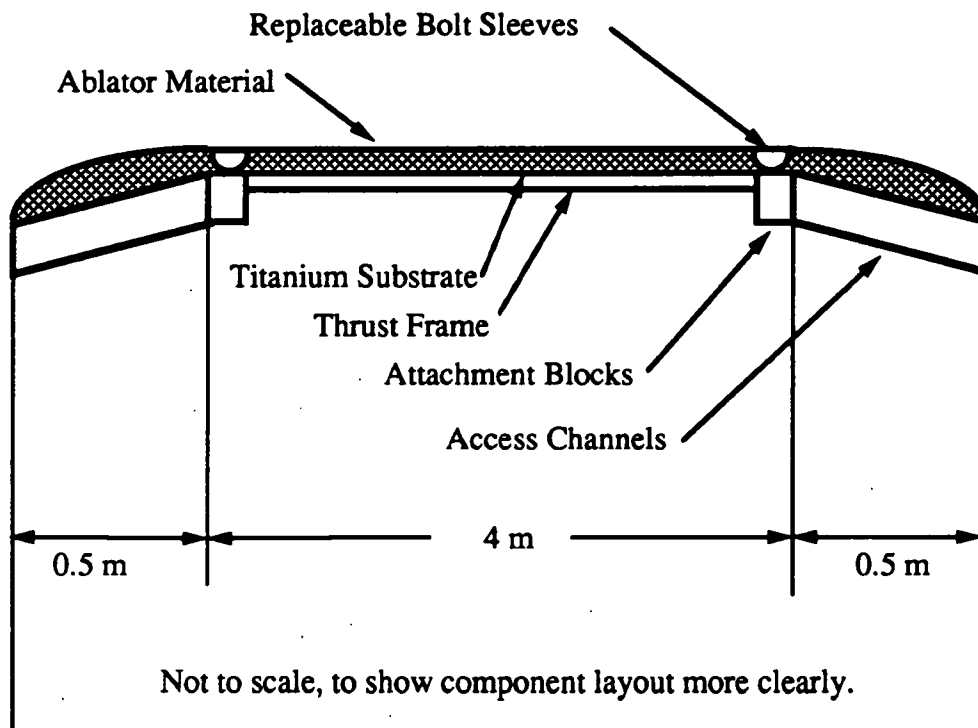
Fig. 3.17. Schematic of Engine Return Unit (ERU) heat shield.

The figure contains the following labels:
- Replaceable Bolt Sleeves
- Ablator Material
- Titanium Substrate
- Thrust Frame
- Attachment Blocks
- Access Channels
- 0.5 m
- 4 m
- 0.5 m
- Not to scale, to show component layout more clearly.

-Drogue parachute deployed to slow vehicle and provide stability.
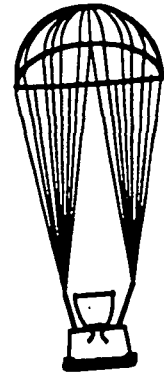
**AREA = 400 m$^2$**
**V= 325 m/s**

-Main parafoil deployed.
Initial high wing loading
to penetrate winds.
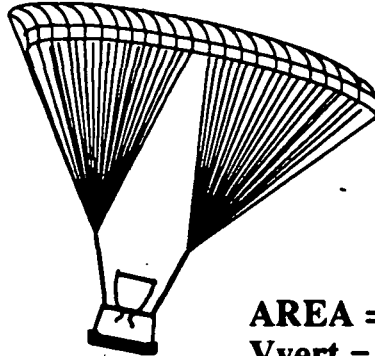
**AREA = 390 m$^2$ (70%)**
**Vvert = 11 m/s**
**Vhor = 25 m/s**
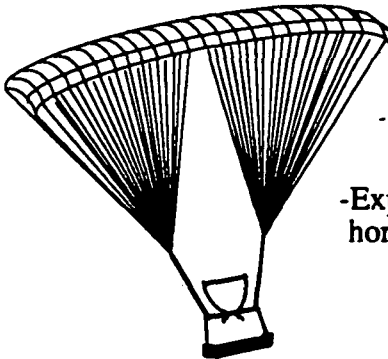
-Expand to low wing loading configuration to reduce
horizontal and vertical velocities for landing.

**AREA = 490 m$^2$ (100%)**
**Vvert = 5m/s**
**Vhor = 17 m/s**

-Dynamic flare reduces touchdown velocities
by rapid trailing edge retraction.
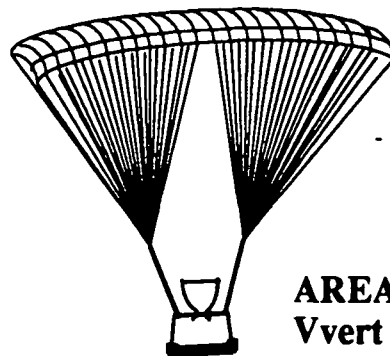
**AREA = 490 m$^2$**
**Vvert = 3.8 m/s**
**Vhor = 14.3 m/s**

Fig. 3.18. ERU descent profile.

# 4.0 PROPELLANT TANKS

The Antares propellant tanks are light, strong, and self-supporting. The light structure is desired to maximize payload capabilities and is achieved by keeping the wall thickness as low as possible and incorporating a common wall bulkhead between the two tanks. The minimum mass of the structure is limited by the tank's ability to withstand various combinations of applied loads prior to launch and during ascent. The relationship between the encountered loads and the ability of the tanks to support these loads determines the structural mass of the tanks. The ability of the tanks to support these combinations of forces and moments is determined by the overall tank strength. The high strength of the thin-walled tanks is achieved by utilizing skin stringers and support rings. In order to ease ground operations the tanks are self-supporting and do not require internal pressurization for their structural integrity.

## 4.1  TANK COMPONENTS AND DIMENSIONS
(David Woodson)

The Antares propellant tanks, illustrated in Fig.4.1, include one oxidizer tank ($140\ m^3$) containing liquid oxygen (LOX), and one fuel tank ($290\ m^3$) containing liquid hydrogen ($LH_2$). The tanks have a maximum capacity of 160,000 kg of $LH_2$ and 19,700 kg of LOX. Figure 4.2 shows the relative size of the Antares propellant tanks compared with the Space Shuttle's external tank, which is also a LOX / $LH_2$ system. A key aspect to the Antares tanks that distinguishes it from the external tank, besides the size, is the intertank structure. The oxidizer and fuel tanks are separated by an evacuated honeycomb common wall bulkhead (Fig. 4.3). The oxidizer and fuel tanks have stiffening rings and stringers located on the inside of the shell walls (Fig. 4.4). The LOX tank has 3 rings spaced 1.9 m apart, while the longer $LH_2$ tank has 8 rings spaced at 2.1 m intervals. Both tanks have 24 stringers evenly spaced running axially along the tank wall. The rings and stringers increase the stiffness and the strength of the tank wall, while adding minimal mass. The rings also serve as baffles to prevent liquid

**PRECEDING PAGE BLANK NOT FILMED**

sloshing (See Section 4.6). Other components included in the tank structure are the insulation for the propellant tanks, and the propellant lines (Fig. 4.5).

## 4.2 TANK ORIENTATION
(David Woodson)

The orientation of the oxidizer and fuel tanks for a liquid hydrogen/oxygen propellant system is determined by the location of the center of mass. The liquid oxygen ($\rho$ = 1400 kg/m$^3$) is placed above the liquid hydrogen ($\rho$ = 70 kg/m$^3$), to keep the center of mass as far forward as possible to minimize aerodynamic stability problems (Fig. 4.1). Unfortunately, the amount of liquid oxygen required is over eight times more massive than the required amount of liquid hydrogen . Therefore the liquid hydrogen tank is designed to be stronger, and heavier, so that it can support the loads imposed by a full liquid oxygen tank.

## 4.3 TANK MATERIAL
(Curt Cartwright)

The material used for the propellant tanks must meet several requirements. A low density material is needed to reduce structural mass, therefore maximizing the payload mass. High strength is also important because the tank walls are the primary load bearing structure of the Antares vehicle. The material also has to maintain its properties at low temperatures. This is because the liquid hydrogen and liquid oxygen will be in direct contact with the tank walls, therefore, the material will be at 20° K in the LH$_2$, and 80° K in the LOX tank. Material cost also needs to be considered. To obtain lower costs, the material must be readily available, and easy to fabricate.

In-depth studies by industry to determine the optimal material to meet these requirements have led to the choice of Aluminum Alloy 2219 for liquid oxygen and hydrogen tanks. This is the material used on the Space Shuttle's External Tank, Japan's H-II launch vehicle, and the core module of the Ariane 5 booster [1]· The primary advantage of Al 2219 is its outstanding properties at cryogenic temperatures. Not only does it maintain ductility, but its

yield strength and ultimate strength both increase by nearly 50% over its room temperature values. It follows that this material was chosen for the Antares' tanks.

## 4.4 TANK ANALYSIS
(David Woodson)

The purpose of the tank analysis is to determine the mass of the structure capable of withstanding the maximum loads encountered by the Antares prior to launch and during ascent. The structural analysis of the propellant tanks is broken down into four separate segments; the strength of the two cylindrical sections, the strength of the hemispherical ends, the strength of the common wall bulkhead (CWB), and the maximum applied loading during launch.

The Antares propellant tank walls are optimized to withstand the various applied moments and forces prior to launch, during launch, and during ascent. The minimum thickness of the tank walls is dependent upon several criteria such as axial rigidity, lateral rigidity, material strength, buckling, and hoop stress. Although all of these criteria will impose limits on the minimum thickness, the minimum buckling load of the cylinders determines the limit on the tank wall thickness. The buckling of the tank walls is a function of the material properties, support ring dimensions, stringer dimensions, wall thickness, dimensions of the tank, and the maximum loads encountered during the launch phase. In order to optimize the mass of the tank walls, the oxidizer and fuel tanks were analyzed separately. Each tank was designed for the minimum thickness capable of withstanding the moments and forces that are applied to that section without buckling or failing. A tank optimization program was developed to determine the mass of the tank structure for the Antares launch vehicle.

### 4.4.1 CYLINDER STRENGTH
(David Woodson)

The strengths of the cylindrical sections of the propellant tanks are determined by calculating the extensional, shear, bending, and coupling stiffness of the structure. These stiffnesses are a function of the dimensions of the cylinder, the rings, the stringers, and the

material properties of Aluminum Alloy 2219. The formulas used to calculate the various stiffnesses of the cylinder are listed below [2]:

Extensional Stiffness:

$$\overline{E}_X = \frac{Et}{1 - \mu^2} + \frac{E_s A_s}{b} \tag{4.1}$$

$$\overline{E}_Y = \frac{Et}{1 - \mu^2} + \frac{E_r A_r}{d} \tag{4.2}$$

$$\overline{E}_{XY} = \frac{\mu Et}{1 - \mu^2} \tag{4.3}$$

Shear Stiffness:

$$\overline{G}_{XY} = \frac{Et}{2(1 + \mu)} \tag{4.4}$$

Bending Stiffness:

$$\overline{D}_X = \frac{Et^3}{12(1 - \mu^2)} + \frac{E_s I_s}{b} + \tilde{z}_s^2 \frac{E_s A_s}{b} \tag{4.5}$$

$$\overline{D}_Y = \frac{Et^3}{12(1 - \mu^2)} + \frac{E_r I_r}{d} + \tilde{z}_r^2 \frac{E_r A_r}{d} \tag{4.6}$$

$$\overline{D}_{XY} = \frac{Et^3}{6(1 + \mu)} + \frac{G_s J_s}{b} + \frac{G_r J_r}{d} \tag{4.7}$$

Coupling Stiffness:

$$\overline{C}_X = \tilde{z}_s \frac{E_s A_s}{b} \tag{4.8}$$

$$\overline{C}_Y = \tilde{z}_r \frac{E_r A_r}{d} \tag{4.9}$$

Once the stiffnesses are determined, the components of the stiffness matrix A are calculated. The A matrix combines the effects of the various stiffnesses and determines the strength of each tank cylinder. The formulas for calculating the A matrix components are listed below.

$$A_{11} = \overline{E}_X \left(\frac{m\pi}{\ell}\right)^2 + \overline{G}_{XY}\left(\frac{n}{r}\right)^2 \tag{4.10}$$

$$A_{22} = \overline{E}_Y \left(\frac{n}{r}\right)^2 + \overline{G}_{XY}\left(\frac{m\pi}{\ell}\right)^2 \tag{4.11}$$

100

$$A_{33} = \overline{D}_X\left(\frac{m\pi}{\ell}\right)^4 + \overline{D}_{XY}\left(\frac{mn\pi}{\ell r}\right)^2 + \overline{D}_Y\left(\frac{n}{r}\right)^4 + \frac{\overline{E}_Y}{r^2} + \frac{2\overline{C}_Y}{r}\left(\frac{n}{r}\right)^2 \quad (4.12)$$

$$A_{12} = A_{21} = \left(\overline{E}_{XY} + \overline{G}_{XY}\right)\frac{m\pi}{\ell}\frac{n}{r} \quad (4.13)$$

$$A_{32} = \frac{\overline{E}_Y}{r}\frac{n}{r} + \overline{C}_Y\left(\frac{n}{r}\right)^3 \quad (4.14)$$

$$A_{13} = \frac{\overline{E}_{XY}}{r}\frac{m\pi}{\ell} + \overline{C}_X\left(\frac{m\pi}{\ell}\right)^3 \quad (4.15)$$

The maximum loads per unit length of the circumference that the cylinder can withstand before failing are determined from the A matrix. The parameters "m" and "n" above represent buckling nodes in two different directions in the thin walls of the tanks. To determine the minimum load that is applied before the structure fails, m is varied until the axial load $N_X$ is at a minimum. In other words, the A matrix is calculated using various integer values of m. The value of m that yields the minimum $N_X$ corresponds to the minimum axial load where the cylinder will buckle.

Axial:

$$N_X = \left(\frac{\ell}{m\pi}\right)^2 \frac{\begin{vmatrix} A_{11} & A_{12} & A_{13} \\ A_{21} & A_{22} & A_{23} \\ A_{31} & A_{32} & A_{33} \end{vmatrix}}{\begin{vmatrix} A_{11} & A_{12} \\ A_{21} & A_{22} \end{vmatrix}} \quad (4.16)$$

Shear:

$$N_{XY} = 0.75N_X \quad (4.17)$$

Lateral:

$$N_Y = \frac{r^2}{n^2} \frac{\begin{vmatrix} A_{11} & A_{12} & A_{13} \\ A_{21} & A_{22} & A_{23} \\ A_{31} & A_{32} & A_{33} \end{vmatrix}}{\begin{vmatrix} A_{11} & A_{12} \\ A_{21} & A_{22} \end{vmatrix}} \quad (4.19)$$

The axial, shear and lateral loads represent the critical buckling load of the cylindrical sections. For example, if an applied axial load exceeds the minimum axial strength load then the cylinder will buckle. To take into account combinations of loads a straightforward relation is used [2].

$$R_c + R_b < 1 \qquad (4.20)$$

Where $R_c$ is the ratio of applied compression loads to the minimum axial strength, and $R_b$ is the ratio of applied bending moments to the minimum allowable shear loads. Knowing the applied lateral and axial loads, and having calculated the strength of the tank using the equations above, the stability of the tank can be determined. The cylindrical sections of the Antares booster are designed for a combination of bending and axial loads such that:

$$R_c + R_b = 0.9. \qquad (4.21)$$

### 4.4.2 HEMISPHERICAL TANK END STRENGTH
(David Woodson)

The rear end of the liquid hydrogen tank must be able to withstand the forces imposed from the propellants located above it. The forward end of the oxidizer tank must withstand the internal pressure of the liquid oxygen tank. The thicknesses of both hemispherical ends are comparable to the thicknesses used for the first stage of the Saturn V rocket, which was a far more massive vehicle than the Antares [3]. The thickness of the liquid oxygen tank end is 2 mm, while that of the liquid hydrogen tank end is 5 mm.

### 4.4.3 COMMON WALL BULKHEAD (CWB)
(David Woodson)

One of the areas where weight is saved is the interface between the liquid hydrogen and liquid oxygen tanks. The top of the fuel tank is concave, while the bottom of the oxidizer tank is convex (Fig. 4.3). Since the radius of each tank is the same, the fuel tank can be attached directly to the bottom of the oxidizer tank. The two tanks combine together to form a common wall bulkhead. The bulkhead consists of two hemispherical sheets of Aluminum 2219 that form a sandwich around a honeycomb core. The core is evacuated to minimize the heat flux

from the liquid oxygen to the liquid hydrogen. The skin panels are 3 mm thick, while the core has a thickness of 2 cm.

## 4.5 LOADS ANALYSIS
(David Woodson)

Various loading cases have been considered in order to determine the maximum loads that are applied on the Antares during various intervals of the launch phase. Some of the cases examined are: fully loaded Antares on launch pad, internal loads at maximum dynamic pressure, and shear loading due to strong winds at maximum dynamic pressure. Loading analysis is done separately for the tank wall, hemispherical ends, and the CWB. The walls of the propellant tanks undergo loads generated by internal pressure, axial loads, and bending moments. The aft hemispherical end has loads imposed from acceleration forces due to the liquid hydrogen. The CWB experiences loadings similar to the hemispherical ends but is also subjected to failure loads created by the pressure difference between the two tanks.

## 4.6 SLOSHING
(David Woodson, Jon Upham)

Liquid sloshing in the fuel and oxidizer tanks is induced by the various forces that are exerted on the booster. Ground winds before launching, axial and lateral excitation from engine thrust, and flight maneuvers all contribute to liquid sloshing [4]. If sloshing is not controlled, bending moments upon the booster and induced dynamic instabilities will increase. The dynamic instabilities are due to the coupling of sloshing with control motions. Sloshing can be controlled by the placement of anti-slosh baffles within the fuel and oxidizer tanks. The design of slosh baffles is dependent upon the frequency of the sloshing liquid, which is dependent upon the geometry and volume of the tank. In practice, the size and number of slosh baffles are determined experimentally and vary for every launch vehicle. Slosh baffles are a necessity for the Antares booster, but their actual design cannot be determined until the propellant tanks have been constructed and sloshing frequencies have been determined.

Presently, the support rings located in the cylindrical sections of the tanks act as slosh baffles. An estimate of the mass of the slosh baffles has been made to calculate structural mass.

## 4.7 INSULATION AND HEAT TRANSFER
(Bruce Detert)

There are three basic types of insulation used in cryogenic containers. The first type is a high vacuum, which may be augmented with radiation shields to reduce heat transfer by radiation. This type of insulation has the lowest effective conductivity, but it is expensive to manufacture and a high vacuum can be difficult to maintain for extended periods. The second type of insulation is powder insulation, which works on the principle of reducing conduction by maintaining a high vacuum between the particles of the powder. The need for a high vacuum again makes this type of insulation impractical.

The third type of insulation is foam. Polyurethane foam insulation was chosen for the Antares vehicles because of its low conductivity (0.036 W /m-K), its simple production, and its low density (46 kg/m$^3$) [5]. Polyurethane foam insulation can be sprayed on the tanks for easy application. This makes the vehicle less likely to have thermal leaks because the insulation can be applied in large continuous sections. Polyurethane foam insulation can also be made structurally durable, so that it can withstand the forces of high speed flight.

The conductivity of a foam can increase by a factor of three or four if its cells are permeated with gaseous hydrogen, therefore the insulation must be placed on the outside of the aluminum walls of the tank. As a design criterion for calculating the amount of insulation needed for the propellant tanks, it was assumed that the tanks are filled with propellant just at its boiling point. It was also assumed that the vehicle would sit on the ground and be refilled continuously until takeoff. The vehicle was assumed to spend a maximum of three minutes in flight in the atmosphere. During this time 0.5% of the propellant would be allowed to boil off. To meet the design criteria, the insulation of the liquid hydrogen tanks must be 10 mm thick

and the insulation of the liquid oxygen tank must be 5 mm thick. The total mass of the insulation is 125 kg.

## 4.8 PROPELLANT LINES
(David Woodson)

The propellant lines for the Antares booster run along the outside of the vehicle as shown in Fig. 4.5. The external propellant line simplifies the inspection of the tanks and fuel lines, and eases the manifolding process needed for multiple modular configurations. The Antares has one liquid hydrogen line and one liquid oxygen line constructed of Inconel 718 [5]. The oxidizer line, having an initial flow rate of 694 kg/sec, has an inside diameter of 10 cm, a wall thickness of 3 mm, and a length of 17 m, transfers LOX to the ERU at a flow speed of 62 m/s. The $LH_2$ line, which has the same cross-sectional area as the LOX line, has a length of only 3 m. Figure 4.5 illustrates how the fuel and oxidizer lines are connected to the tanks and the engine return unit. The fuel and oxidizer lines are insulated with polyurethane foam in order to maintain the cryogenic liquids at their low temperatures as they are pumped into the engine. The estimated combined mass of the propellant lines is 200 kg.

## 4.9 ALTERNATIVE TANK WALL DESIGN
(Curt Cartwright)

As an alternative to stringers and stiffeners, the tank walls of the Antares booster can be made from a honeycomb sandwich. Sandwich construction consists of two thin sheets separated by a lightweight core as shown in Fig. 4.6 [6]. Common facing materials are aluminum, titanium, stainless steel, and reinforced plastic laminate. The honeycomb can also be made from various metals. The face sheets are designed to take axial loads, while the core maintains shear loads. This closely resembles an I-beam. The design of the tank using a honeycomb sandwich must meet five conditions.

• The face sheets must be able to withstand compressive stresses.

• The cylinder walls must resist local buckling.

- The core must have a high enough compressive strength to prevent wall wrinkling.

- The honeycomb cells must be small enough to prevent dimpling of the face sheets.

- The entire cylinder must not buckle as a long column.

With the honeycomb sandwich design, there are several variables that can be adjusted to help meet these requirements. These are:

- Material used for the face sheets.

- Material used for the honeycomb core.

- Thickness of each face sheet. (They need not be the same).

- Thickness of material used in honeycomb core.

- Depth of the core. (Distance between face sheets).

- Size of honeycomb cells.

A honeycomb sandwich design may significantly reduce structural mass. However, it has its limitations. The bond between the core and the face sheets may fail at cryogenic temperatures. Also, these cryogenic temperatures will effectively create a vacuum between the face sheets by condensing the air in between. This will subject the core to high loads caused by the pressure difference. Finally, fabrication of honeycomb material is much more costly than a semi-monocoque structure. Therefore, the semi-monocoque structure with Al 2219 was chosen for preliminary design.

## 4.10   CONCLUSION

The propellant tanks are designed with the hydrogen tank below the oxygen tank and a common wall bulkhead separating the two tanks. The oxidizer and fuel tanks are constructed of Aluminum 2219 and have a wall thickness of 2 and 2.2 mm respectively. The tank structure is 23.5 m long, and has a constant diameter of 5 m. The propellant tanks are stiffened with rings and stringers and thus are self-supporting and do not need to be internally pressurized in order to maintain their structural integrity. An overall schematic of the Antares propellant tanks is shown in Fig. 4.7. The liquid oxygen tank is pressurized to 8.8 atm while the liquid

hydrogen tank is pressurized to 2.4 atm. The propellent tanks are insulated with polyurethane foam 10 mm thick for the liquid hydrogen tank and 5 mm for the liquid oxygen tank. The fuel and oxidizer are transferred to the engine return unit via external lines, constructed of Inconel 718, that have an I.D. of 10 cm. The mass of the complete tank system, including a mass estimation for slosh baffles, is 4200 kg. The breakdown of the mass of each tank component is listed in Table 4.1.

Table 4.1 Tank component structural mass.

| Component | Mass(kg) |
| --- | --- |
| Liquid Oxygen Tank | |
| • Cylindrical Section | 335 |
| • Hemispherical End | 220 |
| • Stiffening Rings | 100 |
| • Stringers | 70 |
| Liquid Hydrogen Tank | |
| • Cylindrical Section | 1440 |
| • Hemispherical end | 440 |
| • Stiffening Rings | 440 |
| • Stringers | 280 |
| Common Wall Bulkhead | 550 |
| Propellant Lines | 200 |
| Insulation | 125 |
| TOTAL TANK STRUCTURAL MASS | 4200 |

## 4.11 NOMENCLATURE

| | |
|---|---|
| A | Cross-sectional area |
| $A_r, A_s$ | Stiffener and ring area, respectively |
| b | Stiffener spacing |
| $\bar{C}_X, \bar{C}_Y$ | Coupling constants |
| $\bar{D}_X, \bar{D}_Y$ | Bending Stiffness per unit circumference of wall |
| $\bar{D}_{XY}$ | Modified twisting stiffness |
| d | Ring spacing |
| E | Young's modulus |
| $E_r, E_s$ | Young's modulus of ring and stiffeners |
| $\bar{E}_X, \bar{E}_Y, \bar{E}_{XY}$ | Extensional stiffness of wall |
| G | Shear modulus |
| $G_s, G_r$ | Shear modulus of stiffeners and rings |
| $\bar{G}_{XY}$ | Shear stiffness of wall |
| $I_r, I_s$ | Moment of inertia of rings and stiffeners about the centroid |
| $J_r, J_s$ | Beam torsion constant of rings and stiffeners |
| $\ell$ | Cylinder length |
| m | Number of buckle half waves in the axial direction |
| $N_X$ | Axial load per unit width of circumference for cylinder subjected to axial compression |
| $N_Y$ | Circumferential load per unit width of circumference for cylinder subjected to lateral pressure |
| $N_{XY}$ | Shear load per unit width of circumference for cylinder subjected to torsion |
| n | Number of buckle waves in the circumferential direction |
| $R_b$ | Ratio of bending moment on cylinder subjected to more than one type of loading to the allowable bending moment for the cylinder when subjected only to bending |

| $R_c$ | Ratio of axial load in cylinder subjected to more than one type of loading to the allowable axial load for the cylinder when subjected only to axial compression |
| --- | --- |
| $r$ | Radius of cylinder |
| $t$ | Skin thickness of isotropic cylinder |
| $\tilde{z}_s, \tilde{z}_r$ | Distance of centroid of stiffeners and rings, respectively, from reference surface (positive when stiffeners or rings are on outside) |
| $\mu$ | Poisson's ratio |

## 4.12  REFERENCES

1.  Eto, T. and Shibato, Y., "The Status of H-II Rocket Development Program," Fifteenth International Symposium on Space Technology and Science, Tokyo, Japan, 1986, pp. 1404.

2.  Anonymous, Buckling of Thin-Walled Circular Cylinders, NASA SP-8007, 1968.

3.  Anonymous, Liquid Rocket Metal Tanks and Tank Components, NASA SP-8088, 1974.

4.  Hellebrand, E.A., "Structural Analysis," pp. 22.36 - 22.41 in Handbook of Astronautical Engineering, Koelle, H.H., ed.,McGraw-Hill Book Co. Inc., New York, 1961.

5.  Williamson, K.D. Jr., et al, "Cryogenics," in Marks' Handbook for Mechanical Engineers Avallone, E.A., and Baumeister III, T., eds., McGraw-Hill Book Co. Inc., New York, 1978.

6.  Bruhn, E.F., Analysis and Design of Flight Vehicle Structures, McGraw-Hill Book Co. Inc., New York, 1965, pp C12.1-C12.52.

LIQUID OXYGEN TANK

Volume: 140 m$^3$
Mass of LOX: 160,000 kg
Thickness: 2.0 mm

LIQUID HYDROGEN TANK

Volume: 290 m$^3$
Mass of LH2: 19,700 kg
Thickness: 2.2 mm

GEO ANTARES

LEO ANTARES
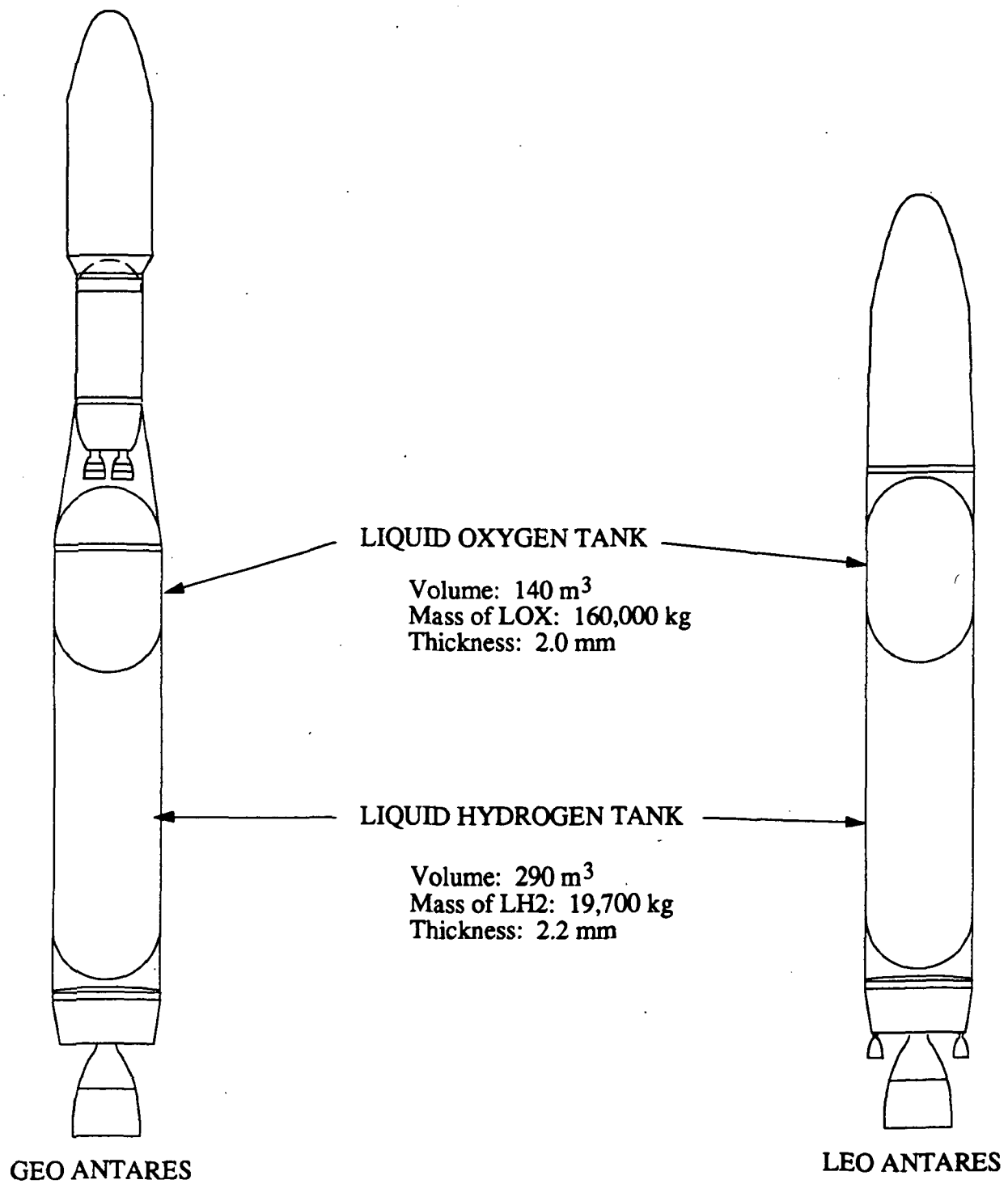
Fig. 4.1. Antares propellant tank orientation and dimensions.

111

8.7 m

LOX

47 m

LH$_2$

5 m

23.5 m

LOX

LH$_2$
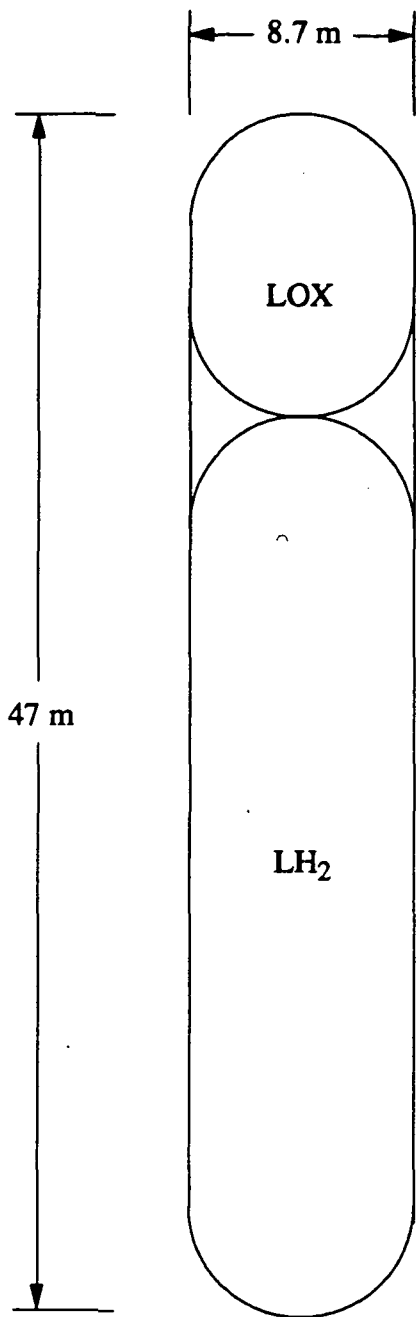
SPACE SHUTTLE
EXTERNAL TANK

ANTARES PROPELLANT
TANKS

Propellant Mass: 703,000 kg

Propellant Mass: 179,708 kg

Fig. 4.2. Comparison of the Antares propellant tanks with the Space Shuttle's External Tank.

EVACUATED HONEYCOMB SANDWICH

LOX

LH2

Fig. 4.3. Common wall bulkhead.

25 mm

STRINGER CROSS-SECTION

25 mm

4 mm

STRINGER ORIENTATION - TOP VIEW

STRINGERS

RINGS

25 mm $LH_2$ RING CROSS-SECTION

50 mm

15 mm LOX RING CROSS-SECTION

50 mm
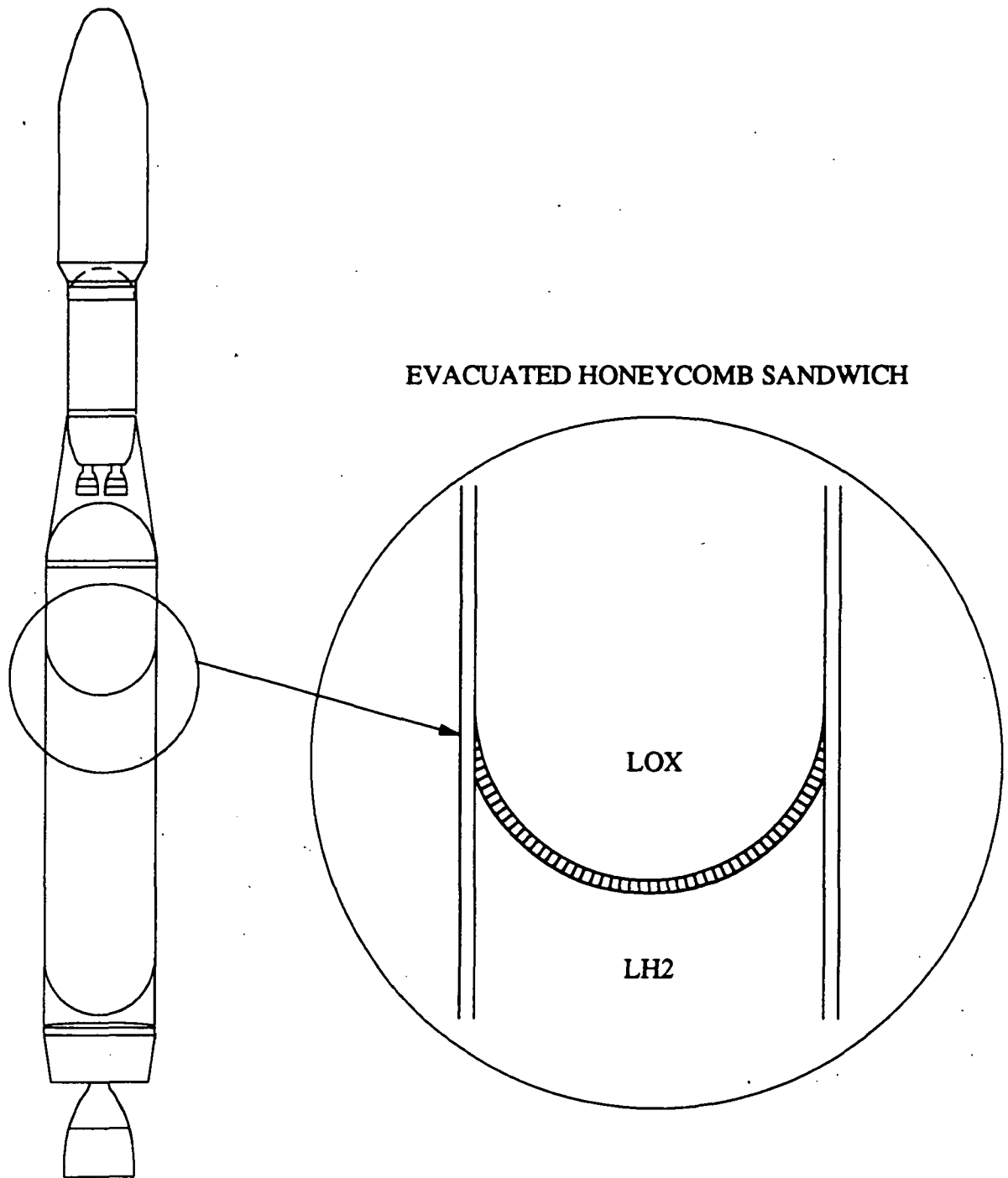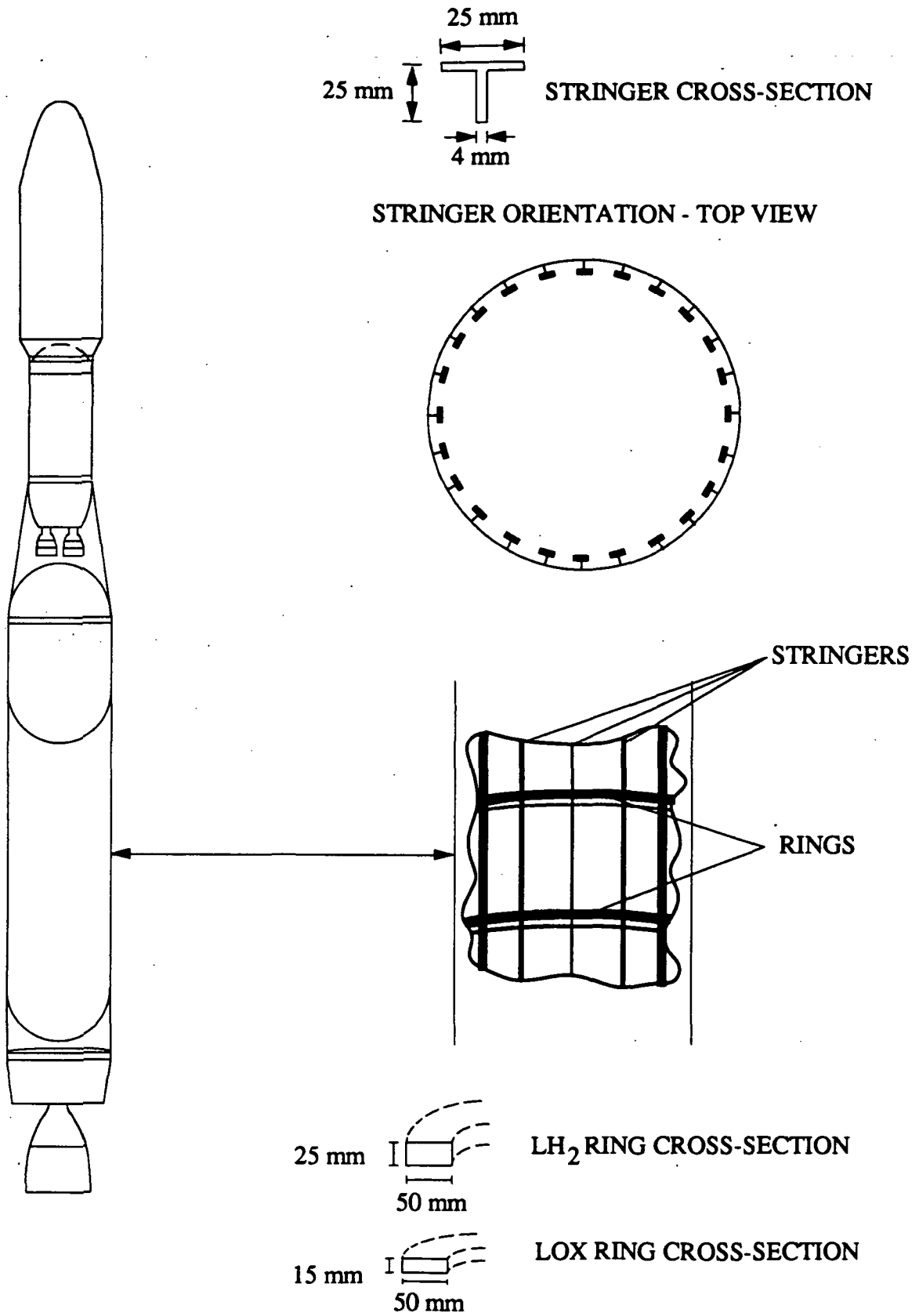
Fig. 4.4. Antares skin-stringers and support rings.

LOX

10 cm

Polyurethane Foam

Inconel 718

Propellant Flow

LH2

Propellant Line

LH2

ERU

ERU
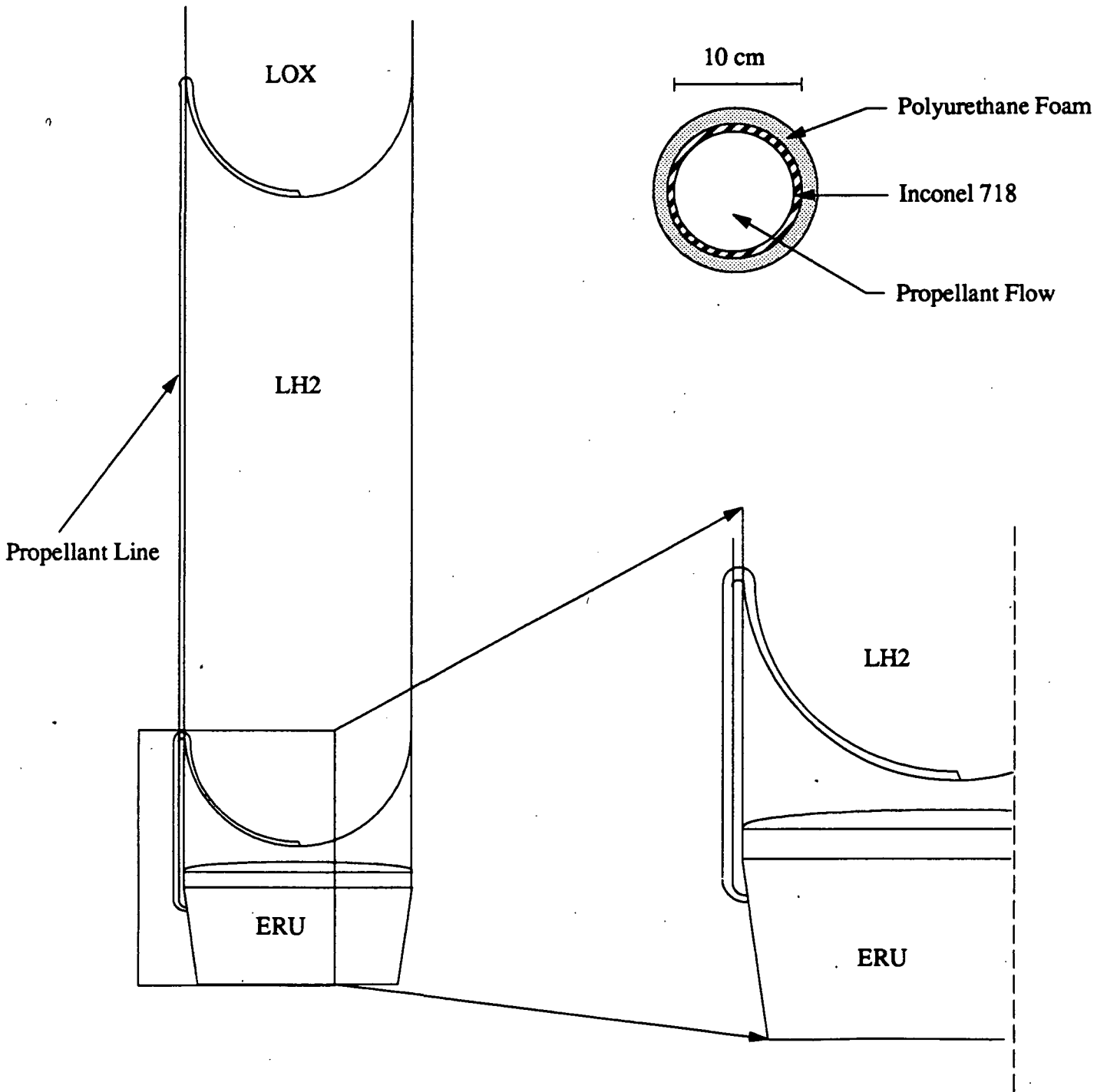
Fig. 4.5. Schematic of Antares propellant lines.

Cross-section of Sandwich Structure

Face Sheet

Honeycomb Core

Face Sheet

Top Cross-section of
Honeycomb Core

Single Ribbon

Fig. 4.6  Honeycomb sandwich.

HARDPOINT ASSEMBLY
LOCATIONS

LOX TANK

COMMON WALL
BULKHEAD

SKIN STRINGERS (24)

SUPPORT RINGS

$LH_2$ TANK

LONGERONS FOR ERU
CONNECTIONS

AFT AERODYNAMIC
FAIRING

ERU

5.0 m

Fig. 4.7. Schematic of Antares propellant tank.

117

# 5.0. STAGE ADAPTERS AND CONNECTIONS
(Steve Solomon)

## 5.1. ERU TO TANK CONNECTION

The main consideration for the connecting structure between the ERU and main tank is to effectively transfer the load between the ERU and the propellant tanks without buckling or failure in shear, while keeping mass to a minimum. Also, the ERU must be able to separate from the main tank upon completion of its mission. The ERU thrust structure transfers the thrust from the main engine to four interface points. From there the load is transferred vertically to four support posts, as shown in Figs. 5.1 and 5.2. A thrust strut is bolted to the top of 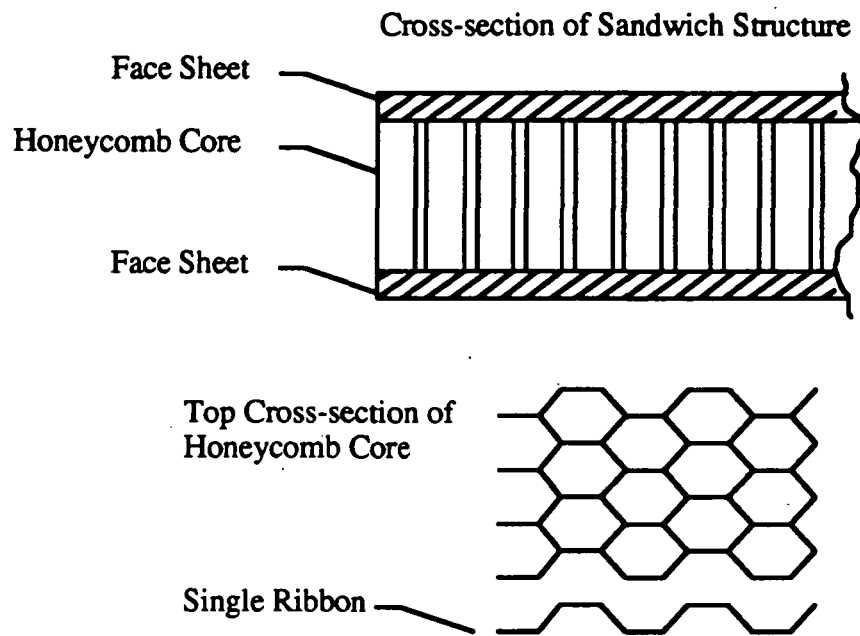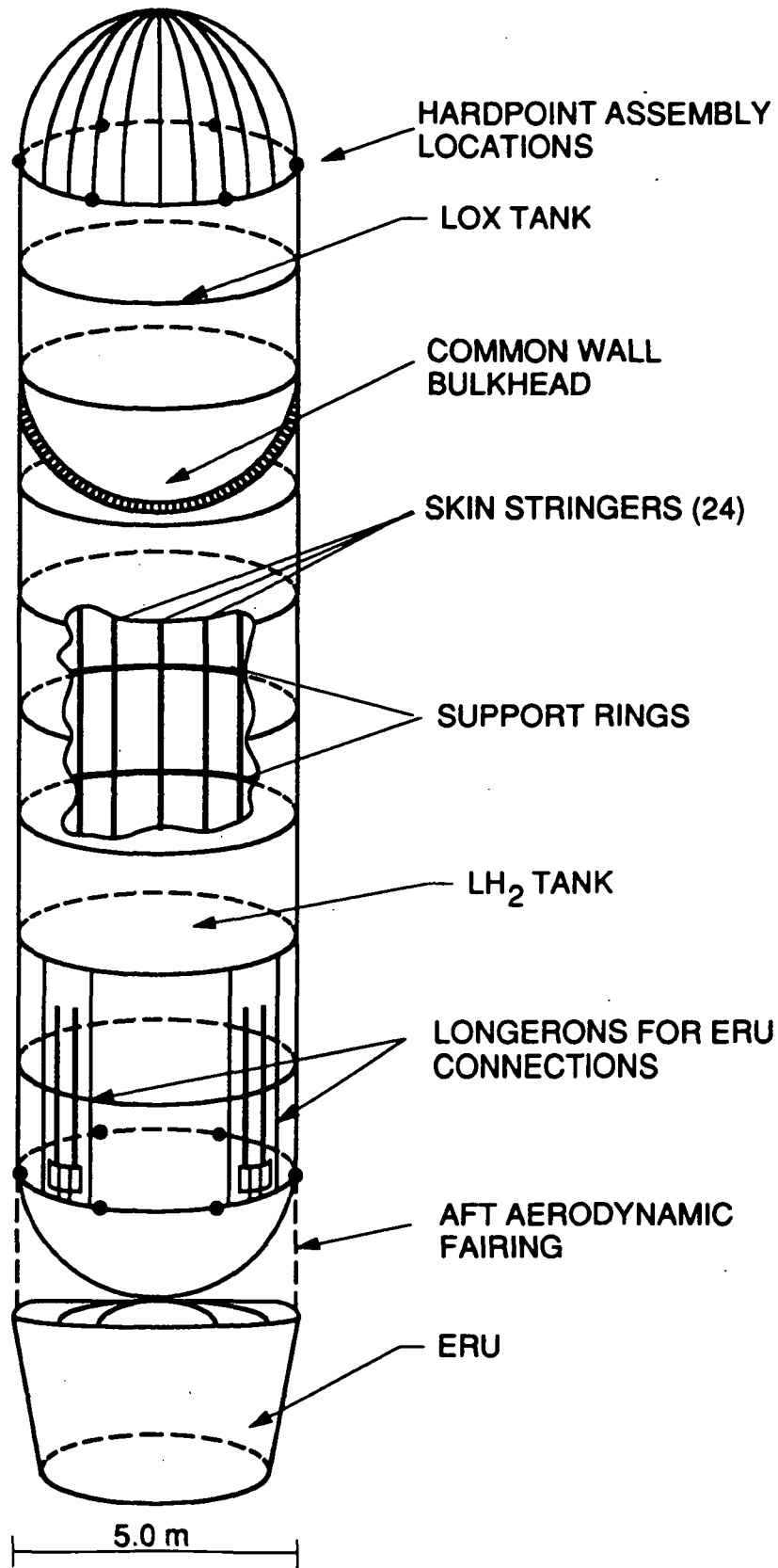each post. The struts are bolted at their top to four longerons that are welded to the bottom sides of the main tank skin, from the lower tank ring vertically to the third ring, and covering two tank stringers (see Fig. 5.1). The support post assembly is held to the ERU structure at the four interface points by four frangible bolts to allow for ERU separation.

### 5.1.1. SUPPORT POST ASSEMBLY (ERU INTERFACE)

Similar in design to the launch pad hold-down system of the Space Shuttle's solid rocket booster, each support post assembly (see Figs. 5.2 and 5.3) consists of a post that transmits axial loads, a spherical bearing to minimize the magnitude of bending induced in the support structures due to loading, and a coil spring to impart a small separation velocity to the ERU. The assembly is joined to the ERU thrust block by the frangible bolt. Each support post is 25 cm tall and has a diameter of 40 cm at the upper flange (Fig. 5.3) Made of 7075-T6 aluminum alloy, it is bell shaped with walls that are 35 mm thick and has a mass of 35 kg. The post tapers from the upper flange to a 15 cm diameter at the bottom, where there is a 90 mm diameter hole taper countersunk to 50.8 mm on the inside to accept the frangible bolt. A 100 mm diameter and 35 mm deep bearing seat is countersunk on the outside bottom to seat the spherical bearing, as shown in Fig. 5.3.

The spherical bearing is hemispherical on one end and has a portion 100 mm diameter x 35 mm high that fits into the bearing seat on the support post as shown in Figs. 5.2 and 5.3. The spherical side has a radius of 50 mm and there is a 50.8 mm diameter hole through the center to allow for the frangible bolt. The bearing is made of 4340 alloy steel and has a mass of 4.5 kg.

The socket has an outside diameter of 16 cm. It is countersunk with a radius of 50 mm on the top side and fits over the ball bearing as shown in Figs 5.2 and 5.3. The opposite side is countersunk 30 mm deep and 125 mm in diameter to seat the separation spring. There is a 50.8 mm hole through the center to pass the frangible bolt. Made of 4340 alloy steel, the socket has a mass 5 kg.

The spring is 125 mm in diameter and fully compressed between the socket and a raised nub on the ERU thrust block (dashed lines on spring in Fig. 5.3); its mass is 5 kg. The steel spring is designed to provide enough force on separation to give the ERU sufficient velocity to clear the main tank stage; the spring is released upon detonation of the frangible bolt. Any flying debris resulting from the explosive severing of the frangible bolt is contained by a dome shaped steel debris catcher mounted on the ERU and a crushable honeycomb bolt stop block on the inside of the support post (see Fig 5.3).

## 5.1.2 THE FRANGIBLE BOLT

The ERU must be able to separate from the tank section upon completion of its mission. To achieve separation frangible bolts are used [10]. These are made of AISI 4340 alloy steel and have a mass of 5.5 kg each. They are 50.8 mm in diameter at the stem and 300 mm long. There is a 25.4 mm diameter hollow core to contain the explosive charge and an internal projectile ( see Fig 5.4 ). The criterion for determining bolt dimensions and material was the tensile stress the alloy would have to endure holding the ERU and main tank sections together. For the given dimensions the axial stress each bolt experiences is well below the ultimate tensile stress (UTS) of 10.5 MN/m$^2$ of the alloy. The bolt is inserted through the

bottom of the ERU interface and secured by the bolt cap (nut) inside the support post. At the time of separation an internal explosive charge fires a projectile down the hollow core of the bolt. The projectile creates high stress concentrations at a frangible section of the bolt ( i.e. at impact about mid-bolt ) breaking it and allowing ERU/tank separation

## 5.1.3 THRUST STRUTS

The thrust struts are steel sections (including main strut, elbow, shim and end fitting) that when joined, transmit the engine thrust load to the longerons and to the Antares' tank section (see Fig. 5.5). The main load bearing strut is tubular AISI 4340 steel in axial compression. The thrust strut assembly combined with the support post assembly make a two force member with the spherical bearing on the lower end and a pinned monoball bearing at the longeron connection, as shown in Fig. 5.5. The thrust strut has an O.D. of 104 mm and an I.D. of 100 mm and a length of 1.7 m. Thicker walls at the elbow section of the strut assembly are necessitated by the bending loads at this point. The mass of one strut assembly is 50 kg. The main criterion for optimizing the strut dimensions (for maximum strength and minimum mass) were Euler buckling and localized cylinder buckling: An axial thrust load of 880 kN (engine thrust + 4 x 1.25 safety factor + cos19°) must be transmitted through each strut. The assembly's elbow section is flared to a 40 cm O.D. flange and is bolted to the support post. At the top, the strut is pinned to an integral joint at the lower end of each longeron by a 100 mm steel shear pin through a 145 mm monoball, as shown in Fig. 5.5. The monoball ensures that the transmitted load is uniaxial along the strut's axis.

The elbow section of the strut assembly also provides a fitting for the crossmember (Fig.5.5). The crossmembers are circular aluminum bars of 20 mm diameter, that are welded to the lower tank ring. Each strut has one crossmember that is oriented at approximately 40° as shown in Figs. 5.1 and 5.5. The purpose of the crossmember is to prevent the ERU from twisting relative to the tank section. Any torque would place the appropriate member in tension and prevent twisting.

### 5.1.4 THE LONGERON

The longerons (Fig. 5.2) are machined from 2219 aluminum alloy forgings to a finished size of 4.2 m long by 1 m wide and a nominal thickness of 6 mm. Each longeron has a mass of 60 kg (front and side views of the longeron are shown in Fig. 5.2). Assembly of the longerons into the aft tank sections is accomplished by fusion butt welding, which is ideal for strength in shear [1]. Four longeron sections are welded into the aft tank skin panels, extending from the lower tank ring vertically to the third tank ring from the bottom and covering two stringers, in order to distribute loads (through shear) transmitted from the thrust end fitting. At the lower tank ring the welds are thicker to handle the horizontal load component transmitted from the thrust strut.

### 5.1.5 AFT TANK SKIRT

The aft tank skirt (Fig. 5.2) is a cylindrical section 5 m in diameter and 3.1 m tall. The assembly is made from welded, corrugated, 2219 aluminum skin panels that are 1 mm thick. The section is fusion welded to the aft tank ring and fitted (not fastened) over the ERU. The total mass of the skirt is 250 kg. The skirt does not transmit any axial loads but rather provides aerodynamic integrity to the lower end of the rocket.

## 5.2 GEO MISSION: UPPER STAGE MODIFICATIONS AND CONNECTIONS

There are three considerations for mounting a Centaur type upper-stage to the Antares vehicle. First, an interstage adapter (ISA) is needed to mount the Centaur on top of the liquid oxygen tank. Then a stub adapter is needed to mount the payload fairing onto the Centaur (see Fig. 5.6). Finally thermal and radiation protection are needed for the exposed Centaur walls for protection during ascent and deep space coast, respectively.

## 5.2.1 INTERSTAGE ADAPTER (ISA)

The ISA allows the Centaur to be mounted on the Antares vehicle, must provide effective load transfer between the two stages, and be tall enough to allow adequate clearance between the Antares LOX tank and the Centaur engines (see Fig. 5.6). Also, the ISA upper interface with the Centaur provides main stage/ upper stage separation hardware. See table 5.1 for ISA data..

## 5.2.2 ISA FORWARD RING/CENTAUR AFT RING INTERFACE

Upon completion of the Antares main engine burn, it is necessary for the upper stage to separate and continue the mission to GEO. This separation will occur at the ISA/Centaur interface (see Fig. 5.7). The ISA forward ring is bolted to the Centaur tank aft ring. A shaped charge (detonation cord) is wrapped around a frangible section of the ISA forward ring, as shown in Fig. 5.7. When ignited, the shaped charge splits this section uniformly around the ring, releasing the upper stage from the main tank section. There is thermal blast protection provided to prevent damage to the Centaur tank [2].

## 5.2.3 STUB ADAPTER

The stub adapter is mounted on top of the Centaur (see Fig 5.6 and Table 5.1). It connects the payload fairing to the Centaur's upper tank assembly and provides the required separation hardware. The adapter also distributes the payload weight evenly to the top of the Centaur [2]. Also provided are flex deflectors, which act as guard rails to prevent the separated nose cone segments from damaging the payload (otherwise, the explosive charge that splits the rails may cause the segments to deform or "flex" and hit the payload when the segments fall away).

## 2.4 CENTAUR INSULATION

Special requirements are necessary to protect the Centaur's exposed walls from aerodynamic heating during ascent and from radiation during deep space coast. This protection is provided by foam insulation enclosed in a 136 kg Kevlar "jacket"[2]. The jacket covers a closed-cell preformed PVC foam insulation as shown in Fig. 5.8. The Kevlar is aluminized for high reflectivity to provide the radiation protection necessary for coast times greater than one-hour (the Centaur was not originally designed for longer coast times).

Table 5.1: Upper Stage Connections

|  | Interstage Adapter | Stub Adapter |
|---|---|---|
| Dimensions | 6.0 m tall<br>3.06 m upper diameter<br>5.0 m lower diameter | 0.635 m tall<br>3.06 m diameter |
| Mass | 1105 kg | 88.5 kg |
| Materials | 2219 Aluminum | 2219 Aluminum |
| Construction | Riveted frame,<br>stringer and skin | Riveted frame,<br>stringer and skin |

## 5.3 REFERENCES

1. Parkman, D., Boeing Defense and Space Group, Seattle, WA, private communications, May, 1991.

2. Lotker, S., General Dynamics, Space System Division, San Diego, CA, private communications, April and May, 1991.

Fig. 5.1 ERU / Main tank connection

126

Antares Tank

Aft Tank Ring

Longeron
(Side View)

Longeron
(Front View)

Mono-Ball and Pin

Thrust Strut Assembly

Aft Skirt

Frangible Bolt Cap

Support Post

Spherical Bearing

Socket

Spring

ERU Interface

Frangible Bolt

Debris Catcher

ERU
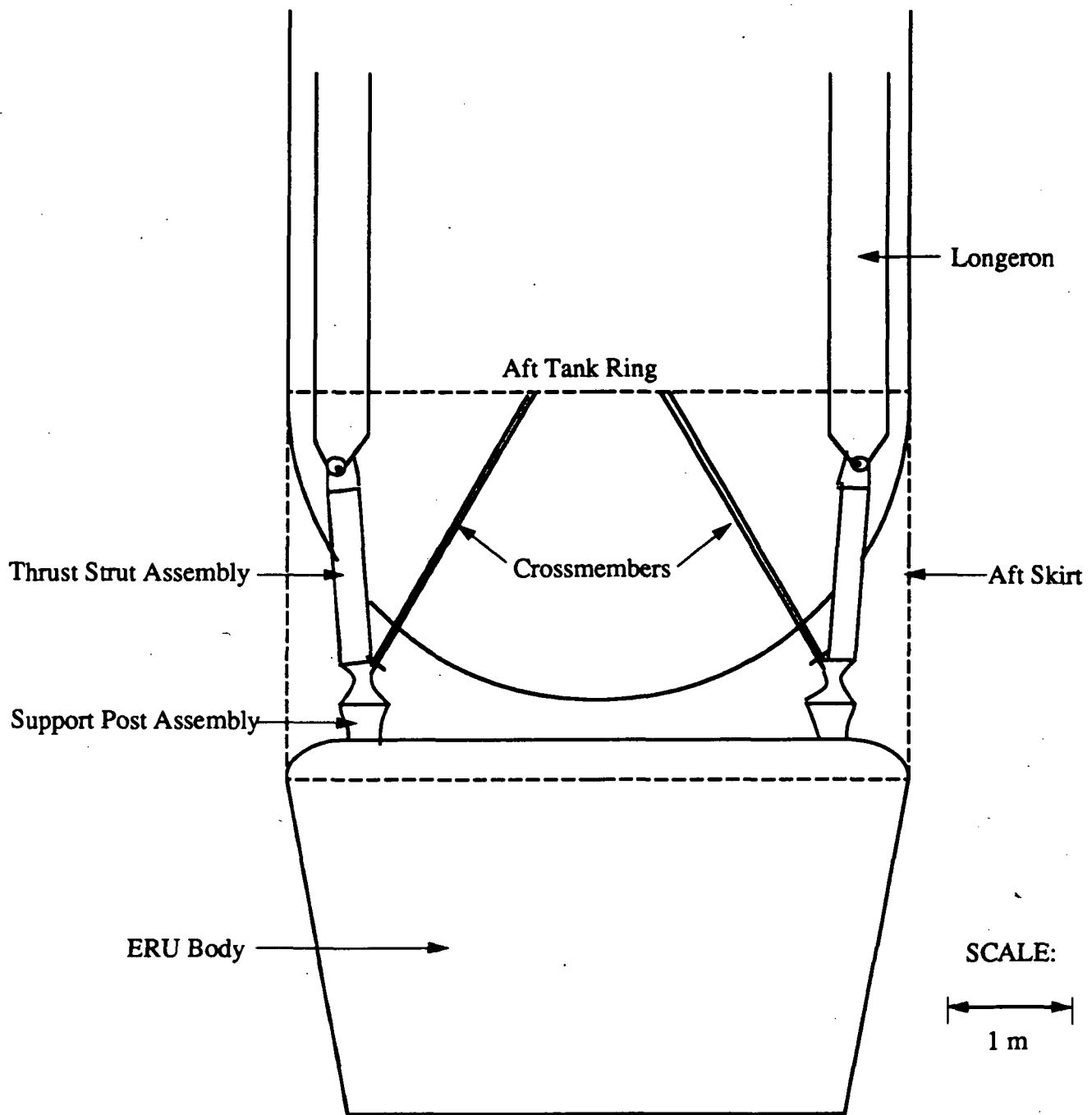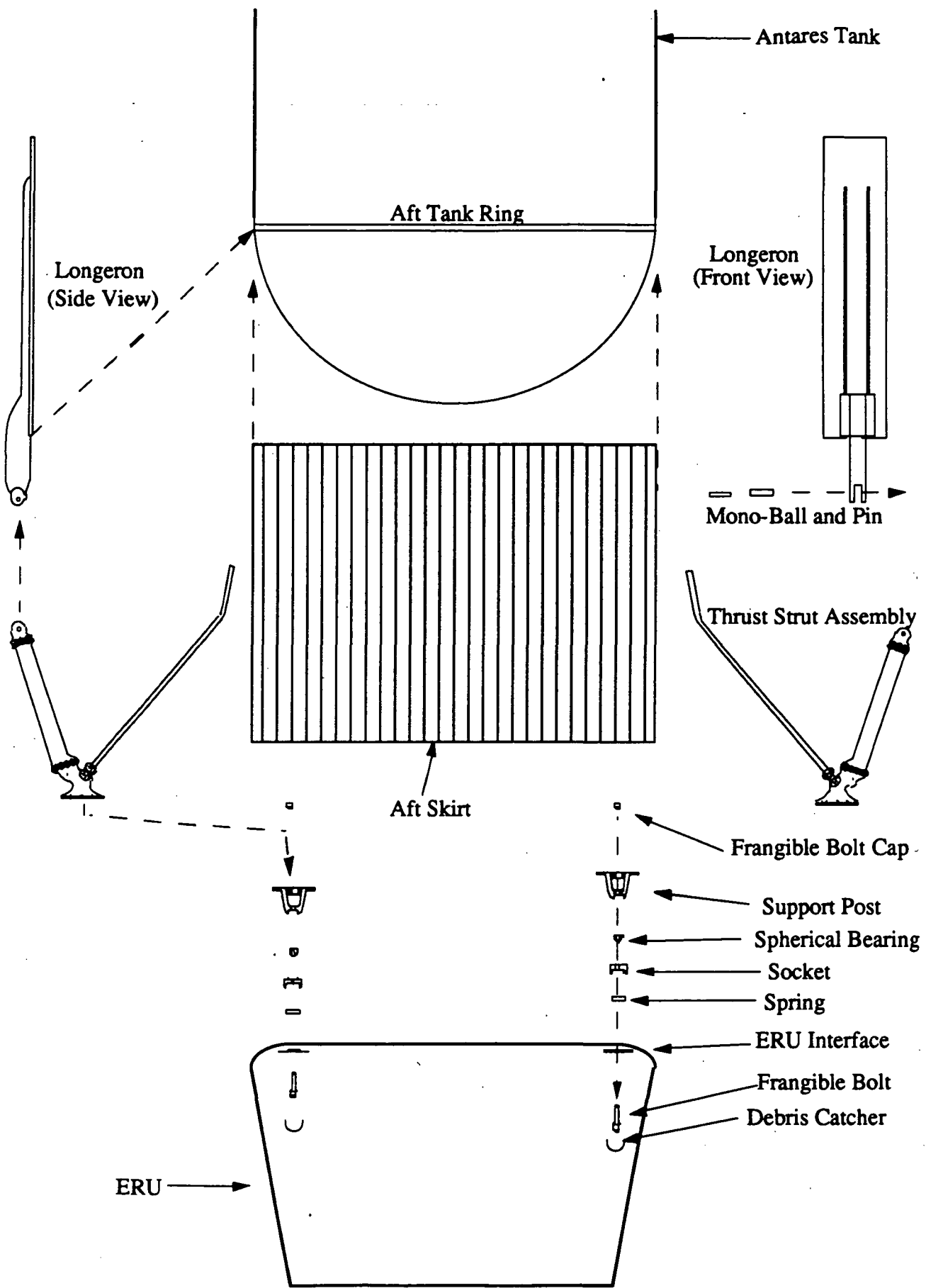
Fig. 5.2  ERU / Main Tank connection (exploded view).

127

Thrust Strut

Thrust Strut Bolt

Stud Decelerator

Support Post

Nut

Spherical Bearing

Frangible Bolt

Socket

Spring

(note raised cylindrical nub that the spring fits over)

ERU Interface

Debris Catcher

SCALE (cm)

0          10

Fig. 5.3  The support post assembly / ERU interface.

90 mm

30 cm

Nut

50.8 mm

Frangible (Break Point) (48.8 mm diameter)

Hollow Core (25.4 mm diameter)

Internal Projectile

Detonation Charge Cap

Fig. 5.4 The frangible bolt.

Longeron Forward End Fitting

End Fitting

Monoball and Shear Pin

Shim

Main Strut

Crossmember

2.3 m

1.7 m

Elbow

Support Post

19°

Pinned Joint

40°

Bearing

Uniaxial
Compression

Fig. 5.5 The thrust strut assembly.

130

Nose Cone Fairing

Flex Deflector

Stub Adapter

Centaur Upper Stage

Interstage Adapter (ISA)

Main Antares Stage
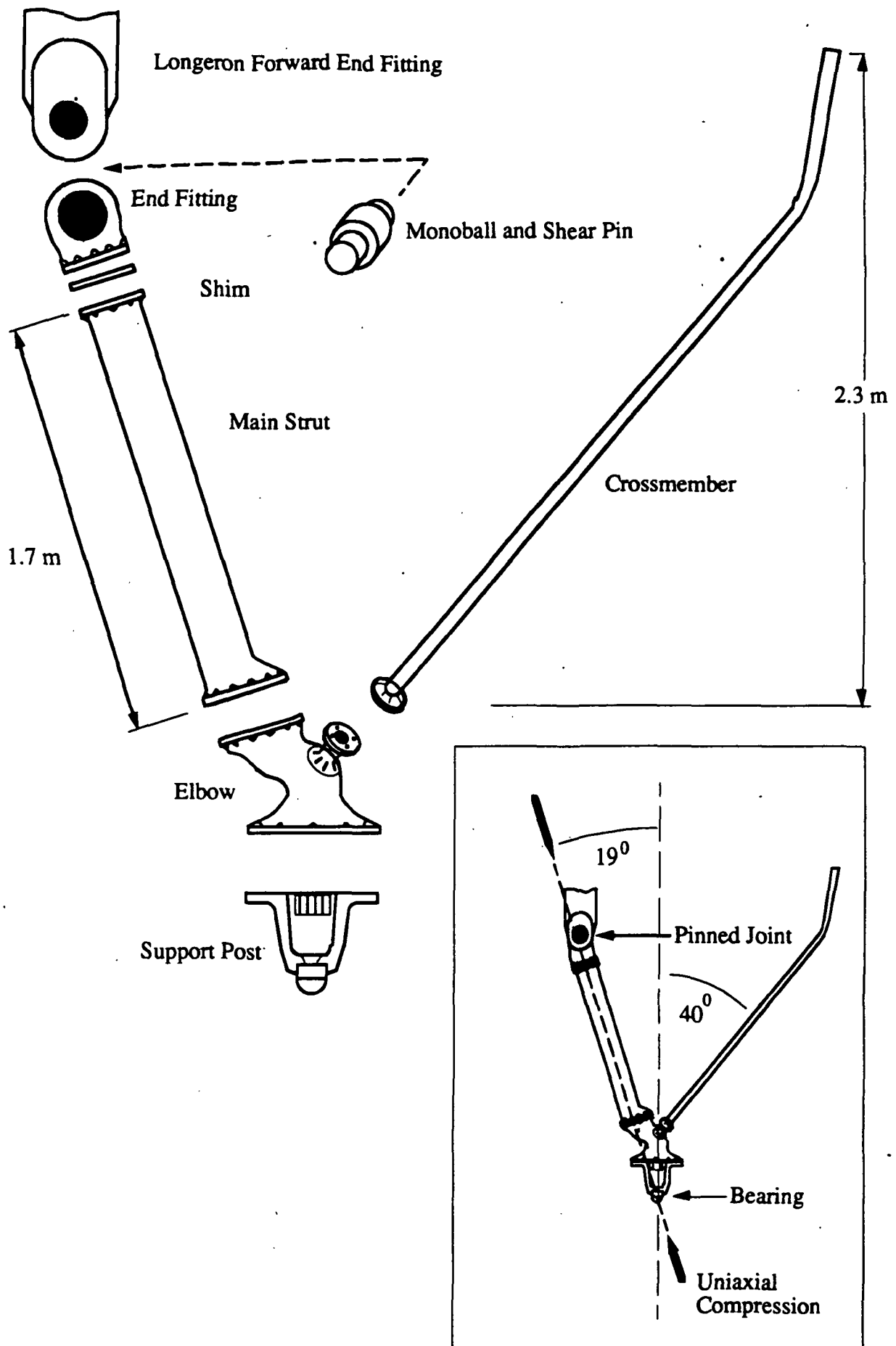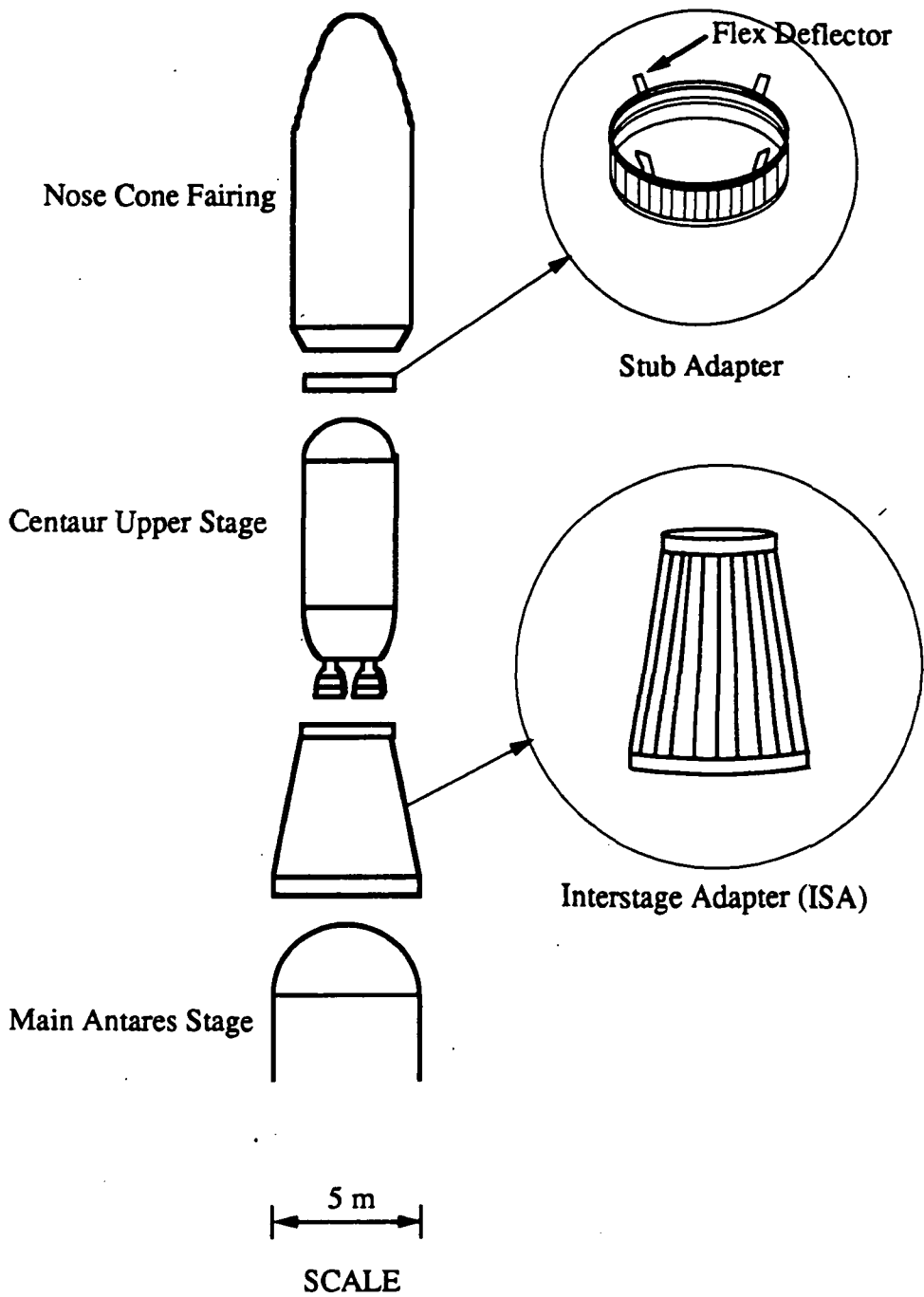
5 m

SCALE

Fig. 5.6 GEO mission-Antares upper section-exploded view.

131
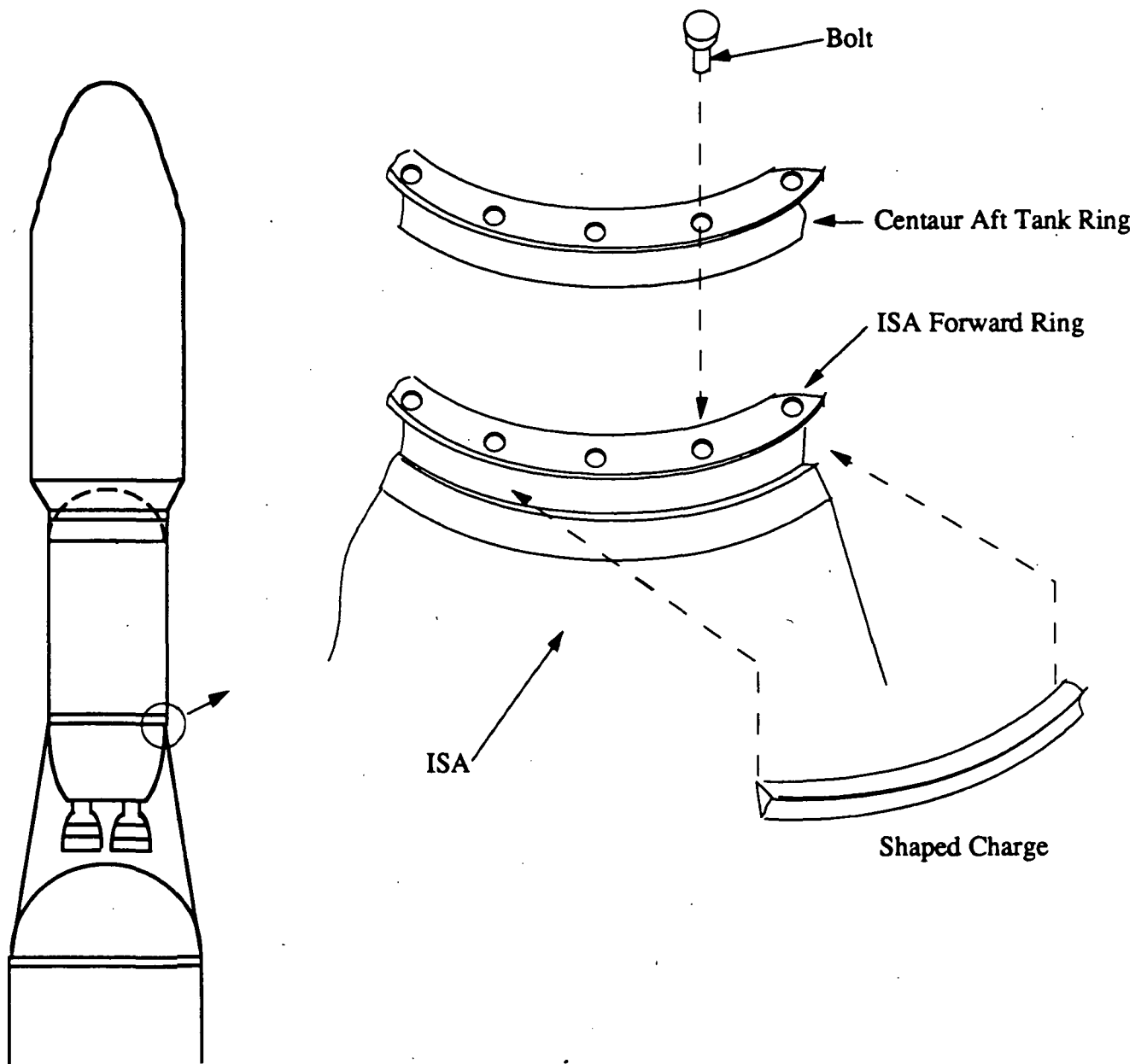
Fig. 5.7  ISA forward ring / Centaur aft tank ring interface.

Tank Skin (0.31mm)

Sidewall Foam Panel
(15.24mm)

Kevlar Jacket

Epoxy Adhesive Bondline
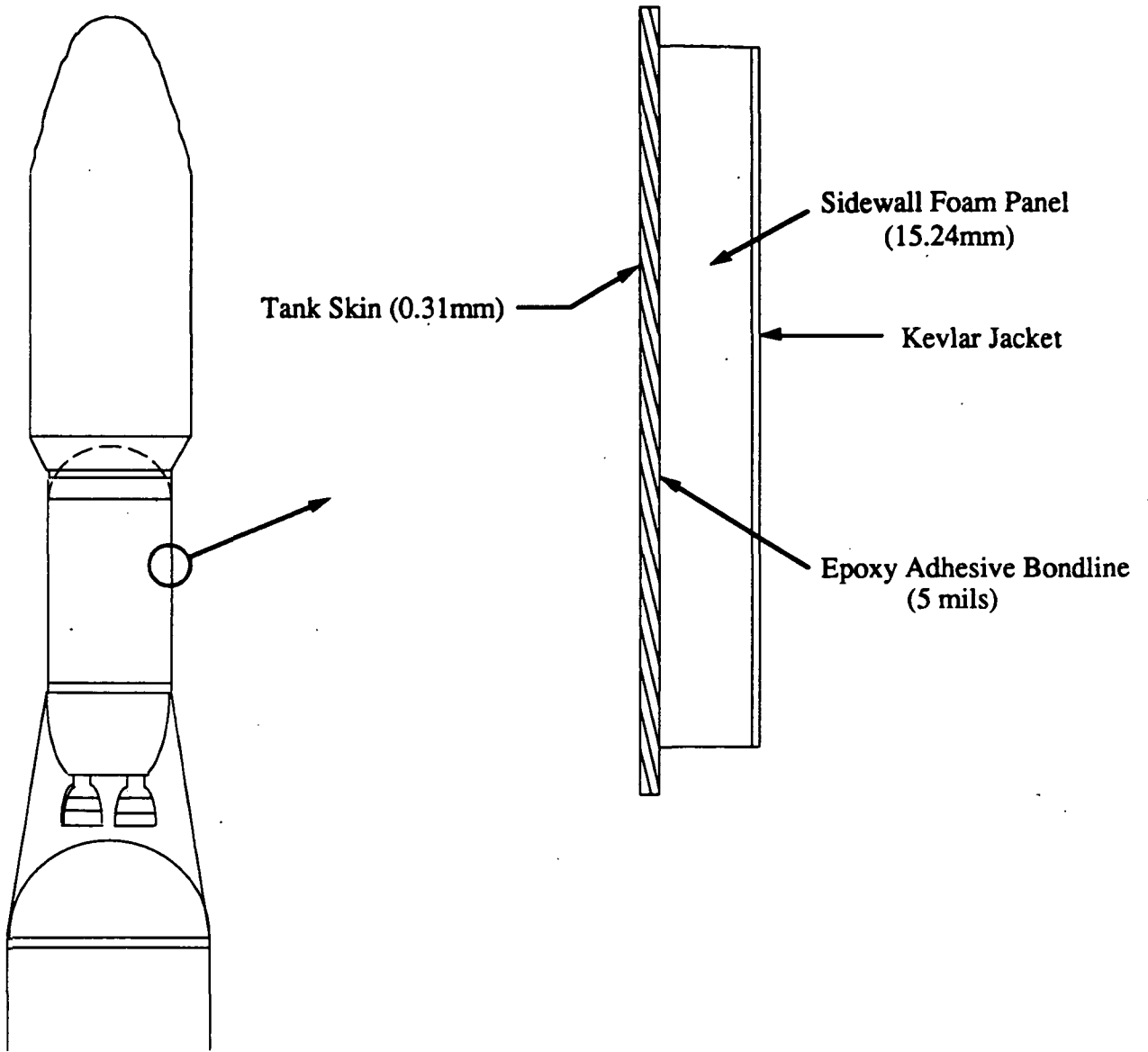(5 mils)

Fig. 5.8  Centaur insulation.

133

# 6.0  PAYLOAD FAIRINGS

## 6.1  PAYLOAD CONSIDERATIONS
(Colin O'Connor)

Geostationary communications satellites have progressed toward increased circuit capacity and longer life span. The more capable spacecraft are larger and heavier than their predecessors. Indications are that future communications satellites will be even larger still. Criteria for the initial geosynchronous orbit (GEO) payload fairing interior dimensions (payload envelope) came from analysis of current communications satellite design and industry projections. Aerodynamic and structural optimizations were then used to produce a desirable payload envelope, while incurring minimal drag and weight. The Antares GEO payload fairing accommodates today's communications satellites and the larger spacecraft of the future (see Fig. 6.1).

NASA's needs and industry projections dictated the initial low earth orbit (LEO) payload envelope dimensions. The Civil Needs Data Base [1], maintained by NASA, contains several hundred entries describing NASA's current and projected payloads for delivery to LEO. A majority of these payloads have widths suited for delivery by the Space Shuttle (4.57 m) and are under 9000 kg (see Fig. 6.1) Such payload widths are accommodated by Antares' standard fairing. The fairing base diameter is dictated by Antares I's body diameter, (5.0 m). The standard LEO payload fairing will service more than 75% of NASA's LEO payloads. The mid-sized payload envelope is the same width as the standard, but is comparable to the shuttle bay's length.

The fairing dimensions of the Antares VII provide a payload envelope that is unique among current or planned U.S. launch vehicles. The envelope's diameter is approximately twice that of the Titan IV's payload envelope. The length corresponds to payload lengths of many larger payloads in the Data Base. The following paragraphs detail the fairing geometry and structure chosen to protect the cargo from aerodynamic forces and hostile environments.

## 6.2 AERODYNAMIC DRAG
(William Chau)

Drag plays an important role in the performance of a rocket in the atmosphere. It creates a force, proportional to the square of the vehicle's velocity, that counteracts the thrust. The effects of drag can be reduced by optimizing the design of the fairing forebody, or nose cone. The drag is computed from:

$$D = C_d \, q \, A \qquad\qquad (6.1)$$

where $D$ = drag force, $C_d$ = total drag coefficient, $q = \frac{1}{2}\rho v^2$ = dynamic pressure, and $A$ = vehicle cross-sectional area.

### 6.2.1 BASIC CONCEPTS

In order to analyze the drag acting on Antares, a basic understanding of the relevant drag components is needed. In this analysis, drag is separated into forebody pressure drag, viscous drag, and base drag.

Forebody pressure drag at subsonic speeds is associated with a change in the pressures on the aft part of the vehicle due to losses in the boundary layer and flow separation. This pressure drag force is affected by the vehicle fineness ratio (vehicle length/diameter) and the skin friction coefficient. Experimental results show that a minimum pressure drag force occurs at a vehicle fineness ratio of 10 - 12 [2]. Forebody pressure drag increases abruptly at transonic and supersonic speeds. This phenomenon, known as wave drag, is associated with shock losses as the vehicle exceeds the speed of sound. Total forebody pressure drag will now be referred to as wave drag for ease of analysis.

Viscous drag, or skin friction, is the result of shearing effects within the boundary layer at the body surface. The amount of viscous drag depends upon whether the flow is laminar or turbulent over the surface. Base drag is produced by a low base pressure over the vehicle base

area, which is less than the free stream pressure. Base drag is a function of the vehicle flight condition and the vehicle base geometry, and cannot be changed by altering the nose cone geometry.

Wave drag, however, is influenced greatly by the nose cone configuration. By optimizing cone geometry, wave drag can be decreased. Wave drag can amount to approximately half of the total vehicle drag, so it is important to optimize the nose cone design. The wave drag on various conical shapes exhibits similar characteristics for a given range of Mach number. A plot of the drag coefficient vs. Mach number is shown in Fig. 6.2 for a nose cone having a fineness ratio, $L_c/D_c$, (cone length/base diameter) of 1.5. This graph is obtained from the following two expressions:

$$\frac{d(C_{d_0})}{dM} = \left(\frac{4}{\gamma+1}\right)\left(1 - 0.5\, C_{d_{01}}\right) \tag{6.2}$$

$$C_{d_0} = 2.1 \sin^2\theta + 0.5\left(\frac{\sin^2\theta}{\sqrt{M^2-1}}\right) \tag{6.3}$$

where $C_{d_0}$ = wave drag coefficient, $C_{d_{01}}$ = wave drag coefficient at M = 1, M = Mach number, $\theta$ = cone half-angle ($\theta$ = 18.4° for $L_c/D_c$ = 1.5), and $\gamma$ = specific heat ratio ($\gamma$ = 1.4 for air). These equations are theoretical expressions which correlate with experimental results performed on conical sections. Equation 6.2, the slope of $C_{d_0}$ as a function of M, is applied at M = 1. Equation 6.3 is valid at Mach numbers greater than 2. The remaining curve is faired based on experimental data from similar curves [3].

## 6.3   NOSE CONE OPTIMIZATION
(William Chau)

Increasing the nose cone fineness ratio, $L_c/D_c$, reduces the wave drag values, but the same general curve shape is retained. This effect is shown clearly in Fig. 6.3, where the wave

drag coefficient vs. $L_C/D_C$ is plotted at a reference Mach number of 2. This figure is derived from [3]:

$$C_{d_o} = \frac{\theta^{1.6}}{360}$$ (6.4)

As seen in Fig. 6.3, values of $L_C/D_C$ less than unity are unacceptable because the drag is too high. Drag is affected greatly in the region of $L_C/D_C$ between 1 and 2. From an aerodynamic standpoint, the nose cone should be as long as possible to reduce drag. However, an $L_C/D_C$ greater than 2 is not practical because the structural weight penalty due to a longer nose cone is too great to justify the small drag improvements. An $L_C/D_C$ between 1 and 2 is therefore a logical choice for the nose cone design. Further structural and payload considerations must also be taken into account before the $L_C/D_C$ ratio can be finalized.

In addition to $L_C/D_C$ ratios, off-conical nose cone geometries will also change $C_{d_o}$ characteristics. In the past, payload fairings have generally been limited to conic or biconic nose cone shapes with a spherical cap, due to the limitations of metal forming. Research has shown, however, that these shapes are not optimal for vehicle drag and weight. Also, conical shapes are not the most efficient structural shapes for resisting collapse pressures experienced during atmospheric flight [4]. Rather, an aerodynamically shaped nose cone made from advanced composite materials would result in improved drag characteristics, higher payload volume, and lighter structures. Aerodynamically curved shapes resist collapse or buckling loads much better than cones, thereby requiring thinner materials and fewer ring stiffeners.

Three promising nose cone configurations are shown in Fig. 6.4. Figure 6.4a, a tangent ogive, is characterized by its large curvature and tangent base. It is defined by the analytical expression [5]:

$$r = \frac{D_c}{2\pi}\left(\pi - \theta_s + \frac{1}{2}\sin 2\theta_s\right)^{\frac{1}{2}}$$ (6.5)

138

where r = nose cone sectional radius and $\theta_s$ = angle between the body axis and the tangent to the body at the point in question. This configuration results in the lightest fairing structure of the three due to its high structural rigidity. However, the tangent ogive results in approximately a 10% increase in wave drag over a pure cone [3]. Figure 6.4b, the three-quarter-power body, is defined by the expression:

$$r = \left(\frac{D_c}{2}\right)\left(\frac{x}{L_c}\right)^{\frac{3}{4}} \qquad (6.6)$$

This shape results in approximately a 10% decrease in wave drag over a cone, but results in the heaviest structure due to its low structural rigidity. Figure 6.4c, the parabolic body, is defined by the expression:

$$r = \left(\frac{D_c}{2}\right)\left(\frac{x}{L_c}\right)^{\frac{1}{2}} \qquad (6.7)$$

This shape results in approximately the same drag characteristics as a cone, but with the advantage of a higher structural rigidity, and hence, lower weight.

A parabolic nose cone design with $L_c/D_c = 1.2$ was selected as the optimal combination of aerodynamic performance, structural weight, and payload capacity. This design minimizes drag for an aerodynamically curved nose cone. The benefits of such a design are that continuously curved shapes resist collapse or buckling loads much better than cones, thereby requiring thinner materials and fewer ring stiffeners. This results in a lighter payload fairing structure. Also, a parabolic design allows a larger portion of the payload to be stowed inside the nose cone. This reduces the required length of the cylindrical part of the payload fairing and, hence, the overall weight.

Also, a small drag improvement can be achieved by optimizing the nose cone bluntness ratio (nose tip radius/nose base radius). The optimal bluntness ratio increases as the Mach number is reduced and is found to be between 0.50 and 0.60 at a Mach number of 1.6 [4]. This Mach number is significant in that the highest dynamic pressures encountered by the Antares occurs in the range of M = 1 to 2. The Antares nose tip radius, $r_t$, is optimized to a bluntness ratio of 0.50 (LEO mission, $r_t = 1.2$ m; GEO mission, $r_t = 0.975$ m).

The combined drag effects of the Antares with the parabolic nose cone described above are shown in Fig. 6.5. Wave drag is calculated using the method outlined earlier. Base drag and skin friction are taken from experimental data performed on projectile bodies [3].

## 6.4 NOSE CONE PRESSURE DISTRIBUTION
(William Chau)

The pressure distribution along the nose cone was obtained using the tangent-cone method outlined by Nielsen [5]. This method assumes the pressure coefficient $C_p$ at any point on a body of revolution corresponds to that of a cone having a semiapex angle, $\theta_s$, equal to the angle between the body axis and the tangent to the body at the point in question. The LEO nose cone profile is approximated by the following analytical expression:

$$r = 0.9956\sqrt{x} \tag{6.8}$$

where r = cone radius and x = distance from the nose cone tip (see Fig. 6.6). Equation 6.8 is used to calculate the slope of the nose cone at different locations along the central axis. This gives the angle of the tangent which is used along with the free stream Mach number and transonic similarity parameters to determine the pressure coefficient $C_p$ [6]. Figure 6.7 shows the pressure coefficient along the Antares nose cone as a function of the distance from the nose tip at maximum dynamic pressure (q = 23,560 N/m$^2$ (492 psf),which occurs at M = 1.09).

140

## 6.5  SHELL DESIGN
### (Jeff Beeghly)

The Antares' payload fairing is partially modeled after the McDonnell Douglas' Titan IV payload fairing. The shell of the Titan IV payload fairing is manufactured from 2 inch thick 6061 aluminum alloy panels, which are milled down into triangular pockets (this is known as an isogrid) [7].

The payload fairing of the Antares uses an isogrid design, as shown in Fig. 6.8, but is made from graphite/epoxy composites. The dimensions of each member of the grid are 20 cm long, 3 cm high, and 0.5 cm thick. The benefit of using an isogrid is that the outer wall of the nose cone can be made thinner, because the forces are transmitted through the "truss" formed by the isogrid.

As Fig. 6.6 shows, the surface of the nose fairing is a function of $\sqrt{x}$ except for the spherical nose tip. In order to withstand the aerodynamic heating which occurs at the higher altitudes, the skin of the nose tip is made from a carbon - carbon composite. The remaining portion of the payload fairing's skin is made of Cycom NCG nickel-coated graphite fiber composite. This composite is specially designed to dissipate electrical charge in the case that lightning should happen to strike the rocket.

## 6.6  ACOUSTIC SHIELDING
### (Jeff Beeghly)

During the beginning of the flight, ground noise from the engine is very intense and can do considerable damage to the payload. To prevent this, the nose cone fairing uses EAR Isodamp C-3002-50 damping foam. The material is a flexible sheet (1.27 cm thick) and is inserted in between the composite beams of the isogrid. The density of this material is 112 kg/m$^3$, which yields 170 kg of acoustic foam for the GEO mission nose cone, and 220 kg of acoustic foam for the single vehicle LEO mission.

## 6.7 JETTISON SYSTEM FOR PAYLOAD FAIRING
### (Steve Solomon)

The nose cone fairing is jettisoned from the vehicle at a prescribed altitude to reduce dead weight and allow the upper stage to continue through the remainder of the mission. To achieve this, rails are used (see Fig. 6.9). Two rails sandwich an explosive charge that, when detonated, splits the fairing along its axis into two or more segments.(similar to Lockheed's Super-Zip). Once split, the segments rotate back on hinges mounted on the stub adapter until they reach an unhinging point, whereupon they fall off. Also mounted on the stub adapter at the base of the segments are flex deflectors (see Sec. 5.2.2 and Fig. 6.10).

### 6.7.1 CONSTRUCTION

The rails are made of 2219 aluminum alloy and are 2.5 mm thick by 152 mm wide; their mass per unit length is 1.05 kg/m. The spacing between two sandwiched rails is 12 mm and there is a linear explosive charge between the two rails, as shown in Fig. 6.9. The rails are held together (and hold the fairing segments together) by closely spaced rivets. During separation the force of expanding gases produced by the explosive charge causes the rails to split uniformly along a frangible seam (Fig. 6.9). The fairing segments must clear the vehicle without damage or debris. To control this problem, the explosive charge is contained in an expandable steel-reinforced rubber seal that does not rupture. Debris and hot gases are contained by the seal. The seal is attached to one of the fairing segments and, upon separation, falls away with that segment. Although aluminum is used for the rails there may be several advantages to using a composite rail i.e., the same material as the fairing: 1) weight savings, 2) compatibility with the fairing i.e., thermal expansion and galvanic corrosion effects, 3) reduced parts and assembly time (i.e. cheaper labor costs), and 4) stiffer shells and reduced warpage (flexing upon separation) and increased dimensional stability.

## 6.8 PAYLOAD FAIRING FOR THE GEO MISSION
(Jeff Beeghly)

The GEO mission is able to accommodate a payload 3.7 m in diameter and 7.0 m long. The nose section of the fairing (see Fig. 6.11) is a function of $\sqrt{x}$ and has a spherical tip with a radius of 0.975 m. It is modeled this way to reduce drag, increase structural stability and reduce the mass of the structure. The central section of the GEO payload fairing is a cylinder 7 m long and 3.9 m in diameter. The fairing then tapers down over a length of 0.75 m to match the 3.05 diameter of the stub adapter which connects to the Centaur.

## 6.9 PAYLOAD FAIRINGS FOR LEO MISSIONS
(Jeff Beeghly)

A different configuration has been designed for each of the three LEO payload envelopes used by the various modular vehicles (see Fig. 6.12). The largest payload diameter that can be accommodated aboard the Space Shuttle, Titan III, or Titan IV is 4.57 m. To meet the needs of the satellite market, the payload fairings of the Antares I and Antares III are 5 m in diameter and are able to enclose a satellite with a diameter of 4.57 m. The Antares I is able to enclose a satellite 7.2 m long (see Fig. 6.6), and the Antares III is able to enclose a satellite 15.24 m long.

If a satellite manufacturer wishes to orbit a satellite that is larger than the Space Shuttle or Titan capacity, the Antares VII is available. This vehicle incorporates a payload fairing that is attached on top of seven boosters and is able to enclose a payload that has a diameter of 9.14 m and a length of 15.24 m (see Fig. 6.13). Like the GEO payload fairing, each of the LEO fairings will utilize the weight saving technique of using an isogrid construction scheme for the shell. Table 6.1 lists the dimensions and masses of the various payload fairings discussed here.

Both the Antares III and Antares VII incorporate additional fairings for aerodynamic reasons (see Figs. 6.14 and 6.15). Both designs are 5 m high and are made of a graphite - epoxy composite isogrid. Since this section is not enclosing the payload, it does not have to be insulated with acoustic foam.
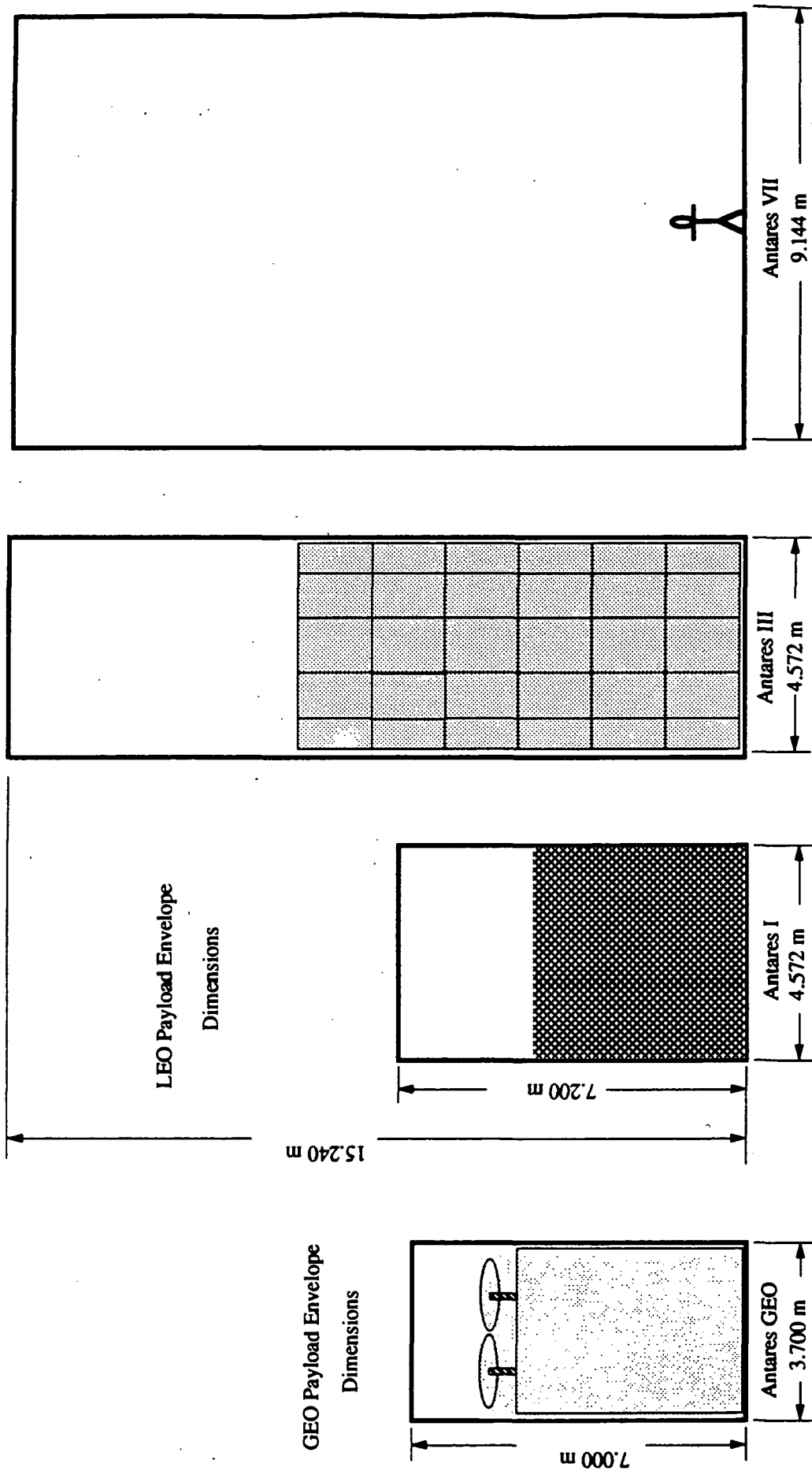
Table 6.1:  Structural Mass of Payload Fairings

| Configuration | Orbit | Payload Length (m) | Payload Diameter (m) | Fairing Mass (kg) |
|---------------|-------|--------------------|----------------------|-------------------|
| Antares I | GEO | 7.0 | 3.8 | 1200 |
| Antares I | LEO | 7.2 | 4.57 | 1400 |
| Antares III | LEO | 15.24 | 4.57 | 2500 |
| Antares VII | LEO | 15.24 | 9.14 | 8500 |

## 6.10 NOMENCLATURE

| | |
|---|---|
| A | Antares cross-sectional area |
| $C_d$ | Total Drag coefficient |
| $C_{d_o}$ | Wave drag coefficient |
| $C_p$ | Pressure coefficient $\left( C_p = \dfrac{p - p_\infty}{q} \right)$ |
| $D_c$ | Nose cone base diameter |
| $L_c$ | Nose cone length |
| $L_c/D_c$ | Nose cone fineness ratio (length/diameter) |
| M | Mach number |
| q | Dynamic pressure $\left( q = \dfrac{1}{2}\rho v^2 \right)$ |
| $r_t$ | Nose tip radius |
| r | Nose cone sectional radius |
| x | Distance from nose cone tip |
| $\gamma$ | Specific heat ratio ($\gamma = 1.4$ for air) |
| $\rho$ | Atmospheric density |
| $\theta$ | Cone half-angle $\left( \theta = \tan^{-1}\left( \dfrac{0.5}{L_c / D_c} \right) \right)$ |
| $\theta_s$ | Semiapex angle equal to the angle between the body axis and the tangent to the body at the point in question |

## 6.11 REFERENCES

1.  NASA TM-103323, <u>Civil Needs Data Base: FY90 Version</u>, Vol. 4, August 1990.

2.  Hemsch, M. and Nielsen, J., <u>Tactical Missile Aerodynamics</u>, American Institute of Aeronautics & Astronautics, New York, 1986, pp.383-401.

3.  Hoerner, S. F., <u>Fluid-Dynamic Drag</u>, Published by author, Great Britain, 1965, Ch. 16 and 18.

4.  Shen, F. and Pope, D., "Fairing Structure For Space Launch Vehicles," <u>Aerospace Engineering</u>, Vol. 11, No. 4, April 1991, pp. 19-22.

5.  Nielsen, J. N., <u>Missile Aerodynamics</u>, McGraw Hill Book Co., New York, 1960, pp. 275-287.

6.  Liepmann, H. and Roshko, A., <u>Elements of Gas Dynamics</u>, John Wiley & Sons, New York, 1957, pp. 262-278.

7.  "Payload Capacity of Titan 4 to Expand with New Fairing," <u>Aviation Week & Space Technology</u>, Vol. 133, No. 19-27, Dec. 10, 1990, pp. 58-62.

LEO Payload Envelope
Dimensions

GEO Payload Envelope
Dimensions

15.240 m

7.200 m

7.000 m

Antares VII
9.144 m

Antares III
4.572 m

Antares I
4.572 m

Antares GEO
3.700 m

A large Space Shuttle Payload
(The Long Duration Exposure Facility)

Average sized Leo Payload.
(From Civil Needs Data base)

Typical Wide Body GEO
Satellite (INTELSAT VI)

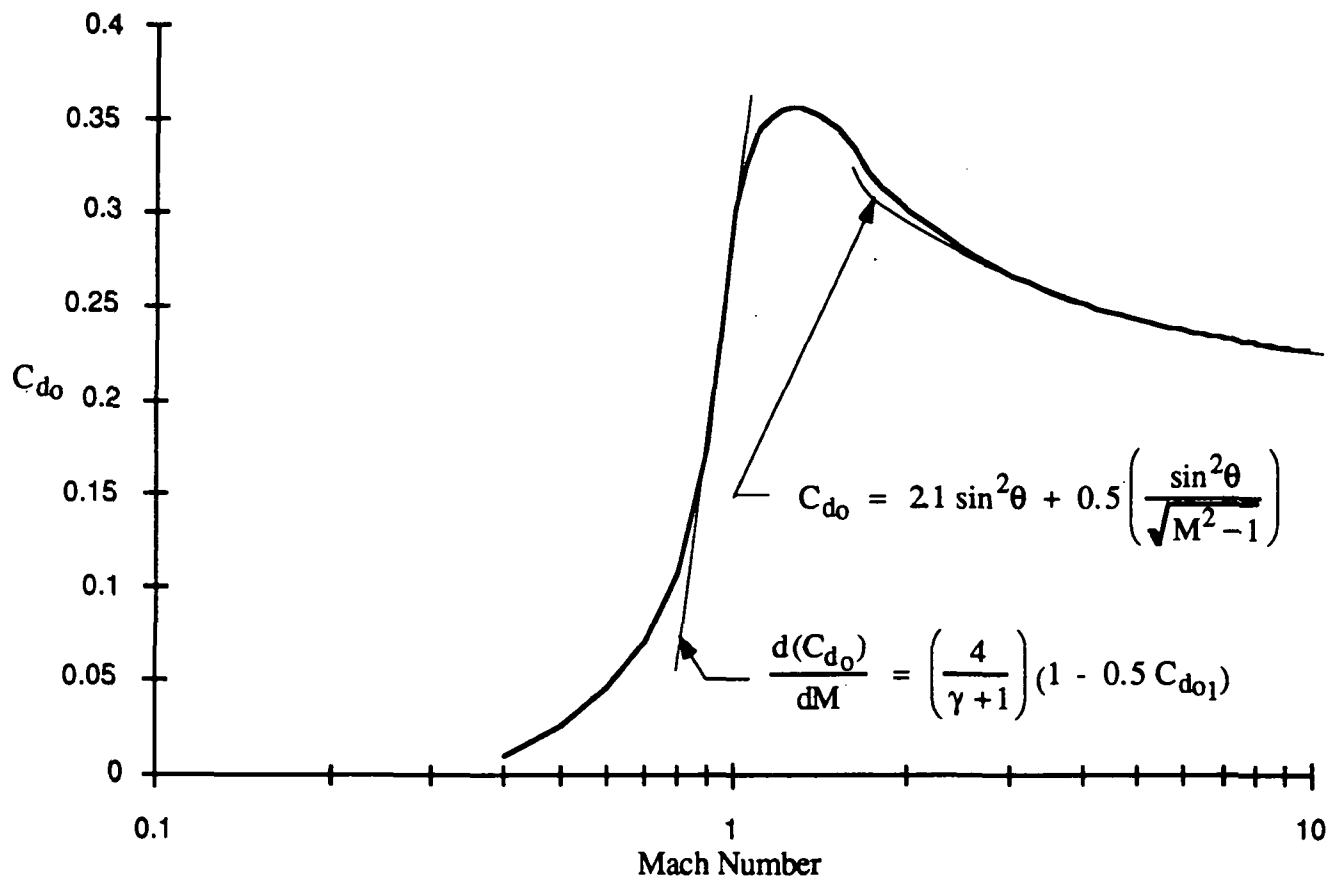Fig. 6.1 Antares payload envelopes.

147

$$C_{do} = 2.1 \sin^2\theta + 0.5\left(\frac{\sin^2\theta}{\sqrt{M^2-1}}\right)$$

$$\frac{d(C_{d_o})}{dM} = \left(\frac{4}{\gamma+1}\right)(1 - 0.5\,C_{do_1})$$

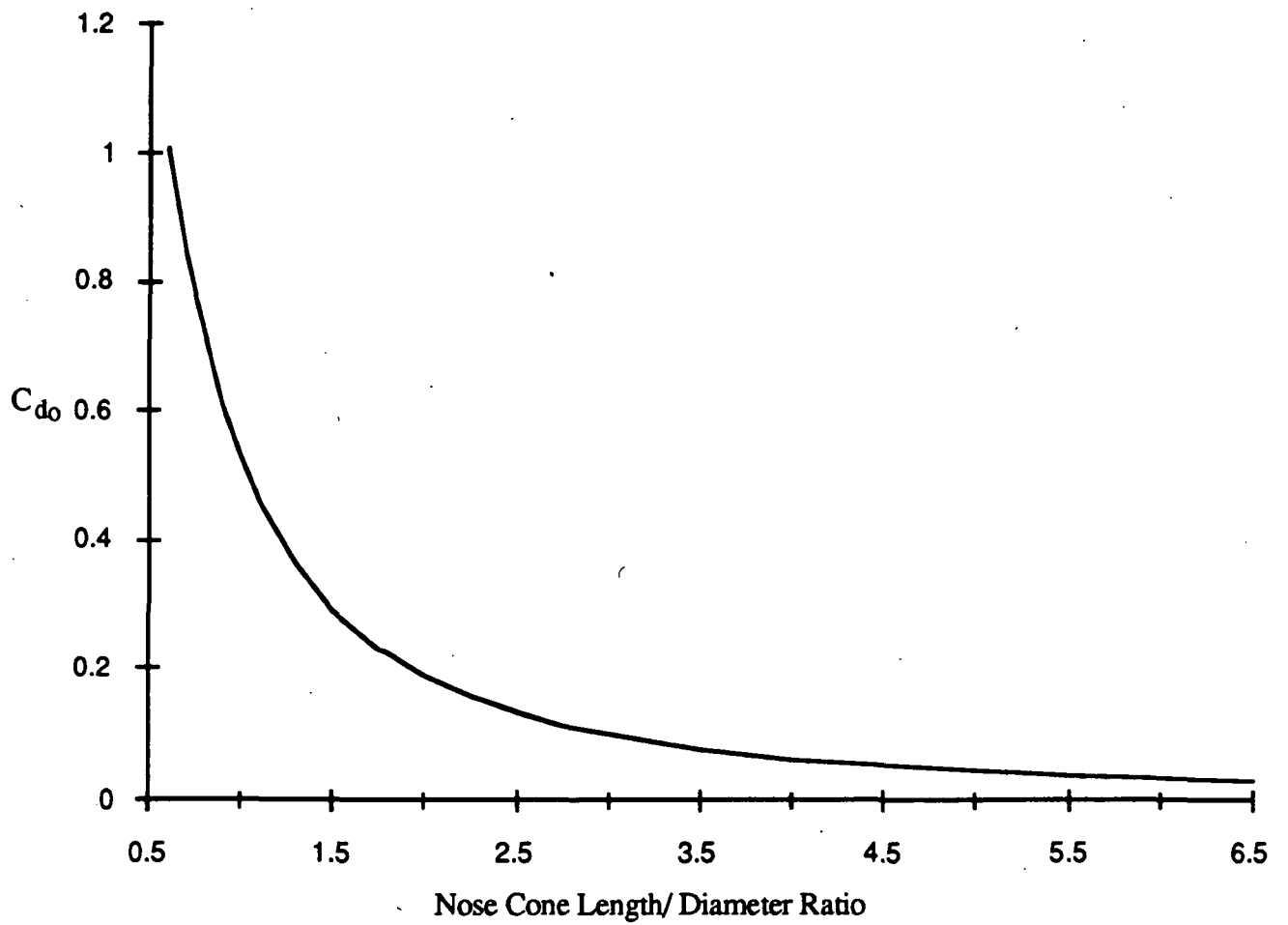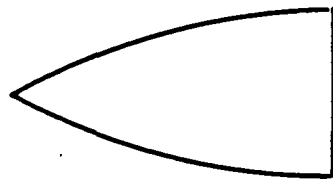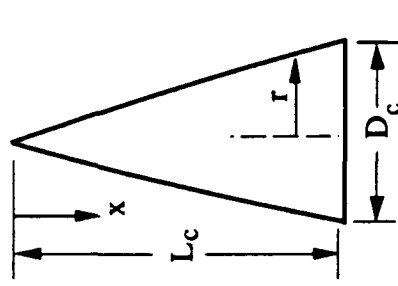Fig. 6.2  Variation of drag coefficient with Mach number of a cone.

148

Fig. 6.3 Drag coefficient of conical sections at M=2.
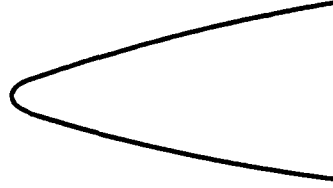
$$r = \frac{D_c}{2\pi}\left(\pi - \theta_s + \frac{1}{2}\sin 2\theta_s\right)^{\frac{1}{2}}$$

a) Tangent Ogive

$$r = \left(\frac{D_c}{2}\right)\left(\frac{x}{L_c}\right)^{\frac{3}{4}}$$

b) Three-Quarter-Power Body

$$r = \left(\frac{D_c}{2}\right)\left(\frac{x}{L_c}\right)^{\frac{1}{2}}$$

c) Parabolic Body

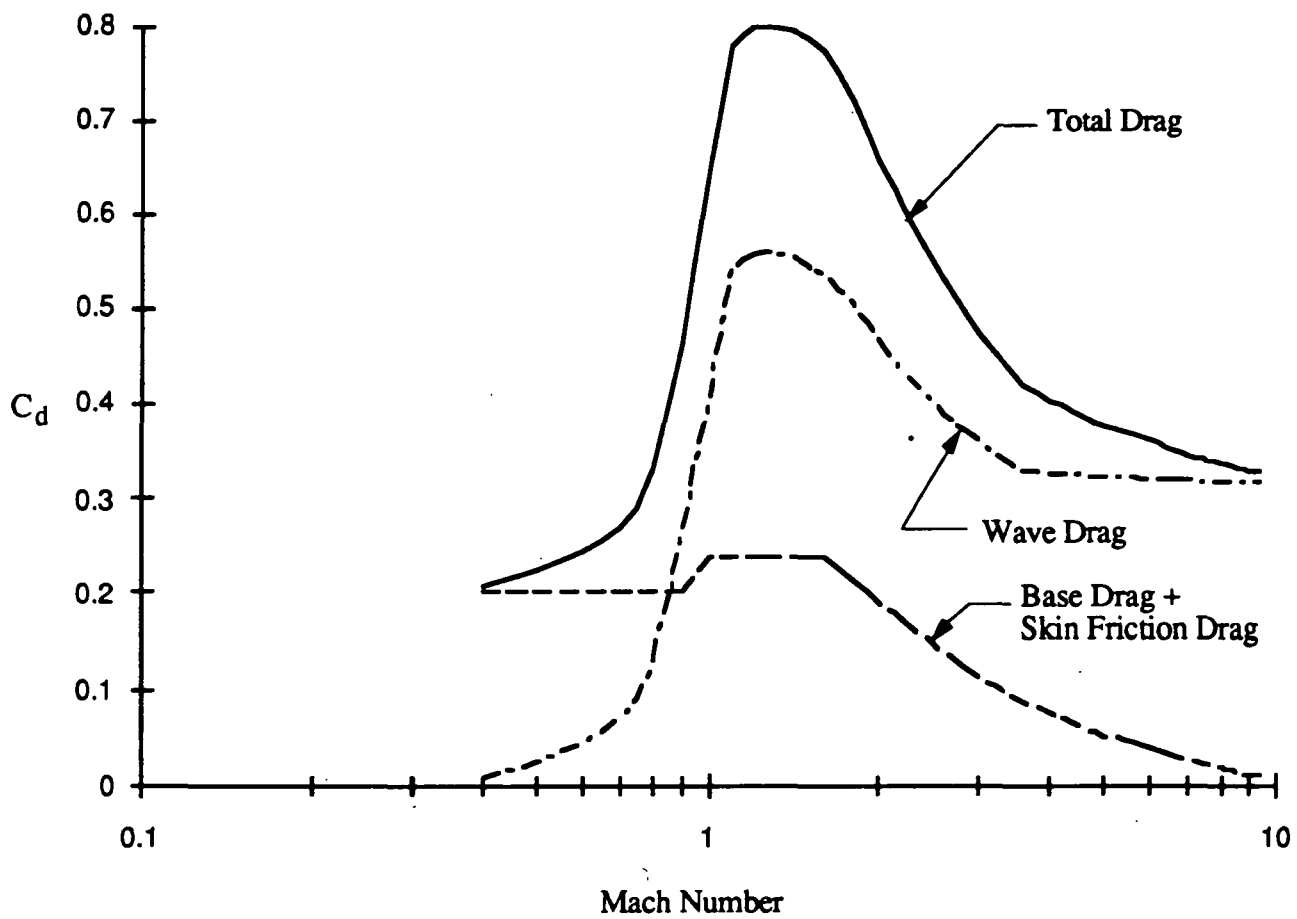Fig. 6.4  Off-conical nose cone shapes.
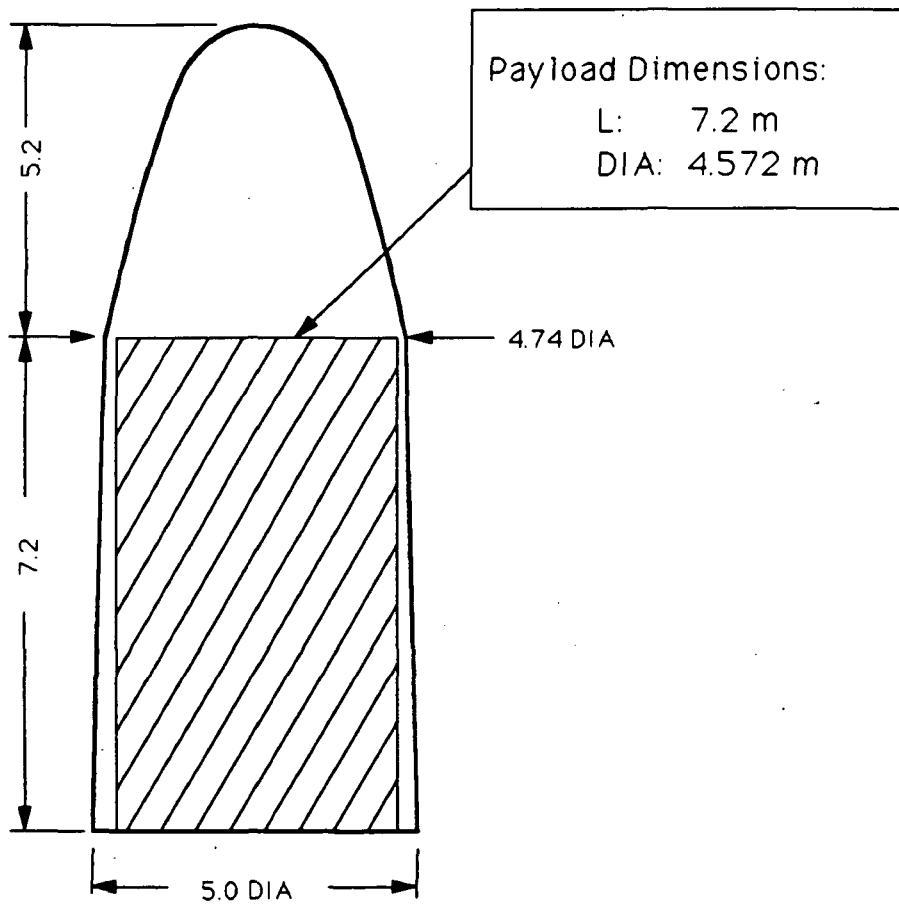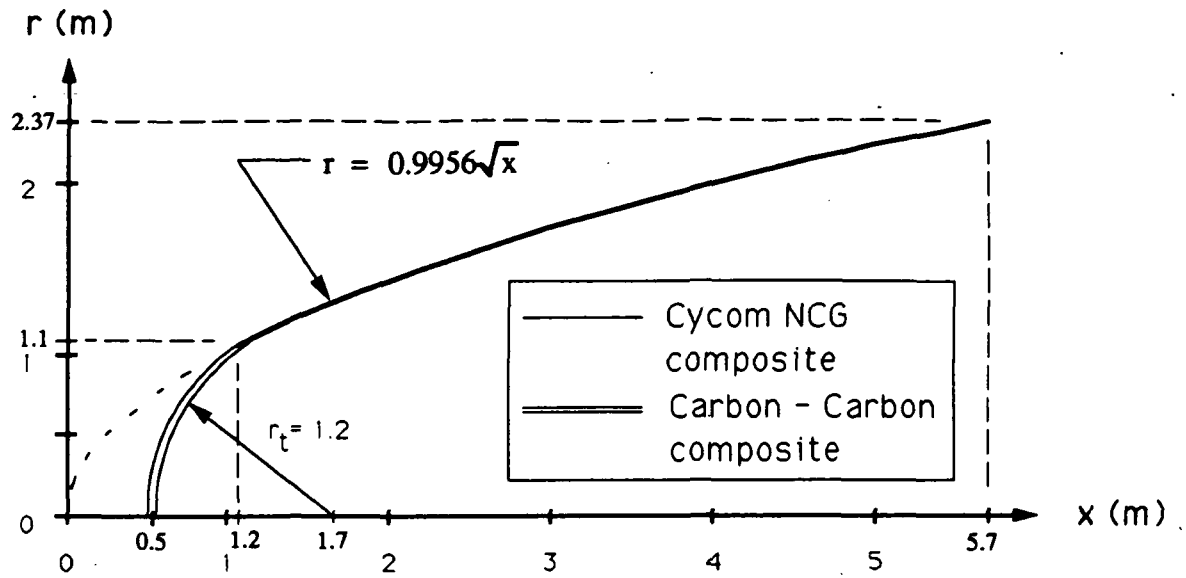
Fig. 6.5 Combined drag effects of Antares.

Fig. 6.6. Payload fairing for Antares I.

Fig. 6.7 Nose cone pressure distribution.

153

0.5 cm

1.5 cm

0.25 cm

Section A-A

1.5 cm

20.0 cm

0.5 cm

Graphite/Epoxy
Composite

Cycom NCG
Composite
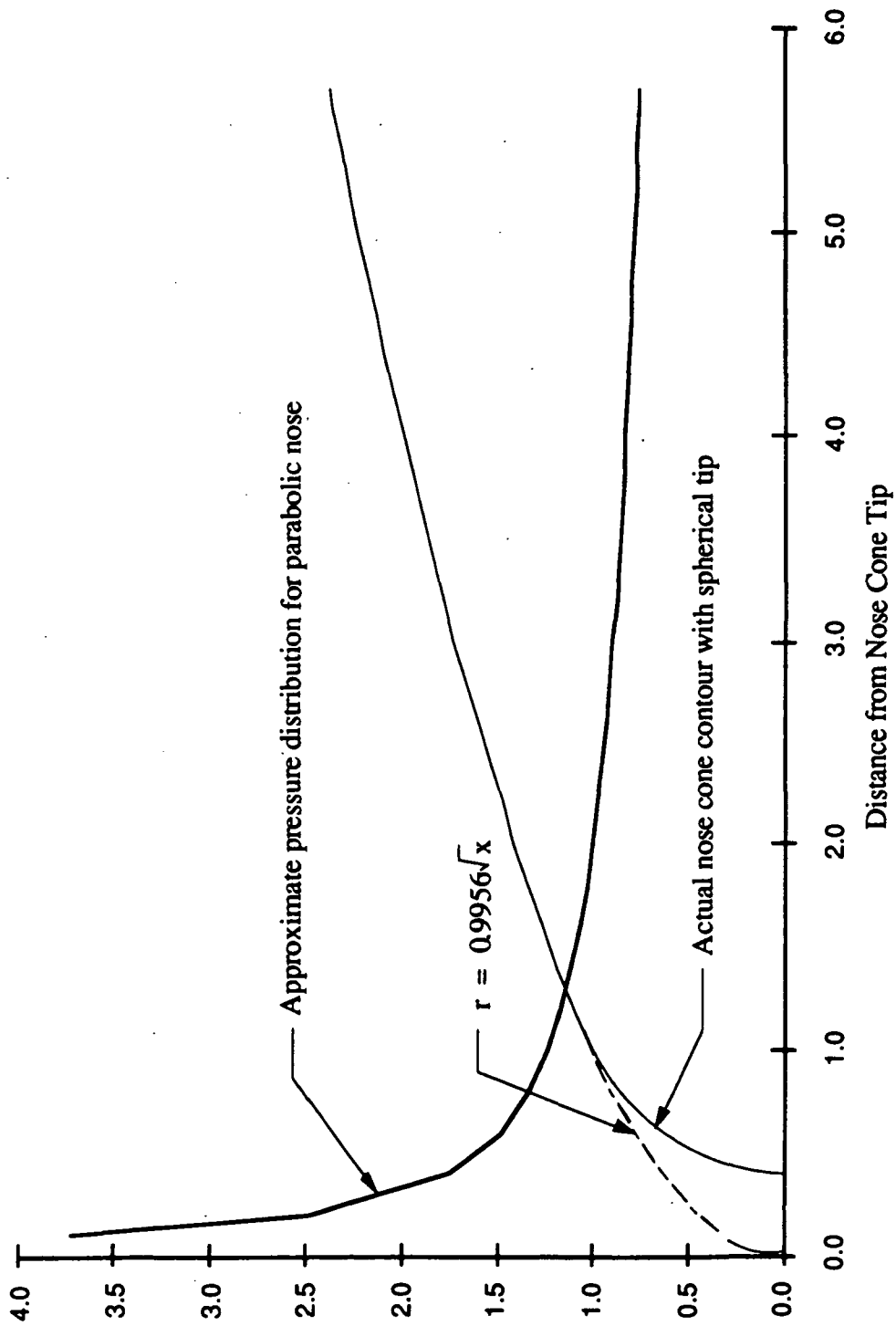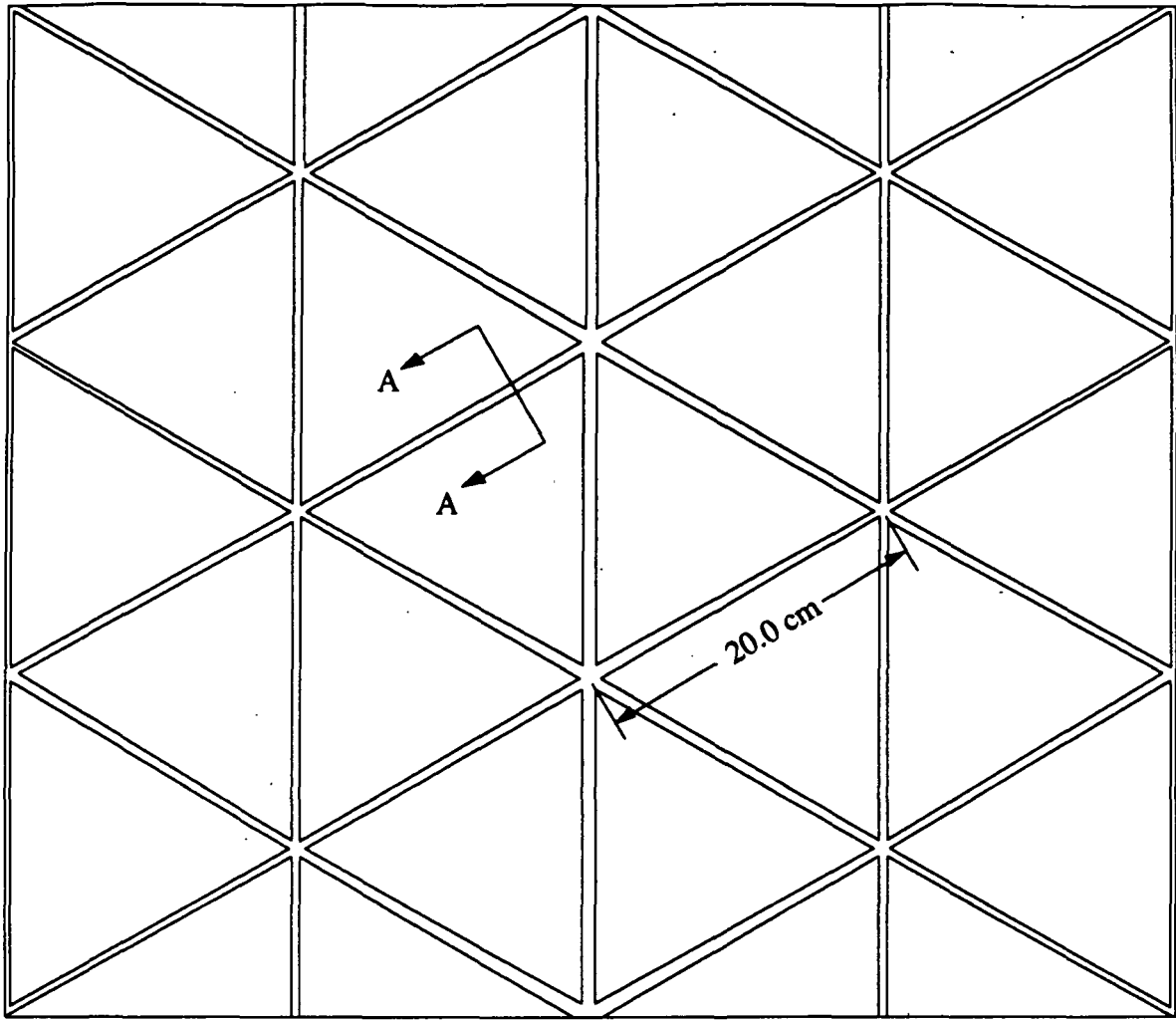
Fig. 6.8. Isogrid configuration.

154

Fairing Section

Inner Rail

Outer Rail

Rivet

Expandable Seal

Frangible Section

Pyrotechnic Charge

Attachment
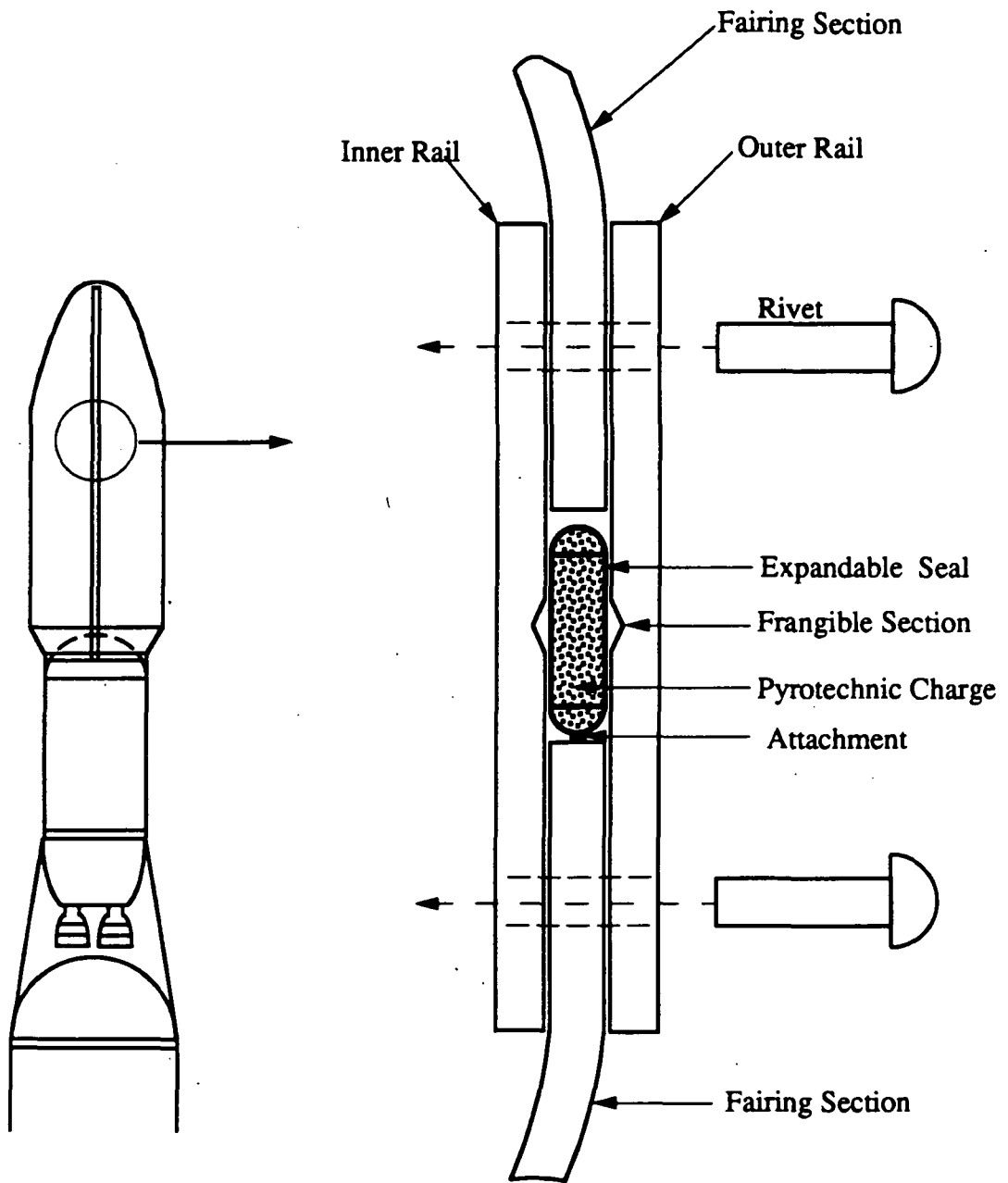
Fairing Section

NOTE: FIGURE NOT DRAWN TO SCALE

Fig. 6.9.  Fairing separation rails.
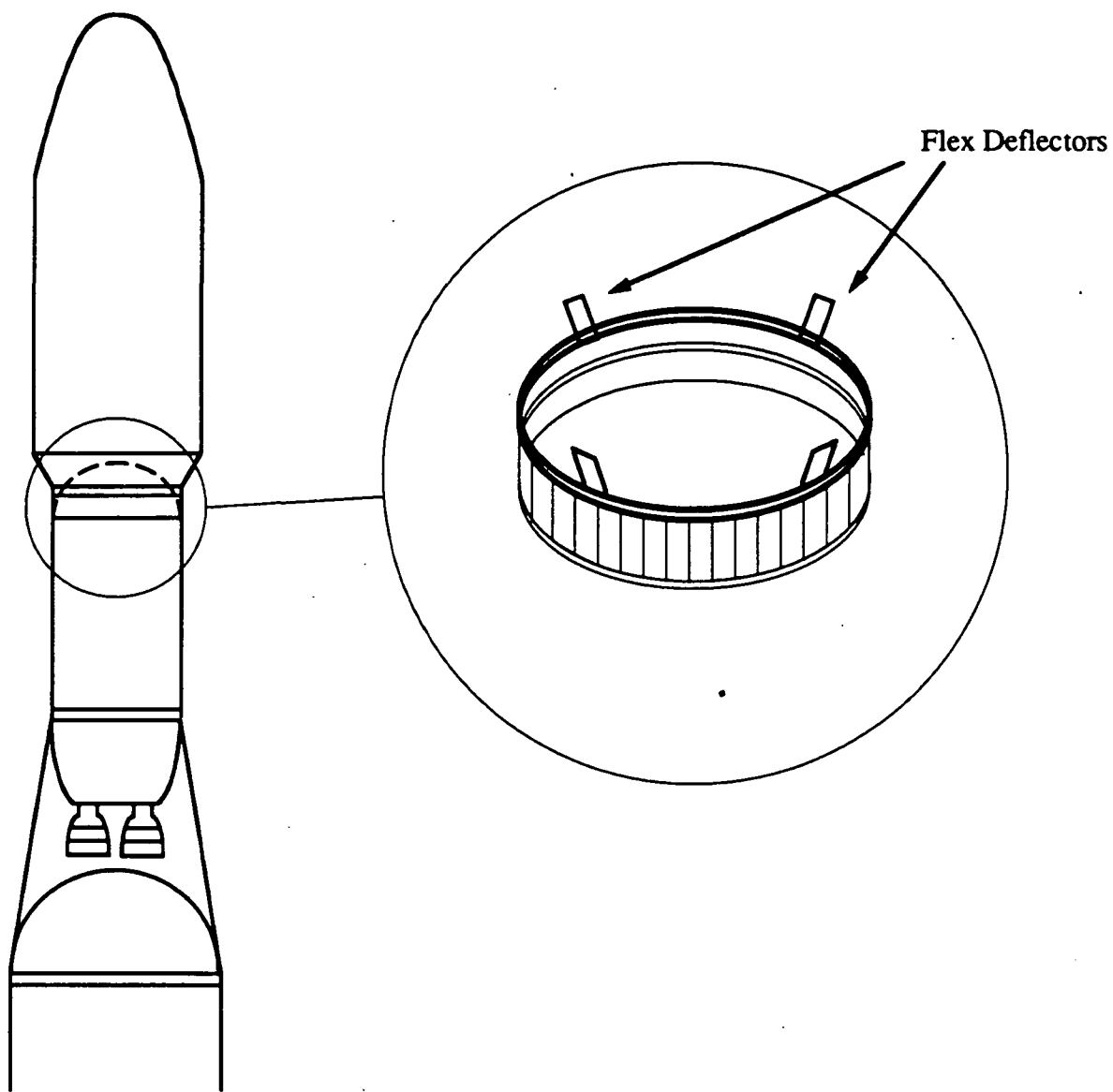
Flex Deflectors

Fig. 6.10. Stub adapter with flex deflectors.

$$r = 0.9092\sqrt{x}$$

Cycom NCG composite

Carbon – Carbon composite

$r_t = 0.975$

Payload Dimensions:
L:    7.0 m
DIA: 3.8 m

3.9 DIA

Stub Adapter

Centaur

Fig. 6.11. Payload fairing for Centaur.

Fig. 6.12. Modular configurations of Antares.
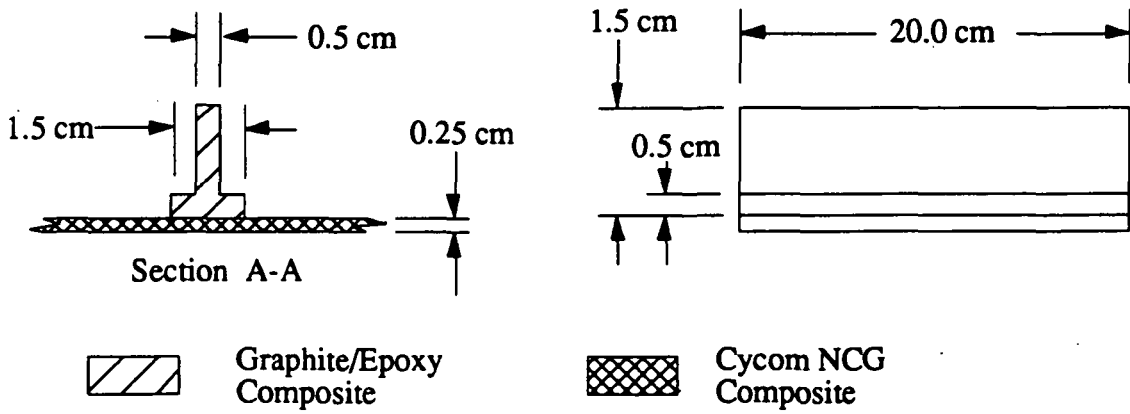
Fig. 6.13. Payload fairing for Antares VII.

159

Fig. 6.14. Additional fairings for Antares III.
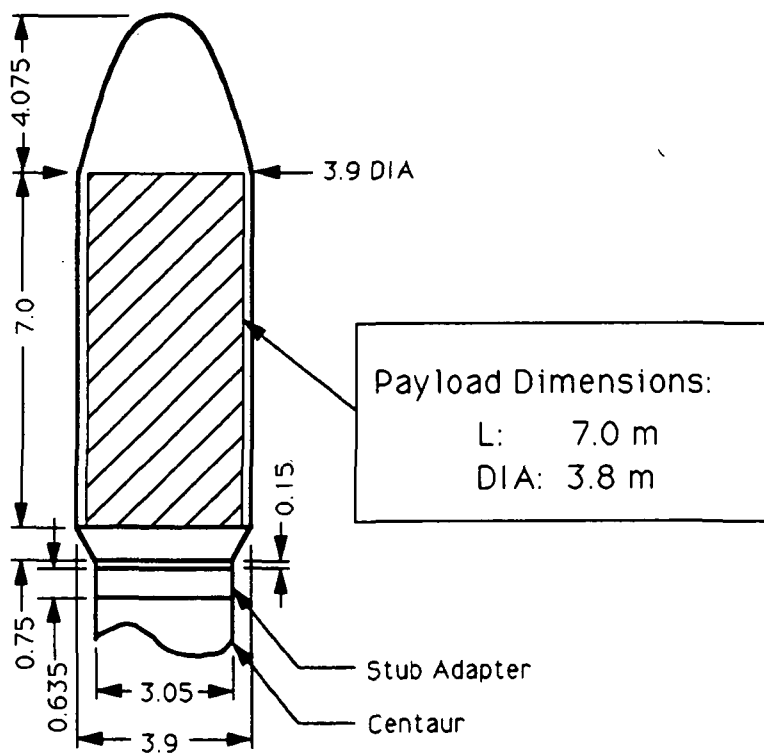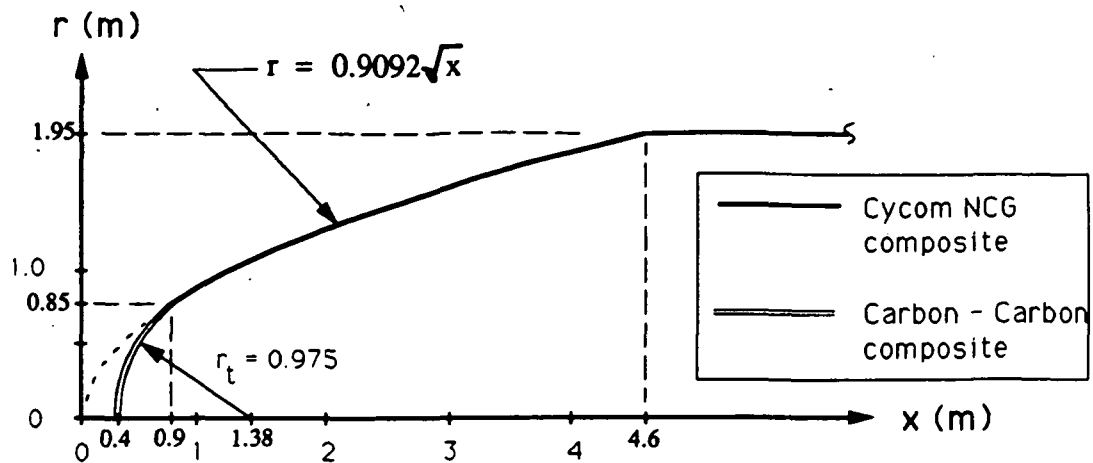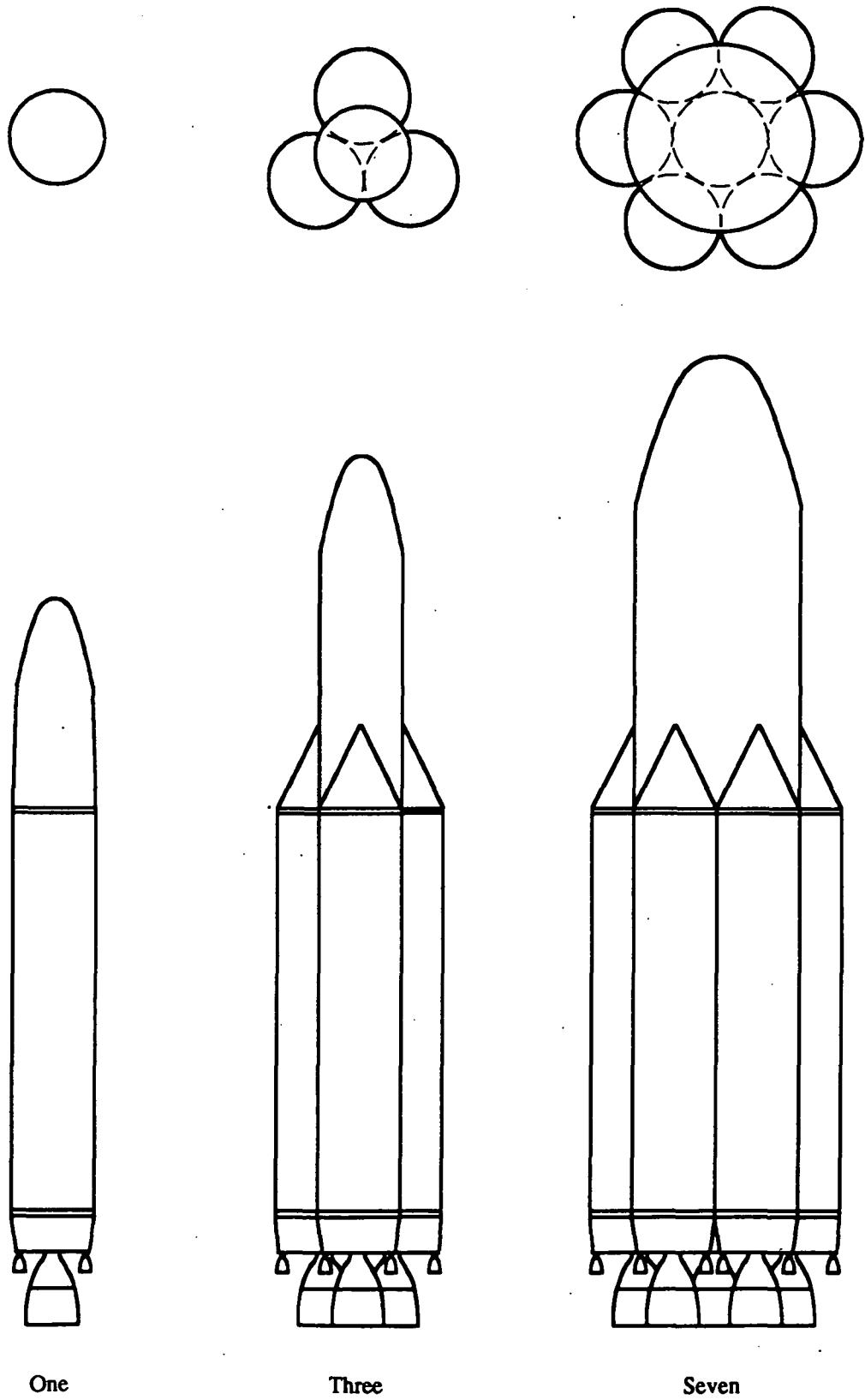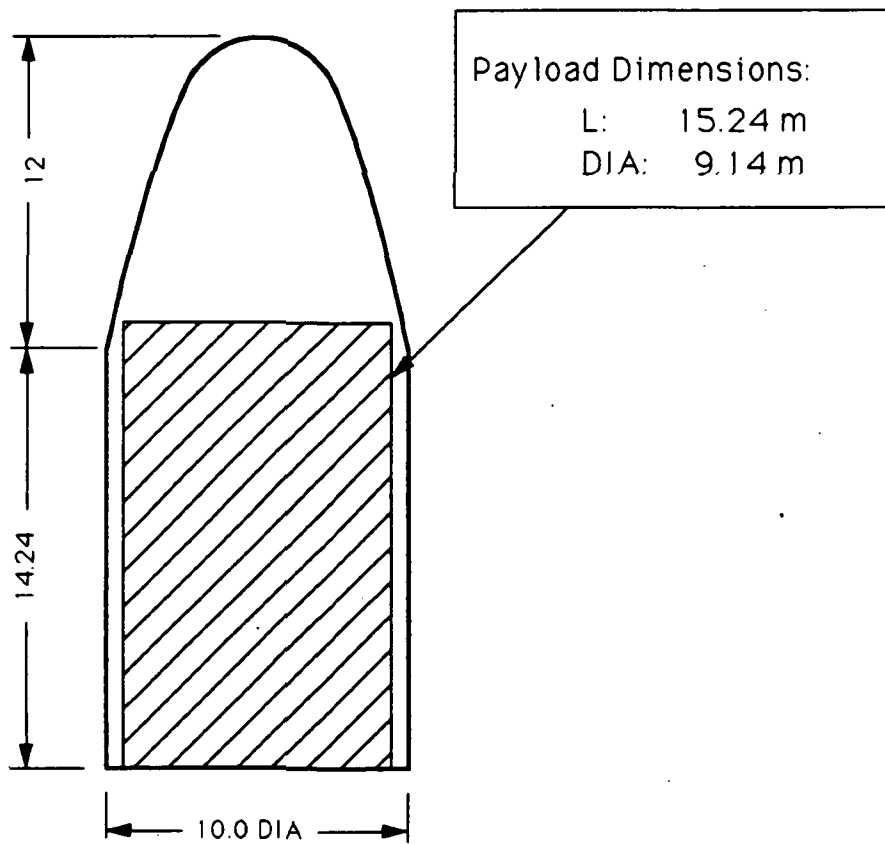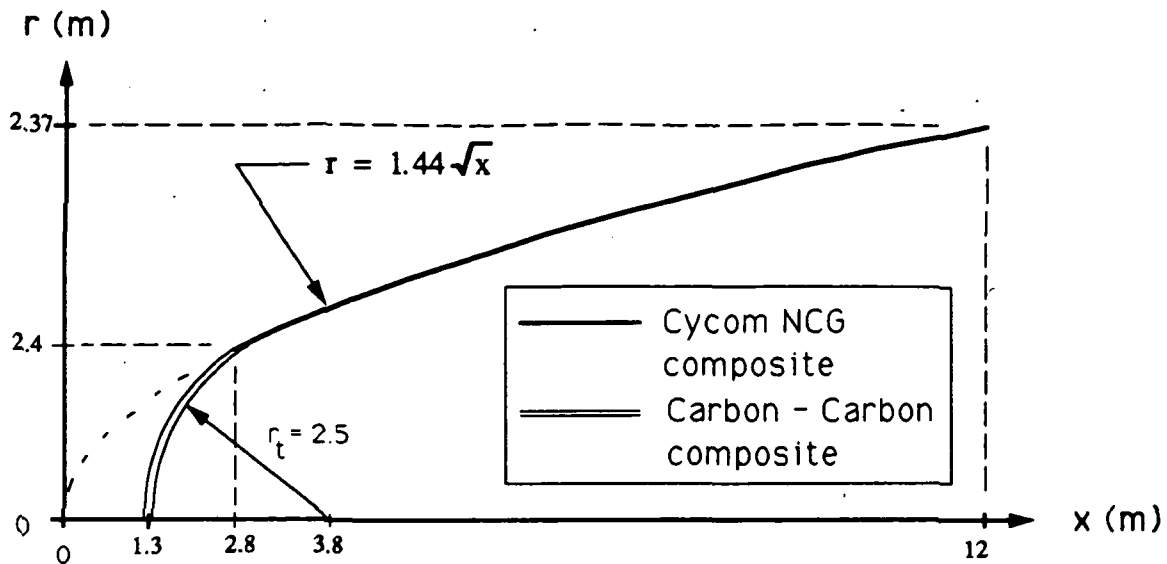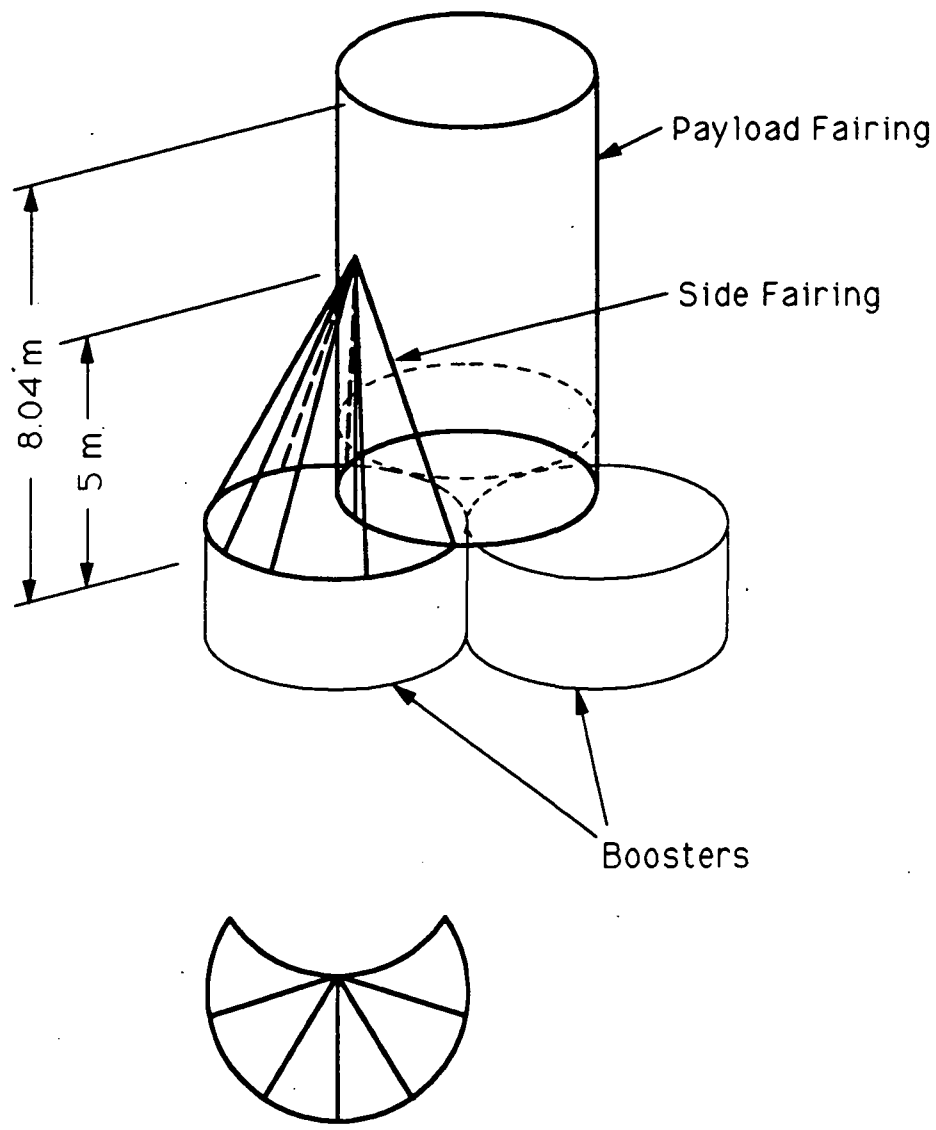
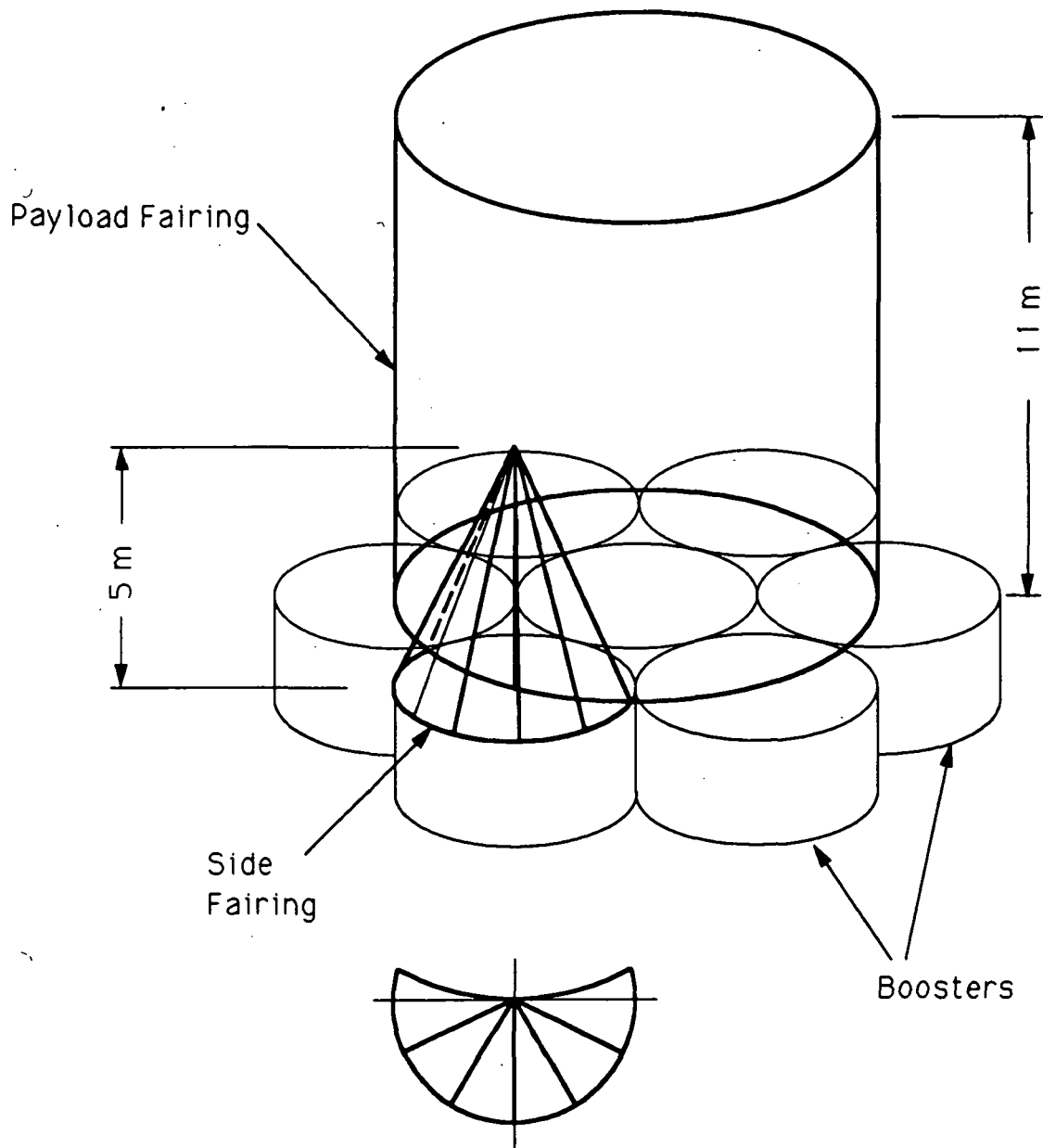Payload Fairing

11 m

5 m

Side
Fairing

Boosters

Fig. 6.15. Additional fairing for Antares VII.

161

# 7.0 CONFIGURATIONS

By far the most distinguishing feature of Antares, setting it apart from other space launch vehicles, is the concept of a completely modular system. The design of such a system was driven toward simplicity in both construction and operation. In this section, the modular capabilities of Antares are described in greater detail. A possible launch facility design and method are also presented. Lastly, the Emergency Propellant Communication System (EPCS) and the capabilities it provides Antares in the event of an engine failure during a LEO mission are discussed.

## 7.1 CAPABILITIES
(Hobie Anderson)

The capabilities of a modular Antares vehicle will largely be at the discretion of the customer, who will have a choice between among offered configurations, each independently operable in low Earth orbit missions. The modular configurations are essentially a group of vehicles attached through the use of structural hard-points.

There are six hard point locations on both the forward and aft tank stiffening rings. An illustration of the hard points is shown in Fig. 7.1. The two hard point rings are capable of withstanding the large bending moments and shearing forces that would be applied if one engine were to become inoperative. The shear forces experienced by the Antares hard points in case of an engine failure are much less than the shear forces experienced by the Space Shuttle's hard points in normal operation. The Space Shuttle's hard points experience shear forces and bending moments due to the dead weight of the external tank, which is much more massive than a single Antares vehicle.

The modular configurations can range from groups of two to seven Antares vehicles, arranged as shown in Fig. 7.2. The payload mass for each configuration is dependent upon the applicable fairing to be used. There will be three sizes of fairings, each of which can be

elongated with corresponding extended mid sections, thus complementing Antares' concept of complete modularity. Descriptions of the fairings employed on the Antares are described in Section 6 of this report. Due to the flexibility in fairing designs, payloads for each configuration are given in Table 7.1 in the form of LEO payload plus fairing weights. This is because each fairing design ultimately affects the amount of payload a particular configuration can deliver to LEO, due to the fairing's weight and atmospheric drag considerations.

To calculate the appropriate modular configuration for a potential customer, one would first calculate the appropriate fairing needed according to the volume of his satellite. Secondly, the customer would then add the weight of his satellite to that of the appropriate fairing. Finally, the customer would then select one of the Antares configurations listed in Table 7.1 to accommodate the necessary payload for launch to LEO.

In addition, some of these configurations may be used at a later date for payloads beyond LEO, should the market develop for this type of launch service. Possible future mission scenarios could include using a modular vehicle to launch heavy GEO payloads or establish the infrastructure necessary for lunar or planetary missions, including manned missions.

Table 7.1: LEO configuration mission capabilities.

| Number of Antares | Payload + Fairing | |
|:---:|:---:|:---:|
| | (kg) | (lbs) |
| 1 | 11,400 | 25,130 |
| 2 | 22,800 | 50,265 |
| 3 | 34,200 | 59,529 |
| 4 | 45,600 | 75,400 |
| 5 | 57,000 | 125,660 |
| 6 | 68,400 | 150,800 |
| 7 | 79,800 | 175,925 |

## 7.2 ENGINE OUT CAPABILITY
(El Mehdi Arzaz)

In the multiple booster configuration, there is a capability of reaching orbit in the event of a non-catastrophic engine failure. This capability is highly dependent on the time at which the failure occurs. If the engine fails too early in the mission, i.e. before the minimum allowable time before failure is reached, then there is no alternative but to abort and destroy the vehicle. In order to minimize ground impacts if the previous scenario occurs, explosive charges are located within the ERU and the payload to destroy the largest sections of the vehicle. However, if the failure occurs late in the flight, the mission can still be accomplished by using the Emergency Propellant Communication System (EPCS), which is discussed in the next section. The minimum times that must elapse before an engine can fail without jeopardizing the mission are tabulated in Table 7.2. These numbers are based on the assumption that the non-functioning engine is kept as dead weight during the remainder of the flight. It can be seen that the more boosters in the configuration, the shorter is the minimum time allowable before engine failure. A comparison of total time to burnout can also be done. The total elapsed time to burnout for a normal flight is 367 seconds for a LEO mission, using the available continuous throttle back on the engine to keep the final acceleration below 4 G. The burnout times for the engine out cases are tabulated in Table 7.2.

Table 7.2: Engine out capabilities.

| Number of Antares Units in Configuration | Minimum Time Acceptable before Engine Failure (sec) | Total Time to Burnout (sec) |
|---|---|---|
| 2 | 190 | 480 |
| 3 | 165 | 430 |
| 4 | 145 | 415 |
| 5 | 130 | 405 |
| 6 | 120 | 400 |
| 7 | 110 | 390 |

Using the NASA requirements on reserve propellant [1] , it was found that a minimum of 500 kg of propellant is needed in each unit .

The reserve fuel was calculated according to the following equations:

$$\Delta v_1 = -U_{e1} * \ln[\frac{(M_s + M_* + M_p - M_{p1})}{(M_p + M_s + M_*)}]$$ (7.1)

$$\Delta v_2 = -U_{e2} * \ln[\frac{(M_s + M_*)}{(M_p - M_{p1} + M_s + M_*)}]$$ (7.2)

$$\delta v_1 = 0.01 * \Delta v_1$$ (7.3)

$$\delta v_2 = 0.01 * \Delta v_2$$ (7.4)

$$M_{pr1} = (M_s + M_* + M_p - M_{p1}) * \exp(\frac{\delta v_1}{U_{e1}})$$ (7.5)

$$M_{pr2} = (M_s + M_*) * \exp(\frac{\delta v_2}{U_{e2}})$$ (7.6)

$$M_{pr} = M_{pr1} + M_{pr2}$$ (7.7)

where:

$M_s$ = Structural mass (kg).
$M_p$ = Minimum propellant mass needed to complete the mission (kg).
$M_*$ = Payload mass (kg).
$M_{p1}$ = Propellant mass used during the 12:1 O/F ratio phase (kg).
$M_{pr}$ = Total mass of reserve fuel (kg).
$M_{pr1}$ = Reserve fuel mass for the 12:1 O/F ratio phase (kg).
$M_{pr2}$ = Reserve fuel mass for the 6:1 O/F ratio phase (kg).
$U_{e1}$ = Exit velocity for the 12:1 O/F ratio phase (m/sec).
$U_{e2}$ = Exit velocity for the 6:1 O/F ratio phase (m/sec).
$\Delta v_1$ = Change in velocity at the end of the 12:1 O/F ratio phase (m/sec).
$\Delta v_2$ = Change in velocity at the end of the 6:1 O/F ratio phase (m/sec).
$\delta v_1$ = 1% of $\Delta v_1$ (m/sec).
$\delta v_2$ = 1% of $\Delta v_2$ (m/sec).

When using two or more boosters, the reserve fuel will be used to accomplish the mission in case of one engine failure.

During the optimization process, jettisoning the failed engine was also considered. The data in Table 7.3 present the results of this alternative scenario, when it is feasible. By comparing Table 7.2 and Table 7.3, it can be seen that the time to failure can be reduced by up

to 50 sec, if the malfunctioning engine is dropped immediately after engine failure occurs. However, this option may not viable at all times during the flight, since the jettisoned engine must not fall on a busy ocean shipping lane. With either of the two scenarios, it can be seen that the Antares spends more time in the atmosphere. The longer burnout time is due to fact that the mission is being completed with one less engine but with the same amount of propellant.

In conclusion, it can be seen that the loss of an engine in a mission does not mean that the mission has to be aborted. If the failure happens after the first minimum time (Table 7.3) is reached, i.e. using the jettison option, the mission can be saved by dropping the failed engine. However, if the vehicle is over a busy ocean shipping lane so that the failed engine cannot be jettisoned, the mission will have to be aborted. On the other hand, if the failure happens anytime after the second minimum time (Table 7.2) is reached, the mission can be accomplished in any case.

Table 7.3: Engine out capabilities after dropping the failed engine.

| Number of Antares Units in Configuration | Minimum Time Acceptable before Engine Failure (sec) | Total Time to Burnout (sec) |
|---|---|---|
| 2 | 145 | 525 |
| 3 | 115 | 455 |
| 4 | 100 | 430 |
| 5 | 90 | 420 |
| 6 | 80 | 408 |
| 7 | 72 | 400 |

## 7.3 EMERGENCY PROPELLANT COMMUNICATION SYSTEM (EPCS)
(El Mehdi Arzaz)

In the multiple booster configurations there is a possibility that an engine may fail, as noted above. In order to have engine out capability, the fuel and oxidizer tanks on each booster must be manifolded in a manner that allows the propellants from the failed booster to be distributed to the other boosters, so that the mission can be completed. The Emergency Propellant Communication System (EPCS) is used to transfer propellants from a faulty booster to the other boosters' engines. Since the fuel and oxidizer lines run along the outside of each booster, connecting the lines between the tanks for EPCS is simple. For example, on the Antares II, each booster has one fuel and one oxidizer line. The EPCS allows each booster access to another boosters' fuel and oxidizer supplies. The propellant lines are designed to take in fuel from either tank. Since the propellant from both tanks can be rerouted, as shown in Fig. 7.3 for the Antares II, the modular vehicle has the capability to use up all of its propellant and complete the mission, even if an engine fails. In the multiple Antares configurations each booster has its own fuel and oxidizer line. Also, each fuel and oxidizer line is interfaced with another tank in a manner that allows the propellants from all the tanks to be interconnected. Figure 7.4 illustrates where the propellant lines are positioned for the multiple configurations of the Antares Launch System.

Each Antares booster is constructed with two ports along the sides of the fuel and oxidizer tanks. One port for the oxidizer tank and one for the fuel tank. These propellant lines run along the sides of the tank until they reach the ERU units, where they are divided and connected to two different ERU's as shown in Fig. 7.3. This concept also helps for the fueling of the rockets - since their fuel and oxidizer tanks are connected, fueling one tank fuels all the others.

## 7.4  GROUND OPERATIONS
(Hobie Anderson, El Mehdi Arzaz)

For the multiple modular configurations to be effective, a new launching system will have to be developed, which will contribute to the flexibility incorporated into the Antares design.  The launch pad will have to be able to accommodate all possible Antares configurations from the Antares I to the Antares VII.  The launch facilities should have a quick turnaround time between launches.  Current launch facilities incorporate the rocket's mission assembly at the site of takeoff, on the launch pad.  The current practice is placing payloads on the vehicle after its delivery to the launch pad.  This translates into long turnaround times between launches, due to the necessity for each vehicle to occupy a pad while undergoing final assembly and payload integration.  The launch facility for the Antares does not necessitate any assembly of the payload or configuration of the vehicle, once it has been positioned at the launch pad.

Our proposed launch facility, which is illustrated in Fig. 7.5, will fully complement the Antares vehicle by its ease in operation and quick launch turnaround time.  The facility is in the vicinity of the main construction plant for the Antares vehicle.  This plant will fully assemble the Antares vehicle, as well as carry out payload integration.  The vehicle will be assembled while lying on its side upon a large railroad car type transporter.  The transporters are constructed with braces which support the Antares vehicle in any configuration as it is assembled and delivered to the launch pad.  An end view schematic of a transporter loaded with an Antares VII vehicle enroute to the launch pad is shown in Fig. 7.6.

The transporter also acts as the lifter for the Antares vehicle upon arrival at the pad, thus it  also includes the necessary hydraulic mechanisms which enable it to stand an Antares configuration up on end when necessary, as shown in Fig. 7.7 for the Antares I and in Fig. 7.8 for the Antares VII.  The method of placing the launch vehicle onto the launch pad through lifting the vehicle from a horizontal position into a vertical position has been used successfully by the Soviet Union.

The transporters carry the Antares vehicle to the launch pad, erect the vehicle and place it upon stations which support the vehicle's weight. The lifter remains extended as a support until just before liftoff when it is retracted and moved away from the launch pad to avoid the intense rocket exhaust during takeoff.

The fueling process is simplified by fueling only one booster and allowing the EPCS to distribute the fuel to all the boosters in the configuration while on the launch pad. Fueling the Antares is the only process which is carried out at the launch pad site. This allows Antares to perform many launches from the same facility with a quicker pad turnaround time than is presently possible. The versatility of this launch system allows Antares to significantly cut ground operations costs.

## 7.5 NOMENCLATURE

| | |
|---|---|
| $M_s$ | Structural mass (kg). |
| $M_p$ | Minimum propellant mass needed to complete the mission (kg). |
| $M_*$ | Payload mass (kg). |
| $M_{p1}$ | Propellant mass used during the 12:1 O/F ratio phase (kg). |
| $M_{pr}$ | Total mass of reserve fuel (kg). |
| $M_{pr1}$ | Reserve fuel mass for the 12:1 O/F ratio phase (kg). |
| $M_{pr2}$ | Reserve fuel mass for the 6:1 O/F ratio phase (kg). |
| $U_{e1}$ | Exit velocity for the 12:1 O/F ratio phase (m/sec). |
| $U_{e2}$ | Exit velocity for the 6:1 O/F ratio phase (m/sec). |
| $\Delta v_1$ | Change in velocity at the end of the 12:1 O/F ratio phase (m/sec). |
| $\Delta v_2$ | Change in velocity at the end of the 6:1 O/F ratio phase (m/sec). |
| $\delta v_1$ | 1% of $\Delta v_1$ (m/sec). |
| $\delta v_2$ | 1% of $\Delta v_2$ (m/sec). |

## 7.6  REFERENCES

1.  Parkman, D., Boeing Defense and Space Group, Seattle, WA, personal communication, April 1991.

Connecting Strut

Hard Points

Assembly Locations

Side View

Antares

Antares

Top View
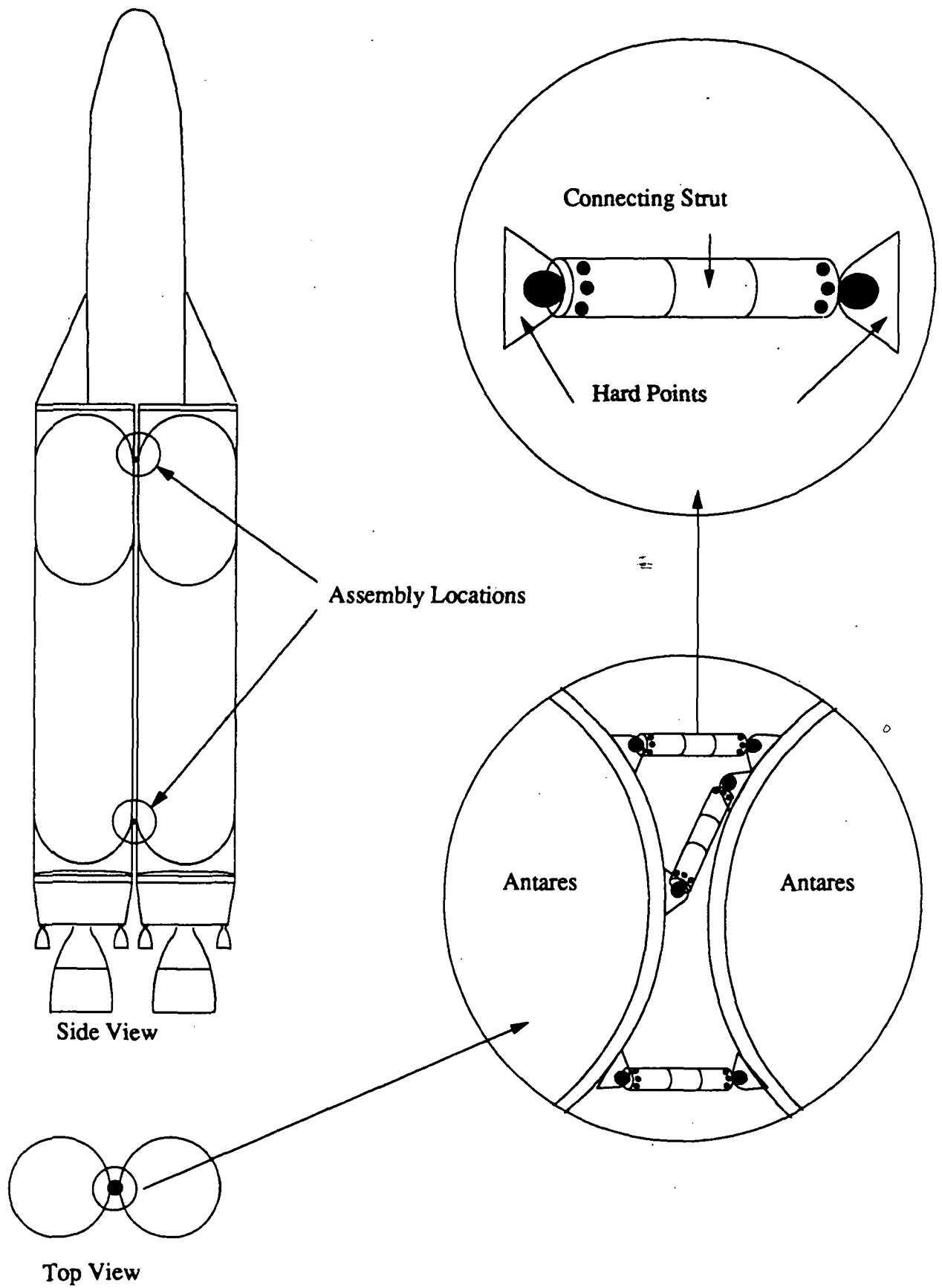
7.1  Hardpoint locations for Antares II.

173

a) Antares II

b) Antares III

c) Antares IV

d) Antares V

e) Antares VI
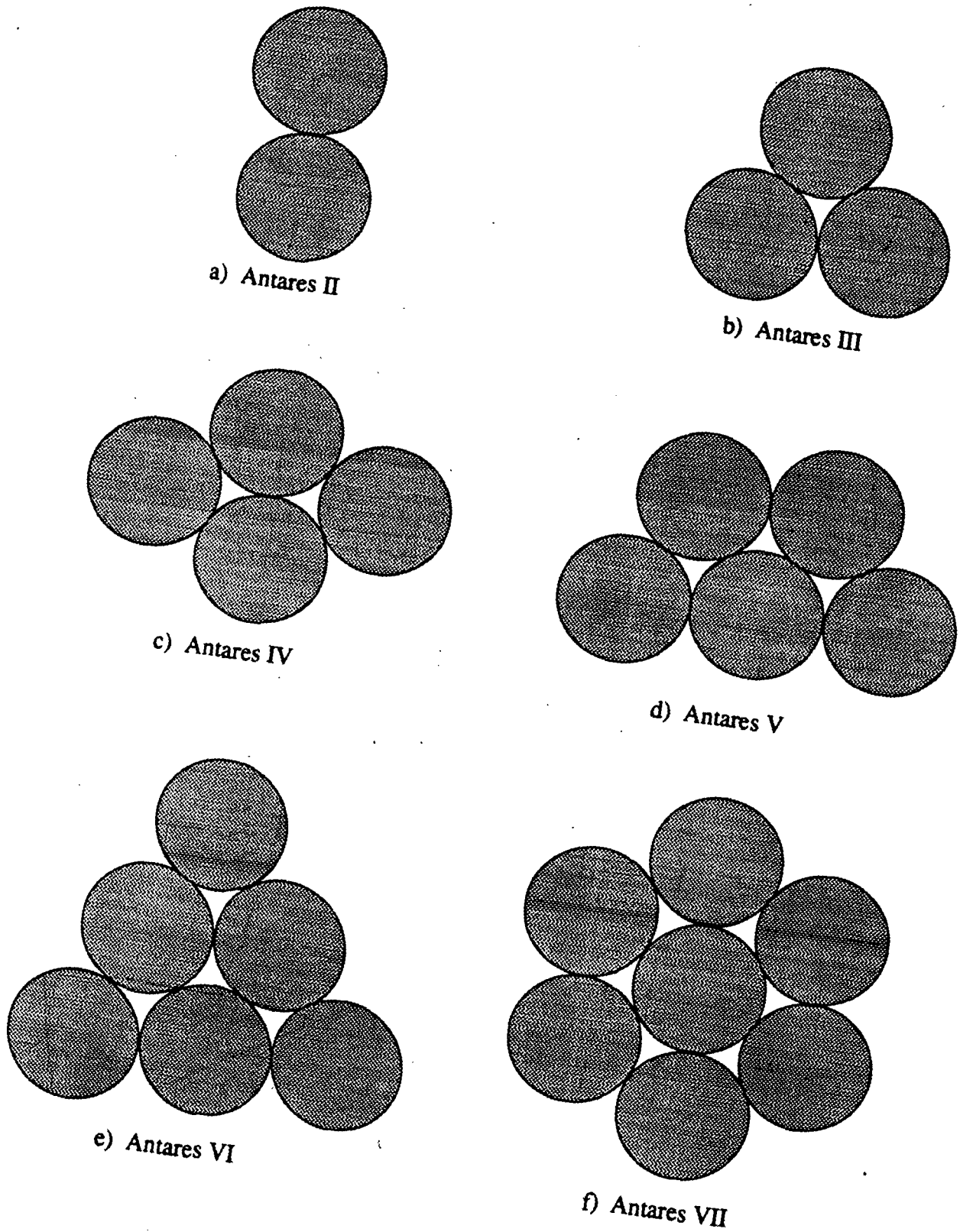
f) Antares VII

Fig 7.2 Plan view of Antares modular configurations.

174
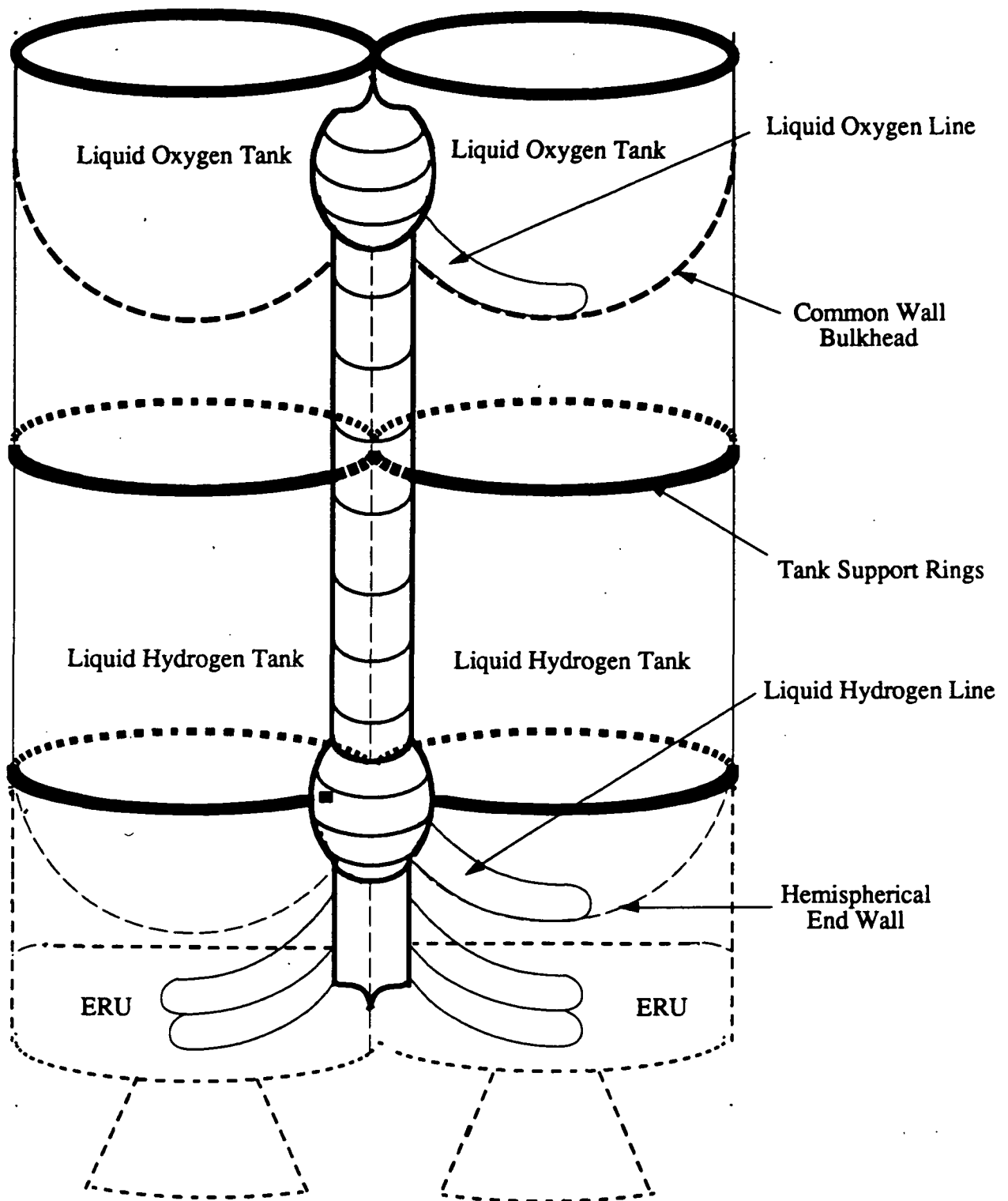
Fig. 7.3 Double configuration Emergency Propellant Communication System (EPCS). (These line are not to scale in order to efficiently illustrate them).

a)  Antares II

b)  Antares III

c)  Antares IV

d)  Antares V

e)  Antares VI

f)  Antares VII

● Liquid Oxygen Line

o Liquid Hydrogen Line

Fig. 7.4 Propellant line orientation for different Antares configurations.

Fig. 7.5 Launch pad facilities.

Fig. 7.6 Tranporter for Antares VII. (Figure not to scale to show different parts).

Fig 7.7  Ground operation for Antares I.

Fig 7.8 Ground operation for Antares VII.

# 8.0 COST ANALYSIS
## (Alvin Jackson)

For the Antares vehicle to establish itself as the premiere launch vehicle in the 21st century it must be cost effective. To achieve this goal the Antares utilizes many cost saving techniques. One of these techniques is utilizing the Engine Return Unit to retrieve the DMRE engine and the avionics, which together can account for up to 70% of total vehi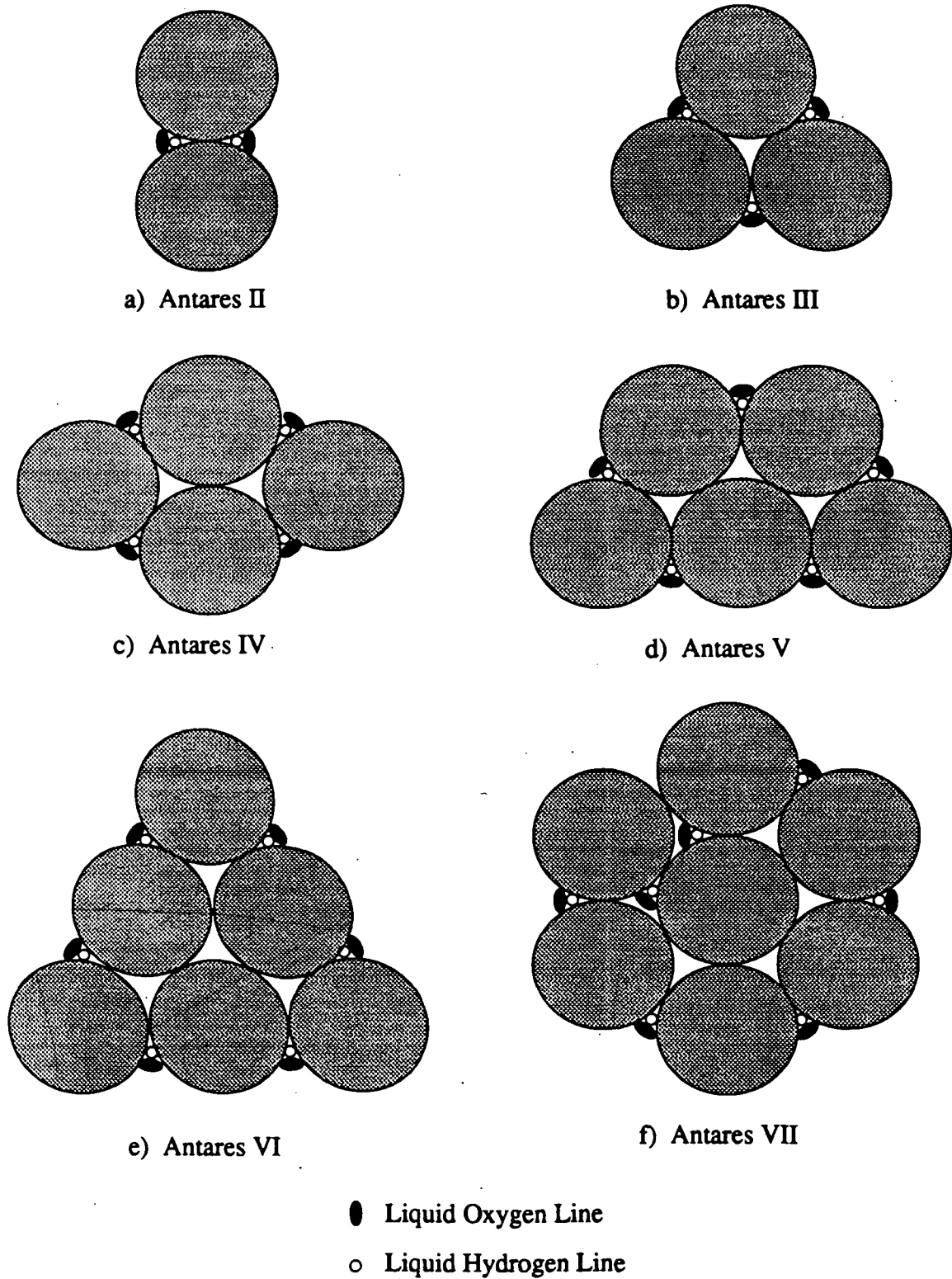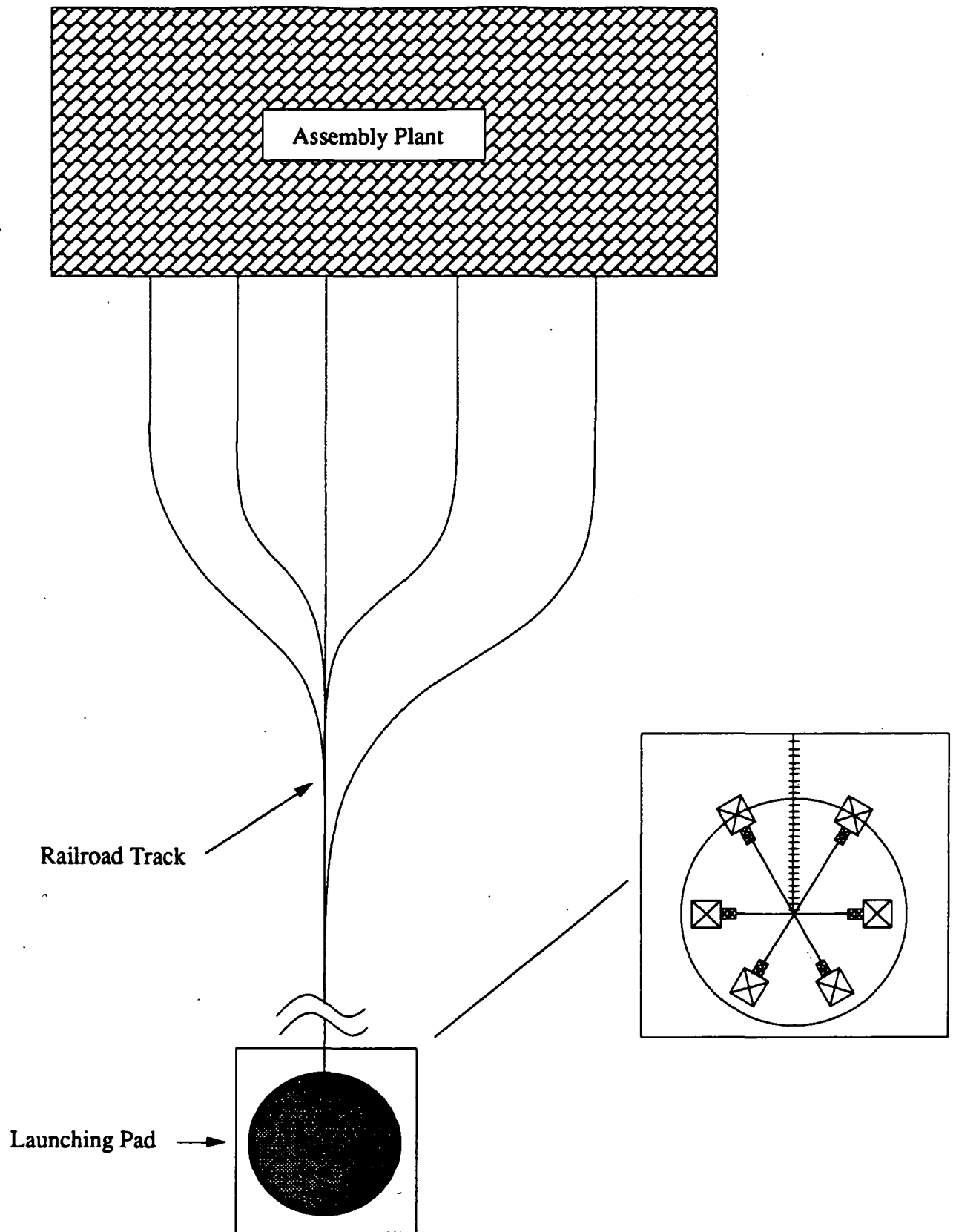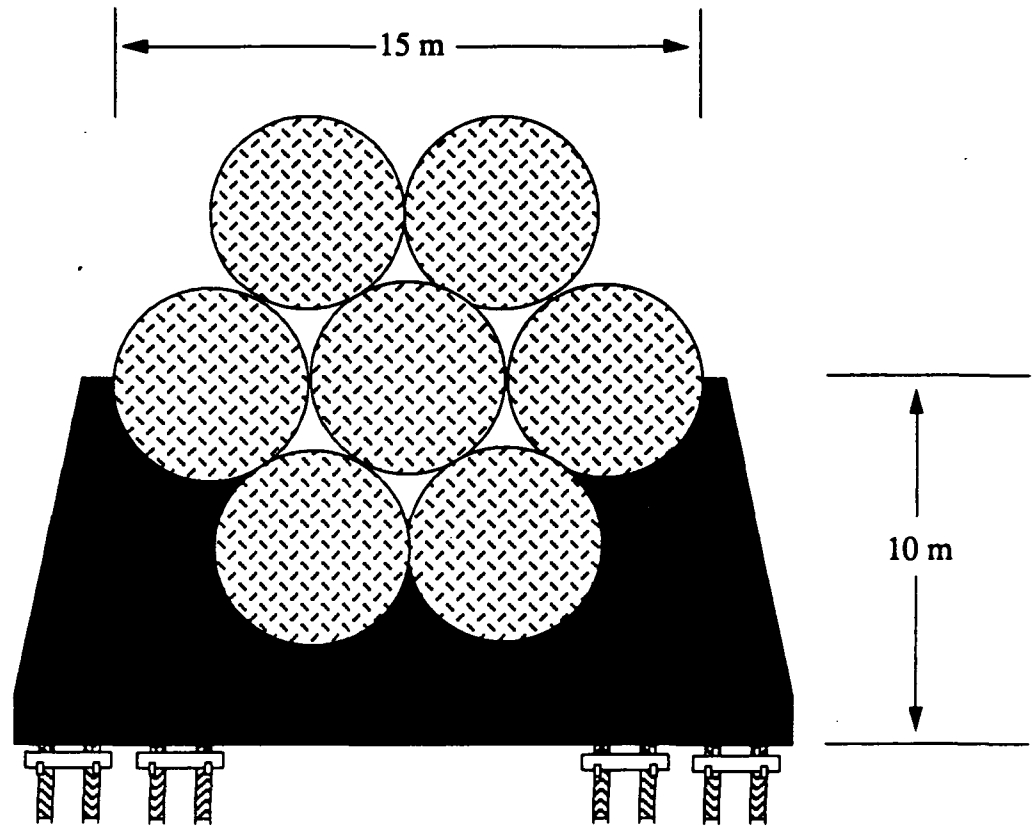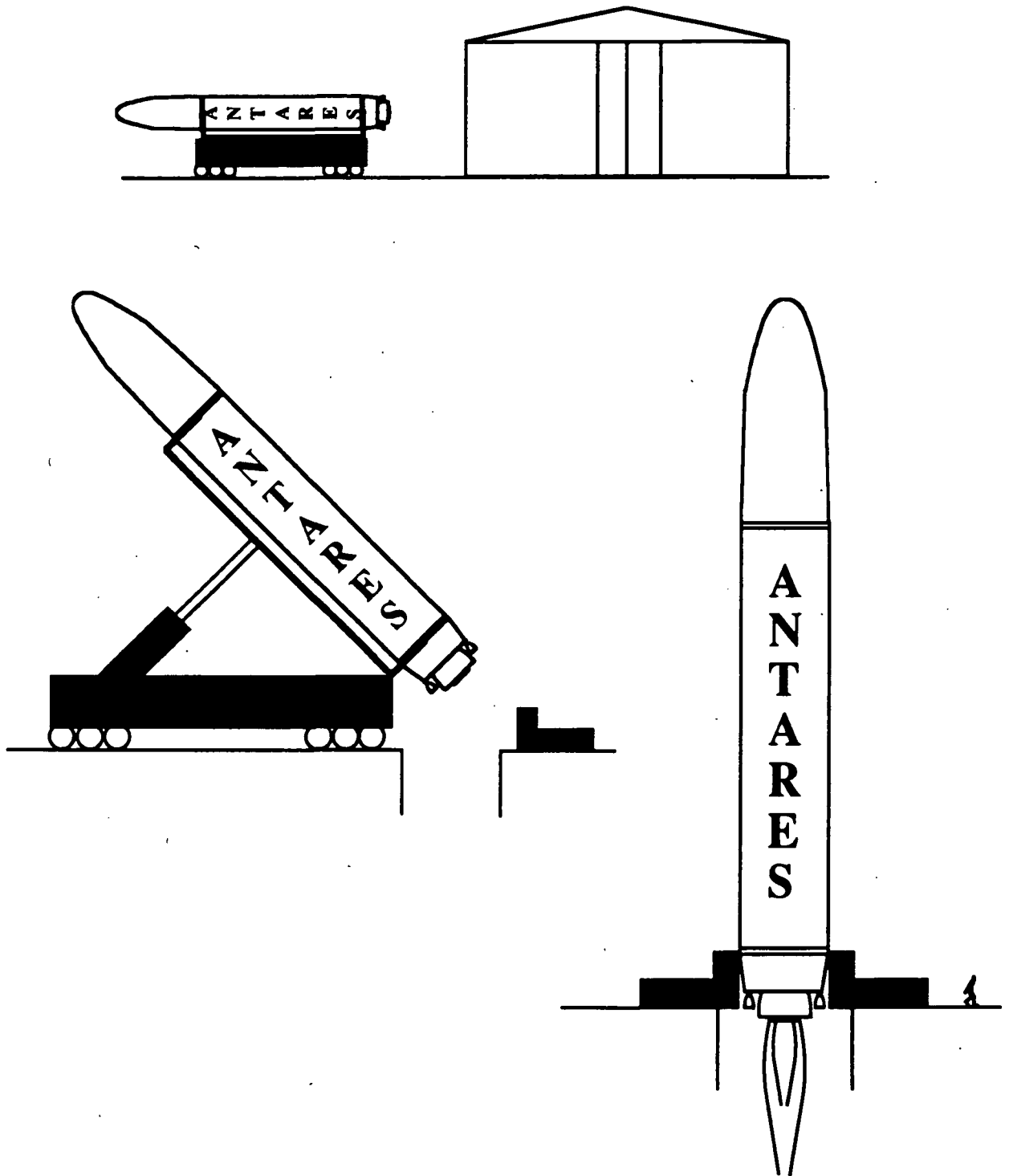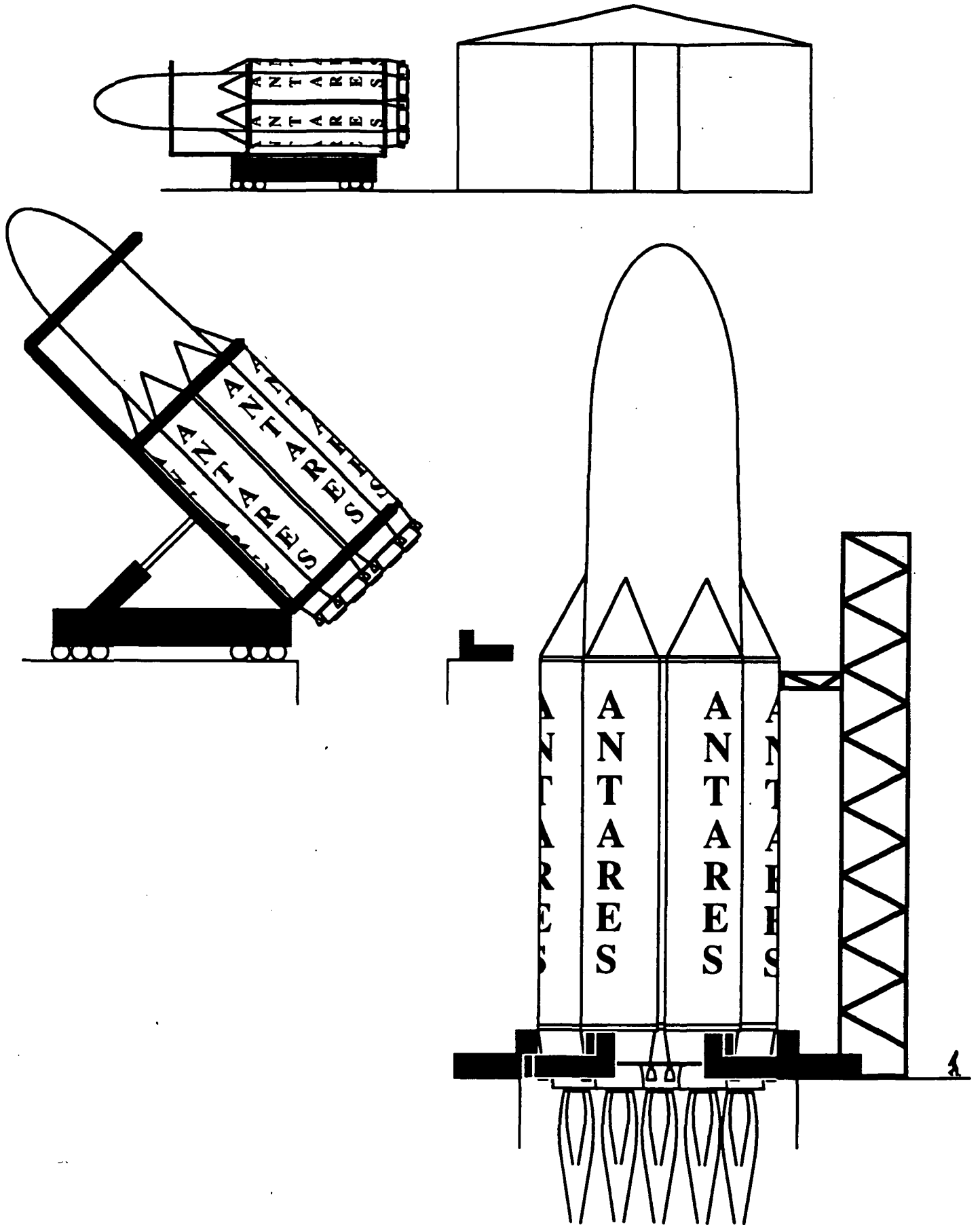cle cost. The savings incurred by reusing the expensive components of the Antares translate directly to a much lower cost per unit payload mass to the customer.

To determine the cost per unit payload mass for Antares many factors were taken into consideration. The cost data were developed using cost per kilogram estimates for the various components of the Antares vehicle [1]. The data obtained were then adjusted, utilizing learning curves of 90% and 85% for the ERU and tank components, respectively. The learning curve adjusts the production costs to account for productivity improvements as more units are produced. Different learning curves were utilized due to the different production rates and complexity of these two components. Once the data were adjusted using the learning curves they were calculated for an average year in the mission model. From this an average cost per unit payload mass was determined.

## 8.1 MISSION MODEL

The mission model for the Antares shows the number of flights in a given year over the lifespan of the Antares vehicle, which was set at 40 years (see Fig. 8.1). The mission model for the Antares fits within the expected growth in launch rates predicted by the Office of Technology Assessment (OTA) [2]. The OTA did not consider the possible increase in launch rates if a low cost vehicle were developed. The mission model is assumed to end after 40 years for cost analysis purposes, but could continue well past the 40 year lifespan. This model is employed to determine the number of Antares vehicles utilized in the cost analysis.

The Antares will begin its first year of providing launch services with five launches, and increase steadily until the 13th year, in which there will be 30 launches. This is the maximum number of launches per year for the mission model utilized. From the 13th year until the 24th year the launch rate remains constant at 30 launches per year. After the 24th year of services the mission model decreases until the 40th year of service when the number of launches will be zero. The total number of Antares launches for the 40 year life span is 900. For the purposes of the cost analysis it is not necessary to specify how many of these launches are single Antares launches or modular configuration launches, since it is assumed that the total launch cost of one of the modular configurations will be a corresponding multiple of the Antares I launch cost.

## 8.2 LIFE CYCLE COST

The life cycle cost of the vehicle is broken up into three components: Research, Development, Test, and Evaluation (RDT&E) cost, the production costs which are a function of the Theoretical First Unit (TFU) cost, and the Operations and Support (O&S) cost. The RDT&E cost includes all of the design, analysis and testing of the Antares vehicle. The TFU cost indicates the production cost for one Antares vehicle and is the basis for computing the cost for multiple units in production. The O&S cost consists of ongoing operations and supplying personnel for launches, and also includes the refurbishment costs for the ERU. All of these costs are necessary to determine the expenditures required to put the Antares on line, and to calculate the cost per unit payload mass.

The determination of total RDT&E and TFU costs for the Antares was done by separating the components of the vehicle into eight categories, which are listed in Table 8.1. Cost per kilogram values for RDT&E and TFU costs were obtained for each of the eight categories [1]. Two separate sets of data were used for the tank and ERU components due to the differing complexities of these units. The total vehicle weight was broken down into the various categories and multiplied by the respective cost per kilogram value to arrive at total

182

RDT&E and TFU costs . The RDT&E costs (see Fig. 8.2) are final after this procedure but the TFU costs (see Fig. 8.3) need to be adjusted utilizing the learning curve.

Table 8.1: Categories for life cycle costs.

| Category | Example of components in Category |
|---|---|
| Structure | Propellant tanks, fairings, ERU thrust frame |
| Thermal Control | Insulation, heat shield, thermal casing |
| Avionics | On board computers, accelerometers, etc. |
| Power | Batteries |
| Main Propulsion | DMRE engine, and associated piping |
| Secondary Propulsion | Maneuvering engines, and associated piping |
| Recovery Systems | Parafoils, flotation devices |
| Staging Ordnance | Explosive bolts, range safety devices |

The learning curve slopes for the tanks and the ERU are assumed to be 85% and 90% respectively. Production costs are obtained by multiplying the TFU cost by the learning curve factor L:

$$\text{Production Cost} = \text{TFU} \times \text{L} \tag{8.1}$$

The learning curve factor is determined from

$$L = N^B \tag{8.2}$$

where
$$B = 1 - \frac{\ln\left(100\%/S\right)}{\ln 2} \tag{8.3}$$

where S is the learning curve slope and N is number of units produced.

For the tanks N was set at 900, the total number of flights, and for the ERU N was set at 14. Only 14 ERU's need to be produced because the DMRE engine is reusable, with a lifespan of approximately one hundred starts [3]. Although 14 ERU's more than meet the necessary 900 launches, this number provides for consecutive Antares VII launches, and spares, if necessary. For the cost analysis it is assumed that all 14 of the ERU's are configured for LEO missions. This is a conservative estimate due to the fact that the LEO ERU is more complex, thus more expensive, than the ERU's configured for GEO missions. The production costs for the ERU and the tanks are calculated for the total number of production units and averaged for each individual flight in a given year.

The Operations and Support costs are calculated using a linear slope approximation:

$$Y = MX + K \hspace{4cm} (8.4)$$

In Eq. 8.4 Y is the O&S cost for the given year, M is a constant value, X is the number of vehicles flown in the given year and K is a constant value which indicates the constant cost per year, which is not a function of launches. To calculate the O&S cost for a certain year the constant values and the number of flights are inserted into Eq. 8.4. The total O&S cost is divided by the number of flights in that year to determine the average O&S cost per flight for that year. By using a linear slope approximation the O&S costs are decreased, on a per flight basis, with more flights taken. Yet, if there are no flights (X = 0) in a given year the, O&S costs are still incurred with the constant K. These trends can be seen in Fig. 8.4.

Other factors that are added into the O&S costs are the propellant costs for the entire vehicle and the refurbishment and recovery costs for the ERU. The propellant costs are determined in a similar matter as the TFU cost in that a cost per kilogram of propellant is given and this value is multiplied by the mass of that propellant. The recovery and refurbishment cost of the ERU includes personnel to recover and refurbish the unit, equipment necessary to refurbish it and all the necessary hardware to recertify the unit for its next flight. The recovery and refurbishment cost for one ERU is assumed to be 2% of the total cost of the ERU. This

184

amounts to approximately $500,000 to recover and refurbish each ERU, which will adequately provide for labor, spare parts, and recertification procedures.

## 8.3  COST PER UNIT PAYLOAD MASS

### 8.3.1  LOW EARTH ORBIT

To determine the cost per unit payload mass for the Antares all of the previous data must be taken into account. The RDT&E costs are spread out over the 900 flights contained in the mission model. A model year is chosen to determine the average cost per unit payload mass - for our analysis the 15th year of service is chosen. In that year 30 launches are scheduled. The values obtained for production costs, and O&S costs are summed up for this number of launches and divided by 30 to determine the average launch cost for one vehicle. A cost per unit payload mass can be obtained by simply dividing the average launch cost by the maximum payload delivered to low Earth orbit. The cost per unit payload mass to LEO computed is listed in Table 8.2.

Table 8.2:  Cost per unit payload mass to LEO (in 1991 dollars).

| Cost per kilogram to LEO | $1,340 |
|---|---|
| Cost per pound to LEO | $610 |

### 8.3.2  GEOSYNCHRONOUS ORBIT

The cost per unit payload mass to geostationary Earth orbit is a direct function of the total LEO launch cost. To calculate the cost per unit payload mass to GEO, there are a few other factors that need to be addressed. These factors are the cost of the Centaur, which is the cost of the vehicle and all O&S necessary to launch it, and the additional components, mostly structure, necessary to attach the Centaur to the Antares. These costs are added directly to the total launch cost (RDT&E, TFU, and O&S) obtained in the LEO analysis. From this the GEO

185

cost per unit payload mass is determined by simply dividing the total GEO launch cost by the Antares payload capabilities to GEO. The cost per unit payload mass to GEO computed in this manner is listed in Table 8.3.

Table 8.3: Cost Per Unit Payload Mass to GEO (In 1991 Dollars)

| Cost per kilogram to GEO | $16,200 |
|---|---|
| Cost per pound to GEO | $7,350 |

### 8.3.3 CONCLUSION

From the preliminary data it is evident that the Antares vehicle is capable of providing launch services at a cost unmatched by any existing launch vehicle. The cost per unit payload mass to LEO for the Antares is approximately one-tenth that of the Space Shuttle's and one-sixth of what the current industry leader, Ariane, offers. For these reasons alone it is evident that the Antares launch vehicle is prepared to make space affordable, and to open this market to the world.

## 8.4 NOMENCLATURE

| | |
|---|---|
| RDT&E | Research Development Test and Evaluation |
| TFU | Theoretical First Unit |
| O&S | Operations and Support |
| L | Learning curve factor |
| N | Number of units produced |
| B | Learning curve exponent |
| Y | Total operations and support cost |
| M | Multiplying factor (constant) |
| X | Number of vehicles flown |
| K | Fixed operations and support cost (constant) |

## 8.5 REFERENCES

1. Jordan, J., Boeing Defense and Space Group, Seattle, WA, personal communication, April, 1991.

2. U.S. Congress, Office of Technology Assessment, Access to Space: The Future of U.S. Space Transportation Systems, OTA-ISC-415, U.S. Government Printing Office, Washington, DC, April 1990, p. 16.

3. Limerick, C.D., "Dual Mixture Ratio $H_2/O_2$ Engine for Single Stage to Orbit Application," Journal of Propulsion and Power, Vol. 7, No. 1, Jan.-Feb. 1991, p. 34.
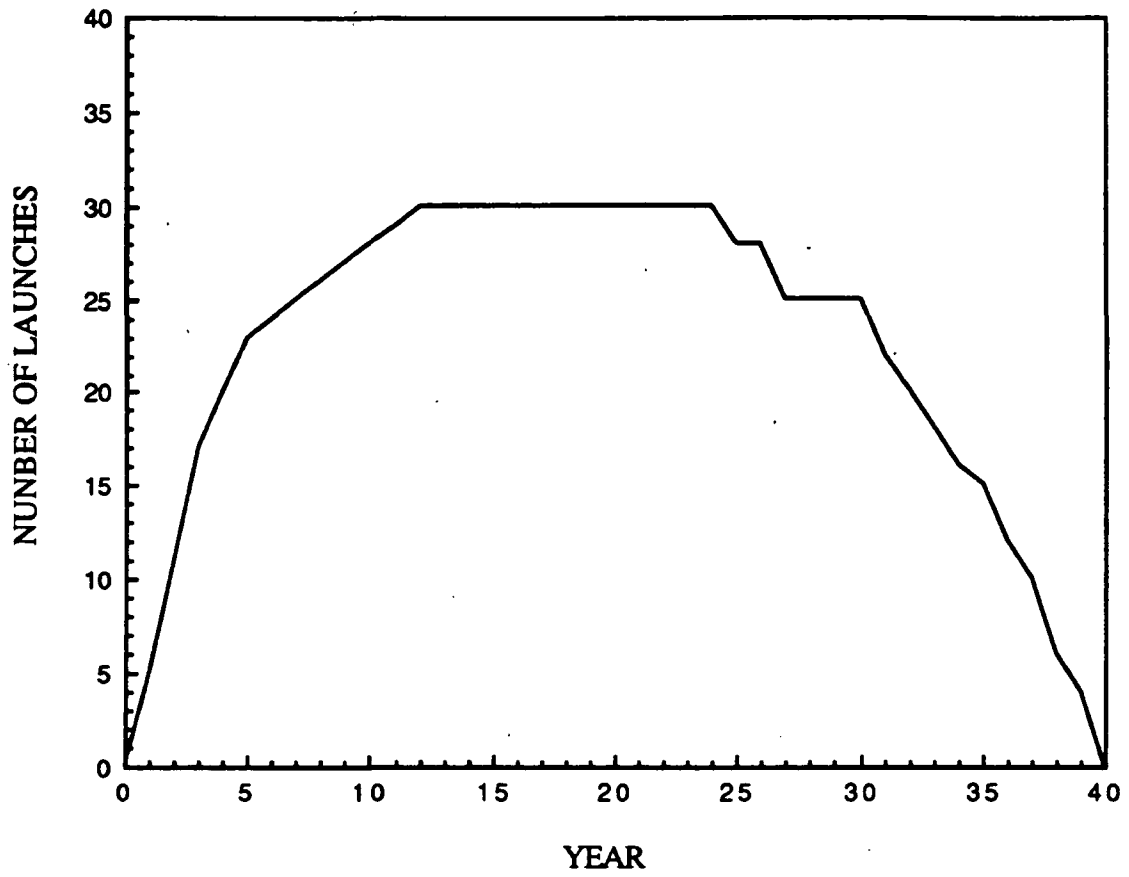
Fig. 8.1. Antares mission model.

CATEGORIES
1 = Structure
2 = Thermal Control
3 = Avionics
4 = Power
5 = Main Propulsion
6 = Secondary Propulsion
7 = Recovery System
8 = Staging/Ordnance

■ Tank Values
▨ ERU Values
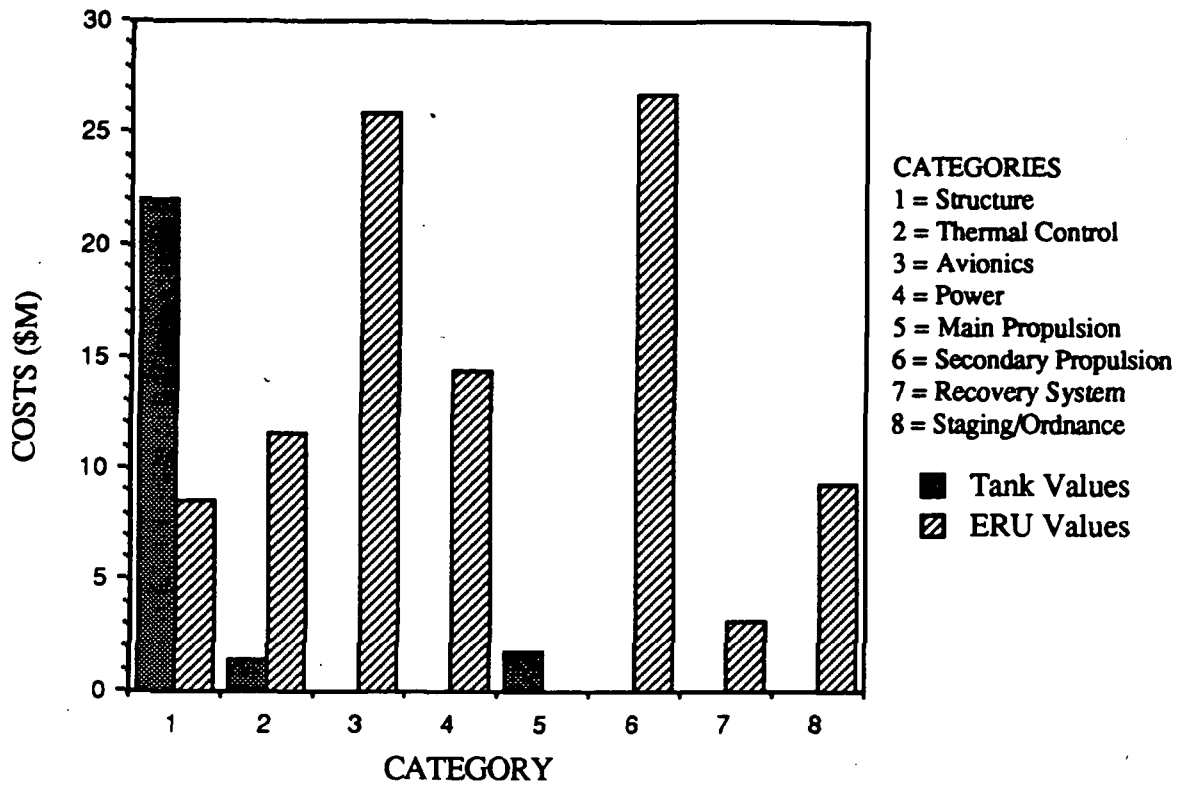
Fig. 8.2. RDT&E costs for tank and ERU components
(in millions of 1991 dollars).

CATEGORIES
1 = Structure
2 = Thermal Control
3 = Avionics
4 = Power
5 = Main Propulsion
6 = Secondary Propulsion
7 = Recovery System
8 = Staging/Ordnance

■ Tank Values
▨ ERU Values
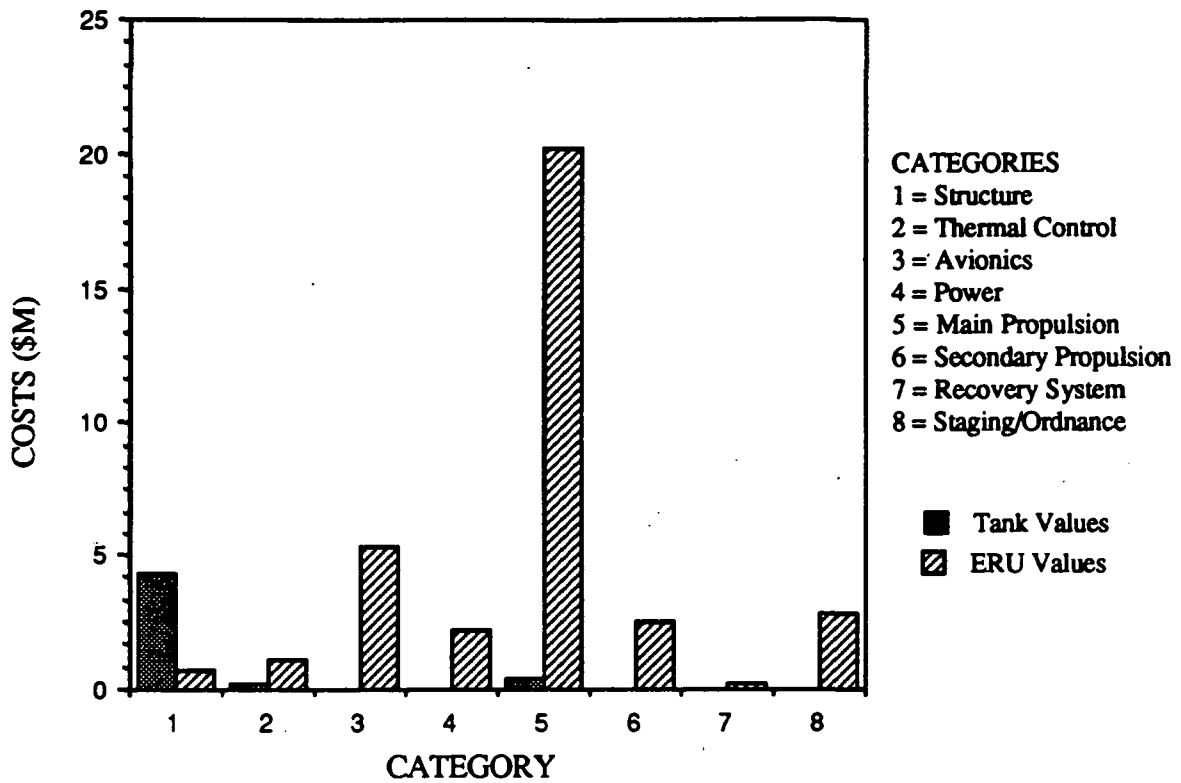
Fig. 8.3. TFU costs for tank and ERU components
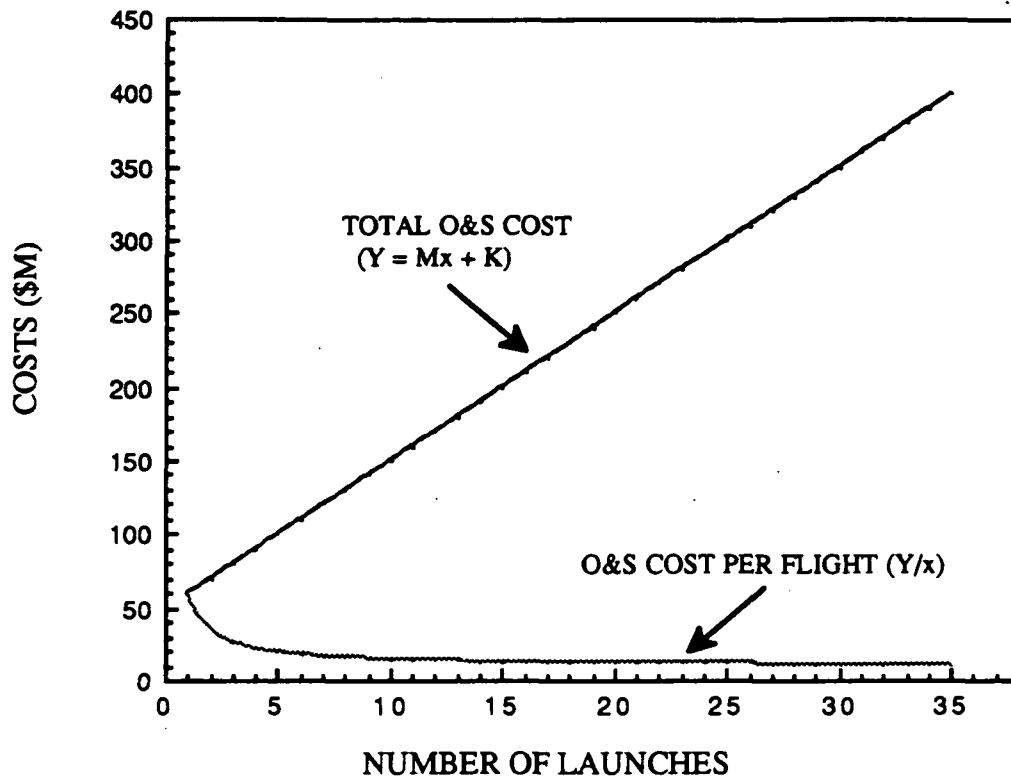(in millions of 1991 dollars).

C-3

Fig. 8.4. Operations and Support cost per launch (in millions of 1991 dollars).

# 9.0 CONCLUSION

The Antares is a single-stage-to-orbit launch vehicle, designed for versatility and low cost. To achieve these goals a modular system based on single identical units is proposed. The basic unit of the modular system, a single Antares vehicle, is aimed at launching approximately 10,000 kg (22,000 lbs) into Low Earth Orbit (LEO). When using the Centaur upper stage it is capable of placing 4,000 kg (8,800 lbs) into Geosynchronous Earth Orbit (GEO). The Antares incorporates a reusable engine, the Dual Mixture Ratio Engine (DMRE), as its propulsive device. This enables Antares to compete and excel in the satellite launch market by dramatically reducing launch costs. Antares' projected launch costs are $1,340 per kg ($610 per lb) to LEO, which offers a tremendous savings over launch vehicles available today.

The most cost-effective aspect of the Antares is its ability to return the main engine and reuse it in future launches. Since the engine accounts for the majority of the total vehicle cost, returning it results in a considerable savings, which can be returned to the customer in the form of a low cost per unit payload mass. Engine reusability is assuredly the new wave of the future, if launching is ever to become economical. The Antares will pioneer the way to developing this new technology.

Antares' modular configurations accommodate a payload range of 10,000 - 70,000 kg to LEO, which is unmatched by any other launch vehicle. The ability to launch multiple booster configurations makes the Antares in itself a family of launch vehicles. Thus the launch cost is greatly reduced because only one vehicle is developed to serve this large range of payload masses. Another cost reducing factor is that the Antares is conducive to inexpensive, large scale production because the main booster is identical in all the modular configuration. This straightforward approach to production, similar to the commercial airplane industry, also assures a high level of reliability in that specific manufacturing methods, unique to the Antares

vehicle, can be implemented because of its inherent long term usefulness as a competitive launch vehicle.

Another feature of the Antares that enables it to reach its design goal is its ability to expand and meet the growing needs of the satellite market. The Antares' modular concept makes this expansion possible. Satellites are no longer bound to the small payload capacities of existing launch vehicles. In addition to an increased payload mass, the modular concept also accommodates an increased volumetric capacity. In effect, the Antares is an all-purpose vehicle ready to expand to future needs.

Antares' innovative design makes it an inexpensive and reliable launch vehicle, and because of Antares' unique features it is capable of encouraging expansion in the satellite industry. By making the one-time dream of low cost vehicles a reality, Antares could help the U.S. regain its dominance in the commercial launch market.

# APPENDICES

# APPENDIX A: TRAJECTORY OPTIMIZATION

## A.1 OPGUID PROGRAM
(Andrew Dawdy)

OPGUID is a program, written at NASA's Marshal Space Center, that is used to optimize the launch parameters and ascent trajectories of launch vehicles. The program has been in use at NASA for many years and is continually updated and modified to meet the requirements of many users. It is capable of performing optimizations on vehicles that use any combination of staging or externally mounted assist boosters. Parameters have been included to account for different atmospheric models, the dropping of payload shrouds, and automatic throttling to meet the G force requirements of the vehicle.

The program performs its calculations in three-dimensional inertial-space (ref. earth center). Position, velocity, and acceleration of the vehicle are output as three-dimensional vectors. The program produces an output of trajectory parameters in relative coordinates by taking the rotation of the earth and the atmosphere into account and adding them to the inertial-space quantities. All other values that describe the position and direction of travel for the vehicle are derived from these vectors.

As inputs, the program requires launch conditions, rocket characteristics, and final orbital characteristics. The launch conditions include the longitude and latitude of the launch site. Preliminary analysis has been performed with NASA's Kennedy Space Center as the launch site. Its location is 28.5° north latitude and -80.5° longitude. The required rocket characteristics include: vacuum thrust, propellant flow rate, nozzle exit area, aerodynamic reference area, drag coefficient vs. Mach number, and base force vs. altitude. The final conditions for the optimization must be one of two types, either specification of final altitude, velocity, inclination and flight path angle, or specification of the final angular momentum of the vehicle as a three component vector.

## A.1.1 OPTIMIZATION PARAMETERS

OPGUID provides for four different types of optimization. Each is performed by iteration of the ascent trajectory, until the optimum solution is obtained. The four types are:

1. Pitch-Over Optimization:

The pitch-over maneuver at the start of the flight is specified by the time at which the maneuver will begin, a first approximation of the rate of pitch, and the time at which it will end. The flight path angle for the ascent is equal to 90° before the pitch-over maneuver starts. During the maneuver the flight path angle is governed by the pitch rate. After the pitch maneuver the vehicle performs a gravity turn until it leaves the atmosphere, after which the flight path angle, $\theta$, is approximated by a first order polynomial ( $\theta = at + b$ ) whose coefficients are determined internally.

2. Gross Liftoff Weight Optimization:

This optimization works well for maximization of the payload taken to orbit. It requires specification of the total propellant available for the flight, and an initial approximation of the gross liftoff weight. The total mass taken to orbit and the liftoff weight are output.

3. Propellant Mass Optimization:

By specifying the initial mass as an input, the program will determine how much of that mass is required as propellant to lift the remaining structure and payload. By determining the structure required to hold this amount of propellant, the payload mass can be found. This option cannot be performed with the Gross Liftoff Weight Optimization.

### 4. Launch Azimuth Optimization:

The program will optimize the launch azimuth upon request. The launch azimuth is defined as the direction that the vehicle will pitch as it begins its ascent. North is conventionally $0°$, while due East is $90°$. A first approximation is needed if the optimization is to be performed, if it is not used, an actual value for the calculation is required.

## A.1.2 VEHICLE PARAMETERS

The optimization of the launch vehicle thus far has included configurations of the Antares for single vehicle LEO missions, Antares/Centaur GEO missions and multiple vehicle LEO missions. All of the mission profiles have several launch parameters in common.

Insertion into a 150 x 300 km elliptical earth orbit of inclination $28.5°$ was performed as a final orbit for all LEO missions, while this orbit was used as a parking orbit before the GEO transfer. This orbit requires a final velocity of 7858 m/s at perigee, with a final flight path angle of $\theta = 0.0°$. The launch site has been chosen to be the Kennedy Space Center in Florida for this preliminary analysis.

Aerodynamic models for lift, drag and base force can be accommodated. Only drag has been accounted for in this analysis. The vehicle parameters that influence drag are the drag coefficient and the aerodynamic reference area. A structure 5.0 m in diameter (see Section 4 for details) has been chosen. This provides for an aerodynamic reference area of 19.6 $m^2$. The drag coefficients were determined theoretically (see section 6.2) and selected values were used as inputs to the program. A linear interpolation was performed at each step of the vehicle's flight. A list of these values is given in Table A.1.

An additional parameter that can be used with the program is base force. The base force term is included in the sum of forces acting on the vehicle. It is the result of interaction between the rocket plume on the aft end of the body and the surrounding atmosphere. Base force will initially be negative to account for the wake drag behind the body, but as the vehicle reaches higher altitudes it becomes positive because of the exhaust pressure on the aft end of

the body. For preliminary analysis the base force term has been neglected, but the wake drag of the vehicle has been accounted for by an increase in the $C_d$ values. This contribution can be seen in Fig. 6.2. The specific vehicle parameters used in this analysis are discussed in Section 2.2.

TABLE A.1: $C_d$ vs. Mach number (taken from Fig. 6.2).

| Mach No. | $C_d$ | Mach No. | $C_d$ |
|----------|-------|----------|-------|
| 0.00 | 0.200 | 1.40 | 0.796 |
| 0.40 | 0.210 | 1.60 | 0.778 |
| 0.60 | 0.245 | 2.00 | 0.666 |
| 0.80 | 0.335 | 2.60 | 0.530 |
| 0.90 | 0.467 | 3.00 | 0.474 |
| 1.00 | 0.648 | 6.00 | 0.363 |
| 1.10 | 0.781 | 10.00 | 0.326 |
| 1.20 | 0.799 | | |

## A.2 LAUNCH TRAJECTORY PROGRAM
(Michael Filbin)

The results of OPGUID were verified with a FORTRAN program written in conjunction with the design of the Antares vehicle. The program employes a fifth-order Runge-Kutta routine to numerically integrate the differential equations of motion for the Antares vehicle.

Atmospheric drag and gravitational effects must be considered in determining the optimal trajectory for the Antares single-stage launch into a low Earth parking orbit. For this

analysis the equations of motion are represented by the following four simultaneous ordinary differential equations ( see Fig A.1):

$$\frac{dv}{dt} = \frac{T}{m} - \frac{1}{2m}C_D A \rho v^2 - \left[ g_0 \left( \frac{R}{R+h} \right)^2 \right] \sin\theta$$

$$\frac{d\theta}{dt} = -\frac{1}{v} \left[ g_0 \left( \frac{R}{R+h} \right)^2 - \frac{(v\cos\theta)^2}{R+h} \right] \cos\theta$$

$$\frac{ds}{dt} = \left( \frac{R}{R+h} \right) v\cos\theta$$

$$\frac{dh}{dt} = v\sin\theta$$

where

| | | | |
|---|---|---|---|
| $v$ | = velocity | $C_D$ | = coefficient of drag |
| $\theta$ | = flight path angle | $A$ | = frontal area |
| $s$ | = downrange distance | $\rho$ | = atmospheric density |
| $h$ | = altitude | $g_0$ | = gravitational acceleration at sea level |
| $m$ | = vehicle mass | $R$ | = radius of the Earth |
| $T$ | = thrust | | |

The program numerically integrates the differential equations of motion over the Antares' launch trajectory from lift-off to main engine cut-off. During the atmospheric phase of the launch, the program applies a gravity assist turn to the vehicle's launch trajectory. At higher altitudes, atmospheric drag and gravitational force have a diminishing effect on the vehicle's pitch rate. Therefore, the launch trajectory program applies an external pitch rate, which physically corresponds to engine gimballing. The applied pitch rate is continuously varied, depending on the vehicle's altitude, velocity, flight path angle, and remaining

propellant. The launch trajectory program optimizes this upper phase of the trajectory so that orbital altitude and velocity are obtained at main engine cut-off.

Other features of the launch trajectory program include engine staging and throttle capability. The program varies the thrust profile to model the dual mixture ratio characteristic of the DMRE. In addition, the thrust profile is varied with altitude as a function of the ambient pressure. The program also throttles back the thrust as the Antares reaches the 4 G acceleration limit. Once the throttle-back is initiated, the thrust is continually throttled until main engine cut-off.

The inputs to the launch trajectory program include the vehicle's structural mass, and estimates for the propellant and payload masses. With these inputs, the program determines the optimal tilt angle that is required at take-off to initiate the gravity assist turn. Once the initial tilt angle is determined, the program optimizes the initial propellant mass required to launch a given payload into low Earth orbit. If this optimization is successful, the payload mass is increased until a maximum is reached, above which orbital altitude and velocity cannot be reached, regardless of the amount of propellant used.

## A.3 DEORBIT ANALYSIS PROGRAM
### (Michael Filbin)

The deorbit analysis program incorporates the fifth-order Runge-Kutta routine that was used in the launch trajectory program. The Antares encounters two different deorbit profiles, corresponding to the geostationary (GEO) and low Earth orbit (LEO) mission profiles. Technically, the Antares' tank and ERU do not reach orbit in the GEO mission profile, however the trajectory analysis is the same as for the LEO deorbit.

The differential equations of motion that apply to the Antares for the unpowered deorbit trajectory are similar to the equations used for the powered launch analysis, with the exception that the thrust terms are omitted (see Fig. A.2):

$$\frac{dv}{dt} = -\frac{1}{2m}C_D A\rho v^2 + \left[g_0\left(\frac{R}{R+h}\right)^2\right]\sin\theta$$

$$\frac{d\theta}{dt} = \frac{1}{v}\left[g_0\left(\frac{R}{R+h}\right)^2 - \frac{(v\cos\theta)^2}{R+h}\right]\cos\theta$$

$$\frac{ds}{dt} = \left(\frac{R}{R+h}\right)v\cos\theta$$

$$\frac{dh}{dt} = -v\sin\theta$$

where      $v$ = velocity                    $C_D$ = coefficient of drag

$\theta$ = flight path angle          $A$ = frontal area

$s$ = downrange distance       $\rho$ = atmospheric density

$h$ = altitude                      $g_0$ = gravitational acceleration at sea level

$m$ = vehicle mass              $R$ = radius of the Earth

These equations are numerically integrated from the beginning of the deorbit trajectory until the vehicle intercepts the Earth's surface. The inputs to the deorbit analysis program include initial altitude, velocity, flight path angle, vehicle mass, and frontal area. For GEO mission launches the inputs to the deorbit analysis program correspond to the Antares' altitude, velocity, and flight path angle at main engine cut-off. For LEO missions, the program inputs correspond to the flight conditions at the apogee of the low.Earth parking orbit, following the deorbit burn. Therefore the initial deorbit velocity is the difference of the apogee velocity and the $\Delta v$ provided by the deorbit maneuver. Also, the vehicle's flight path angle at the apogee is exactly zero.

The output of the deorbit analysis program is the downrange distance travelled from the point where the deorbit trajectory was initiated to the point where the trajectory intercepts the

Earth's surface. The Earth's rotation is taken into account in calculating the downrange distance travelled. This determines the area on Earth where the Antares vehicle returns.
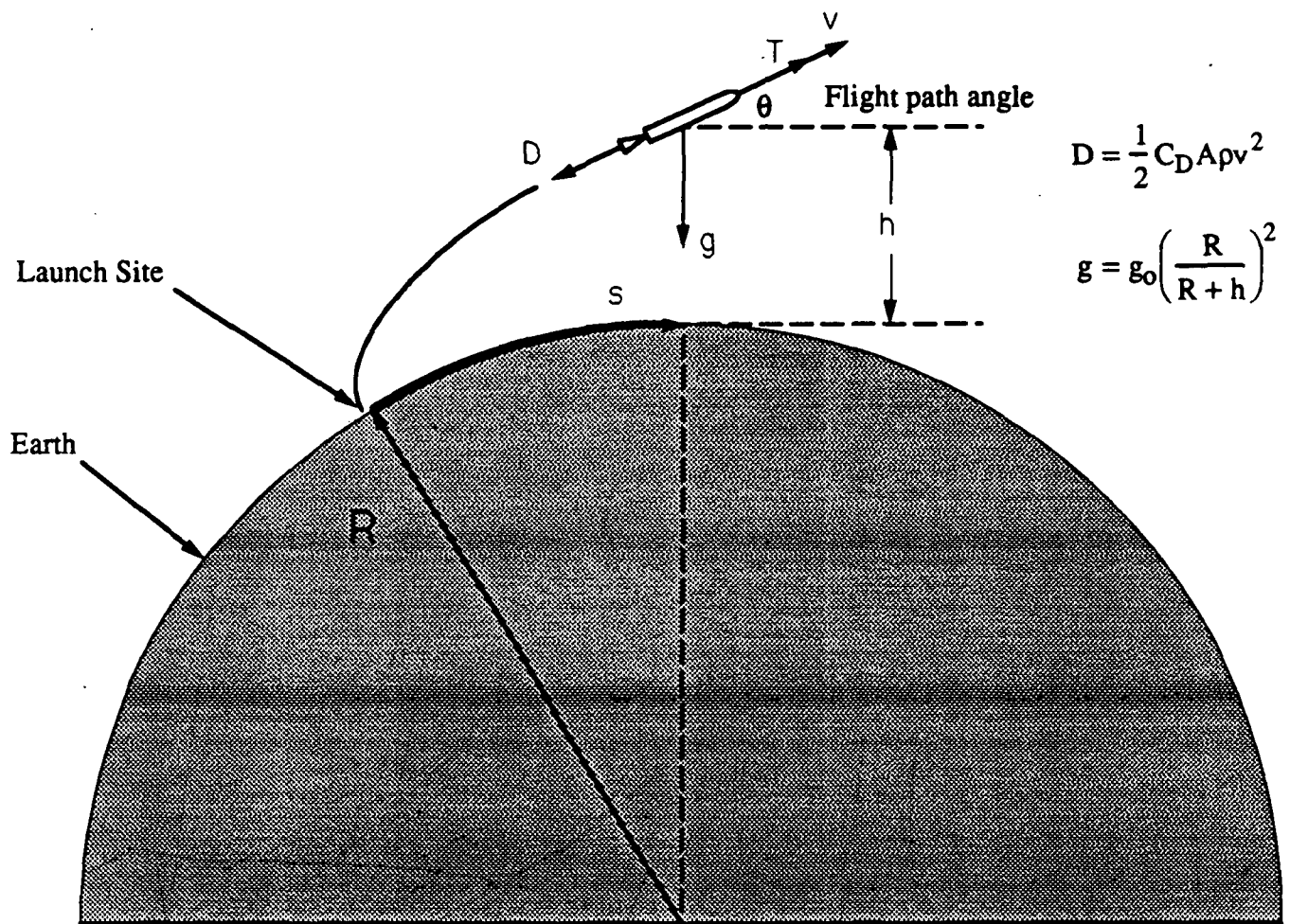
The figure shows the flight trajectory with vectors labeled $T$, $v$, $D$, $g$, angle $\theta$, "Flight path angle", $h$, $s$, $R$, "Launch Site", and "Earth".

$$D = \frac{1}{2}C_D A \rho v^2$$

$$g = g_o\left(\frac{R}{R+h}\right)^2$$

Fig. A.1. Flight trajectory parameters for launch.

$$D = \frac{1}{2} C_D A \rho v^2$$

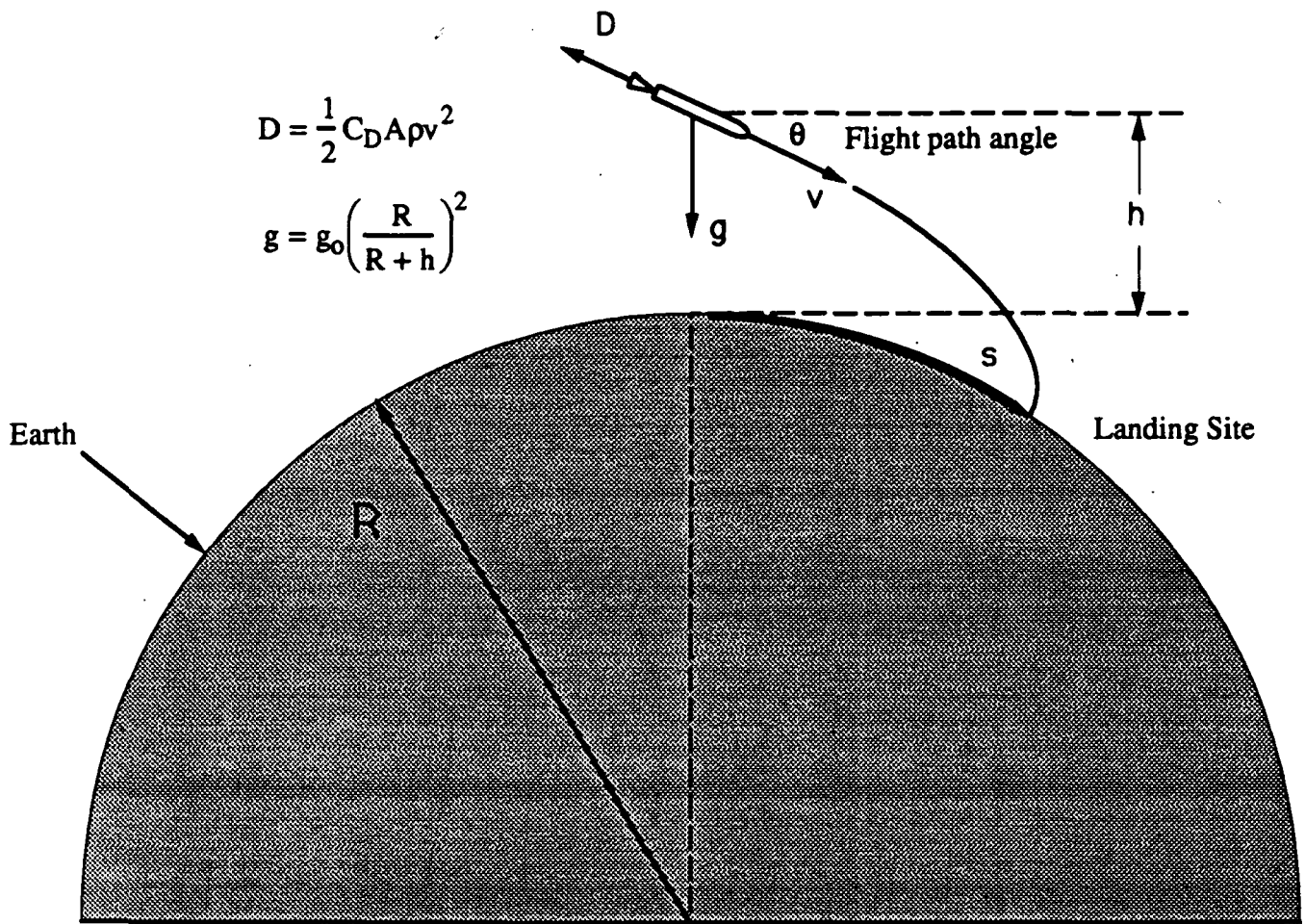$$g = g_o \left( \frac{R}{R+h} \right)^2$$



Fig. A.2. Flight trajectory parameters for deorbit.

# APPENDIX B: REUSABLE ENGINE COMPARISON
## (Steve Nicholls)

Three types of reusable rocket engines were considered in the design of the Antares. Of these three, only the Space Shuttle Main Engine (SSME) is currently in use. The remaining two engines, the Space Transportation Main Engine (STME) and the Dual Mixture Ratio Engine (DMRE) are currently under development and research, respectively.

Table B.1 lists the characteristics of the various engines. Two versions of the STME were considered. One version produces approximately 2,580 kN of vacuum thrust, the other produces approximately 2,850 kN of vacuum thrust. The DMRE performance characteristics are given in two entries. The first corresponds to values with the nozzle extension retracted. The second corresponds to values with the nozzle extended. Note that the SSME and DMRE use a staged combustion cycle, while the STME uses a gas generator cycle. Figure B.1 is a propellant flow schematic for a staged combustion cycle. Figure B.2 shows propellant flow for a gas generator cycle.

Table B.2 lists the characteristics of a single Antares mission to low earth orbit. The last column refers to the point to which the engine must be throttled back, in percent of maximum throttle, to stay under a 4 G acceleration limit. This limit is imposed to protect payloads from excessive g loading. The Antares using the DMRE delivers the maximum payload to low earth orbit.

Table B.1: Comparison of reusable engine characteristics.

| | DMRE [1] | SSME | STME (A) [2] | STME (B) [2] |
|---|---|---|---|---|
| Engine Cycle | Staged Combustion | Staged Combustion | Gas Generator | Gas Generator |
| Propellants | LOX / LH$_2$ | LOX / LH$_2$ | LOX / LH$_2$ | LOX / LH$_2$ |
| Mixture Ratio (LOX/LH$_2$) | 12:1 / 6:1 | 6:1 | 6:1 | 6:1 |
| Chamber Pressure (MPa) | 27.6 / 18.6 | 20.7 | 15.5 | 15.5 |
| Mass Flow Rate (kg/sec) | 751 / 403 | 466 | 617 | 617 |
| Nozzle Area Ratio (A$_e$/A$_t$) | 40 / 150 | 77.5 | 40 | 40 |
| Thrust (kN) Sea Level | 2460 / NA | 1670 | 2237 | 2470 |
| Thrust (kN) Vacuum | 2670 / 1850 | 2091 | 2580 | 2850 |
| Specific Impulse (sec) Sea Level | 334 / NA | 361 | 370 | 370 |
| Specific Impulse (sec) Vacuum | 362 / 467 | 453 | 428 | 428 |
| Dry Mass (kg) | 2272 | 3125 | 2689 | 2689 |

[1] Where two parameters are given, the first denotes the condition with nozzle extension retracted, the second denotes the condition with nozzle extended.

[2] Two types of the Space Transportation Main Engine are proposed. One would produce 2580 kN of vacuum thrust (A), the other would produce 2850 kN of vacuum thrust (B).

Table B.2: Antares LEO mission using various engines.

| Engine Used | $M_O$ (kg) | $M_p$ (kg) | $M_S$ (kg) | $M_*$ (kg) | 4 G Throttle |
|---|---|---|---|---|---|
| SSME | 136,080 | 118, 670 | 12,700 | 4500 | 30 % |
| STME (A) [1] | 179,900 | 159,800 | 12,700 | 7000 | 28 % |
| STME (B) [1] | 202,900 | 180,300 | 12,700 | 8500 | 29 % |
| DMRE | 197,600 | 174,000 | 12,700 | 10,000 | 47 % |

$M_O$ : Liftoff mass of Antares vehicle

$M_p$ : Propellant mass of Antares vehicle

$M_S$ : Structural mass of Antares vehicle

$M_*$ : Payload to Low Earth Orbit of Antares vehicle

4 G Throttle : Throttle back point to keep acceleration of vehicle under 4 G

[1] Two types of the Space Transportation Main Engine are proposed. One would produce 2580 kN of vacuum thrust (A), the other would produce 2850 kN of vacuum thrust (B).
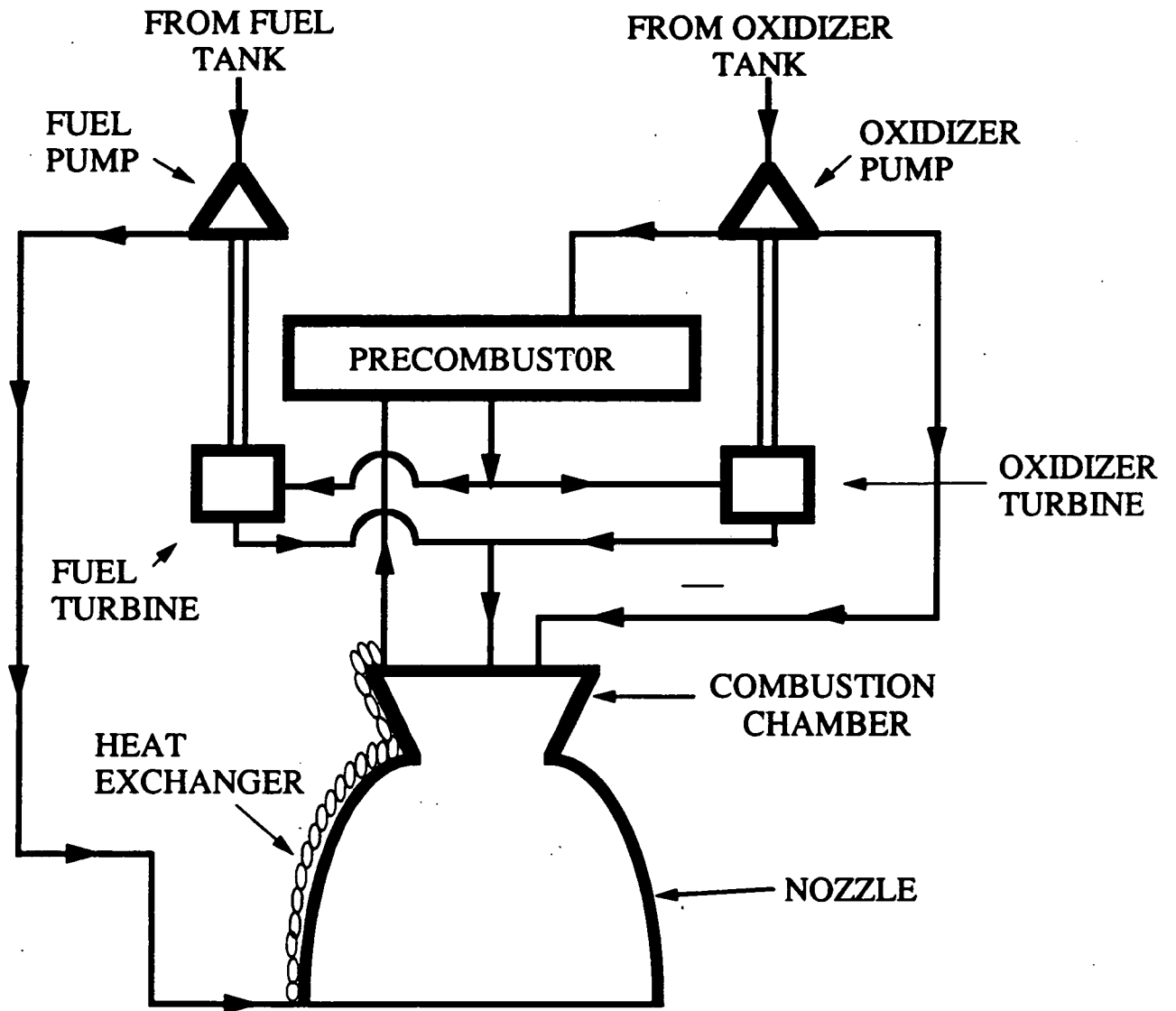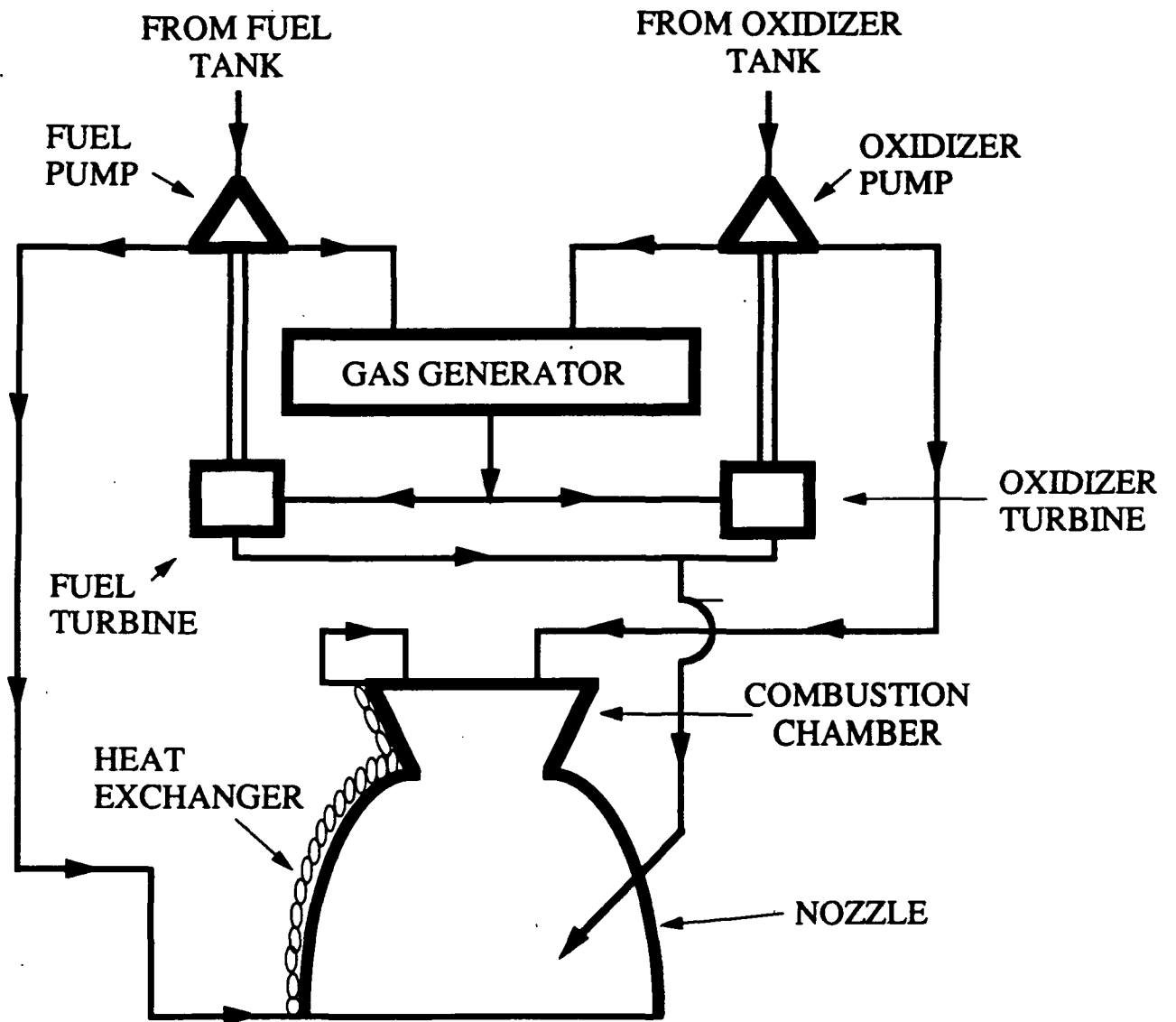
Fig. B.1. Staged combustion propellant flow schematic.

Fig. B.2. Gas generator propellant flow schematic.